ON A CLASS OF ABCS

by

SRIDEVI LALGUDI

Presented to the Faculty of the Graduate School of

The University of Texas at Arlington in Partial Fulfillment

of the Requirements

for the Degree of

MASTER OF SCIENCE IN PHYSICS

THE UNIVERSITY OF TEXAS AT ARLINGTON

August 2005

ACKNOWLEDGEMENTS

I would like to thank Dr. A. K. Ray for his mentorship throughout the course of my academics and research work. I would like to extend my gratitude to the members of my thesis committee: Dr. M. Cuntz, and Dr. N. Fazleev and also to the other faculty members of Physics department for having enriched my knowledge in the area of Physics. I am thankful to the Physics Department for providing an excellent environment for work. I gratefully acknowledge the financial support of the Welch Foundation, Houston Texas and the Department of Physics at the University of Texas at Arlington.

It was fun working with my research group members and I appreciate their resourceful ideas and valuable opinions. I would like to thank the members of Physics office; Amy, Margie and Jean and also Doug for their friendliness and help they offered me during my stay at UTA. I owe a lot to my parents for their support and encouragement. Finally, I would like to dedicate this work to my fiancé Prasanna, for his undying patience and encouragement that he offered without which it would have been difficult to have completed this work.

July 20, 2005

ABSTRACT

ON A CLASS OF ABCS

Publication No. _____

Sridevi Lalgudi Ganapathy

The University of Texas at Arlington, 2005

Supervising Professor: Dr. A. K. Ray

The local density approximation to density functional theory (LDA-DFT) has been used to study the different possible relaxations and reconstructions of In-rich InSb (100) surface. Various electronic and geometric structure properties such as, bond lengths, cohesive energies, band gaps and density of states of the ideal (1x1) surface and the (2x1), (4x2) and c(8x2) reconstructed InSb surfaces are reported. Adsorptions of lithium atom as well as other halogen atoms such as chlorine, bromine and iodine on the (1x1), (2x1), (4x2) and c (8x2) InSb surfaces in the different symmetric sites, such as, top, bridge, hollow, cave, trough and also interstitial cage site have been investigated. Details of energetics of the chemisorption process, such as

chemisorption energies, and also the adatom separation distances, charge distributions, energy band gaps and density of states are discussed. The changes in the InSb surfaces due to these different atomic adsorptions are analyzed. In the final phase of this study, we address the question of whether the molecular adsorption of iodine on the InSb surface is feasible. The results of molecular as well as dissociative adsorptions are reported and it was found that dissociation is favored in many of the approaches in energetics point of view. The changes in the atomic charge distributions of the InSb surface due to the I_2 adsorption, both molecularly as well as dissociatively are investigated. The variations in the HOMO-LUMO gaps when the I_2 molecule is adsorbed are reported with the DOS plots illustrating these changes.

TABLE OF CONTENTS

LIST OF ILLUSTRATIONS

Figure Page

LIST OF TABLES

CHAPTER 1

INTRODUCTION

1.1 Surface Science of InSb(100) Surface – Technological Point of View

Indium antimonide (InSb) belongs to a class of antimony-based compound semiconductors (ABCS). ABCS is a new class of compound semiconductors with superior electronic properties and lower turn-on voltages compared to those offered by semiconductors based on silicon, Gallium Arsenide and Indium Phosphide [1]. ABCS are expected to produce world's fastest circuits with lowest consumed power, in defense and space applications. In addition to this, ABCS technology has commercial applications too, particularly in high frequency wireless applications, light wave communication and integrated optoelectronic circuits [2]. In particular, transistors made of InSb enable research devices to operate at very low power. The research results obtained from the quantum well transistors research showed a ten percent lower power consumption for the same performance, or conversely improvement by a factor of three in transistor performance for the same consumption, as compared to today's traditional transistors [3].

Among the compound semiconductor materials, InSb is the exception from the point of view of band-gap energy, as it has a smaller band-gap of 0.165 eV, about one sixth of that of Si. This band-gap predicts that the energy resolution of InSb detector is less than 60 eV for 6 keV x rays. In addition, the mobilities of electrons and holes of

InSb are found to be 40 and 1.5 times greater than those of Si, respectively. The high atomic number of In(49) and Sb(51), and it high density(5.78 g/cm^3) make InSb a more attractive material for radiation detectors, especially for the measurements of high-energy photons [4]. In this work by Kanno *et al.* [4], the InSb detector was found to have a wide temperature operating range. Nakamura *et al.* [5] showed that the use of an InSb semiconductor is advantageous at low-temperature operation because of its high carrier mobility. Within the last decade, III-V semiconductors including InSb have become extremely relevant for fabricating high-speed electronic and optoelectronic devices owing to these potential applications. Layer growth and epitaxial behavior, which are strongly influenced by the morphology of the substrate surface, play an important role for the fabrication process. Thus, detailed knowledge about the geometric structure of the surface is essential [6].

The most frequently used surface of III-V compound semiconductors in device technology is the (100) surface. Also, the industry standard for growing InSb by molecular beam epitaxy (MBE) is the (100) surface [7, 8] . This surface has the highest aerial density of dangling surface bonds, greater than the (110) or (111) surface. Ideally, the (100) surface of zinc-blende structure of InSb is made up of alternating layers of anions and cations and hence the ideal unreconstructed surface is electrostatically unstable. Each surface atom possesses two dangling bonds which makes the surface to reconstruct by the formation of dimers, the basic mechanism responsible for the minimization of total energy [9]. Depending upon preparation, temperature, and especially whether group-III- or group-V-rich conditions are dominant, the (100)

surfaces of III-V compound semiconductors show a wealth of different surface reconstructions [6]. A brief summary of some of the relevant literature concerning the InSb(100) surface follows.

The most prominent reconstruction of In-rich InSb(100) surface discussed in the literature is the c (8x2) structure. The surface structures of InSb films grown on (111)A, (111)B and (001)-oriented InSb substrates by molecular beam epitaxy were investigated *in situ* with a reflection high-energy electron diffraction (RHEED) technique by Oe *et al.* [10] and the surface structures observed with RHEED were (111)A – (2x2), (111)B – (3x3) and (001)-c(8x2) at room temperature. Data obtained by Noreika *et al.*[11] supplement and extend the work of Oe *et al.*, but include some corroborative duplication for comparison. Here, the films of InSb were grown homoepitaxially on (111)A-, (111)B-, and (001)-oriented InSb substrates and heteroepitaxially on (001)-oriented InAs and GaAs over a wide temperature range, $250^{\circ}<T<450^{\circ}$C. Surface-atom reconstructions for Sb-stabilized and In-stabilized films were identified. For $J_{Sb}/J_{In} < 1$, only an In stabilized c(8x2) structure was observed and basically, the RHEED data substantiate the surface reconstructions on (001) InSb surface by Oe *et al.* and supplement them with the addition of complex (7x5) Sb-stabilized structure. In the study by John *et al.*[12], the InSb (100) surface was grown using the techniques of molecular-beam epitaxy and the surface was found to undergo several reconstructions, including a c(4x4), a c(8x2), an asymmetric (1x3), a symmetric (1x3), and a (1x1). The c(4x4) surface was found to be terminated with 1-3/4 monolayers of Sb, while 3/4 monolayer of In was found to be the termination of the c(8x2) surface. In the surface

study of Jones *et al*.[13], the formation of clean, antimony rich, c(4x4) reconstructed surface of Insb (001) by chemical means is described. Here it has been reported that a clean, indium rich surface formed by noble gas ion bombardment and annealing of a bulk sample, displayed a disordered (4x2) low energy electron diffraction (LEED) pattern with sharp (4x1) features and this surface, when saturated to monolayer coverage with either iodine or chlorine and heated to 300 C resulted in the desorption of the halogen species leaving a clean, antimony rich c(4x4) surface. There has been another LEED study of InSb (001) in which a sharp (4x1) structure, with faint streaks, was also observed [14]. There has also been a scanning tunneling microscopy (STM) study of the InSb(100) – c(8x2) surface by Schweitzer *et al.* [15]. In this study, both STM and LEED had been used to assess the quality of sputtered and annealed InSb(100) surfaces and to elucidate the atomic structure of the c(8x2) surface reconstruction. It has been found that although the LEED pattern clearly exhibits a c(8x2) surface periodicity, the real space STM image suggests a (4x1) periodicity. The apparent conflict between the (4x1) periodicity as observed by STM and the c(8x2) pattern seen in LEED has been resolved by considering the structural model originally proposed for this surface by John *et al.*. Close inspection of this model discussed by Schweitzer *et al.* shows that the full translational symmetry of the surface is c (8x2) surface consistent with the low energy electron diffraction (LEED) results. Again the same fact has been established by an STM study where several different reconstructions of InSb (100) surface has been studied and discussed in detail [16]. In this study, cycles of low-energy ion bombardment and annealing result in the formation of In-rich surface

with a c(8x2) diffraction pattern. Filled-state images were found to indicate a (4x1) periodicity arising from imaging occupied lone-pair orbitals on exposed second-layer Sb atoms. The controlled deposition of Sb_4 from a Knudsen effusion source onto the c(8x2) surface at elevated temperatures led to the formation of a (1x1), c(4x4), and an asymmetric (1x3) structure, in order of decreasing Sb/In ratio. Filled- and empty-states STM images of all these Sb-rich reconstructions were generated and the coexistence of the different structures was also found to be observed. Surface reconstructions of InSb(001) during molecular beam epitaxy(MBE) using reflection high energy electron diffraction(RHEED) were studied by Liu *et al.* where several previously unreported reconstruction regimes; namely (1x1), co-existence of (4x2) with c(8x2), and co-existence of Sb-terminated and In-terminated structures were reported and also the pseudo-(1x3) pattern was believed to result from a mixture of different (2x4) phases, rather than a single surface structure [17]. It is claimed that (4x2) and c(8x2) structures are simply related by atomic displacement of In-dimers in the direction of the 2x periodicity and therefore they are readily interchangeable. Jones *et al.* reported a surface X-ray diffraction study of the indium-rich InSb(001)-c(8x2) reconstruction, which gives a detailed picture of the atomic structure. The proposed structure is consistent with the STM images and represents a significant departure from the models previously suggested for the c(8x2) reconstruction on any of the III-V (001) surfaces [18]. In one another surface x-ray diffraction study by Kumpf *et al.*, the atomic structure of the c(8x2) reconstructions of InSb-, InAs-, and GaAs-(001) surfaces are presented where subsurface dimerization of group III atoms is found to occur [6, 19].

Indium antimonide (InSb) belongs to a class of antimony-based compound semiconductors (ABCS). ABCS is a new class of compound semiconductors with superior electronic properties and lower turn-on voltages compared to those offered by semiconductors based on silicon, Gallium Arsenide and Indium Phosphide [1]. ABCS are expected to produce world's fastest circuits with lowest consumed power, in defense and space applications. In addition to this, ABCS technology has commercial applications too, particularly in high frequency wireless applications, light wave communication and integrated optoelectronic circuits [2]. In particular, transistors made of InSb enable research devices to operate at very low power. The research results obtained from the quantum well transistors research showed a ten percent lower power consumption for the same performance, or conversely improvement by a factor of three in transistor performance for the same consumption, as compared to today's traditional transistors [3].

Among the compound semiconductor materials, InSb is the exception from the point of view of band-gap energy, as it has a smaller band-gap of 0.165 eV, about one sixth of that of Si. This band-gap predicts that the energy resolution of a InSb detector is less than 60 eV for 6 keV x rays. In addition, the mobilities of electrons and holes of InSb are found to be 40 and 1.5 times greater than those of Si, respectively. The high atomic number of In(49) and Sb(51), and it high density(5.78 g/cm^3) make InSb a more attractive material for radiation detectors, especially for the measurements of high-energy photons [4]. In this work by Kanno *et al.* [4], the InSb detector was found to have a wide temperature operating range. Nakamura *et al.* [5] showed that the use of an

InSb semiconductor is advantageous at low-temperature operation because of its high carrier mobility. Within the last decade, III-V semiconductors including InSb have become extremely relevant for fabricating high-speed electronic and optoelectronic devices owing to these potential applications. Layer growth and epitaxial behavior, which are strongly influenced by the morphology of the substrate surface, play an important role for the fabrication process. Thus, detailed knowledge about the geometric structure of the surface is essential [6].

The most frequently used surface of III-V compound semiconductors in device technology is the (100) surface. Also, the industry standard for growing InSb by molecular beam epitaxy (MBE) is the (100) surface [7, 8] . This surface has the highest aerial density of dangling surface bonds, greater than the (110) or (111) surface. Ideally, the (100) surface of zinc-blende structure of InSb is made up of alternating layers of anions and cations and hence the ideal unreconstructed surface is electrostatically unstable. Each surface atom possesses two dangling bonds which makes the surface to reconstruct by the formation of dimers, the basic mechanism responsible for the minimization of total energy [9]. Depending upon preparation, temperature, and especially whether group-III- or group-V-rich conditions are dominant, the (100) surfaces of III-V compound semiconductors show a wealth of different surface reconstructions [6]. A brief summary of some of the relevant literature concerning the InSb(100) surface follows.

The most prominent reconstruction of In-rich InSb(100) surface discussed in the literature is the c (8x2) structure. The surface structures of InSb films grown on (111)A,

(111)B and (001)-oriented InSb substrates by molecular beam epitaxy were investigated *in situ* with a reflection high-energy electron diffraction (RHEED) technique by Oe *et al.* [10] and the surface structures observed with RHEED were (111)A – (2x2), (111)B – (3x3) and (001)-c(8x2) at room temperature. Data obtained by Noreika *et al.*[11] supplement and extend the work of Oe *et al.*, but include some corroborative duplication for comparison. Here, the films of InSb were grown homoepitaxially on (111)A-, (111)B-, and (001)-oriented InSb substrates and heteroepitaxially on (001)-oriented InAs and GaAs over a wide temperature range, 250°<T< 450°C. Surface-atom reconstructions for Sb-stabilized and In-stabilized films were identified. For $J_{Sb}/J_{In} < 1$, only an In stabilized c(8x2) structure was observed and basically, the RHEED data substantiate the surface reconstructions on (001) InSb surface by Oe *et al.* and supplement them with the addition of complex (7x5) Sb-stabilized structure. In the study by John *et al.*[12], the InSb (100) surface was grown using the techniques of molecular-beam epitaxy and the surface was found to undergo several reconstructions, including a c(4x4), a c(8x2), an asymmetric (1x3), a symmetric (1x3), and a (1x1). The c(4x4) surface was found to be terminated with 1-3/4 monolayers of Sb, while 3/4 monolayer of In was found to be the termination of the c(8x2) surface. In the surface study of Jones *et al.*[13], the formation of clean, antimony rich, c(4x4) reconstructed surface of Insb (001) by chemical means is described. Here it has been reported that a clean, indium rich surface formed by noble gas ion bombardment and annealing of a bulk sample, displayed a disordered (4x2) low energy electron diffraction (LEED) pattern with sharp (4x1) features and this surface, when saturated to monolayer

coverage with either iodine or chlorine and heated to 300 C resulted in the desorption of the halogen species leaving a clean, antimony rich c(4x4) surface. There has been another LEED study of InSb (001) in which a sharp (4x1) structure, with faint streaks, was also observed [14]. There has also been a scanning tunneling microscopy (STM) study of the InSb(100) – c(8x2) surface by Schweitzer *et al.* [15]. In this study, both STM and LEED had been used to assess the quality of sputtered and annealed InSb(100) surfaces and to elucidate the atomic structure of the c(8x2) surface reconstruction. It has been found that although the LEED pattern clearly exhibits a c(8x2) surface periodicity, the real space STM image suggests a (4x1) periodicity. The apparent conflict between the (4x1) periodicity as observed by STM and the c(8x2) pattern seen in LEED has been resolved by considering the structural model originally proposed for this surface by John *et al.*. Close inspection of this model discussed by Schweitzer *et al.* shows that the full translational symmetry of the surface is c (8x2) surface consistent with the low energy electron diffraction (LEED) results. Again the same fact has been established by an STM study where several different reconstructions of InSb (100) surface has been studied and discussed in detail [16]. In this study, cycles of low-energy ion bombardment and annealing result in the formation of In-rich surface with a c(8x2) diffraction pattern. Filled-state images were found to indicate a (4x1) periodicity arising from imaging occupied lone-pair orbitals on exposed second-layer Sb atoms. The controlled deposition of Sb_4 from a Knudsen effusion source onto the c(8x2) surface at elevated temperatures led to the formation of a (1x1), c(4x4), and an asymmetric (1x3) structure, in order of decreasing Sb/In ratio. Filled- and empty-states

STM images of all these Sb-rich reconstructions were generated and the coexistence of the different structures was also found to be observed. Surface reconstructions of InSb(001) during molecular beam epitaxy(MBE) using reflection high energy electron diffraction(RHEED) were studied by Liu *et al.* where several previously unreported reconstruction regimes; namely (1x1), co-existence of (4x2) with c(8x2), and co-existence of Sb-terminated and In-terminated structures were reported and also the pseudo-(1x3) pattern was believed to result from a mixture of different (2x4) phases, rather than a single surface structure [17]. It is claimed that (4x2) and c(8x2) structures are simply related by atomic displacement of In-dimers in the direction of the 2x periodicity and therefore they are readily interchangeable. Jones *et al.* reported a surface X-ray diffraction study of the indium-rich InSb(001)-c(8x2) reconstruction, which gives a detailed picture of the atomic structure. The proposed structure is consistent with the STM images and represents a significant departure from the models previously suggested for the c(8x2) reconstruction on any of the III-V (001) surfaces [18]. In one another surface x-ray diffraction study by Kumpf *et al*., the atomic structure of the c(8x2) reconstructions of InSb-, InAs-, and GaAs-(001) surfaces are presented where subsurface dimerization of group III atoms is found to occur [6, 19].

1.2 Metal-Semiconductor Contacts

Metal-semiconductor interfaces have been of major interest to both experimentalists and theoreticians to understand both Ohmic and Schottky barrier contacts as well as the extensive industrial applications of semiconductor devices [9, 20, 21, 22]. The electronic properties of metal-semiconductor, metal-oxide-semiconductor,

and semiconductor-semiconductor junctions are widely used in the formulation of increasingly complex and versatile device concepts. Since Li is a simple metal atom, in the initial phase of this study, we investigate the surface chemistry and physics of lithium adsorption on the different InSb (100) surfaces. To the best of our knowledge, this is the first *ab-initio* study on the adsorption of Li on the InSb surface.

1.3 Importance of halogen reactions with semiconductor surfaces

The field of surface science has matured sufficiently over the past 30 years that investigation of model systems aid in studies of more complex real-life processes. One such real-life process that has received considerable attention in recent years is the etching of semiconductor surfaces by halogen compounds [23]. At sufficiently high temperatures and pressures, halogens or halogen-containing compounds can etch III-V semiconductors, which make these reactions appropriate for use in device processing. Hence, it is technologically important to understand how halogens react with semiconductor surfaces. Also, in addition to the industrial importance, halogens are an excellent class of adsorbates for studying chemisorption and are thus also interesting from a purely academic point of view. Halogen adsorbates are ideal for structural studies because they form strong, directional, monovalent bonds to semiconductor surfaces. As a result of their large electronegativities, halogens withdraw an appreciable amount of charge from a neighboring atom in forming a bond.

Simpson and Yarmoff [23] have presented a good review about the basic chemical reactions of simple molecular halogens (XeF_2, Cl_2, Br_2, I_2) on III-V (GaAs, GaSb, InP, InAs, InSb) semiconductor surfaces and the properties of the surfaces

following reaction. Cl_2 has been observed, in some cases, to form a 1x1 overlayer on GaAs(110) [24, 25, 26], GaAs(001)-c(8x2) [26], InSb(001)-4x1 [13], and InP(001)-4x2 [27]. At other times, however, Cl_2 adsorption leads to the complete removal of the low-energy electron diffraction (LEED) pattern, thereby indicating that the surface has become disordered. This has been seen for Cl_2 adsorption on GaAs(110) [28], on InP(110) [29], and on InP(001)-4x2 [27]. In this study, it has been commented that the adsorption of I_2 on many surfaces, including InSb(001) – 4x1 [13], InSb(001)-c(4x4)[13], InSb(001)-c(8x2) [30,31,32], GaAs(001)-(4x1) [33,34,35], GaAs(001)-4x6 [33,34,35], GaAs(001)-c(2x8)[33, 34, 35] and InAs(001)-c(8x2)[33, 34, 35]- relaxes the clean surface reconstruction and forms a highly ordered 1x1 overlayer. In one of the studies dealing with the reaction of I_2 with the InSb(001) surfaces of GaAs, InAs, and InSb, Varekemp *et al.*[34] have provided evidence for the room temperature etching of InSb(001) surface from an analysis of scanning tunneling microscopy(STM) images and synchrotron soft x-ray photoelectron spectroscopy(SXPS) data as a function of I_2 exposure. In this study, InAs(001)-c(8x2), InSb(001)-c(8x2), and several reconstructions of GaAs(001) were exposed at room temperature to iodine molecules(I_2). It was found that the InSb(001)-c(8x2) reconstruction is removed by I_2 adsorption, and a strong 1x1 LEED pattern is formed. It was reported that one of the predominant feature of the STM image was found to occupy a 1x1 unit cell with the same spacing as bulk-terminated InSb(001). This observation of an ordered overlayer during etching at room temperature is in contrast to the reactions of GaAs with chlorine and fluorine, where the reaction produced disorder in the near-surface region. This

tendency for I_2 to be a "gentler" etchant is important in semiconductor device processing, where a minimal amount of etchant-induced disorder is desired. All these interesting properties of the halogen reactions with semiconductor surfaces prompted us to investigate the chemisorption process of halogens, such as chlorine, bromine and iodine on the InSb surface.

From the review of Simpson *et al*.[23], several trends were already found to be apparent in the results of investigations of halogens with the III-V semiconductors. One among them is that halogens dissociatively chemisorb during their reactions with III-V semiconductors, forming first monohalides and then di- and trihalides. But still, the reactions of halogens, such as, Br and I with III-V semiconductors other than GaAs are found to be lesser studied [2]. Hence, in the last phase of the study, considerable effort has been taken towards the understanding of interactions of molecular halogens (I_2) with the InSb(100) surface. And also, more focus was given as to find out if dissociative adsorption is favored. It has been claimed by Varekemp *et al.*[33] that though the atomic structures of all (001) surfaces are not completely agreed upon, the c(8x2), c(2x8), and c(4x4) reconstructions present on the (001) crystal face are commonly believed to be superstructures composed of 4x2 unit cells. We also report the changes in geometric and electronic structure properties of InSb(100) surface after both molecular and dissociative adsorptions. More emphasis was given on the analysis of atomic charge distribution of the (4x2) surface before and after dissociative chemisorption of I_2.

In the next chapter, we outline the theoretical formalism used in this work. In Chapter 3, the energetics and the geometric and electronic structure properties of the

different In-rich InSb(100) surface are discussed. In Chapter 4, the results of the detailed analysis of the atomic adsorptions, such as Li, Cl, Br and I on the different InSb(100) surface are reported. In Chapter 5, we present the results of molecular as well as dissociative adsorption of I_2 with the (4x2) surface of In-rich InSb(100) surface in different sites along various approaches. Also, a detailed analysis of the changes in the (4x2) surface is made with respect to the mulliken charge distribution, HOMO-LUMO gaps, density of states and energetics, due to I_2 adsorption from both molecular as well as dissociative point of view. Finally, in chapter 6, we discuss the overall conclusions of our study. In our future work, we plan to extend our current work on the molecular adsorption of halogens, by increasing the coverage of the adatoms on the InSb surface to analyze the changes in the energetics as well as the geometric and electronic structure properties of the surface.

CHAPTER 2

THEORY

2.1 Introduction

Currently, there are primarily two computational methods based on two different theories to solve the many-body problems; the Hartree-Fock theory and the density functional theory (DFT). DFT is one of the most popular and successful quantum mechanical approaches to matter. Conceptually simpler and formally rigorous density functional theory provides an elegant way of mapping a *N* variable system to a single variable, the system's density, and hence reducing the computational cost significantly over the traditional *ab initio* theories such as Hartree-Fock theory, while retaining the much of the computational accuracy. Here is a short description of density functional theory following mostly the reviews of Yang and Parr [36], Capelle [37] and Nagy [38].

2.2 Hohenberg-Kohn Theorems

At the heart of DFT is the Hohenberg-Kohn theorem. Let us consider a system of *N* electrons under the influence of some time-independent external potential. Hohenberg-Kohn theorem [39] states that, the external potential $v(\vec{r})$ is determined solely by the electron density $\rho(\vec{r})$, within a trivial additive constant. The basic difference from the traditional quantum mechanics is that in density functional theory

we solve for the density rather than the wave functions. Of course densities are defined from the wave function in a very trivial manner:

$$\rho(\vec{r}_1) = N\int \Psi^*(\vec{x}_1,\vec{x}_2,\ldots,\vec{x}_N)\Psi(\vec{x}_1,\vec{x}_2,\ldots,\vec{x}_N)ds_1 d\vec{x}_2 d\vec{x}_3 \ldots d\vec{x}_N \tag{2.1}$$

where Ψ is assumed to be normalized to unity; and $\vec{x}_i$'s include both spin and spatial variables which, in equation (1) are integrated out for i = 2 to N, including the spin part of the first particle. So once the density of electrons is known the other electronic properties can also be computed. For example, the total number of electrons is given by:

$$N = \int \rho(\vec{r})d\vec{r} \tag{2.2}$$

Also from Kato's theorem [40], which is applicable only to the Coulomb potential, we get:

$$Z_\beta = -\frac{1}{2\rho(\vec{r})}\frac{\partial\rho(\vec{r})}{\partial r}\bigg|_{r=R_\beta} \tag{2.3}$$

where the partial derivatives are taken at the nuclei β. So from the equation (3) we see that from the cusps of the density define the position of the nuclei, R_β, and the atomic number Z_β. In general $v(\vec{r})$ in the Hohenberg-Kohn theorem is not restricted to the Coulomb potentials.

Let us now proceed to prove the Hohenberg-Kohn theorem following the original approach of their papers. The original proof was both simple and elegant, and was done by reduction ad absurdum, basically for the non-degenerate systems. However the general conclusion is applicable to degenerate system as well. The proof follows like this:

Let us suppose that, in addition to $v(\vec{r})$ there exists another potential $v'(\vec{r})$ due to the same density $\rho(\vec{r})$, and that $v(\vec{r}) \neq v'(\vec{r}) + c$, where c is just an additive constant. Now due to this two potentials we will have two ground state wave functions Ψ and Ψ' corresponding to two Hamiltonian H and H' with the ground state energies of E and E', respectively. The Hamiltonians are defined as:

$$H = T + V_{ee} + \sum_{i}^{N} v(\vec{r}_i), \tag{2.4}$$

where T and V_{ee} are the kinetic energy and electron-electron repulsion operators defined as below:

$$T = -\frac{1}{2}\sum_{i}^{N} \nabla_i^2 , \tag{2.5}$$

$$V_{ee} = \sum_{i<j}^{N} \frac{1}{r_{ij}}, \tag{2.6}$$

Here we use the atomic units where

$$e^2 = \hbar = m_e = 1 .$$

where e is the electronic charge, $\hbar$ is the Plank's constant and m_e is the electron mass. In this unit energies are given in Hertrees, $1H$ = 27.2116 eV = 627.4 kcal/mol and the distances are in Bohr, $a_o = 0.529$ Å.

From Rayleigh_Ritz variational principal it follows that

$$\begin{aligned} E_0 = \langle \Psi | H | \Psi \rangle < \langle \Psi' | H | \Psi' \rangle &= \langle \Psi' | H | \Psi' \rangle + \langle \Psi' | H - H' | \Psi' \rangle \\ &= E_0' + \int \rho(\vec{r}) [v(\vec{r}) - v'(\vec{r})] dr \end{aligned} \tag{2.7}$$

Similarly, using the variational principle for the Hamiltonian H' with the trial wave function Ψ, we have

$$E_0' = \langle \Psi' | H' | \Psi' \rangle < \langle \Psi | H' | \Psi \rangle = \langle \Psi | H | \Psi \rangle + \langle \Psi | H' - H | \Psi \rangle$$
$$= E_0' + \int \rho(\vec{r})[v(\vec{r}) - v'(\vec{r})]dr \tag{2.8}$$

Addition of equation (2.7) and (2.8) leads to

$$E_0 + E_0' < E_0' + E_0 \tag{2.9}$$

which clearly is a contradiction, so we can conclude that given the electronic density, the external potential is determined, so as all the other electronic properties, for example total energy.

Let us write the total energy as,

$$E_v(\rho) = T(\rho) + V_{ne}(\rho) + V_{ee}(\rho)$$
$$= \int \rho(\vec{r}) v(\vec{r}) d\vec{r} + F_{HK}[\rho] \tag{2.10}$$

where,

$$F_{HK}[\rho] = T(\rho) + V_{ee}[\rho] \tag{2.11}$$

Here, V_{ee} includes both the classical and non-classical (for example, Coulomb and exchange interactions) contributions and F_{HK} is the Hohenberg-Kohn functional, which does not depend on the external potential as can be seen from equation (2.11) and so is a universal functional of $\rho(\vec{r})$.

The second Hohenberg-Kohn theorem states that for a trial density $\tilde{\rho}(\vec{r})$, such that $\tilde{\rho}(\vec{r}) \geq 0$, and $\int \tilde{\rho}(\vec{r}) d\vec{r} = N$,

$$E_0 \leq E_v[\tilde{\rho}] \tag{2.12}$$

where, $E_v[\tilde{\rho}]$ is the energy functional of equation (2.10). The proof will be done by the use of variational principle. For any trial density $\tilde{\rho}(\vec{r})$, according to the Hohenberg-Kohn first theorem, it has its won potential $v(\vec{r})$, Hamiltonian *H* and wave function $\tilde{\Psi}$. So we get following equation (2.10),

$$\left\langle \tilde{\Psi} \middle| H \middle| \tilde{\Psi} \right\rangle = \int \tilde{\rho}(\vec{r}) v(\vec{r}) d\vec{r} + F_{HK} = E_v[\tilde{\rho}] \geq E_v[\rho] \tag{2.11}$$

Now the variation of total energy with the constraint that the total electrons are fixed, we get,

$$\delta\left\{E_v[\rho] - \mu\left[\int \rho(\vec{r}) d\vec{r} - N\right]\right\} = 0 \tag{2.12}$$

which leads to the Euler-Lagrange equation

$$\mu = \frac{\delta E_v[\rho]}{\delta \rho(\vec{r})} = v(\vec{r}) + \frac{\delta F_{HK}}{\delta \rho(\vec{r})} \tag{2.13}$$

where the Lagrange multiplier μ is the chemical potential. Now if the exact form of the functional F_{HK} is known, the equation (2.12) then would be an exact equation for the ground state electron density. The functional F_{HK} is defined only for those trials $\rho(\vec{r})$ which are *v*-representable, meaning that the $\rho(\vec{r})$ corresponds to a anti-symmetric ground state wave function of some Hamiltonian with external potentials $v(\vec{r})$. The conditions for the density to be *v*-representable is yet unknown. However it turned out that the density functional theory can be formulated on a density which satisfies a weaker constraint than that of *v*-representability, namely *N*-representability. A density is *N*-representable if it can be derived from some anti-symmetric wave functions. Based on the *N*-representable density, Levy's constrained search method is described below

which eliminates the degeneracy limitations in the proof of original Hohenberg-Kohn theorem.

2.2.1 The Method of Constrained Search

This method was first developed by Levy and Lieb [41-43]. A Universal function $F[\rho]$ defined as a sum of kinetic and Coulomb repulsion energies:

$$F[\rho] = \underset{\Psi\to\rho}{Min}\langle\Psi|T+V_{ee}|\Psi\rangle \tag{2.14}$$

$F[\rho]$ searches all wave functions Ψ which yield the fixed trial density ρ, and ρ need not to be *v*-representable.

Now the ground state energy can be written as:

$$E_0 = \underset{\Psi\to\rho}{Min}\langle\Psi|T+V_{ee}+\sum_i^N v(r_i)|\Psi\rangle \tag{2.15}$$

$$= \underset{\rho}{Min}\left\{\underset{\Psi\to\rho}{Min}\langle\Psi|T+V_{ee}+\sum_i^N v(r_i)|\Psi\rangle\right\}$$

$$= \underset{\rho}{Min}\left\{\left[\underset{\Psi\to\rho}{Min}\langle\Psi|T+V_{ee}|\Psi\rangle + \int v(\vec{r})\rho(\vec{r})d\vec{r}\right]\right\} \tag{2.16}$$

Now using the definition of $F[\rho]$ from equation (2.14) we can write equation (2.16) as:

$$E_0 = \underset{\rho}{Min}\left\{F[\rho] + \int v(\vec{r})\rho(\vec{r})d\vec{r}\right\}$$

$$= \underset{\rho}{Min}\, E[\rho] \tag{2.17}$$

where

$$E[\rho] = F[\rho] + \int v(\vec{r})\rho(\vec{r})d\vec{r}. \tag{2.18}$$

In the constrained search formula for the functional $F[\rho]$ there is no reference that ρ needs to be *v*-representable ground state density, as long as it is constructed from an anti-symmetric wave function. However, when ρ is *v*-representable we get:

$$F[\rho] = F_{HK}[\rho] \tag{2.19}$$

The functional $F[\rho]$ is universal because it does not depend on the external potential $v(\vec{r})$. This constrained search method remove the degeneracy problem from the original Hohenberg-Kohn theorem, for in the approach only one of a set of degenerate wave functions is selected which is corresponding to the given ρ.

2.3 The Kohn-Sham Method

The ground state electron density can be in principle determined by solving the Eular-Lagrange equation (13)

$$\frac{\delta F(\rho)}{\delta \rho} + v(\vec{r}) = \mu. \tag{2.20}$$

where μ is the Lagrange multiplier associated with the constraint:

$$\int \rho(\vec{r}) d\vec{r} = N$$

Here the exact form of the functional $F[\rho]$ in equation (2.20) is not known:

$$F(\rho) = T[\rho] + V_{ee}[\rho]. \tag{2.21}$$

As can be seen from the above equation the basic problem is to evaluate the kinetic energy term. Kohn-Sham proposed [44] an indirect approach to this problem, which is described in the following.

Let us consider a non-interacting system where electrons move independently in a common local potential v_s, where the electronic density $\rho(\vec{r})$ is the same as the interacting electronic system. This can be done as long as we ensure that the wave functions, from which $\rho(\vec{r})$ is constructed, are *N*-representable. Hamiltonian is:

$$H_s = \sum_i^N \left(-\frac{1}{2}\nabla_i^2 \right) + \sum_i^N v_s(\vec{r}_i). \tag{2.22}$$

In the above Hamiltonian there is non electron-electron repulsion term. For this system we can write the non-interacting wave-function as the Slater determinant:

$$\Psi_s = \frac{1}{\sqrt{N!}} \det[\psi_1 \psi_2 \cdots \psi_N] \tag{2.23}$$

where ψ_i are the *N* lowest eigenstates of the one-electron Hamiltonian h_s:

$$h_s \psi_i = \left[-\frac{1}{2}\nabla_i^2 + v_s(\vec{r}_i) \right] \psi_i = \varepsilon_i \psi_i \tag{2.24}$$

The kinetic energy of this non-interacting system is,

$$T_s[\rho] = \langle \Psi_s | \sum_{i=1}^N \left(-\frac{1}{2}\nabla_i^2 \right) | \Psi_s \rangle = \sum_i^N \langle \psi_i | -\frac{1}{2}\nabla_i^2 | \psi_i \rangle \tag{2.25}$$

while the density of the non-interacting system

$$\rho(\vec{r}) = \sum_i^N |\psi_i(\vec{x}_i)|^2 \tag{2.26}$$

is equal to that of the interacting one.

The kinetic energy functional $T[\rho]$ in equation (2.21), as mentioned before, is unknown, so we simply take the kinetic energy functional $T_s[\rho]$ of non-interacting

system instead of $T[\rho]$. Let the difference between this two functional is $T_c = T - T_s$, and substituting this in equation (21) we get:

$$F[\rho] = T_s[\rho] + V_{ee}[\rho] + T_c[\rho] \tag{2.27}$$

The last two terms in the right hand side of equation (2.27) representing the electron-electron interaction and we can rewrite them as the Coulomb and exchange-correlation terms, respectively:

$$V_{ee}[\rho] + T_c[\rho] = J[\rho] + E_{xc}[\rho] \tag{2.28}$$

So equation (2.27) can be written as:

$$F[\rho] = T_s[\rho] + J[\rho] + E_{xc}[\rho] \tag{2.29}$$

So with the above functional the total energy of equation (2.18) can be written as:

$$E[\rho] = T_s[\rho] + J[\rho] + E_{xc}[\rho] + \int \rho(\vec{r})v(\vec{r})d\vec{r}\,. \tag{2.30}$$

Now the variation of equation (2.30) gives the Euler-Lagrange equation:

$$\mu = \frac{\delta E[\rho]}{\delta\rho} = \frac{\delta}{\delta\rho}\int \rho(\vec{r})v(\vec{r})d\vec{r} + \frac{\delta T_s[\rho]}{\delta\rho} + \frac{\delta J[\rho]}{\delta\rho} + \frac{\delta E_{xc}[\rho]}{\delta\rho}$$

$$= v(\vec{r}) + \frac{\delta T_s[\rho]}{\delta\rho} + \frac{\delta J[\rho]}{\delta\rho} + \frac{\delta E_{xc}[\rho]}{\delta\rho} \tag{2.31}$$

$$= v_{eff}(\vec{r}) + \frac{\delta T_s[\rho]}{\delta\rho} \tag{2.32}$$

where the Kohn-Sham effective potential is defined by:

$$v_{eff} = v(\vec{r}) + \frac{\delta J[\rho]}{\delta\rho} + \frac{\delta E_{xc}[\rho]}{\delta\rho}$$

$$= v(\vec{r}) + \int \frac{\rho(\vec{r}')}{|\vec{r} - \vec{r}'|}d\vec{r}' + v_{xc}(\vec{r}) \tag{2.33}$$

here we also defined the exchange-correlation potential as:

$$v_{xc}(\vec{r}) = \frac{\delta E_{xc}(\rho)}{\delta \rho} \tag{2.34}$$

Now let us rewrite equation (2.30) in terms of one electron orbitals:

$$E(\rho) = \sum_{i}^{N} \int \psi_i^* \left(-\frac{1}{2} \nabla^2 \right) \psi_i d\vec{r} + J(\rho) + E_{xc}[\rho] + \int v(\vec{r}) \rho(\vec{r}) d\vec{r} \tag{2.35}$$

and the electron density is, as in equation (2.26):

$$\rho(\vec{r}) = \sum_{i}^{N} |\psi_i|^2$$

So in equation (2.35) energy is expressed in terms of *N* orbitals.

Now taking the variation of energy in equation (2.35) with respect to the one-electron orbital ψ_i, along with the constraint that these oribitals are orthonormal to each other:

$$\int \psi_i^* \psi_j d\vec{x} = \delta_{ij} \tag{2.36}$$

We get,

$$\delta \left[E[\rho] - \sum_{i}^{N} \sum_{j}^{N} \varepsilon_{ij} \int \psi_i^*(\vec{x}) \psi_i(\vec{x}) d\vec{x} \right] = 0 \tag{2.37}$$

In equation (2.37) ε_{ij} are the Lagrange multipliers. Let us now consider the variation in the energy $E[\rho]$ given by the equation (2.35),

$$\delta E[\rho] = \left[\frac{\delta}{\delta \psi_i^*} \sum_{i}^{N} \int \psi_i^* \left(-\frac{1}{2} \nabla^2 \right) \psi_i d\vec{r} + \frac{\delta J}{\delta \psi_i^*} + \frac{\delta E_{xc}}{\delta \psi_i^*} + \frac{\delta}{\delta \psi_i^*} \int v(\vec{r}) \left(\sum_{i}^{N} |\psi_i|^2 \right) d\vec{r} \right] \delta \psi_i^* \tag{2.38}$$

Using chain rule for functional derivative, the first term in the right hand side gives,

$$\frac{\delta}{\delta\psi_i^*}\sum_i^N\int\psi_i^*\left(-\frac{1}{2}\nabla^2\right)\psi_i d\vec{r}=\frac{\partial\psi_i^*}{\partial\psi_i^*}\left(-\frac{1}{2}\nabla^2\right)\psi_i+\psi_i^*\frac{\partial}{\partial\psi_i^*}\left\{\left(-\frac{1}{2}\nabla^2\right)\psi_i\right\}$$

$$=-\frac{1}{2}\nabla^2\psi_i \tag{2.39}$$

where derivative in the second term is zero. Similarly the last term in the variation of energy in equation (2.38) gives,

$$\frac{\delta}{\delta\psi_i^*}\int v(\vec{r})\left(\sum_i^N|\psi_i|^2\right)d\vec{r}=v(\vec{r})\psi_i \tag{2.40}$$

So from equation (2.37), for any arbitrary variation of $\delta\psi_i^*$, we get using equations (2.39) and (2.40),

$$h_{eff}\psi_i=\left[-\frac{1}{2}\nabla^2+\frac{\delta J[\rho]}{\delta\rho}+\frac{\delta E_{xc}[\rho]}{\delta\rho}+v(\vec{r})\right]\psi_i=\sum_j^N\varepsilon_{ij}\psi_j$$

$$\Rightarrow h_{eff}\psi_i=\left[-\frac{1}{2}\nabla^2+v_{eff}(\vec{r})\right]\psi_i=\sum_j^N\varepsilon_{ij}\psi_j \tag{2.41}$$

where $v_{eff}(\vec{r})$ is defined by equation (2.33). Now in equation (2.41) the Hamiltonian h_{eff} is a Hermitian operator, hence ε_{ij} is a Hermitian matrix which can be diagonalize by unitary transformation, which leads to the Kohn-Sham equations:

$$\left[-\frac{1}{2}\nabla^2+v_{eff}(\vec{r})\right]\psi_i=\varepsilon_i\psi_i \tag{2.42}$$

Equation (2.42) (or equation (2.41)) is the central equation in the application of density function theory. These equations are usually solved by self-consistent methods which can be represented by the following flow-chart:

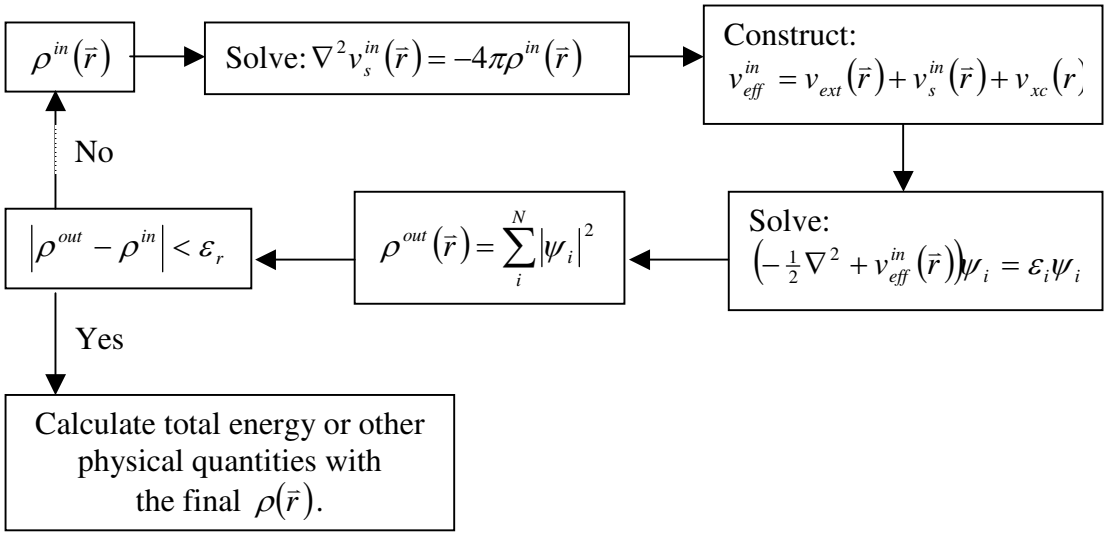

Figure 2.1 Flow-chart for DFT self-consistency loop

The solution of Kohn-sham equation is in principle is exact, but as can be seen from the above discussion of the Kohn-Sham procedure that, it does not give any prescription of obtaining the exchange-correlation functionals. Depending on the system at hand, different levels of approximations were made to deal with this functional. In the following we will describe the local and generalized density approximations to these functionals.

2.4 The Local Density Approximation (LDA)

Historically local density approximation to the functionals is the most used approach in the condensed matter physics. In this approximation the functionals are local, that is they depend only on the local variable. Formally, a functional *F* is local if,

$$F[\rho] = \int f(\rho(\vec{r}))d\vec{r} \tag{2.43}$$

where the functional F depends on $\vec{r}$ only through the density $\rho(\vec{r})$. Physically this approximation would be correct in the limit where the charge density is a slowly varying function with respect to the spatial variable, $\vec{r}$. Within the LDA the exchange and correlation energy becomes,

$$E_{xc}^{LDA}[\rho] = \int \rho(\vec{r}) \varepsilon_{xc}(\rho) d\vec{r} \tag{2.44}$$

where $\varepsilon_{xc}(\rho)$ is the exchange and correlation energy per particle of a uniform electron gas of density $\rho(\vec{r})$. The exchange-correlation potential then is given by,

$$v_{xc}^{LDA}(\vec{r}) = \frac{\delta E_{xc}^{LDA}}{\delta \rho(\vec{r})} = \varepsilon_{xc}(\rho(\vec{r})) + \rho(\vec{r}) \frac{\partial \varepsilon_{xc}}{\partial \rho} \tag{2.45}$$

Then the Kohn-Sham equation can be written as,

$$\left[-\frac{1}{2}\nabla^2 + v(\vec{r}) + \int \frac{\rho(\vec{r})}{|\vec{r} - \vec{r}'|} d\vec{r}' + v_{xc}^{LDA}(\vec{r}) \right] \psi_i = \varepsilon_i \psi_i \tag{2.46}$$

Now the function $\varepsilon_{xc}(\rho)$ can be divided into exchange and correlation contribution [36],

$$\varepsilon_{xc}(\rho) = \varepsilon_x(\rho) + \varepsilon_c(\rho) \tag{2.47}$$

where $\varepsilon_x(\rho)$ is the Dirac exchange energy,

$$\varepsilon_x(\rho) = -\frac{3}{4}\left(\frac{3}{\pi}\right)^{1/3} \rho(\vec{r})^{1/3} \tag{2.48}$$

and $\varepsilon_c(\rho)$ is the correlation energy per particle of a homogeneous electron gas,

$$\varepsilon_c(\rho) = \begin{cases} 0.0311 \ln r_s - 0.048 + r_s (A \ln r_s + C) & \text{for } r_s << 1 \\ \frac{1}{2}\left(\frac{g_0}{r_s} + \frac{g_1}{r_s^{3/2}} + \frac{g_2}{r_s^2} + \cdots \right) & \text{for } r_s >> 1 \end{cases} \tag{2.49}$$

where, r_s is the Wigner_seitz radius,

$$\frac{4}{3}\pi r_s^3 = \frac{1}{n} \tag{2.50}$$

We can extend the LDA to include spin for so-called unrestricted calculations. We can divide the total electronic density in two parts for spin up density (ρ_α) and spin down (ρ_β), so that,

$$\rho_\alpha(\vec{r}) + \rho_\beta(\vec{r}) = \rho(\vec{r}). \tag{2.51}$$

Then in the local spin density approximation the exchange-correlation functional can be written as,

$$E_{xc}^{LSD}[\rho_\alpha, \rho_\beta] = \int \rho(\vec{r}) \varepsilon_{xc}(\rho_\alpha(\vec{r}), \rho_\beta(\vec{r})) d\vec{r} \tag{2.52}$$

As mentioned earlier, LDA (or LSD) is based upon the idealization that the system is a homogeneous electron gas with equal (or slowly varying) density. It is obvious that any real system could behave in a drastically different manner. However, the success and importance of the local density approximation in condensed matter physics is noteworthy. It gives results comparable or better than the Hartree-Fock approximation.

CHAPTER 3

RELAXATIONS AND RECONSTRUCTIONS OF InSb(100) SURFACES

One of the primary considerations involved in ab initio calculations of the type reported here are the type of basis sets[45] and the type of exchange-correlation functional(xc) to be used. The calculations reported in this work have been performed within the local density approximation [46, 47] to density functional theory (LDA-DFT) [39, 44, 48-50]. The selection of basis set is a trade-off between computational cost and the accuracy that one desires in the calculations. Keeping this in mind, we have elected to represent fairly large systems like indium and antimony by effective core potentials, specifically the Hay - Wadt (HW) effective core potentials [51, 52]. The Hay Wadt effective core potentials and associated basis sets for indium and antimony are shown in table 3.1-3.3. This basis set has been tested at the atomic and dimer level for In and Sb and at the bulk level for InSb. The ionization potentials and electron affinities for In and Sb are given in tables 3.4 and 3.5 respectively and compared with the available experimental data [53-55]. The dimer bondlengths and binding energies of In_2, Sb_2, In-H, Sb-H and In-Sb are shown in tables 3.6 and 3.7 respectively along with the available experimental results [53, 56]. Also, the bulk properties of InSb such as lattice constant [13], binding energy per unit cell [57], and energy band gap [4, 58] are provided along with the available experimental results in table 3.8. These results clearly indicate that the above described choices of the basis set and the xc functional should provide a good description of the systems studied in this work.

All the total energy calculations were performed using repeated slab geometry where the unit cell is repeated in two dimensions using the Periodic Boundary Conditions (PBC) [59-62].

The surfaces are modeled by a 3-layered slab with In atoms in the top layer followed by Sb atoms in the middle layer which is in turn followed by In atoms in the bottom layer. Hydrogen atoms are used to saturate the dangling bonds of In atoms in the bottom layer to simulate the semi-infinite effect of the surface. This treatment is similar to that of our previous works [63-72]. All the computational simulations are carried out using the Gaussian 03 suite of programs [73] utilizing the computational resources available at the University of Texas at Arlington.

The models for the different surfaces, such as, (1x1), (2x1), (4x2) and c(8x2) are shown in the figures 3.1,3.2,3.3 and 3.4 respectively. In all these figures, the In atoms are the ones colored in blue and the Sb atoms are colored in red. For modeling all these relaxations and reconstructions, the unit cell is composed of three layers, though the number of atoms per layer is dependent on the type of reconstruction that is modeled. As a first step of the process, the InSb (100) surface is relaxed. This relaxed surface is called as ideal (unreconstructed) (1x1) surface since the relative positions of the different In and Sb atoms are same as that of the bulk InSb and the top view of it is shown in figure 3.1. For modeling the (1x1) surface, the first layer was made of four In atoms followed by four Sb atoms in the next layer and four In atoms in the third layer and two hydrogen atoms were used for saturate the dangling bonds of each of the In atoms in the third layer. An energy optimized bond length of 1.88 Å was used as the dimer bond length of In-H. This optimized bond length is consistent with the available experimental data [53] as verified from the table 3.6. The total energy optimization of the lattice constant was carried out for modeling the (1x1) surface of the InSb(100) surface. The relaxed lattice constant was found to be 6.675 Å and the corresponding surface In-In distance of the surface square mesh of In-rich InSb (100) surface was found to be 4.72 Å. This is comparable to the zinc blende experimental lattice constant of 6.479 Å and the corresponding In-In distance of 4.58 Å[13]. Table 3.9 gives

the binding energy per atom and the value of energy band gap for the (1x1) surface. The binding energy per atom is calculated from

$E_b = xE(In) + yE(Sb) + zE(H) - E(In_xSb_yH_z)/(x+y+z)$ 3.1

Where x is the number of In atoms, y is the number of Sb atoms and z is the number of H atoms used for saturating the In atoms of the last layer found in the unit cell modeling the surface [63-72].

As seen from the table 3.4, the surface energy for the ideal relaxed (1x1) surface is found to be 2.31 eV/atom. As there are no comparable surface energy values available for InSb in the literature, we take the surface energy for Ga-rich GaAs (100) surface of 1.77 eV/atom [71,72] and 2.02 eV/atom for comparison [74] to be compared with our value of 2.31 eV/atom. Taking into consideration the overestimation of cohesive energy by LDA calculations [57], we find a good agreement with the available values.

The (2x1) surface adapted in this study is shown in the figure 3.2 and it is the same 2x1-Ga dimer model proposed by Qian et al [74] for the Ga-rich GaAs (100) surface and also it is the same as the (2x1) surface represented by the cluster $Ga_7As_6H_{19}$ in one of our previous works on the cluster study of chemisorption of atomic Cs on Ga-rich GaAs (100) (2x1), (2x2) and (4x2) surface [63-65]. The (2x1) surface was found to be metallic in the work of Qian *et al.* during the first principles study of Ga-rich GaAs (100) surface. For modeling the different reconstructions, the In-In dimer bondlength in the top layer was varied and the total energy optimization was performed for modeling the different reconstructions [63-72]. In modeling the (2x1) dimer model of In-terminated InSb (100) surface, the total energy is lowered in each step of dimerization. In the process of optimization of the of the top surface In-In dimer bond length, the dimer bond length was found to have reduced from unreconstructed ideal and relaxed value

of 4.72 Å to 3.02 Å. The total energy was found to have been lowered by 0.73 eV/ dimer from (1x1) surface to the (2x1) dimer model which is comparable to that of Ga-terminated GaAs (100) surface [74]. The values of binding energy per atom and energy band gap for this (2x1) surface are listed in the table 3.9 as compared to the ideal and relaxed (1x1) surface. Comparing the energy band gaps of dimerized (2x1) dimer model with respect to the (1x1) unreconstructed surface from the table 3.9, it is noted that the energy band gap (that is the HOMO-LUMO Gap) is reduced from 0.05 eV to 0.01 eV .

The energy band gap is also shown by plotting the DOS (Density of States) plot for the surfaces using the Gaussian broadening scheme [75] in which a Gaussian $\exp(-\alpha x^2)$ is assigned to each of the orbital eigenvalues with $\alpha=2x10^8$ that corresponds to the full width half maximum of 0.005eV for all the dos plots. The density of states was plotted for the (1x1) and (2x1) surfaces as shown in the figures 3.6 and 3.7 respectively. We note that the band gap is wider for the (1x1) surface corresponding to 0.05 eV with respect to the (2x1) surface which has a band gap of 0.01 eV. This observed difference in the energy band gaps of these two surfaces allows us to conclude that the dimerized (2x1) dimer model surface is metallic which is in good agreement with the first principles calculations for the dimerized (2x1) dimer model of GaAs found by Qian *et al.* [74]. Also from the results of table 3.9, it is clear that the (2x1) surface, though not experimentally observed has the highest binding energy and hence it is suggested that the (2x1) reconstruction of In-Rich InSb(100) surface possibly exists, though not experimentally reported yet. Further experimental studies in this area would be welcome.

The (4x2) and c(8x2) surfaces are modeled as per the original missing dimer model proposed by John. *et al.* [12] and are shown in the figures 3.3 and 3.4 respectively. In our work, in both the cases of (4x2) and c(8x2) reconstruction, the surface dimer bond length was found to

have been reduced from the ideal and relaxed value of 4.72 Å to 3.07 Å during our process of energy minimization by dimerization. It was noted that the total energy is reduced by 0.73 eV/ dimer in the case of (4x2) reconstruction and by 0.74 eV/dimer for the c(8x2) surface. Our results show that (4x2) and c (8x2) structures have comparable energy band gaps and also the binding energy per atom are exactly the same as can be seen from the table 3.9. Both these (4x2) and c(8x2) surfaces were found to be semiconducting in nature with band gaps of 0.07 eV and 0.09 eV respectively as against the metallic nature of the (2x1) surface. The graphs for the (1x1), (2x1), (4x2) and c(8x2) surfaces are shown in the figure 9.

The Mulliken population analysis [76-78] was carried out for the (1x1), (2x1), (4x2) and c(8x2) surfaces of InSb and for the scale of brevity, we have shown only the atomic charge distributions for (2x1) and (4x2) surfaces in the tables 3.10 and 3.11 respectively. Also these atomic charge distribution diagrams were schematically represented using the visualization software called Gauss View 3.0 [79]. This Gauss view enables us to color the different atoms in the unit cell according to the charges gained or lost by a particular atom. The figures 3.9 and 3.10 show the atomic charge distributions for the different atoms in the unit cell of (1x1) and (2x1) surfaces respectively. As seen in figure 3.9, it is seen that the hydrogen atoms are neutral and the indium atoms lose charges as seen from the numbers which are positive and also from the green color. On the other hand, the antimony atoms are seen in red and the negative values displayed against each of the atom indicating that the antimony atoms gain charges. This is a very consistent trend that has been noted through out this study. This is consistent with the electronegativities of these elements. Apart from this fact, in the atomic charge distribution of (1x1) surface, it is seen that the distribution is very symmetric, that is charges gained or lost by atoms in the same layer are very close to each other. But, if we look at the atomic charge

distribution for (2x1) surface, it is observed that the amount of charges lost by the indium atoms of the first layer is slightly less than that of the corresponding atoms in the (1x1) surface. The similar trend is noted for the antimony atoms in the second layer, that is the charges gained by the Sb atoms in the second layer for (2x1) surface is slightly less than that of the corresponding atoms of the (1x1) surface. But, in the third layer of (2x1) surface, the In atoms labeled 5 and 7 seem to lose more charges and the In atoms labeled 6 and 8 seem to lose less charges when compared to the corresponding atoms in the third layer of (1x1) surface. Hence there is a slightly unsymmetrical distribution found for (2x1) surface as compared to the (1x1) surface.

The atomic charge distribution of (4x2) surface is shown in figure 3.11. We noted that the charge distribution of the subsurface of (4x2) surface has a similar distribution as that of (2x1) surface. For example, the first layer In atoms such as 1, 2, 3, 4, 5 and 6 and also the second layer Sb atoms with labels 16, 17, 19 and 22 have a distribution similar to that of (2x1) surface. Again, same is the case with the In atoms labeled 7, 10, 12 and 13 . This is because these atoms of the (4x2) surface have an atmosphere similar to that of the (2x1) surface. But, if we take a look at the In atoms labeled 8, 9, 11 and 14, it is seen that the charge lost by these indium atoms are very different from that of the third layer In atoms of the (2x1) surface. That is the charge lost by these indium atoms is very less compared to the corresponding atoms of the (4x2) surface. Again, if we consider the Sb atoms of the second layer in the case of (4x2) surface, it is seen that the atoms labeled 15, 18, 20 and 21 are distinctly darker in red compared to the other Sb atoms of the (4x2) surface or for that matter the corresponding atoms of the (2x1) surface. This again shows that these four atoms gain less charges compared to the corresponding atoms in the (2x1) surface. This is because of the fact that the two In atoms of the top-most layer are missing in the (4x2) surface and hence the interaction of these four Sb atoms with the number of In atoms is

limited as compared to the (2x1) surface. Also, it was observed that the charge distribution of c(8x2) surface exactly the same as that of (4x2) surface as seen in the figure 3.12 and hence all the arguments made for the (4x2) surface holds good for this surface also.

Table 3.1 Hay-Wadt Pseudopotential for In atom

	n_k	ζ_k	d_k
	f potential		
0	0.1802071	-0.06390310	
1	33.0176528	-29.90829010	
2	9.7219749	-63.34468240	
2	2.3481578	-19.00584280	
2	0.7226853	-2.51619210	
	s-f potential		
0	173.1403228	3.23016070	
1	58.2752431	76.78091400	
2	21.1294304	245.47707600	
2	5.9581061	79.28927210	
2	1.4830272	26.40894600	
	p-f potential		
0	35.9438033	4.46902900	
1	11.2431083	43.64733990	
2	3.5340830	50.75654060	
2	1.4120937	-48.67300170	
2	1.2828947	58.76926530	
	d-f potential		
0	42.6276817	3.10207700	
1	14.5649330	36.54450900	
2	5.5505378	48.80418080	
2	1.8351485	19.43623610	
2	0.5288122	3.98556470	

Table 3.2 Hay-Wadt Pseudopotential for Sb atom

	n_k	ζ_k	d_k
	f potential		
0	227.2723558	-0.06922610	
1	77.1429882	-31.54347120	
2	26.0116501	-115.84073060	
2	9.1421159	-42.02242120	
2	2.9281082	-20.04639380	
2	0.9231136	-2.87960280	
	s f potential		
0	116.0010888	2.93313030	
1	59.6755065	44.11048190	
2	27.6135849	228.01980500	
2	7.8045081	92.56101620	
2	1.6934418	31.25372440	
	p f potential		
0	27.8050796	4.99473690	
1	10.3929685	38.02238600	
2	3.6381067	62.05206540	
2	1.9839681	-49.54893890	
2	1.5546562	51.36660000	
	d f potential		
0	83.2183030	2.97384700	
1	30.3070501	41.64958250	
2	13.2014120	104.59195620	
2	3.6961611	42.31878570	
2	0.7711144	7.94135030	

Table 3.3 Basis Functions for In and Sb atoms

Indium

Exponents(α_i)	Coefficients(c_i)
s orbitals	
0.49150	-1.081556
0.34040	1.141886
0.07740	0.813418
p orbitals	
0.97550	-0.061050
0.15500	0.518554
0.04738	0.594588

Antimony

Exponents(α_i)	Coefficients(c_i)
s orbitals	
0.58630	-1.459644
0.42930	1.568921
0.10780	0.752990
p orbitals	
1.11100	-0.099467
0.23650	0.592487
0.07999	0.526790

Table 3.4 Ionization potentials(eV) for In and Sb

Element	This work	Exp.[53]
In	6.11	5.79
Sb	9.6	8.64

Table 3.5 Electron affinities(eV) for In and Sb

Element	This work	Exp.
In	0.63	(0.85±0.15)[54],(0.40±0.009)[55],(0.3±0.2)[53]
Sb	0.98	1.02±0.005[53]

Table 3.6 Dimer bondlengths (Å) for In_2, Sb_2, In-H, Sb-H and In-Sb

Dimer	This work	Exp[53]	Exp[56]
In_2	3.20	NA	3.14
Sb_2	2.60	NA	2.34
In-H	1.88	1.84	NA
Sb-H	1.77	1.70*	NA
In-Sb	3.06	NA	NA

* The bondlength is the one as found in the compound SbH_3

Table 3.7 Binding energies(eV) for In_2, Sb_2, In-H, Sb-H and In-Sb

Dimer	This work	Exp [53]	Exp [56]
In_2	1.05	1.04	0.83
Sb_2	3.33	3.1	3.09
In-H	3.03	2.52	NA
Sb-H	2.91	NA	NA
In-Sb	1.99	1.57	NA

Table 3.8 Bulk properties of InSb

Property	This work	Exp.
Lattice constant(Å)	6.63	6.48[13]
Binding energy(eV)	6.46	5.79[57]
Band gap(eV)	0.15	0.17[4,58]

Table 3.9 Binding energies and band gaps for different InSb surfaces

Surface	Binding energy per atom (eV)	Band Gap (eV)
(1x1)	2.31	0.05
(2x1)	2.39	0.01
(4x2)	2.32	0.07
c(8x2)	2.32	0.09

Table 3.10 Atomic charge distribution for the InSb(100) (2x1) surface

Layer	Atom label	Type of Atom	(2x1) surface
1st	1	In	0.22
1st	2	In	0.20
1st	3	In	0.20
1st	4	In	0.22
2nd	5	Sb	-0.41
2nd	6	Sb	-0.41
2nd	7	Sb	-0.41
2nd	8	Sb	-0.41
3rd	9	In	0.30
3rd	10	In	0.20
3rd	11	In	0.30
3rd	12	In	0.20
4th	13	H	-0.02
4th	14	H	-0.04
4th	15	H	-0.02
4th	16	H	-0.04
4th	17	H	-0.02
4th	18	H	-0.04
4th	19	H	-0.02
4th	20	H	-0.04

Table 3.11 Atomic charge distribution for the InSb(100) (4x2) surface

Layer	Atom label	Type of atom	(4x2) surface
1st	1	In	0.21
1st	2	In	0.21
1st	3	In	0.22
1st	4	In	0.22
1st	5	In	0.21
1st	6	In	0.21
2nd	7	Sb	-0.24
2nd	8	Sb	-0.40
2nd	9	Sb	-0.40
2nd	10	Sb	-0.25
2nd	11	Sb	-0.40
2nd	12	Sb	-0.24
2nd	13	Sb	-0.25
2nd	14	Sb	-0.40
3rd	15	In	0.31
3rd	16	In	0.16
3rd	17	In	0.21
3rd	18	In	0.21
3rd	19	In	0.20
3rd	20	In	0.31
3rd	21	In	0.21
3rd	22	In	0.16
4th	23	H	-0.03
4th	24	H	-0.04
4th	25	H	-0.02
4th	26	H	-0.03
4th	27	H	-0.03
4th	28	H	-0.03
4th	29	H	-0.03
4th	30	H	-0.03
4th	31	H	-0.03
4th	32	H	-0.03
4th	33	H	-0.03
4th	34	H	-0.03
4th	35	H	-0.02
4th	36	H	-0.03
4th	37	H	-0.03
4th	38	H	-0.04

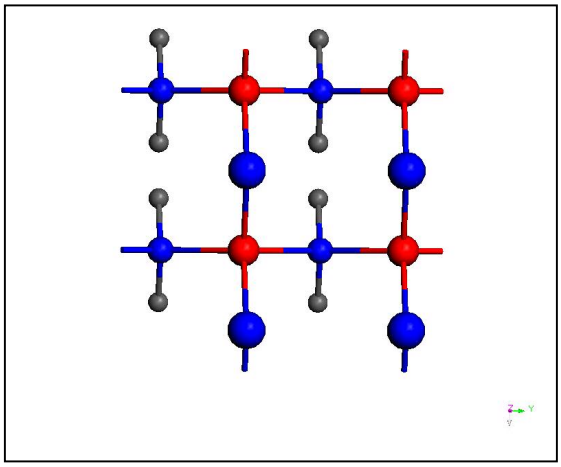

Figure 3.1 Top view of InSb(100) (1x1) surface

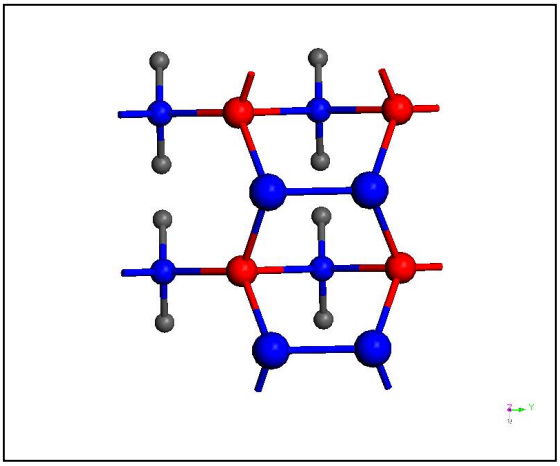

Figure 3.2 Top view of InSb(100) (2x1) surface

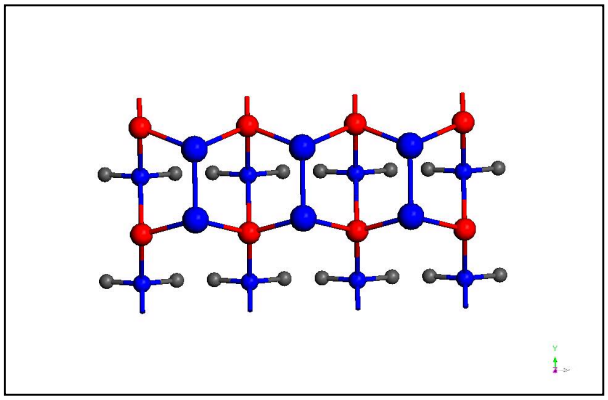

Figure 3.3 Top view of InSb(100) (4x2) surface

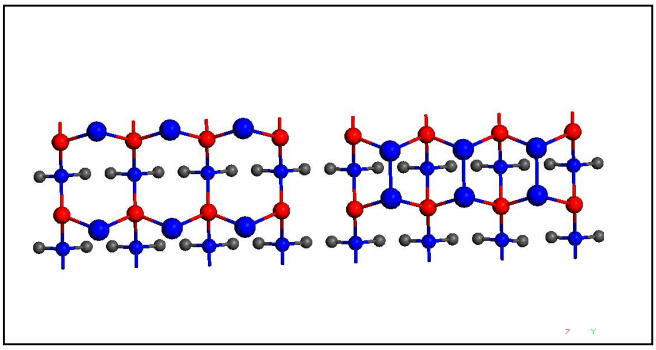

Figure 3.4 Top view of InSb(100) c(8x2) surface

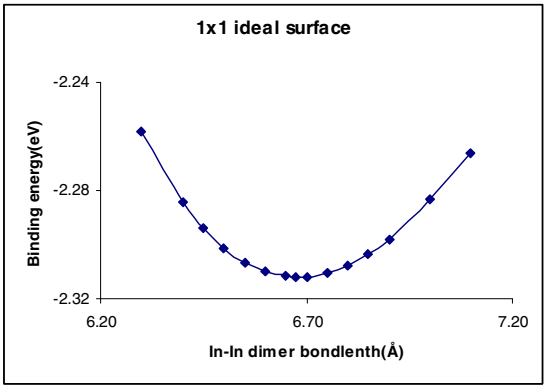

(a)

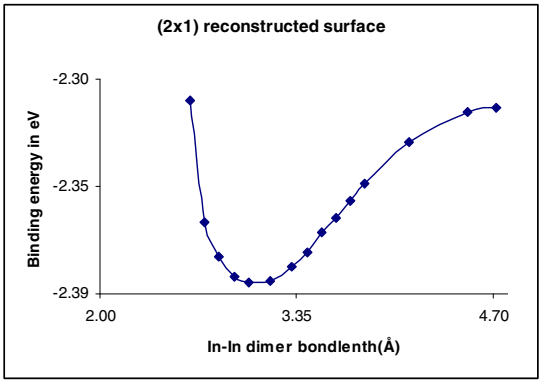

(b)

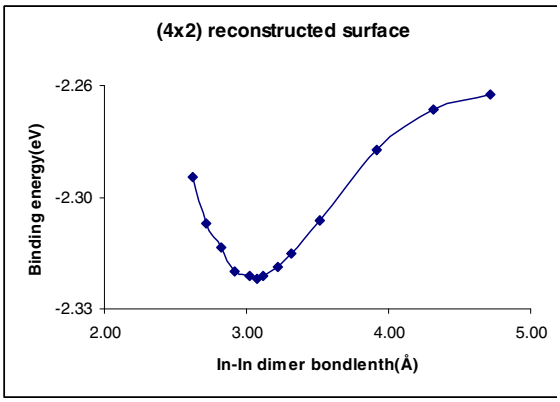

(c)

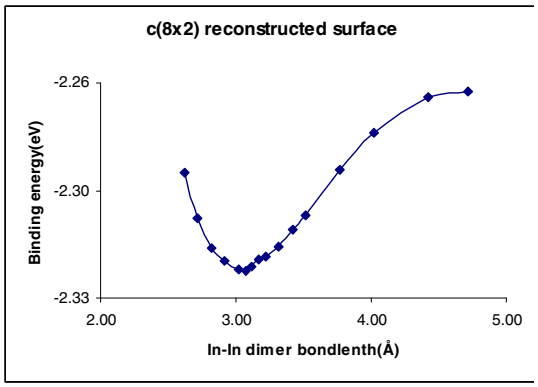

(d)

Figure 3.5 Binding energy(eV) vs. dimer bondlength(Å) for ideal (1x1)(a) (2x1)(b) (4x2)(c) and c(8x2)(d) InSb surfaces

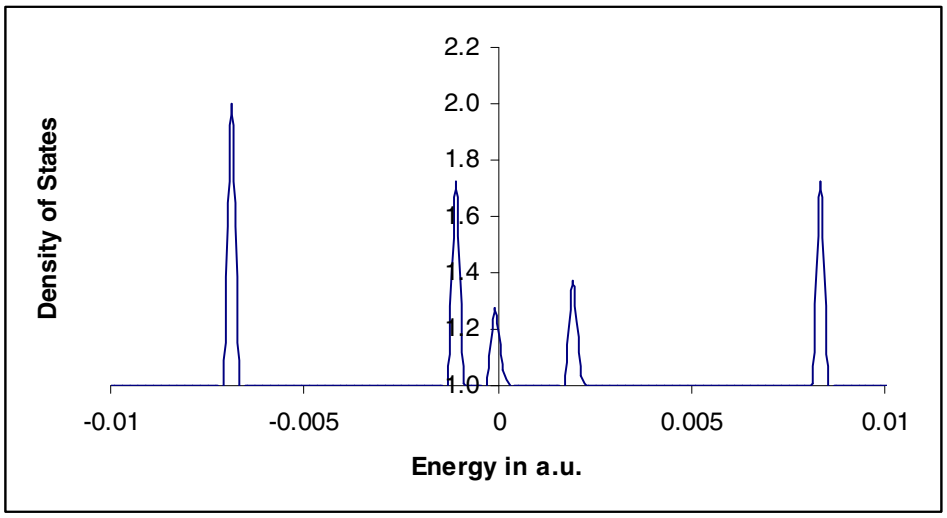

Figure 3.6 Dos Plot of (1x1) surface

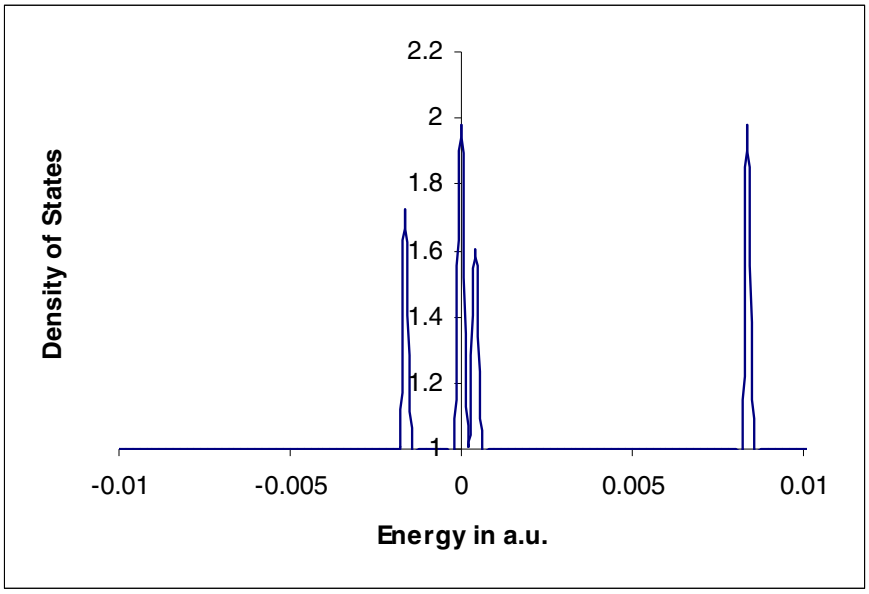

Figure 3.7 DOS plot of (2x1) surface

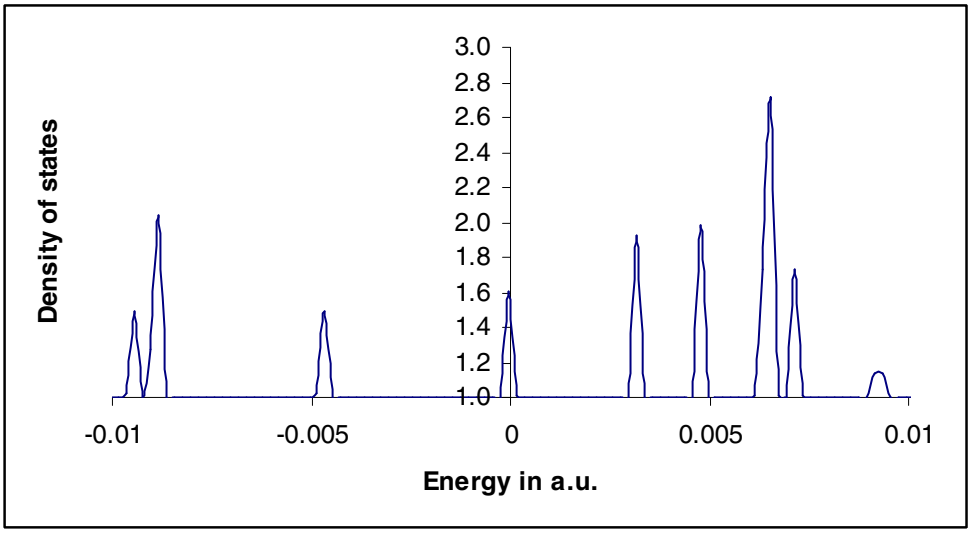

Figure 3.8 DOS Plot of c(8x2) surface

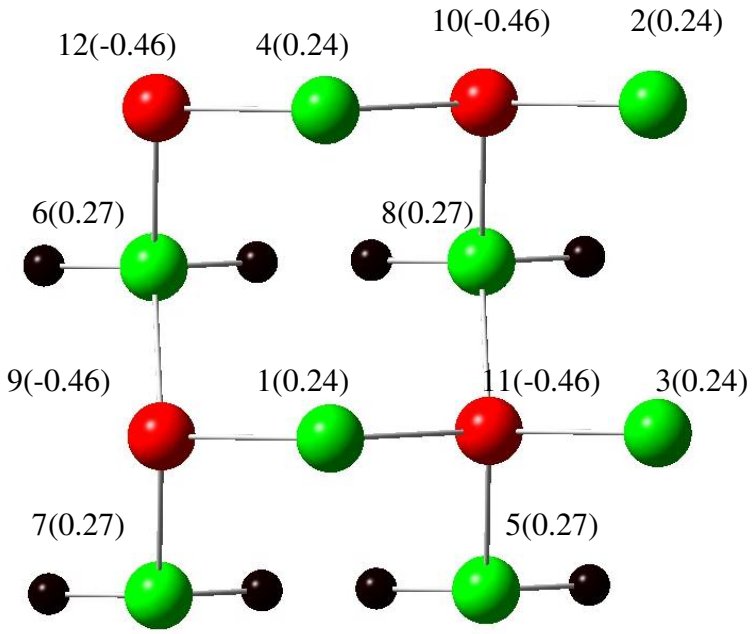

Figure 3.9 Atomic charge distribution of (1x1) surface

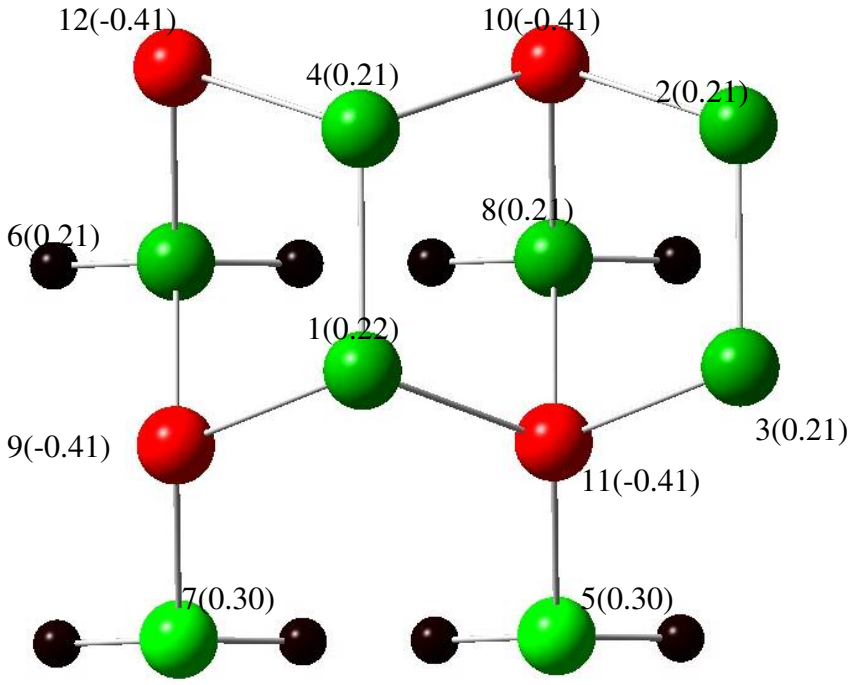

Figure 3.10 Atomic charge distribution of (2x1) surface

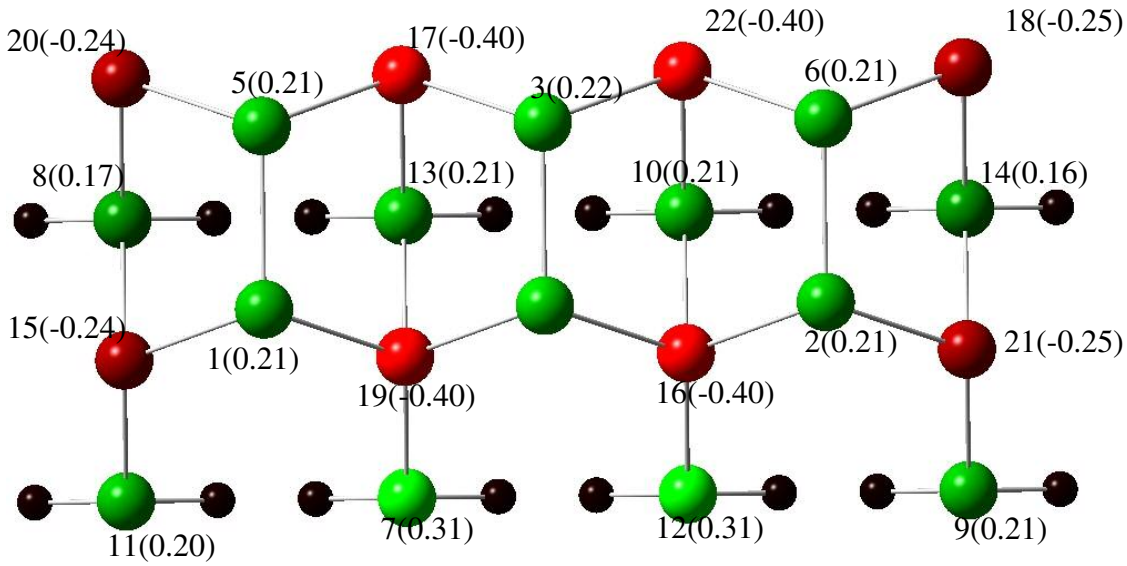

Figure 3.11 Atomic charge distribution of (4x2) surface

In all these atomic charge distribution figures, the bright red color represents the highest amount of charge gained by the particular atom while the darker red color represents a slight decrease in the amount of charges gained and the bright green color represents the highest amount of charge gained by a particular atom while the darker green color represents the slight decrease in the amount of charges lost.

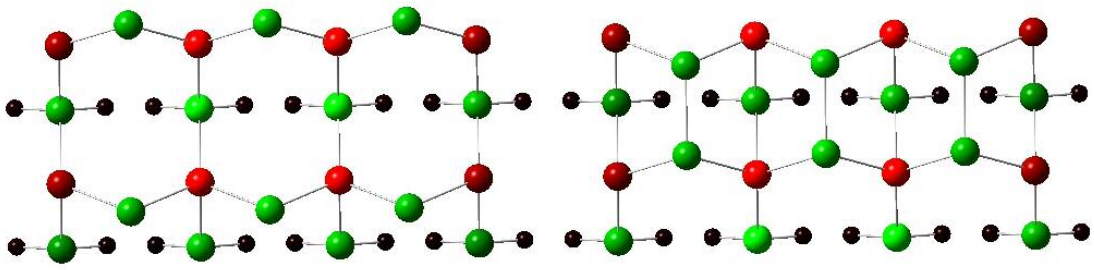

Figure 3.12 Atomic charge distribution of c(8x2) surface

CHAPTER 4

ATOMIC ADSORPTIONS ON InSb SURFACES

4.1 Results and Discussions of Li Adsorption

4.1.1 Energetics and geometric structure properties

The *ab initio* calculations were performed on the chemisorption of Li on the (1x1), (2x1), (4x2) and c(8x2) if the InSb(100) surfaces. Considering the importance of selection of basis set to represent any system, we decided to use the Dunning/Huzinga valence double zeta basis set [80] to study the behavior of Li with the different InSb(100) surfaces. This basis set is shown in the table 4.1. The atomic properties were tested for Li using this basis set and the values of the ionization potential and electron affinity for the Li atom are given in the table 4.6 in comparison with the available experimental data [53]. Again, the basis set LANL2DZ was used for In and Sb and all the calculations were performed within the local density approximation to density functional theory.

The different sites of adsorption of Li on (1x1), (2x1), (4x2) and c(8x2) surfaces are shown in figures 4.1, 4.2, 4.3 and 4.4 respectively. In this study of atomic Li adsorption , we have considered six adsorption sites of high symmetry on the In-rich InSb (100) (4x2) and c (8x2) surfaces, namely, the top, bridge, hollow, cave, trough and one of the interstitial site, namely the cage site. For all the atomic adsorption studies, a one-dimensional optimization of the adatom nearest surface neighbor bondlength, in other words, height of the adatom from the surface is performed [63-72]. All the sites were chosen because of their associated point symmetries. The top, bridge and the cage sites

were chosen for their σ_v inversion symmetry [63-72] through a plane perpendicular to the surface dimer mid-point. The cave, hollow and trough sites were chosen for their C_{4v} point rotational symmetry about an axis normal to the (100) plane. In the top site, the position of the adatom is just above one of the In atoms in the top surface. The bridge site is exactly above the mid-point of the In-In dimer in the first layer. The hollow site on the other hand is located in the mid-point of the two In atoms that are moving apart. The cage site is same as the bridge site, but located interstitially. The cave site is located above the center of four In atoms forming a rectangle formed by a set of In dimers in the top surface. The trough site is four fold coordinated and located in the center of the four Sb atoms which are bonded only to one of the In atoms in the top-most layer. Through out this work, there are two different types of top, bridge, hollow and cage sites for the (4x2) and c(8x2) surfaces because of the differences in the surrounding atoms that that adatom sees while reacting with these surfaces; for example, there are two different top sites, top site 1 and top site 2 for both (4x2) and c(8x2) surfaces as seen from figures 4.3 and 4.4 respectively.

The results of adatom heights from the surface, chemisorption energies, HOMO(Highest Occupied Molecular Orbital) –LUMO (Lowest Unoccupied Molecular Orbital) gaps and the difference in band gaps(Δ Gaps) of the Li adsorbed surfaces with respect to the bare surfaces for the different sites of (1x1), (2x1), (4x2) and c(8x2) surfaces are tabulated in tables 4.7, 4.8, 4,9, and 4.10 respectively. The adatom heights are calculated with respect to the top layer of InSb(100) surface that is solely composed of In atoms. Here the chemisorption energy (CE) is defined as

$$E_c(Li/In_xSb_yH_z) = E(Li) + E(In_xSb_yH_z) - E(LiIn_xSb_yH_z) \qquad 4.1$$

This energy is indicative of whether the adsorption is possible or not. If this energy is positive, then adsorption is possible, on the other hand, a negative energy implies that the adsorption is not probable. During the adsorption studies of Li on the different InSb(100) surface, we found that all the chemisorption energies are positive which means that Li adsorption is favored on all the InSb (100) surfaces at all the sites. The parameter ΔGap is illustrative of whether the band gap of the Li adsorbed system has increased or decreased from that of the corresponding bare surface, positive value indicating that the band gap of the adsorbed system has increased with respect to the corresponding bare surface and vice versa for the negative value of ΔGap.

One important thing that was noted in this study of Li adsorption is that the adatom was found to penetrate the surface during adsorptions in the case of hollow, cage and trough sites of (2x1), (4x2) and c(8x2) surfaces. For example, during the adsorption of Li in the hollow site of (2x1) surface, the adatom was found to lie at 2.1 Å below the InSb surface.

In the case of adsorption on (1x1) surface, the most favorable site is the center site with the highest coordination number as seen from table 4.7. From tables 4.9 and 4.10, it is noted that the chemisorption energies and adatom heights at each site of c(8x2) surface is comparable to the corresponding site of (4x2) surface. It is found that in both the cases of c (8x2) and (4x2), the trough site is most favored and the top site is the least favored and also the order of preferred sites is one and the same in both cases of c(8x2) and (4x2) surfaces. The overall trend of the order of preferred sites in the case of (2x1) surface is same as that of other reconstructed surfaces like c(8x2) and (4x2) surfaces which follows from tables 4.8, 4.9 and 4.10. In the case of adsorption on (2x1) surfaces,

the chemisorption energies follow the same pattern as that of the other dimerized surfaces like (4x2) and c(8x2) surfaces. All of the graphs concerned with the adsorption of Li on the c(8x2), (4x2), (2x1) and (1x1) surfaces are shown in figures 4.5, 4.6, 4.7 and 4.8 respectively. These graphs show the variation in chemisorption energy with respect to the height of the adatom from the surface.

In summary, during the adsorption of Li on the (1x1) surface, the center site was found to be the most preferred site and in the case of (4x2) and c(8x2) surfaces, trough site was found to be the most preferred site. The justification for this lies in the fact that both trough and the center sites have the maximum coordination number, that is, the adatom sees more nearest neighboring atoms. These results for (4x2) and c(8x2) surfaces are in good agreement with the previous work done by our group [63-65,71,72], which deals with the cesium and also aluminum adsorption on the Ga- terminated GaAs (100) surfaces. Also, it is known from many of the previous works [63-72, 81-83] that the top site is rarely preferred adsorption site on a semiconductor surface. Again the most preferred site in the case of (2x1) surface is the hollow site and that is because if we look at tables 4.9 and 4.10, the next preferred site to the trough site is the hollow site and there is no trough site in the case of (2x1) surface. Hence the general trend is maintained the same during adsorption of Li on all the reconstructed surfaces.

4.1.2 Electronic structure properties and charge distributions

One of the main focuses of this study is to see if there could be any possibilities of metallization in the InSb surface due to the interaction with lithium. Direct evidence of metallization is provided by the HOMO-LUMO gap or the 'band gap' [63-65, 71, 72]. Looking at the band gaps and Δ Gaps of the systems after the adsorption of

lithium, as seen from tables 4.7, 4.9 and 4.10, it is clear that for Li adsorption on the (1x1), (4x2) and c(8x2) surfaces, there is a considerable reduction in the energy band gap which is evident from the calculated Δ Gaps. DOS plots(figures 4.22 a and b) indicate this for Li adsorption in the trough site on the c(8x2) surface. This trend continues for the (4x2) and (1x1) surfaces. Similar kinds of results were obtained by the study of metallization of Ga-rich GaAs (100) surface in this group. In the case of Li adsorption on the (2x1) surface which was already metallic, the surface turns out to be non-metallic, that is there is a prominent increase in the band gaps of the Li adsorbed system compared to that of the bare (2x1) surface as seen from the ΔGaps shown in Table 4.8 for the (2x1) surface. Figures 4.21 a and b shows DOS plots of the bare (2x1) and Li adsorbed (2x1) surface from which we can see the increase in the band gap for the Li adsorbed system. All these DOS plots are shown only for the cases of most preferred sites for both (2x1) (hollow site) and c(8x2) (trough site) surfaces.

The Mulliken population analysis was carried for the Li adsorption on all the InSb(100) surfaces. Through out this study, it was noted that the Li atom loses charges and these charges are gained by the In or Sb atoms, whichever lies near to this Li atom depending upon the adsorptions in different sites. During the adsorption of Li on both (1x1) and (2x1) surfaces, it was found that the charge loss of Li was 0.37 e in the case of center site which is the most preferred site in the case of (1x1) surface and the highest charge loss of 0.30 e occurred in the case of hollow site which is the most preferred site of adsorption for the (2x1) surface. The Mulliken charge distributions for the (1x1) surface before and after Li adsorption in the most favorable center site are shown in the figures 4.27 and 4.28 respectively**.** From figure 4.28, it is seen that the four In atoms in

the top most layer which are closer to the adsorbed Li atom have become darker in green color as compared to the corresponding atoms in the figure 4.27 indicating that these four In atoms have gained charges from Li atom. The atomic charge distributions for Li adsorption on InSb (2x1) and (4x2) surfaces at various sites are shown in tables 4.23 and 4.24 respectively. It was noted that the charges are distributed as per the electronegativities of the different atoms.

In the case of (4x2) and c(8x2) surfaces also, the lithium atom loses charge in all cases and the atoms nearest to the adatom gains maximum charges, except for the cage site in which the Li adatom gains a very negligible amount of charge. Again, it is found that the highest charge transfer occurs in the case of trough site for on (4x2) and c(8x2) surfaces, which is the most preferred site in terms of chemisorption energy for both the surfaces. For our enhanced understanding of the charge distribution, the atomic charge distributions for c(8x2) surface is schematically represented as shown in figures 4.29 and 4.30 which depicts the difference between bare c(8x2) surface and the c(8x2) surface after Li adsorption. It is seen from the figure 4.30 that Li adatom is very light green in color showing it loses charges wherein these charges are picked up by the four Sb atoms (these four atoms seem to lose the dark red color and become more brighter) which are close to the Li adatom and also by the two In atoms in the third layer and these two In atoms have grown thicker in green color indicating charge gain. The same arguments and charge distribution patterns hold good for the adsorption on the (4x2) surface and hence not shown.

In summary, Li adatom loses charges and the atoms near the adatom gain charges except for the cage site in which negligible amount of charge is gained. The highest

amount of charge is lost by the lithium adatom in all the cases in case of the most preferred site. For example, highest charge loss of 0.45e and 0.47e occurs in the adsorption of Li atom in the trough site of c(8x2) and (4x2) surfaces respectively, 0.30 e in the case of hollow site of (2x1) surface and 0.37 e in the case of center site of (1x1) surface.

4.2 Results and Discussions of Halogen(Cl, Br and I) Adsorptions

If your work contains more than four chapters, add additional template chapters to your template now before continuing. To add additional chapters to those that come with your template you will need to use Word 2000 text selection and copy operations. (If you do not know how to select and copy text in a Word 2000 document, consult an introductory Word 2000 manual before continuing further.) For example, if your work contains five chapters, select and copy the template's entire Chapter IV using Word 2000 text selection and copy operations. Then, paste your copy of Chapter IV immediately after the template's Chapter IV using Word 2000 text paste operations. Once you have done this, be sure to change the chapter title in the added fifth template chapter to Chapter V from Chapter VI.

4.2.1 Energetics and geometric structure properties

Chemisorption of halogens on semiconductor surface continues to be a field of active research owing to the usage of these reaction techniques in the etching process in the manufacture of optoelectronic devices. This work focuses on investigating the electronic and geometric structure properties of the InSb surface due to chemisorption of different halogen atoms like Chlorine, Bromine and Iodine. *Ab initio* calculations were performed within local density approximation [46,47] to density functional theory [39,

44, 48-50] with the Hay - Wadt (HW) effective core potentials [51, 52] used as basis set for all the elements, such as, In, Sb, Cl, Br and I. The effective core potentials for Cl, Br and I are shown in tables 4.2, 4.3 and 4.4 respectively and the associated basis sets for Cl, Br and I are shown in table 4.5. The atomic properties of chlorine, bromine and iodine were verified against the available experimental data [53] as can be seen from table 4.6.

Adsorption studies of different halogens such as chlorine, bromine and iodine were done on the In-Rich InSb(100) (1x1), (2x1), (4x2) and c(8x2) surfaces at various symmetric sites. The (1x1, (2x1), (4x2) and c(8x2) surfaces are the ones that were described in Chapter 3. The different symmetric sites are exactly the same as the ones mentioned afore in the first part of this chapter (figures 4.1-4.4). Again, for all these adsorption studies, an one-dimensional optimization of the adatom nearest surface neighbor bondlength is performed.

The results of adatom heights from the surface, chemisorption energies, HOMO(Highest occupied Molecular Orbital) –LUMO (Lowest Unoccupied Molecular Orbital) gaps and the difference in band gaps(Δ Gap) of the halogen adsorbed surfaces with respect to the bare surfaces for the different sites of chlorine, bromine and iodine adsorption on (1x1), (2x1), (4x2) and c(8x2) surfaces are tabulated in tables 4.11-4.22. The chemisorption energy is calculated using equation 4.1, except for the fact that the Li atom is replaced by Cl, Br or I.

In this work, all the chemisorption energies were found to be positive for the chemisorption studies of chlorine, whereas the cage sites alone were not bound for the cases of atomic adsorptions of bromine and iodine. It is believed the size of the adatom is an important factor that determines this and hence owing to the sizes of bromine and

iodine, the adsorption of these on the cage site, which is an interstitial site, was not found to be feasible. From the tables 4.11, 4.15 and 4.19, it is noted that the pattern of chemisorption energies are exactly the same for the cases of atomic adsorption of Cl, Br and I on the (1x1) surface. The bridge site 1 is the most favored followed by top site, center site and bridge site 2. In the case of adsorption of chlorine on the (2x1), (4x2) and c(8x2) surfaces, the top site was the most preferred site and cage site was the least preferred one. In the case of adsorption of bromine on the (2x1), (4x2) and c(8x2) surfaces, the top site was again the most preferred site and trough site was the least favored site in the case of (4x2) and c(8x2) surfaces(since the cage site was not bound), and the cave site was the least preferred site in the case of (2x1) surface. It was found that for the case of adsorption of iodine on the (2x1), (4x2) and c(8x2) surfaces, hollow site was the most favored and trough site was the least favored for the adsorption on (4x2) and c(8x2) and cave site was the least favored for the (2x1) surface. But in the case of Iodine, if we look into the tables 4.20-4.22, it is noticed that though the hollow site is the most favored, the second preferred top site does not vary much in terms of chemisorption energy when compared to the hollow site(where as we can see that for the adsorption of Cl and Br, the top site chemisorption energies were higher than that of the hollow site by a greater energy) and the least preferred site was found to the trough site (where the cage site is not bound) in the case of (4x2) and c(8x2) surfaces and cave site in the case of (2x1) surface. Overall, it can be summarized that the top site is the most preferred site in the case of adsorption of halogens on the InSb surface and this is justified because as discussed in the introduction, it is a well known fact that the halogens form strong, directional mono-valent bond and top site is the site which meets the criteria. Also, if we

see the least preferred site in each case, it is the cage, trough or the cave site and it is known that all these sites are with highest coordination with the neighboring atoms and hence not suited for the halogen adsorption.

During the adsorption study of each halogen atom on the InSb surface, it was noted that the distance of the adatom from the surface decreases in the order of Top>Bridge>Cave> Hollow>Trough site in the cases of (2x1), (4x2) and c(8x2) surface and the order is Top>Bridge 2>Bridge1>center site in the case of each of the halogen adsorption on the (1x1) surface.

In the cases of adsorption on the (4x2) and c(8x2) surfaces, there was a unique one to one correspondence in the order of preferred sites when the results were compared for each of the cases of chlorine , bromine and iodine adsorptions. This was the same trend that was observed while Li adsorption was studied on the (4x2) and c(8x2) surfaces as discussed in the section 4.1 in the first part of this chapter. One another point that is obvious from tables 4.13, 4.14 , 4.17, 4.19, 4.21, and 4.22 is that in all the cases of halogen adsorption on the (4x2) and c(8x2) surfaces, the #2 sites are more preferred compared to their respective #1 counterparts; for example, Top site 2 is more preferred compared to the top site 1.

Again, comparing the chemisorption energies for adsorption of iodine on the different surfaces of InSb from the tables 4.19-4.22, it is seen that all the chemisorption energies for InSb(100) (1x1) surface are higher compared to that of the InSb(100) (2x1), (4x2) and c(8x2) surfaces which suggests us that during the chemisorption of Iodine on the different InSb surfaces, the chemisorption on InSb(100) (1x1) surface is particularly more favorable. This is a very interesting result because the same feature was observed

during some experimental studies as discussed in the introduction. In those studies, the STM images of an I_2-saturated surface were found to exhibit an ordered square lattice of spots separated by 4.6 Angstroms in both [110] and [$1\bar{1}0$] directions, which agrees with the size of the InSb(001) surface unit cell. Also in our studies of chemisorption of chlorine and bromine on the InSb surfaces, our results shows the same pattern, that is the chemisorption on the (1x1) surfaces are correspondingly more favorable than on that of the other surfaces. This can be verified from the tables 4.15-4.22.

If we look into the tables 4.11-4.22 carefully, it is noticed that the overall chemisorption energies for the adsorption of chlorine on each of the sites is in general higher compared to that of bromine which is higher than that of iodine. This allows us to conclude that chlorine is the most reactive and Iodine is the least reactive on the InSb surface which is expected owing to the electronegativities of Cl>Br>I and also it is seen by the analysis of Mulliken charge distribution that the charge gained follows the pattern Cl>Br>I. It was also noted that the halogen-In dimer bondlengths generally was found to increase in the order of Cl<Br<I. This could be justified by taking into account the fact that the size of the different adatoms.

4.2.2 Electronic structure properties and charge distributions

We now discuss Mulliken charge analysis for Cl, Br and I adsorption on the (1x1), (2x1), (4x2) and c(8x2) surfaces. We find that the halogen adatom gains charges from the atoms that lie closer to the adatom. The charge distribution tables for the Cl, Br and I adsorptions in the different sites of (2x1) and (4x2) surfaces of InSb are shown in the tables 4.25, 4.26, 4.27, 4.28, 4.29 and 4.30 in comparison with their corresponding bare surfaces.

The highest charge transfer occurs in the case of hollow site in the cases of (2x1), (4x2) and c(8x2) surfaces and in the center site in the case of (1x1) surface during the adsorption studies of chlorine, bromine and iodine. Also comparing each of the corresponding sites in the case of chemisorption of chlorine, bromine and iodine on the different InSb surfaces, it is observed that the chlorine gains more charges compared to that of bromine which in turn gains more charges compared to that of iodine. The atomic charge distributions for the bare (1x1) surfaces as compared to the iodine adsorbed (1x1) surface are shown in the figures 4.31 and 4.32 respectively. Also, the atomic charge distributions are shown for the bare (4x2) surface and the iodine adsorbed (4x2) surface in the top site 2. It is observed that when the adsorption of iodine occurs on the top site 2 of (4x2) surface, the atom labeled 3 in figure 4.33 colored in dark green in figure 4.33 turns to brighter green in figure 4.34 which indicates that the In atom located just below the adatom loses more charge to the adatom as compared to the other In atoms on the surface.

Looking into the energy band gaps, it is seen that the band gap of the halogen adsorbed system was less compared to the respective bare system in the cases of (1x1), (4x2) and c(8x2) surfaces with the exception of the bridge site 1 and top site of the (1x1) surface in each of the cases of chlorine, bromine and iodine adsorption. In the case of adsorption of these atoms in the case of (2x1) surface, the band gap of the halogen adsorbed system was found to increase compared to the bare (2x1) surface. DOS plots were plotted for the bare (1x1) surface and also for the (1x1) surface after Cl adsorption was done in the bridge site 1 as shown in the figures 4.23 a and b respectively. These figures clearly illustrate the increase in band gap for the Cl adsorbed (1x1) surface.

Similar observation was found during the iodine adsorption on the (1x1) surface as seen from the figures 4.25. a and b . The DOS plots were also plotted for the bare (4x2) surface and also for the (4x2) surface after Cl adsorption in the top site 2 as shown in the figures 4.24 a and b respectively. These figures clearly illustrate the decrease in band gap for the Cl adsorbed (4x2) surface. This trend is also observed for iodine adsorption on the (4x2) surface as evident from the figures 4.26 a and b.

Table 4.1 Basis functions for Li

Lithium

Exponents(α_i)	Coefficients(c_i)
s orbitals	
921.3000	0.001367000067
138.7000	0.010425000510
31.94000	0.049859002450
9.3530	0.160701007900
3.1580	0.344604016900
1.1570	0.425197020900
0.4446	0.169468008300
0.4446	-0.22231097350
0.07666	1.11647686700
0.02864	1.00000000000
p orbitals	
1.48800	0.03877001547
0.26670	0.23625709430
0.07201	0.83044833150
0.02370	1.00000000000

Table 4.2 Hay-Wadt Pseudopotential for Cl atom

n_k	ζ_k	d_k
	d potential	
1	94.8130	-10.000000
2	165.6440	66.272917
2	30.8317	-28.968595
2	10.5841	-12.866337
2	3.7704	-1.710217
	s-d potential	
0	128.8391	3.000000
1	120.3786	12.852851
2	63.5622	275.672398
2	18.0695	115.677712
2	3.8142	35.060690
	p-d potential	
0	216.5263	5.000000
1	46.5723	7.479486
2	147.4685	613.032000
2	48.9869	280.800685
2	13.2096	107.878824
2	3.1831	15.343956

Table 4.3 Hay-Wadt pseudopotential for Br atom

n_k	ζ_k	d_k
	f potential	
1	213.6143969	-28.000000
2	41.0585380	-134.926885
2	8.7086530	-41.927191
2	2.6074661	-5.933642
	s-f potential	
0	54.1980682	3.000000
1	32.9053558	27.343064
2	13.6744890	118.802884
2	3.0341152	43.435487
	p-f potential	
0	54.2563340	5.000000
1	26.0095593	25.050425
2	28.2012995	92.615746
2	9.4341061	95.824901
2	2.4341061	26.268498
	d-f potential	
0	87.63287216	3.000000
1	61.73733770	22.553355
2	32.43851040	178.124198
2	8.75371990	76.992416
2	1.66331890	9.481827

Table 4.4 Hay-Wadt pseudopotential for I atom

n_k	ζ_k	d_k
	f-potential	
0	1.0715702	-0.0747621
1	44.1936028	-30.0811224
2	12.9367609	-75.3722721
2	3.1956412	-22.0563758
2	0.8589806	-1.6979585
	s f potential	
0	127.9202670	2.93800036
1	78.6211465	41.24712670
2	36.5146237	287.86800950
2	9.9065681	114.37585060
2	1.9420086	37.65477140
	p f potential	
0	13.0035304	2.2222630
1	76.0331404	39.4090831
2	24.1961684	177.4075002
2	6.4053433	77.9889462
2	1.5851786	25.7547641
	d f potential	
0	40.4278108	7.0524360
1	28.9084375	33.3041635
2	15.6268936	186.9453875
2	4.1442856	71.9688361
2	0.9377235	9.3630657

Table 4.5 Basis functions for Cl, Br and I

Chlorine

Exponents(α_i)	Coefficients(c_i)
s orbitals	
2.23100	-0.295892
0.47200	0.757313
0.16310	0.435100
p orbitals	
6.29600	-0.034865
0.63330	0.556255
0.18190	0.556988

Bromine

Exponents(α_i)	Coefficients(c_i)
s orbitals	
1.15900	-0.869134
0.71070	0.964261
0.19050	0.773809
p orbitals	
2.69100	-0.067338
0.44460	0.589984
0.13770	0.525115

Iodine

Exponents(α_i)	Coefficients(c_i)
s orbitals	
0.72420	-1.173761
0.46530	1.374971
0.13360	0.653103
p orbitals	
1.29000	-0.118932
0.31800	0.627256
0.10530	0.508219

Table 4.6 Atomic properties of Li, Cl, Br and I

Element	IP		EA	
	This work	Exp.[53]	This work	Exp.[53]
Li	5.84	5.40	0.74	0.62
Cl	13.76	12.97	3.87	3.61
Br	12.45	11.81	3.58	3.36
I	11.29	10.45	3.64	3.06

Table 4.7 Results of Li adsorption on InSb (1x1) surface

Site	Adatom Height	CE	Band gap	Δ Gap
Center	0.2	2.27	0.04	-0.01
Bridge 2	1.4	2.21	0.01	-0.04
Bridge 1	1.8	2.13	0.07	0.02
Top	2.7	1.7	0.03	-0.02

Table 4.8 Results of Li adsorption on InSb (2x1) surface

Site	Adatom Height	CE	Band gap	Δ Gap
Hollow	2.1	2.62	0.10	0.09
Cage	2.8	2.50	0.03	0.02
Cave	0.2	2.12	0.09	0.08
Bridge	2.3	1.46	0.02	0.01
Top	2.7	1.13	0.04	0.03

Table 4.9 Results of Li adsorption on InSb (4x2) surface

Site	Adatom Height	CE	Band gap	Δ Gap
Trough	1.27	3.28	0.01	-0.06
Hollow 1	1.9	2.86	0.07	0.0
Hollow 2	1.6	2.62	0.06	0.0
Cage 1	2.7	2.7	0.05	-0.01
Cage 2	2.8	2.44	0.08	0.01
Cave	0.0	2.19	0.05	-0.02
Bridge 1	2.3	1.53	0.04	-0.02
Bridge 2	2.3	1.46	0.05	-0.02
Top 1	2.7	1.19	0.04	-0.03
Top 2	2.7	1.14	0.04	-0.03

Table 4.10 Results of Li adsorption on InSb c(8x2) surface

Site	Adatom Height	CE	Band gap	Δ Gap
Trough	1.27	3.23	0.02	-0.07
Hollow 1	2.0	2.87	0.03	-0.06
Hollow 2	1.90	2.62	0.05	-0.03
Cage 1	2.80	2.69	0.01	-0.07
Cage 2	2.80	2.41	0.05	-0.04
Cave	0.0	2.19	0.05	-0.04
Bridge 1	2.4	1.51	0.02	-0.07
Bridge 2	2.4	1.48	0.03	-0.06
Top 1	2.7	1.18	0.02	-0.07
Top 2	2.8	1.14	0.03	-0.06

Table 4.11 Results of Cl adsorption on InSb (1x1) surface

S. No	Site	Adatom height	CE	Band Gap	ΔGap
1	Bridge 1	1.20	4.64	0.09	0.04
2	Top	2.40	4.05	0.09	0.04
3	Center	0.9	3.53	0.04	-0.01
4	Bridge 2	1.7	3.30	0.04	-0.01

Table 4.12 Results of Cl adsorption on InSb (2x1) surface

S. No.	Site	Adatom height	CE	Band Gap	ΔGap
1	Top	2.50	3.80	0.03	0.02
2	Bridge	2.40	3.42	0.07	0.06
3	Cave	1.50	3.37	0.08	0.07
4	Hollow	0.50	3.28	0.03	0.02
5	Cage	-2.10	1.87	0.03	0.02

Table 4.13 Results of Cl adsorption on InSb (4x2) surface

S. No.	Site	Adatom height	CE	Band gap	ΔGap
1	Top 2	2.40	3.72	0.01	-0.06
2	Top 1	2.50	3.58	0.06	-0.01
3	Bridge 2	2.30	3.36	0.08	0.01
4	Hollow 2	0.30	3.32	0.01	-0.06
5	Bridge 1	2.30	3.30	0.10	0.03
6	Cave	1.50	3.26	0.02	-0.05
7	Hollow 1	0.40	3.12	0.06	-0.01
8	Trough	-1.17	2.74	0.01	-0.06
9	Cage 2	-2.00	1.81	0.07	0.00
10	Cage 1	-2.00	1.64	0.03	-0.04

Table 4.14 Results of Cl adsorption on InSb c(8x2) surface

S.No.	Site	Adatom height	CE	Band Gap	ΔGap
1	Top2	2.50	3.75	0.03	-0.06
2	Top 1	2.40	3.53	0.03	-0.06
3	Bridge 2	2.30	3.40	0.02	-0.07
4	Hollow 2	0.50	3.33	0.03	-0.06
5	Bridge 1	2.30	3.30	0.02	-0.07
6	Cave	1.40	3.21	0.03	-0.06
7	Hollow 1	0.30	3.09	0.03	-0.06
8	Trough	-1.27	2.63	0.03	-0.06
9	Cage 2	-2.10	1.85	0.04	-0.05
10	Cage 1	-2.10	1.66	0.09	0.00

Table 4.15 Results of Br adsorption on InSb (1x1) surface

S. No.	Site	Adatom height	CE in eV	Band gap	ΔGap
1	Bridge 1	1.50	4.11	0.09	0.04
2	Top	2.60	3.55	0.07	0.02
3	center	1.10	3.27	0.03	-0.02
4	Bridge 2	1.90	2.95	0.04	-0.01

Table 4.16 Results of Br adsorption on InSb (2x1) surface

S. No.	Site	Height in Angstroms	CE in eV	Band Gap in eV	ΔGap
1	Top	2.60	3.30	0.04	0.03
2	Hollow	0.70	3.09	0.05	0.04
3	Bridge	2.60	2.95	0.06	0.05
4	Cave	1.80	2.95	0.08	0.07

Table 4.17 Results of Br adsorption on InSb (4x2) surface

S. No.	Site	Height in Angstroms	CE in eV	Band gap in eV	ΔGap
1	Top2	2.60	3.23	0.02	-0.05
2	Hollow 2	0.70	3.11	0.01	-0.06
3	Top 1	2.60	3.09	0.06	-0.01
4	Bridge 2	2.60	2.93	0.06	-0.01
5	Hollow 1	0.70	2.92	0.06	-0.01
6	Cave	1.80	2.87	0.04	-0.03
7	Bridge 1	2.50	2.84	0.09	0.02
8	Trough	-0.97	2.55	0.01	-0.06

Table 4.18 Results of Br adsorption on InSb c(8x2) surface

S. No.	Site	Adatom height	CE in eV	Band Gap in eV	ΔGap
1	Top2	2.70	3.25	0.03	-0.06
2	Hollow 2	1.10	3.08	0.03	-0.06
3	Top 1	2.60	3.04	0.03	-0.06
4	Bridge 2	2.60	2.93	0.02	-0.07
5	Hollow 1	0.80	2.92	0.03	-0.06
6	Cave	1.90	2.87	0.03	-0.06
7	Bridge 1	2.60	2.82	0.02	-0.07
8	Trough	-0.97	2.46	0.02	-0.07

Table 4.19 Results of I adsorption on InSb (1x1) surface

S. No.	Site	Adatom height	CE in eV	Band Gap in eV	ΔGap
1	Bridge 1	1.8	3.61	0.09	0.04
2	Top	2.7	3.12	0.08	0.03
3	Center	1.5	3.02	0.01	-0.04
4	Bridge 2	2.2	2.60	0.05	0.00

Table 4.20 Results of I adsorption on InSb (2x1) surface

S. No.	Site	Adatom height	CE in eV	Band Gap in eV	ΔGap
1	Hollow	1.10	2.88	0.04	0.03
2	Top	2.80	2.85	0.04	0.03
3	Cave	2.20	2.54	0.08	0.07
4	Bridge	2.80	2.53	0.05	0.04

Table 4.21 Results of I adsorption on InSb (4x2) surface

S. No.	Site	Adatom Height (Å)	CE (eV)	Band Gap (eV)	ΔGap
1	Hollow 2	1.20	2.90	0.02	-0.05
2	Top 2	2.80	2.79	0.02	-0.05
3	Hollow 1	1.20	2.70	0.05	-0.02
4	Top 1	2.90	2.64	0.06	-0.01
5	Bridge 2	2.80	2.50	0.04	-0.03
6	Cave	2.30	2.47	0.05	-0.02
7	Bridge 1	2.37	2.38	0.08	0.01
8	Trough	-0.77	2.34	0.00	-0.07

Table 4.22 Results of I adsorption on InSb c(8x2) surface

S.No	Site	Adatom Height (Å)	CE (eV)	Band Gap (eV)	ΔGap
1	Hollow2	1.40	2.87	0.03	-0.06
2	Top2	2.80	2.79	0.03	-0.06
3	Hollow 1	1.20	2.71	0.03	-0.06
4	Top 1	2.60	2.62	0.03	-0.06
5	Bridge 2	2.9	2.51	0.02	-0.07
6	Cave	2.50	2.41	0.03	-0.06
7	Bridge 1	2.70	2.37	0.02	-0.07
8	Trough	-0.57	2.24	0.02	-0.07

Table 4.23 Charge distribution of (2x1) surface before and after Li adsorption

Layer	Atom label	Type of atom	Bare (2x1) surface	Hollow	Cage	Cave	Bridge	Top
Adatom	1	Li	-	0.30	-0.06	-0.08	0.21	0.27
1st	2	In	0.22	0.24	0.22	0.22	0.17	0.17
1st	3	In	0.20	0.19	0.19	0.22	0.16	0.09
1st	4	In	0.20	0.19	0.19	0.22	0.16	0.14
1st	5	In	0.22	0.24	0.22	0.22	0.17	0.17
2nd	6	Sb	-0.41	-0.47	-0.40	-0.39	-0.39	-0.40
2nd	7	Sb	-0.41	-0.47	-0.40	-0.32	-0.39	-0.37
2nd	8	Sb	-0.41	-0.47	-0.40	-0.32	-0.39	-0.40
2nd	9	Sb	-0.41	-0.47	-0.40	-0.39	-0.39	-0.37
3rd	10	In	0.30	0.28	0.26	0.25	0.29	0.28
3rd	11	In	0.20	0.21	0.29	0.17	0.19	0.20
3rd	12	In	0.30	0.28	0.26	0.27	0.29	0.28
3rd	13	In	0.20	0.21	0.29	0.20	0.19	0.20
4th	14	H	-0.02	-0.03	-0.02	-0.03	-0.03	-0.03
4th	15	H	-0.04	-0.04	-0.04	-0.04	-0.04	-0.04
4th	16	H	-0.02	-0.03	-0.03	-0.02	-0.02	-0.03
4th	17	H	-0.04	-0.04	-0.04	-0.03	-0.03	-0.04
4th	18	H	-0.02	-0.03	-0.03	-0.03	-0.02	-0.03
4th	19	H	-0.04	-0.04	-0.04	-0.04	-0.03	-0.04
4th	20	H	-0.02	-0.03	-0.02	-0.02	-0.03	-0.03
4th	21	H	-0.04	-0.04	-0.04	-0.03	-0.04	-0.04

Table 4.24 Charge distribution of (4x2) surface before and after Li adsorption

Layer	Label	Atom	(4x2) surface	Trough	Hollow 1	Hollow 2	Cage 1	Cage 2
Adatom	1	Li	-	0.47	0.31	0.44	-0.02	-0.01
1st	2	In	0.21	0.20	0.21	0.21	0.21	0.20
1st	3	In	0.21	0.20	0.17	0.21	0.19	0.21
1st	4	In	0.22	0.23	0.24	0.17	0.22	0.21
1st	5	In	0.22	0.23	0.24	0.17	0.22	0.21
1st	6	In	0.21	0.20	0.21	0.21	0.21	0.20
1st	7	In	0.21	0.20	0.17	0.21	0.19	0.20
2nd	8	Sb	-0.24	-0.33	-0.25	-0.25	-0.23	-0.25
2nd	9	Sb	-0.40	-0.40	-0.45	-0.46	-0.39	-0.41
2nd	10	Sb	-0.40	-0.40	-0.41	-0.46	-0.41	-0.40
2nd	11	Sb	-0.25	-0.33	-0.28	-0.25	-0.25	-0.26
2nd	12	Sb	-0.40	-0.40	-0.41	-0.46	-0.41	-0.40
2nd	13	Sb	-0.24	-0.33	-0.25	-0.25	-0.26	-0.25
2nd	14	Sb	-0.25	-0.33	-0.28	-0.25	-0.25	-0.25
2nd	15	Sb	-0.40	-0.40	-0.45	-0.46	-0.39	-0.41
3rd	16	In	0.31	0.30	0.31	0.25	0.31	0.28
3rd	17	In	0.16	0.10	0.16	0.16	0.15	0.15
3rd	18	In	0.21	0.23	0.18	0.20	0.17	0.20
3rd	19	In	0.21	0.20	0.22	0.23	0.26	0.30
3rd	20	In	0.20	0.23	0.21	0.20	0.19	0.20
3rd	21	In	0.31	0.30	0.25	0.25	0.29	0.28
3rd	22	In	0.21	0.20	0.20	0.23	0.20	0.30
3rd	23	In	0.16	0.10	0.17	0.16	0.26	0.16
4th	24	H	-0.03	-0.02	-0.03	-0.03	-0.03	-0.03
4th	25	H	-0.04	-0.04	-0.04	-0.04	-0.04	-0.04
4th	26	H	-0.02	-0.02	-0.03	-0.02	-0.02	-0.01
4th	27	H	-0.03	-0.03	-0.04	-0.02	-0.03	-0.03
4th	28	H	-0.03	-0.02	-0.02	-0.03	-0.02	-0.01
4th	29	H	-0.03	-0.04	-0.03	-0.03	-0.03	-0.04
4th	30	H	-0.03	-0.02	-0.03	-0.03	-0.03	-0.04
4th	31	H	-0.03	-0.04	-0.04	-0.04	-0.04	-0.03
4th	32	H	-0.03	-0.02	-0.03	-0.03	-0.01	-0.04
4th	33	H	-0.03	-0.04	-0.03	-0.04	-0.03	-0.03
4th	34	H	-0.03	-0.02	-0.03	-0.03	-0.03	-0.01
4th	35	H	-0.03	-0.04	-0.04	-0.03	-0.04	-0.04
4th	36	H	-0.02	-0.02	-0.02	-0.02	-0.01	-0.01
4th	37	H	-0.03	-0.04	-0.02	-0.02	-0.03	-0.03
4th	38	H	-0.03	-0.02	-0.03	-0.03	-0.03	-0.03
4th	39	H	-0.04	-0.04	-0.02	-0.04	-0.04	-0.03

Table 4.24 - *Continued*

Layer	Label	Atom	(4x2) surface	Cave	Bridge 1	Bridge 2	Top 1	Top 2
Adatom	1	Li	-	0.03	0.28	0.27	0.35	0.35
1st	2	In	0.21	0.20	0.19	0.17	0.19	0.17
1st	3	In	0.21	0.20	0.14	0.19	0.13	0.17
1st	4	In	0.22	0.22	0.20	0.17	0.19	0.10
1st	5	In	0.22	0.22	0.20	0.17	0.20	0.17
1st	6	In	0.21	0.21	0.19	0.17	0.18	0.16
1st	7	In	0.21	0.20	0.14	0.19	0.06	0.17
2nd	8	Sb	-0.24	-0.26	-0.27	-0.27	-0.23	-0.25
2nd	9	Sb	-0.40	-0.33	-0.39	-0.40	-0.40	-0.40
2nd	10	Sb	-0.40	-0.40	-0.40	-0.39	-0.40	-0.38
2nd	11	Sb	-0.25	-0.23	-0.25	-0.25	-0.24	-0.26
2nd	12	Sb	-0.40	-0.40	-0.40	-0.40	-0.40	-0.40
2nd	13	Sb	-0.24	-0.25	-0.25	-0.24	-0.28	-0.26
2nd	14	Sb	-0.25	-0.26	-0.24	-0.23	-0.26	-0.24
2nd	15	Sb	-0.40	-0.33	-0.39	-0.40	-0.38	-0.37
3rd	16	In	0.31	0.29	0.31	0.30	0.31	0.30
3rd	17	In	0.16	0.16	0.17	0.17	0.17	0.17
3rd	18	In	0.21	0.19	0.20	0.20	0.19	0.20
3rd	19	In	0.21	0.20	0.19	0.20	0.20	0.21
3rd	20	In	0.20	0.20	0.21	0.20	0.21	0.20
3rd	21	In	0.31	0.27	0.30	0.29	0.30	0.30
3rd	22	In	0.21	0.20	0.21	0.21	0.21	0.22
3rd	23	In	0.16	0.15	0.15	0.16	0.16	0.17
4th	24	H	-0.03	-0.03	-0.03	-0.03	-0.03	-0.03
4th	25	H	-0.04	-0.04	-0.03	-0.04	-0.03	-0.04
4th	26	H	-0.02	-0.02	-0.02	-0.02	-0.02	-0.02
4th	27	H	-0.03	-0.03	-0.03	-0.03	-0.03	-0.04
4th	28	H	-0.03	-0.02	-0.03	-0.02	-0.03	-0.02
4th	29	H	-0.03	-0.03	-0.04	-0.04	-0.04	-0.04
4th	30	H	-0.03	-0.03	-0.02	-0.03	-0.03	-0.02
4th	31	H	-0.03	-0.04	-0.03	-0.03	-0.03	-0.04
4th	32	H	-0.03	-0.03	-0.03	-0.02	-0.02	-0.02
4th	33	H	-0.03	-0.03	-0.03	-0.03	-0.03	-0.03
4th	34	H	-0.03	-0.03	-0.02	-0.02	-0.02	-0.02
4th	35	H	-0.03	-0.04	-0.03	-0.04	-0.03	-0.04
4th	36	H	-0.02	-0.02	-0.02	-0.03	-0.02	-0.03
4th	37	H	-0.03	-0.03	-0.03	-0.04	-0.03	-0.04
4th	38	H	-0.03	-0.03	-0.03	-0.03	-0.04	-0.03
4th	39	H	-0.04	-0.03	-0.04	-0.04	-0.04	-0.04

Table 4.25 Charge distribution of (2x1) surface before and after Cl adsorption

Layer	Label	Atom	(2x1) surface	Top	Bridge	Cave	Hollow	Cage
Adatom	1	Cl	-	-0.37	-0.37	-0.41	-0.42	-0.34
1st	2	In	0.22	0.29	0.28	0.33	0.26	0.26
1st	3	In	0.20	0.38	0.34	0.33	0.31	0.27
1st	4	In	0.20	0.31	0.34	0.33	0.31	0.27
1st	5	In	0.22	0.32	0.28	0.33	0.26	0.26
2nd	6	Sb	-0.41	-0.42	-0.40	-0.43	-0.34	0.30
2nd	7	Sb	-0.41	-0.41	-0.40	-0.39	-0.34	0.25
2nd	8	Sb	-0.41	-0.42	-0.40	-0.39	-0.34	0.30
2nd	9	Sb	-0.41	-0.41	-0.40	-0.43	-0.34	0.25
3rd	10	In	0.30	0.30	0.29	0.28	0.31	0.28
3rd	11	In	0.20	0.20	0.19	0.19	0.15	0.20
3rd	12	In	0.30	0.30	0.29	0.30	0.31	0.28
3rd	13	In	0.20	0.20	0.19	0.19	0.15	0.20
4th	14	H	-0.02	-0.03	-0.03	-0.03	-0.03	-0.05
4th	15	H	-0.04	-0.04	-0.04	-0.03	-0.03	-0.03
4th	16	H	-0.02	-0.03	-0.02	-0.03	-0.04	-0.05
4th	17	H	-0.04	-0.04	-0.04	-0.03	-0.03	-0.04
4th	18	H	-0.02	-0.03	-0.02	-0.03	-0.04	-0.05
4th	19	H	-0.04	-0.04	-0.04	-0.03	-0.03	-0.04
4th	20	H	-0.02	-0.03	-0.03	-0.03	-0.03	-0.05
4th	21	H	-0.04	-0.04	-0.04	-0.03	-0.03	-0.03

Table 4.26 Charge distribution of (4x2) surface before and after Cl adsorption

Layer	Label	Atom	(4x2) surface	Top 2	Top 1	Bridge 2	Hollow 2	Bridge 1
Adatom	1	Cl	-	-0.35	-0.37	-0.36	-0.41	-0.35
1st	2	In	0.21	0.25	0.24	0.25	0.23	0.23
1st	3	In	0.21	0.24	0.30	0.25	0.23	0.33
1st	4	In	0.22	0.39	0.28	0.33	0.31	0.26
1st	5	In	0.22	0.31	0.27	0.33	0.31	0.26
1st	6	In	0.21	0.26	0.24	0.24	0.23	0.23
1st	7	In	0.21	0.25	0.37	0.25	0.23	0.33
2nd	8	Sb	-0.24	-0.24	-0.25	-0.24	-0.24	-0.24
2nd	9	Sb	-0.40	-0.42	-0.43	-0.40	-0.35	-0.40
2nd	10	Sb	-0.40	-0.41	-0.41	-0.40	-0.35	-0.40
2nd	11	Sb	-0.25	-0.23	-0.25	-0.28	-0.24	-0.21
2nd	12	Sb	-0.40	-0.43	-0.41	-0.40	-0.35	-0.40
2nd	13	Sb	-0.24	-0.25	-0.21	-0.27	-0.24	-0.24
2nd	14	Sb	-0.25	-0.24	-0.26	-0.25	-0.24	-0.23
2nd	15	Sb	-0.40	-0.40	-0.41	-0.40	-0.35	-0.39
3rd	16	In	0.31	0.31	0.32	0.30	0.33	0.31
3rd	17	In	0.16	0.15	0.15	0.16	0.16	0.17
3rd	18	In	0.21	0.20	0.20	0.20	0.20	0.19
3rd	19	In	0.21	0.22	0.21	0.22	0.17	0.21
3rd	20	In	0.20	0.21	0.21	0.20	0.20	0.20
3rd	21	In	0.31	0.31	0.31	0.30	0.33	0.30
3rd	22	In	0.21	0.21	0.20	0.22	0.17	0.21
3rd	23	In	0.16	0.15	0.15	0.17	0.16	0.16
4th	24	H	-0.03	-0.04	-0.03	-0.03	-0.03	-0.03
4th	25	H	-0.04	-0.03	-0.03	-0.04	-0.04	-0.05
4th	26	H	-0.02	-0.03	-0.03	-0.01	-0.03	-0.02
4th	27	H	-0.03	-0.03	-0.03	-0.03	-0.04	-0.03
4th	28	H	-0.03	-0.03	-0.03	-0.02	-0.02	-0.02
4th	29	H	-0.03	-0.04	-0.03	-0.04	-0.04	-0.04
4th	30	H	-0.03	-0.02	-0.02	-0.02	-0.02	-0.02
4th	31	H	-0.03	-0.03	-0.02	-0.04	-0.03	-0.04
4th	32	H	-0.03	-0.02	-0.03	-0.02	-0.02	-0.02
4th	33	H	-0.03	-0.02	-0.03	-0.04	-0.03	-0.04
4th	34	H	-0.03	-0.03	-0.03	-0.02	-0.03	-0.03
4th	35	H	-0.03	-0.04	-0.03	-0.04	-0.04	-0.04
4th	36	H	-0.02	-0.03	-0.02	-0.01	-0.03	-0.02
4th	37	H	-0.03	-0.04	-0.03	-0.03	-0.04	-0.04
4th	38	H	-0.03	-0.04	-0.03	-0.02	-0.03	-0.03
4th	39	H	-0.04	-0.04	-0.03	-0.03	-0.04	-0.04

Table 4.26 - *Continued*

Layer	Label	Atom	(4x2) surface	Cave	Bridge 1	Trough	Cage 2	Cage 1
Adatom	1	Cl		-0.41	-0.42	-0.29	-0.33	-0.33
1st	2	In	0.21	0.23	0.22	0.22	0.22	0.21
1st	3	In	0.21	0.31	0.30	0.22	0.22	0.26
1st	4	In	0.22	0.32	0.26	0.24	0.27	0.24
1st	5	In	0.22	0.32	0.26	0.24	0.27	0.24
1st	6	In	0.21	0.23	0.22	0.22	0.22	0.21
1st	7	In	0.21	0.31	0.30	0.22	0.22	0.26
2nd	8	Sb	-0.24	-0.24	-0.26	-0.14	-0.22	-0.25
2nd	9	Sb	-0.40	-0.39	-0.36	-0.40	-0.38	-0.39
2nd	10	Sb	-0.40	-0.41	-0.40	-0.41	-0.38	-0.41
2nd	11	Sb	-0.25	-0.25	-0.19	-0.23	-0.26	-0.21
2nd	12	Sb	-0.40	-0.41	-0.40	-0.40	-0.38	-0.40
2nd	13	Sb	-0.24	-0.25	-0.25	-0.21	-0.27	-0.26
2nd	14	Sb	-0.25	-0.25	-0.17	-0.16	-0.25	-0.22
2nd	15	Sb	-0.40	-0.39	-0.36	-0.41	-0.38	-0.39
3rd	16	In	0.31	0.31	0.31	0.30	0.31	0.31
3rd	17	In	0.16	0.16	0.17	0.21	0.17	0.17
3rd	18	In	0.21	0.20	0.22	0.18	0.21	0.20
3rd	19	In	0.21	0.21	0.16	0.20	0.28	0.26
3rd	20	In	0.20	0.21	0.20	0.18	0.21	0.21
3rd	21	In	0.31	0.29	0.32	0.30	0.31	0.31
3rd	22	In	0.21	0.21	0.21	0.20	0.28	0.22
3rd	23	In	0.16	0.16	0.11	0.20	0.17	0.25
4th	24	H	-0.03	-0.03	-0.02	-0.03	-0.03	-0.02
4th	25	H	-0.04	-0.03	-0.03	-0.03	-0.03	-0.04
4th	26	H	-0.02	-0.02	-0.02	-0.02	-0.03	-0.02
4th	27	H	-0.03	-0.03	-0.03	-0.04	-0.03	-0.03
4th	28	H	-0.03	-0.03	-0.04	-0.02	-0.03	-0.04
4th	29	H	-0.03	-0.04	-0.04	-0.04	-0.04	-0.04
4th	30	H	-0.03	-0.02	-0.02	-0.05	-0.02	-0.04
4th	31	H	-0.03	-0.03	-0.03	-0.03	-0.03	-0.03
4th	32	H	-0.03	-0.03	-0.02	-0.05	-0.02	-0.02
4th	33	H	-0.03	-0.03	-0.03	-0.02	-0.03	-0.03
4th	34	H	-0.03	-0.02	-0.02	-0.02	-0.03	-0.02
4th	35	H	-0.03	-0.03	-0.03	-0.04	-0.04	-0.04
4th	36	H	-0.02	-0.02	-0.03	-0.02	-0.03	-0.03
4th	37	H	-0.03	-0.03	-0.04	-0.04	-0.03	-0.04
4th	38	H	-0.03	-0.03	-0.03	-0.02	-0.03	-0.04
4th	39	H	-0.04	-0.04	-0.04	-0.03	-0.03	-0.03

Table 4.27 Charge distribution of (2x1) surface before and after Br adsorption

Layer	Label	Atom	(2x1) surface	Top	Hollow	Bridge	Cave
Adatom	1	Br	-	-0.33	-0.42	-0.35	-0.40
1st	2	In	0.22	0.29	0.27	0.29	0.33
1st	3	In	0.20	0.35	0.31	0.32	0.33
1st	4	In	0.20	0.31	0.31	0.32	0.33
1st	5	In	0.22	0.32	0.27	0.29	0.33
2nd	6	Sb	-0.41	-0.42	-0.35	-0.40	-0.42
2nd	7	Sb	-0.41	-0.40	-0.36	-0.40	-0.39
2nd	8	Sb	-0.41	-0.42	-0.35	-0.40	-0.39
2nd	9	Sb	-0.41	-0.40	-0.36	-0.40	-0.42
3rd	10	In	0.30	0.29	0.31	0.28	0.29
3rd	11	In	0.20	0.20	0.16	0.20	0.19
3rd	12	In	0.30	0.29	0.31	0.28	0.30
3rd	13	In	0.20	0.20	0.16	0.20	0.19
4th	14	H	-0.02	-0.03	-0.03	-0.03	-0.03
4th	15	H	-0.04	-0.04	-0.04	-0.04	-0.04
4th	16	H	-0.02	-0.03	-0.03	-0.03	-0.03
4th	17	H	-0.04	-0.04	-0.04	-0.03	-0.03
4th	18	H	-0.02	-0.03	-0.03	-0.03	-0.03
4th	19	H	-0.04	-0.04	-0.04	-0.03	-0.04
4th	20	H	-0.02	-0.03	-0.03	-0.03	-0.03
4th	21	H	-0.04	-0.04	-0.04	-0.04	-0.03

Table 4.28 Charge distribution of (4x2) surface before and after Br adsorption

Layer	Label	Atom	(4x2) surface	Top 2	Hollow 2	Top 1	Bridge 2
Adatom	1	Br	-	-0.34	-0.42	-0.33	-0.35
1st	2	In	0.21	0.25	0.23	0.22	0.25
1st	3	In	0.21	0.24	0.23	0.30	0.25
1st	4	In	0.22	0.33	0.31	0.28	0.32
1st	5	In	0.22	0.31	0.31	0.26	0.32
1st	6	In	0.21	0.26	0.24	0.23	0.25
1st	7	In	0.21	0.25	0.23	0.33	0.25
2nd	8	Sb	-0.24	-0.25	-0.24	-0.26	-0.22
2nd	9	Sb	-0.40	-0.42	-0.36	-0.43	-0.40
2nd	10	Sb	-0.40	-0.40	-0.35	-0.40	-0.40
2nd	11	Sb	-0.25	-0.27	-0.24	-0.22	-0.23
2nd	12	Sb	-0.40	-0.42	-0.35	-0.40	-0.40
2nd	13	Sb	-0.24	-0.20	-0.22	-0.20	-0.27
2nd	14	Sb	-0.25	-0.23	-0.25	-0.23	-0.26
2nd	15	Sb	-0.40	-0.40	-0.36	-0.41	-0.40
3rd	16	In	0.31	0.30	0.32	0.31	0.30
3rd	17	In	0.16	0.16	0.15	0.16	0.16
3rd	18	In	0.21	0.20	0.21	0.19	0.20
3rd	19	In	0.21	0.22	0.18	0.21	0.22
3rd	20	In	0.20	0.20	0.21	0.20	0.20
3rd	21	In	0.31	0.31	0.33	0.30	0.30
3rd	22	In	0.21	0.21	0.17	0.21	0.22
3rd	23	In	0.16	0.16	0.16	0.15	0.16
4th	24	H	-0.03	-0.03	-0.04	-0.03	-0.03
4th	25	H	-0.04	-0.04	-0.04	-0.03	-0.04
4th	26	H	-0.02	-0.03	-0.04	-0.02	-0.02
4th	27	H	-0.03	-0.04	-0.04	-0.03	-0.03
4th	28	H	-0.03	-0.03	-0.03	-0.03	-0.03
4th	29	H	-0.03	-0.04	-0.03	-0.04	-0.04
4th	30	H	-0.03	-0.02	-0.02	-0.02	-0.03
4th	31	H	-0.03	-0.03	-0.03	-0.03	-0.03
4th	32	H	-0.03	-0.02	-0.03	-0.03	-0.03
4th	33	H	-0.03	-0.03	-0.03	-0.03	-0.03
4th	34	H	-0.03	-0.03	-0.03	-0.02	-0.03
4th	35	H	-0.03	-0.04	-0.03	-0.03	-0.03
4th	36	H	-0.02	-0.03	-0.03	-0.02	-0.02
4th	37	H	-0.03	-0.03	-0.03	-0.03	-0.03
4th	38	H	-0.03	-0.03	-0.03	-0.04	-0.03
4th	39	H	-0.04	-0.04	-0.03	-0.04	-0.04

Table 4.28 - *Continued*

Layer	Label	Atom	(4x2) surface	Hollow 1	Cave	Bridge 1	Trough
Adatom	1	Br	-	-0.42	-0.40	-0.31	-0.24
1st	2	In	0.21	0.23	0.23	0.23	0.22
1st	3	In	0.21	0.30	0.31	0.30	0.23
1st	4	In	0.22	0.26	0.32	0.26	0.22
1st	5	In	0.22	0.26	0.32	0.26	0.22
1st	6	In	0.21	0.23	0.23	0.23	0.22
1st	7	In	0.21	0.30	0.31	0.30	0.23
2nd	8	Sb	-0.24	-0.26	-0.25	-0.23	-0.21
2nd	9	Sb	-0.40	-0.36	-0.40	-0.40	-0.40
2nd	10	Sb	-0.40	-0.41	-0.41	-0.41	-0.41
2nd	11	Sb	-0.25	-0.19	-0.26	-0.23	-0.22
2nd	12	Sb	-0.40	-0.41	-0.41	-0.41	-0.41
2nd	13	Sb	-0.24	-0.24	-0.24	-0.26	-0.21
2nd	14	Sb	-0.25	-0.19	-0.25	-0.22	-0.22
2nd	15	Sb	-0.40	-0.36	-0.40	-0.40	-0.40
3rd	16	In	0.31	0.31	0.29	0.31	0.30
3rd	17	In	0.16	0.16	0.16	0.16	0.20
3rd	18	In	0.21	0.22	0.19	0.19	0.20
3rd	19	In	0.21	0.17	0.20	0.21	0.21
3rd	20	In	0.20	0.20	0.20	0.21	0.20
3rd	21	In	0.31	0.32	0.27	0.31	0.30
3rd	22	In	0.21	0.21	0.20	0.21	0.20
3rd	23	In	0.16	0.11	0.15	0.16	0.20
4th	24	H	-0.03	-0.02	-0.03	-0.03	-0.02
4th	25	H	-0.04	-0.03	-0.03	-0.04	-0.03
4th	26	H	-0.02	-0.02	-0.02	-0.02	-0.02
4th	27	H	-0.03	-0.03	-0.03	-0.03	-0.04
4th	28	H	-0.03	-0.03	-0.03	-0.02	-0.02
4th	29	H	-0.03	-0.04	-0.04	-0.03	-0.03
4th	30	H	-0.03	-0.02	-0.02	-0.03	-0.04
4th	31	H	-0.03	-0.03	-0.03	-0.03	-0.03
4th	32	H	-0.03	-0.03	-0.03	-0.03	-0.05
4th	33	H	-0.03	-0.03	-0.03	-0.03	-0.03
4th	34	H	-0.03	-0.02	-0.02	-0.03	-0.02
4th	35	H	-0.03	-0.03	-0.03	-0.03	-0.03
4th	36	H	-0.02	-0.02	-0.02	-0.02	-0.01
4th	37	H	-0.03	-0.03	-0.03	-0.03	-0.04
4th	38	H	-0.03	-0.04	-0.03	-0.03	-0.02
4th	39	H	-0.04	-0.04	-0.04	-0.03	-0.03

Table 4.29 Charge distribution of (2x1) surface before and after I adsorption

Layer	Label	Atom	(2x1) surface	Hollow	Cage	Cave	Bridge
Adatom	1	I	-	-0.41	-0.31	-0.34	-0.30
1st	2	In	0.22	0.29	0.29	0.31	0.29
1st	3	In	0.20	0.29	0.28	0.31	0.29
1st	4	In	0.20	0.29	0.32	0.31	0.29
1st	5	In	0.22	0.29	0.32	0.31	0.29
2nd	6	Sb	-0.41	-0.36	-0.42	-0.42	-0.39
2nd	7	Sb	-0.41	-0.36	-0.39	-0.39	-0.39
2nd	8	Sb	-0.41	-0.36	-0.42	-0.39	-0.39
2nd	9	Sb	-0.41	-0.36	-0.39	-0.42	-0.39
3rd	10	In	0.30	0.30	0.29	0.30	0.28
3rd	11	In	0.20	0.17	0.19	0.19	0.20
3rd	12	In	0.30	0.30	0.29	0.29	0.28
3rd	13	In	0.20	0.17	0.19	0.19	0.20
4th	14	H	-0.02	-0.03	-0.03	-0.03	-0.03
4th	15	H	-0.04	-0.03	-0.04	-0.04	-0.04
4th	16	H	-0.02	-0.03	-0.03	-0.03	-0.03
4th	17	H	-0.04	-0.04	-0.03	-0.03	-0.04
4th	18	H	-0.02	-0.03	-0.03	-0.03	-0.03
4th	19	H	-0.04	-0.04	-0.03	-0.04	-0.04
4th	20	H	-0.02	-0.03	-0.03	-0.03	-0.03
4th	21	H	-0.04	-0.03	-0.04	-0.03	-0.04

Table 4.30 Charge distribution of (4x2) surface before and after I adsorption

Layer	Atom label	Atom	(4x2) surface	Top 2	Hollow 2	Top 1	Bridge 2
Adatom	1	I	-	-0.31	-0.41	-0.33	-0.30
1st	2	In	0.21	0.25	0.25	0.24	0.25
1st	3	In	0.21	0.24	0.25	0.30	0.25
1st	4	In	0.22	0.28	0.29	0.29	0.29
1st	5	In	0.22	0.31	0.29	0.27	0.29
1st	6	In	0.21	0.26	0.25	0.24	0.25
1st	7	In	0.21	0.26	0.25	0.27	0.25
2nd	8	Sb	-0.24	-0.22	-0.23	-0.23	-0.26
2nd	9	Sb	-0.40	-0.42	-0.36	-0.43	-0.40
2nd	10	Sb	-0.40	-0.39	-0.36	-0.41	-0.39
2nd	11	Sb	-0.25	-0.24	-0.25	-0.20	-0.22
2nd	12	Sb	-0.40	-0.42	-0.36	-0.40	-0.39
2nd	13	Sb	-0.24	-0.27	-0.25	-0.25	-0.24
2nd	14	Sb	-0.25	-0.24	-0.25	-0.24	-0.26
2nd	15	Sb	-0.40	-0.38	-0.36	-0.40	-0.39
3rd	16	In	0.31	0.31	0.32	0.32	0.30
3rd	17	In	0.16	0.16	0.16	0.16	0.16
3rd	18	In	0.21	0.20	0.21	0.19	0.20
3rd	19	In	0.21	0.22	0.19	0.21	0.22
3rd	20	In	0.20	0.20	0.21	0.20	0.20
3rd	21	In	0.31	0.30	0.32	0.31	0.30
3rd	22	In	0.21	0.21	0.18	0.21	0.22
3rd	23	In	0.16	0.16	0.16	0.15	0.16
4th	24	H	-0.03	-0.03	-0.03	-0.03	-0.03
4th	25	H	-0.04	-0.04	-0.03	-0.03	-0.04
4th	26	H	-0.02	-0.03	-0.03	-0.02	-0.02
4th	27	H	-0.03	-0.03	-0.03	-0.03	-0.03
4th	28	H	-0.03	-0.02	-0.03	-0.03	-0.02
4th	29	H	-0.03	-0.03	-0.04	-0.04	-0.03
4th	30	H	-0.03	-0.02	-0.02	-0.02	-0.03
4th	31	H	-0.03	-0.04	-0.03	-0.03	-0.03
4th	32	H	-0.03	-0.03	-0.02	-0.03	-0.03
4th	33	H	-0.03	-0.03	-0.03	-0.03	-0.03
4th	34	H	-0.03	-0.03	-0.03	-0.02	-0.02
4th	35	H	-0.03	-0.03	-0.04	-0.03	-0.03
4th	36	H	-0.02	-0.03	-0.03	-0.02	-0.02
4th	37	H	-0.03	-0.04	-0.03	-0.03	-0.03
4th	38	H	-0.03	-0.02	-0.03	-0.03	-0.03
4th	39	H	-0.04	-0.04	-0.03	-0.04	-0.04

Table 4.30 - *Continued*

Layer	Label	Atom	(4x2) surface	Hollow 1	Cave	Bridge 1	Trough
Adatom	1	I	-	-0.41	-0.37	-0.27	-0.14
1st	2	In	0.21	0.23	0.24	0.23	0.24
1st	3	In	0.21	0.30	0.30	0.28	0.24
1st	4	In	0.22	0.27	0.31	0.26	0.22
1st	5	In	0.22	0.27	0.31	0.26	0.22
1st	6	In	0.21	0.23	0.24	0.23	0.24
1st	7	In	0.21	0.30	0.30	0.28	0.24
2nd	8	Sb	-0.24	-0.26	-0.24	-0.25	-0.23
2nd	9	Sb	-0.40	-0.38	-0.40	-0.39	-0.40
2nd	10	Sb	-0.40	-0.40	-0.42	-0.40	-0.40
2nd	11	Sb	-0.25	-0.17	-0.24	-0.22	-0.26
2nd	12	Sb	-0.40	-0.40	-0.42	-0.40	-0.40
2nd	13	Sb	-0.24	-0.27	-0.24	-0.26	-0.26
2nd	14	Sb	-0.25	-0.17	-0.25	-0.21	-0.24
2nd	15	Sb	-0.40	-0.38	-0.40	-0.40	-0.41
3rd	16	In	0.31	0.32	0.30	0.31	0.30
3rd	17	In	0.16	0.16	0.16	0.17	0.18
3rd	18	In	0.21	0.19	0.20	0.18	0.23
3rd	19	In	0.21	0.18	0.21	0.22	0.20
3rd	20	In	0.20	0.21	0.20	0.20	0.23
3rd	21	In	0.31	0.31	0.30	0.30	0.30
3rd	22	In	0.21	0.22	0.21	0.21	0.21
3rd	23	In	0.16	0.11	0.15	0.17	0.18
4th	24	H	-0.03	-0.03	-0.03	-0.03	-0.02
4th	25	H	-0.04	-0.04	-0.03	-0.04	-0.04
4th	26	H	-0.02	-0.02	-0.02	-0.01	-0.01
4th	27	H	-0.03	-0.02	-0.04	-0.03	-0.04
4th	28	H	-0.03	-0.03	-0.03	-0.03	-0.02
4th	29	H	-0.03	-0.03	-0.04	-0.04	-0.04
4th	30	H	-0.03	-0.02	-0.02	-0.02	-0.04
4th	31	H	-0.03	-0.03	-0.03	-0.03	-0.03
4th	32	H	-0.03	-0.03	-0.02	-0.02	-0.05
4th	33	H	-0.03	-0.02	-0.03	-0.04	-0.03
4th	34	H	-0.03	-0.01	-0.02	-0.03	-0.02
4th	35	H	-0.03	-0.03	-0.03	-0.04	-0.03
4th	36	H	-0.02	-0.03	-0.02	-0.02	-0.01
4th	37	H	-0.03	-0.04	-0.04	-0.04	-0.04
4th	38	H	-0.03	-0.05	-0.03	-0.03	-0.02
4th	39	H	-0.04	-0.05	-0.04	-0.04	-0.04

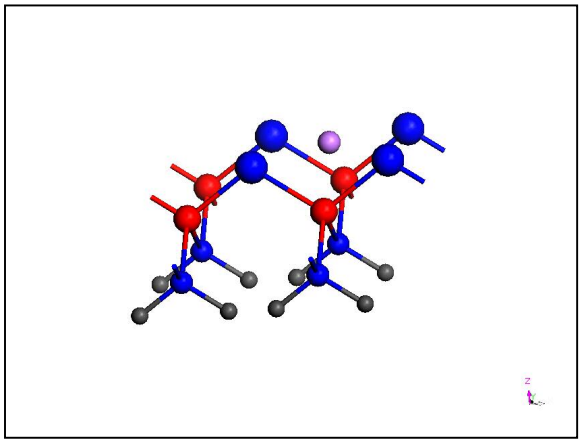

(a)

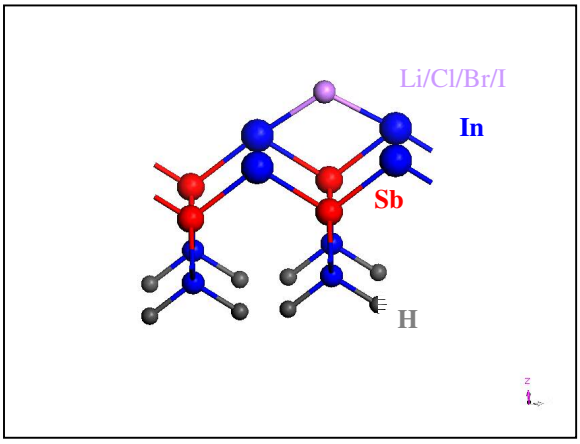

(b)

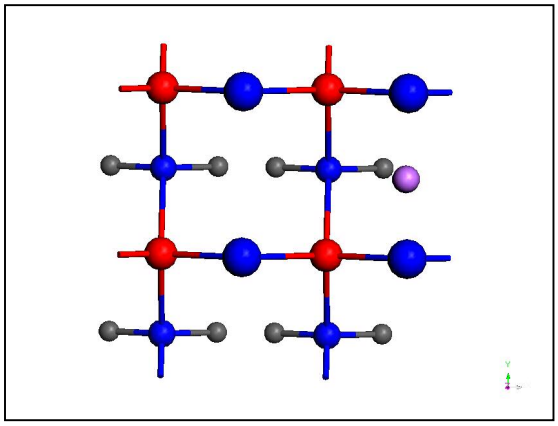

(c)

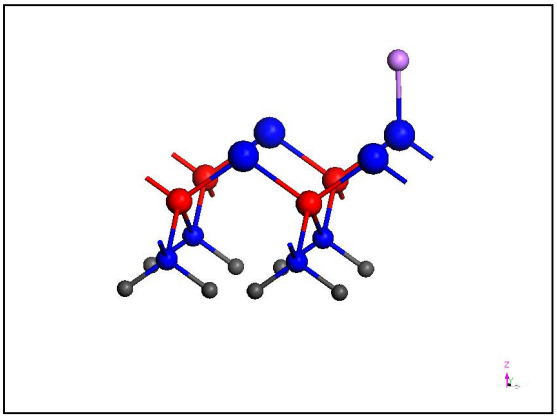

(d)

Figure 4.1 Atomic adsorption on InSb(100) (1x1) surface in center(a) bridge 2(b) bridge1(c) and top(d) sites

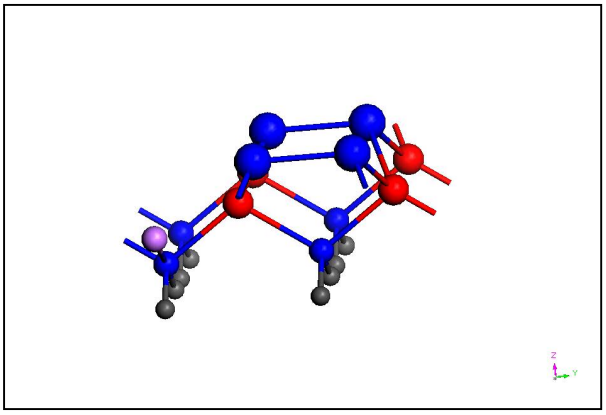

(a)

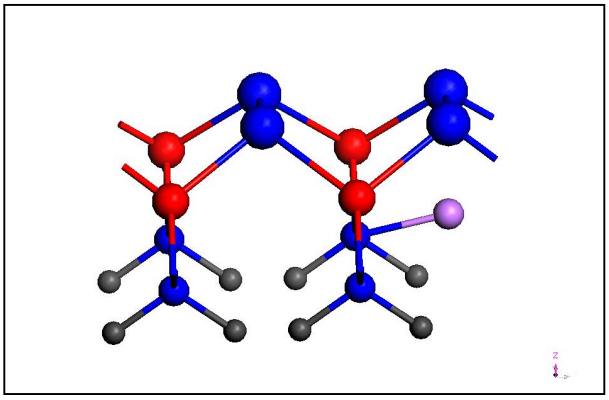

(b)

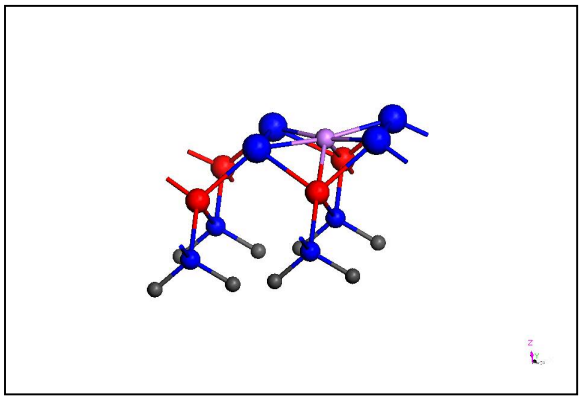

(c)

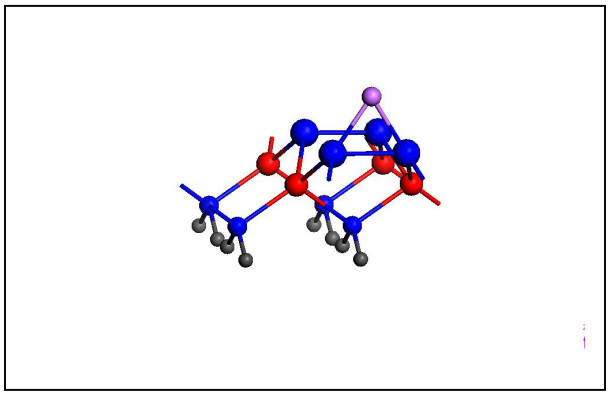

(d)

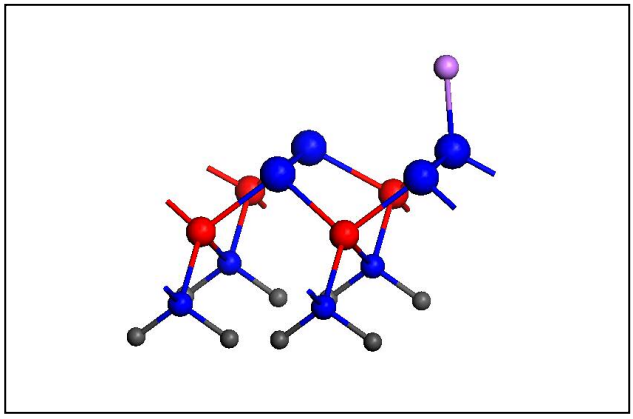

(e)

Figure 4.2 Atomic adsorption on InSb(100) (2x1) surface in hollow(a) cage(b) cave(c) bridge(d) top(e) sites

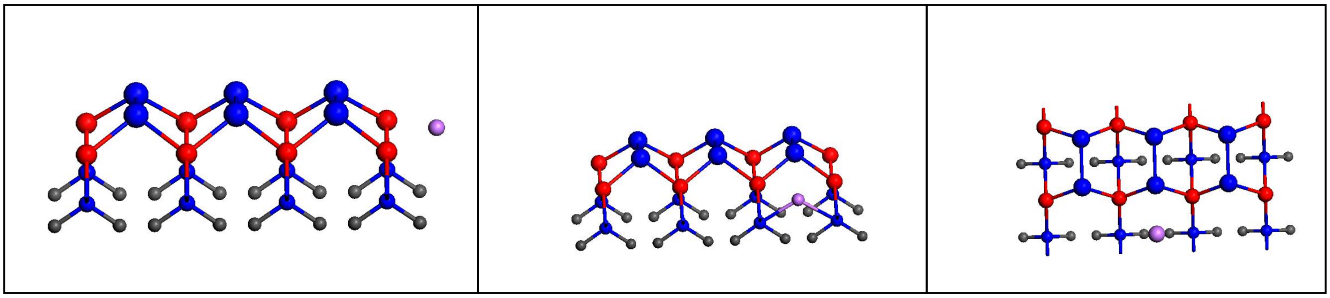

(a) (b) (c)

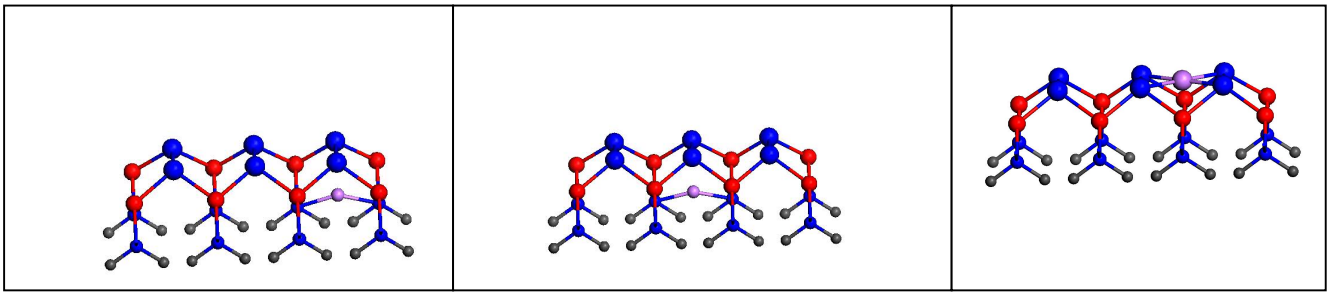

(d) (e) (f)

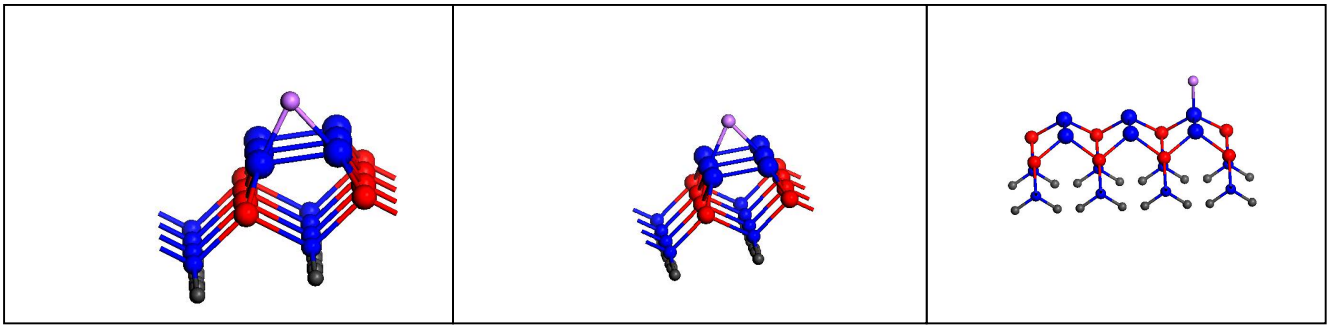

(g) (h) (i)

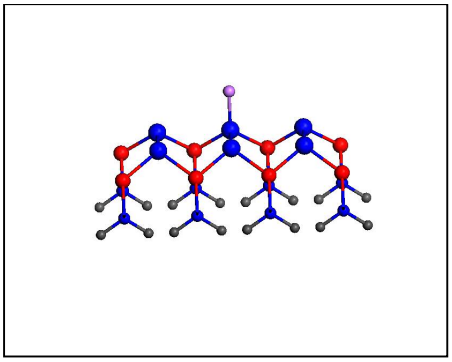

(j)

Figure 4.3 Atomic adsorption on InSb (4x2) surface in trough(a) hollow 1(b) hollow 2(c) cage 1(d) cage 2(e) cave(f) bridge 1(g) bridge 2(h) top 1(i) top 2(j) sites

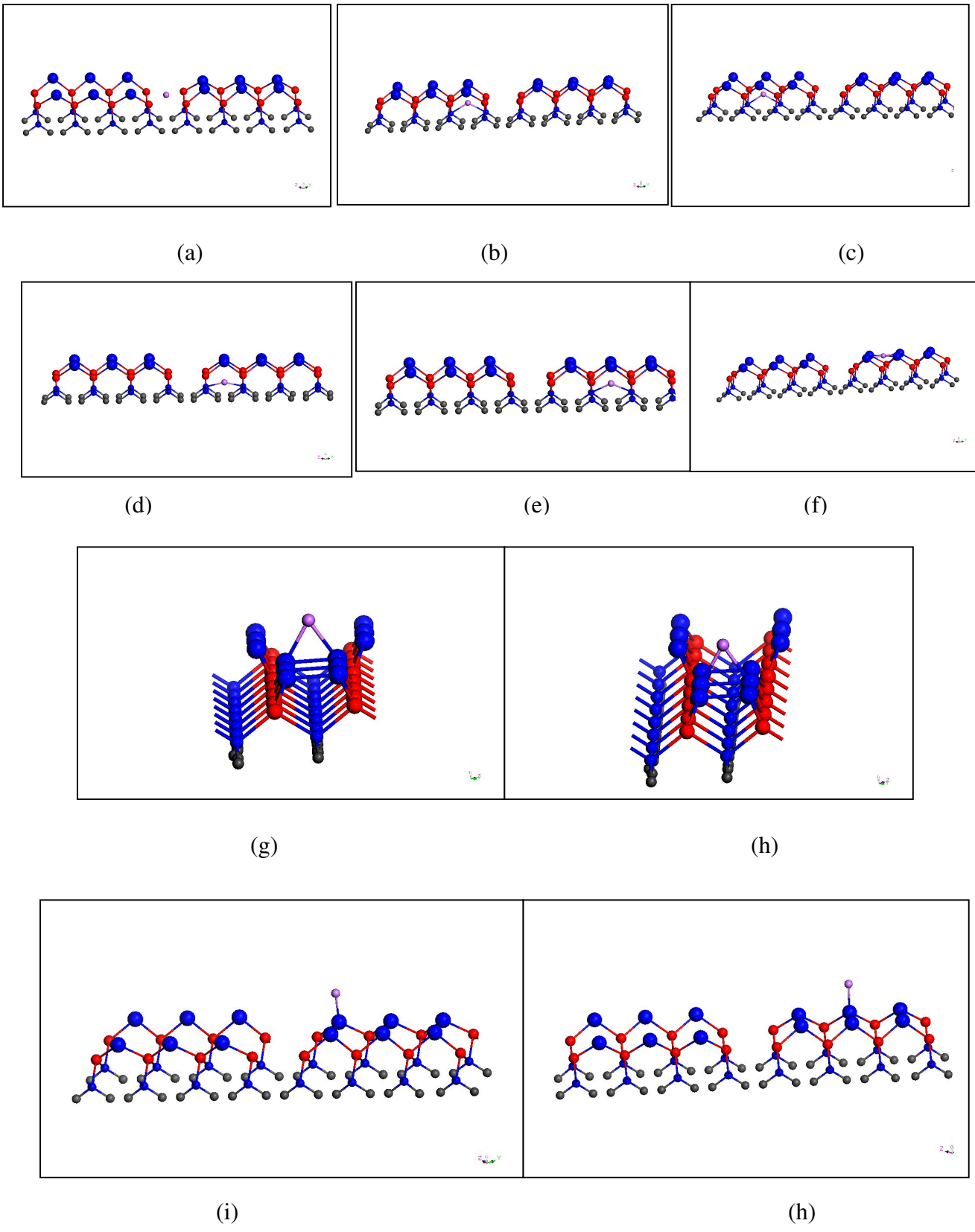

Figure 4.4 Atomic adsorption on InSb c(8x2) surface on trough(a) hollow 1(b) hollow 2(c) cage 1(d) cage 2(e) cave(f) bridge 1(g) bridge 2(h) top 1(i) top 2(j) sites

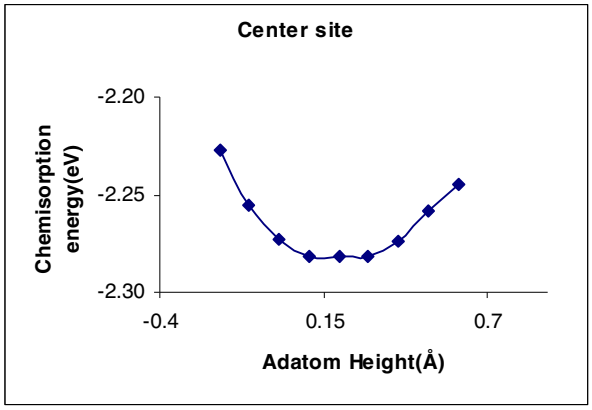

(a)

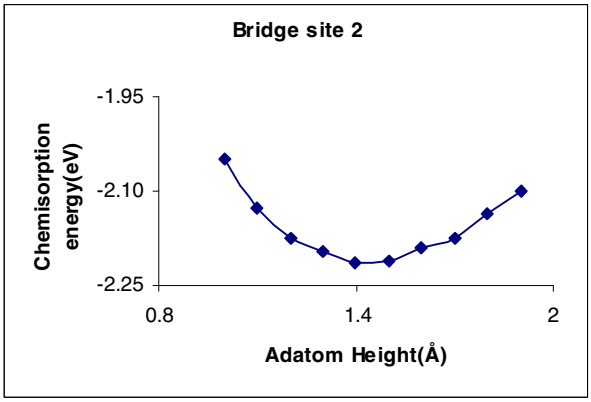

(b)

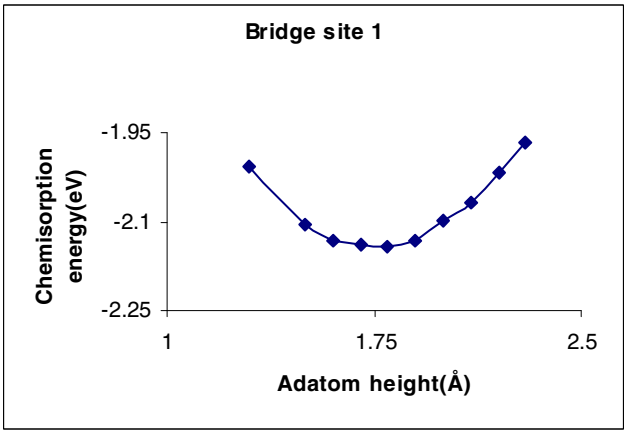

(c)

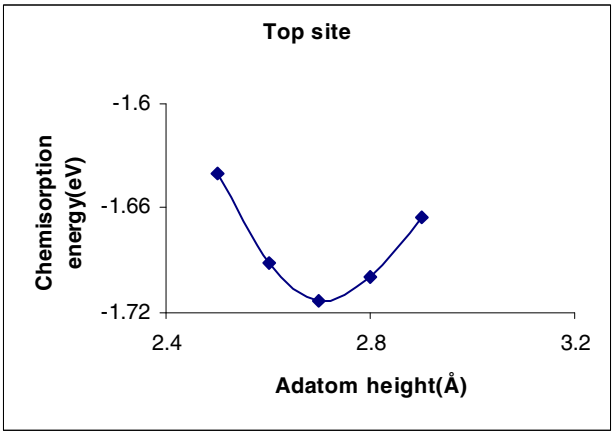

(d)

Figure 4.5 Chemisorption energy(eV) vs. adatom height(Å) for Li adsorption on the InSb(100) (1x1) surface in center(a) bridge 2(b) bridge 1(c) and top(d) sites

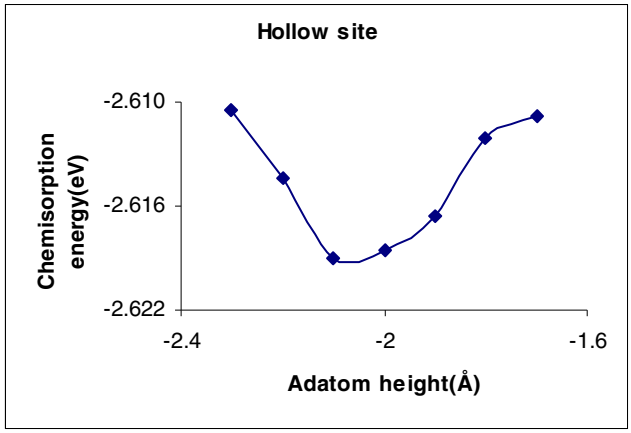

(a)

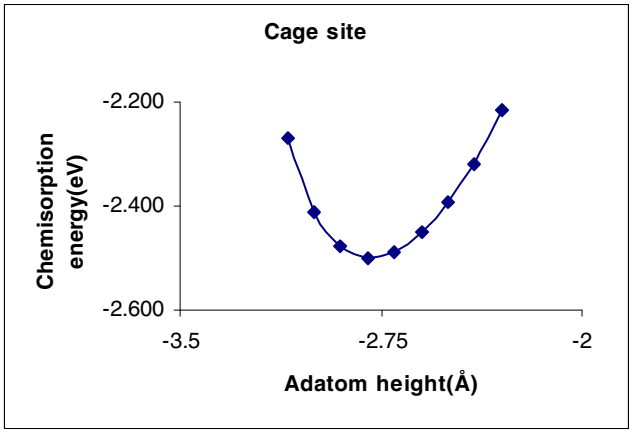

(b)

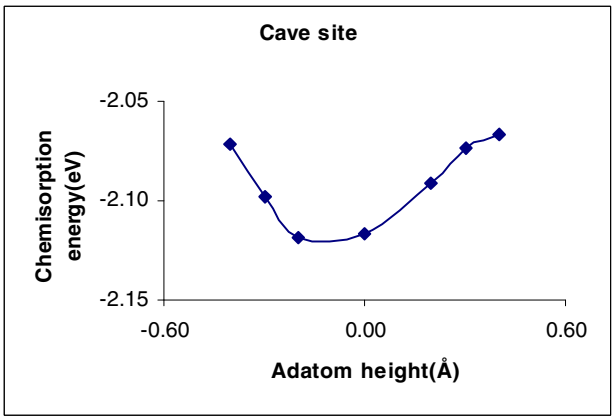

(c)

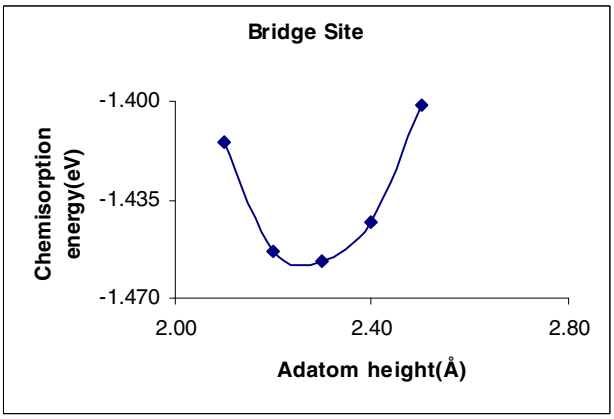

(d)

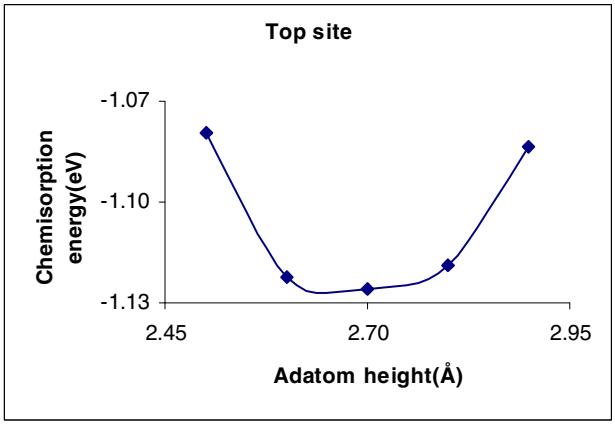

(e)

Figure 4.6 Chemisorption energy(eV) vs. adatom height (Å) for Li adsorption on the InSb(100) (2x1) surface in hollow(a) cage(b) cave(c) bridge(d) and top(e) sites

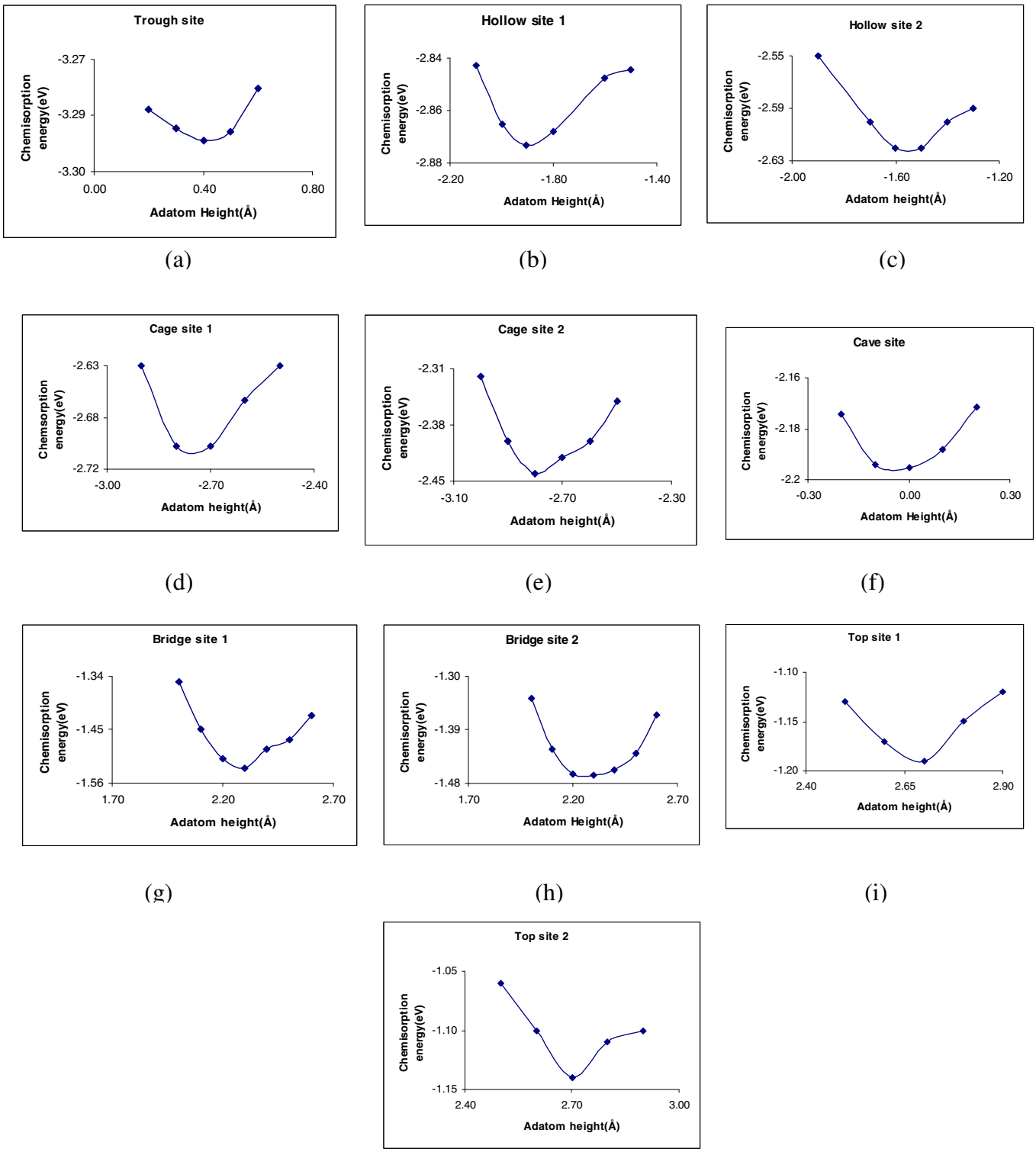

Figure 4.7 Chemisorption energy(eV) vs adatom height(Å) for Li adsorption on the InSb(100) (4x2) surface in trough(a) hollow 1(b) hollow 2(c) cage 1(d) cage 2(e) cave(f) bridge 1(g) bridge 2(h) top 1(i) and top 2(j) sites

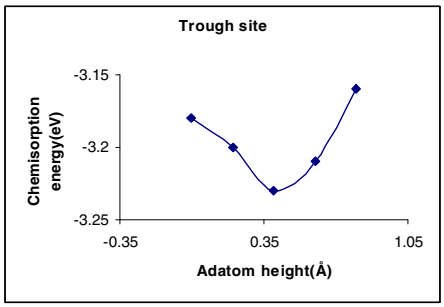

(a)

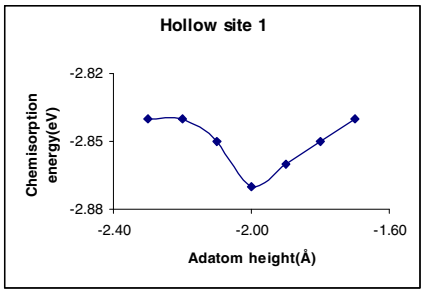

(b)

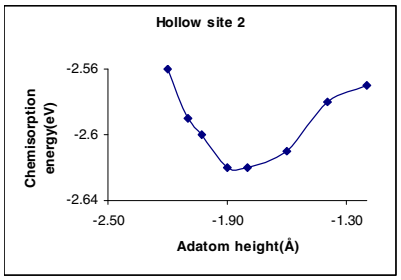

(c)

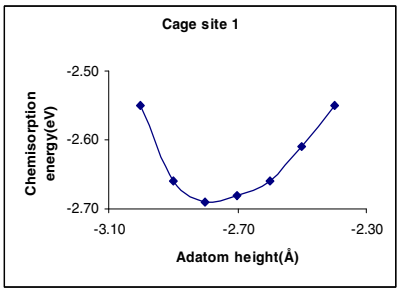

(d)

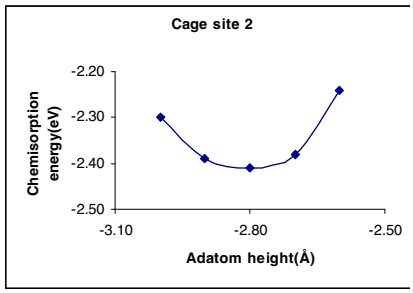

(e)

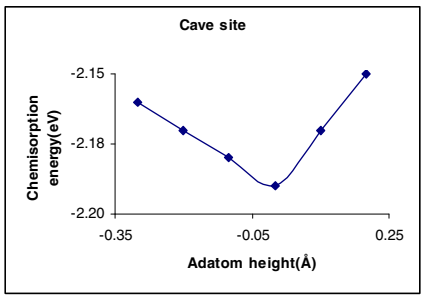

(f)

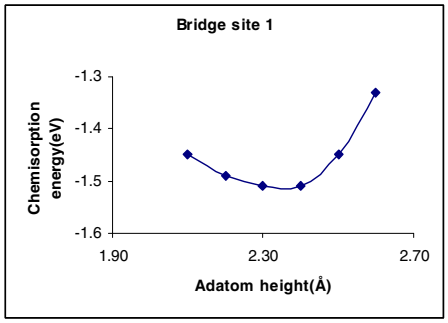

(g)

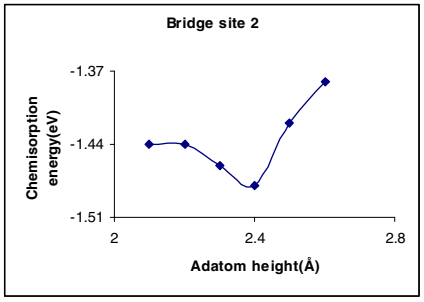

(h)

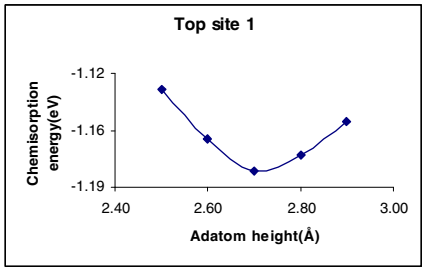

(i)

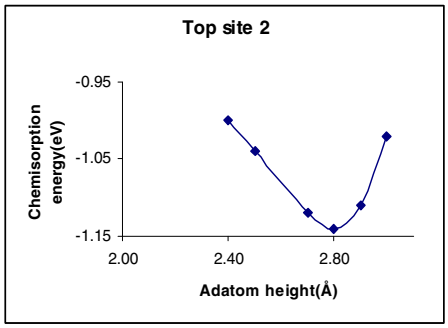

(j)

Figure 4.8 Chemisorption energy(eV) vs. adatom height(Å) for Li adsorption on the InSb(100) c(8x2) surface in trough(a) hollow 1(b) hollow 2(c) cage 1(d) cage 2(e) cave(f) bridge 1(g) bridge 2(h) top 1(i) and top 2(j) sites

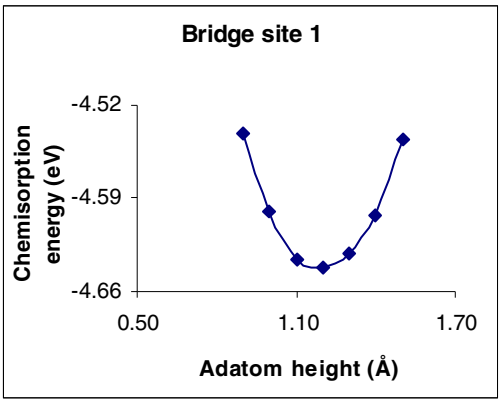

(a)

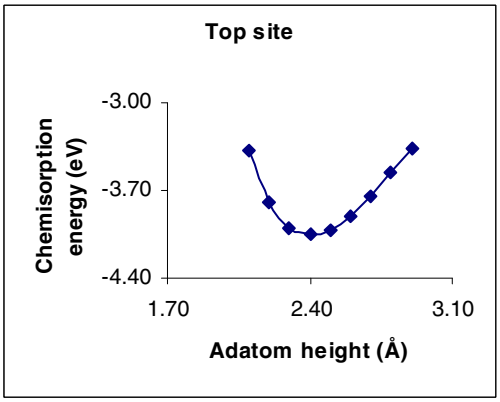

(b)

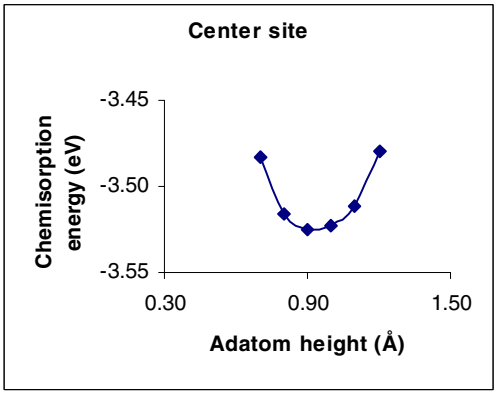

(c)

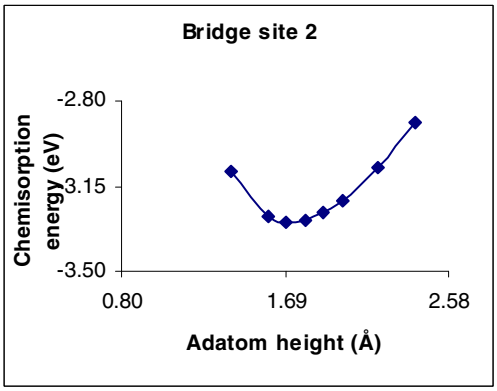

(d)

Figure 4.9 Chemisorption energy(eV) vs. adatom height(Å) for Cl adsorption on the InSb(100) (1x1) surface in bridge 1(a) top(b) center(c) and bridge 2(d) sites

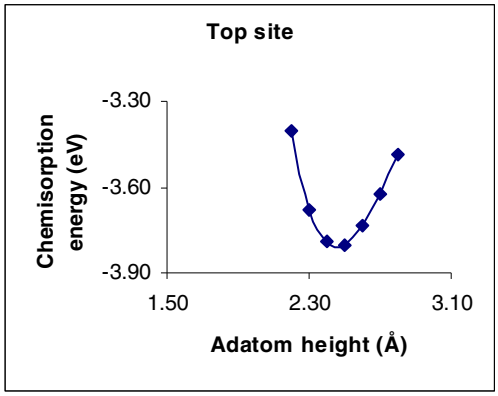

(a)

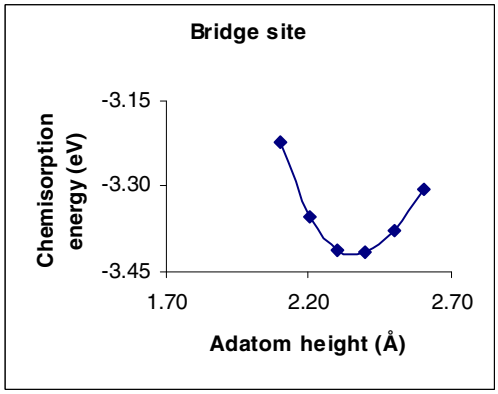

(b)

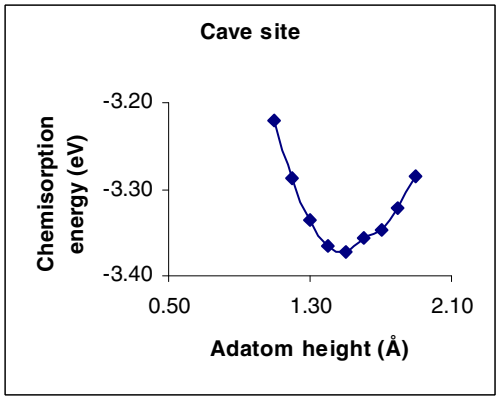

(c)

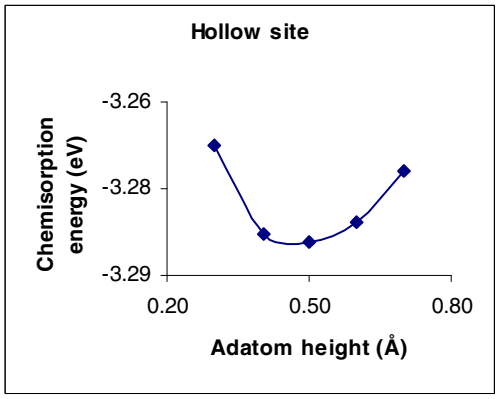

(d)

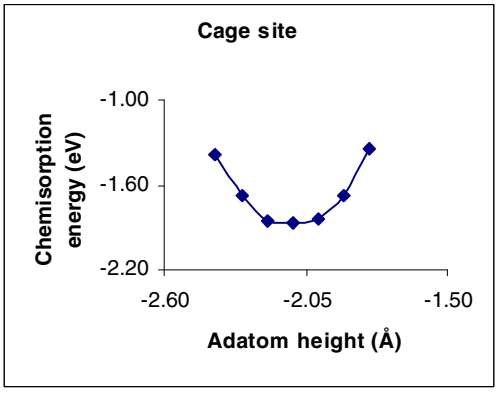

(e)

Figure 4.10 Chemisorption energy(eV) vs. adatom height(Å) for Cl adsorption on the InSb(100) (2x1) surface in top(a) bridge(b) cave(c) hollow(d) and cage(e) sites

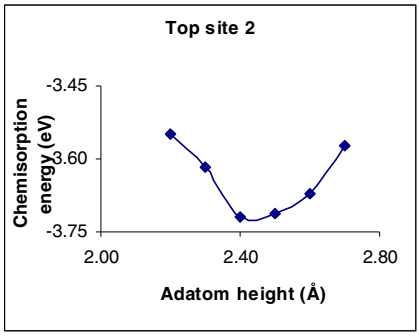

(a)

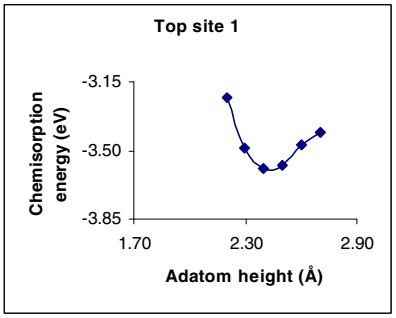

(b)

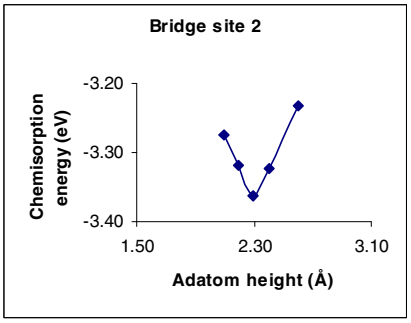

(c)

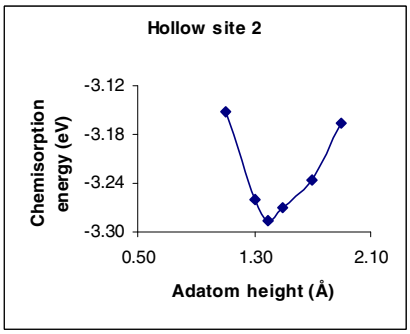

(d)

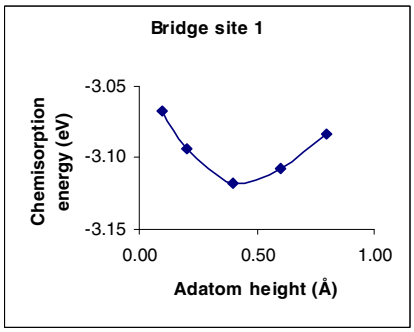

(e)

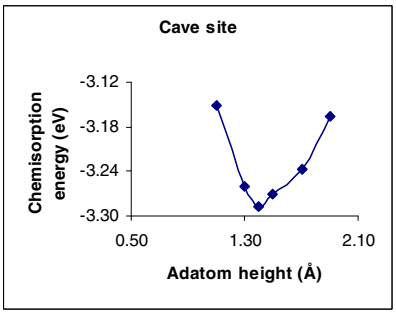

(f)

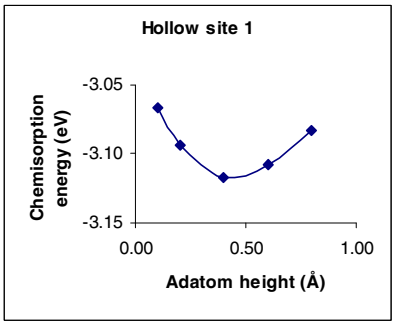

(g)

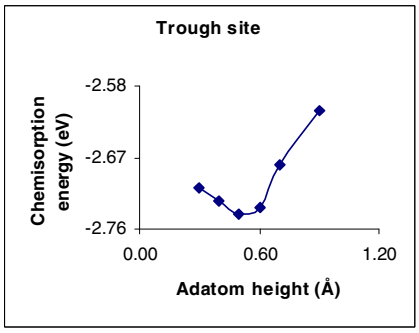

(h)

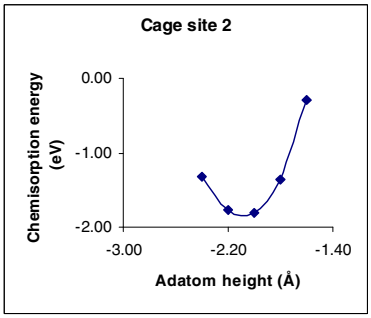

(i)

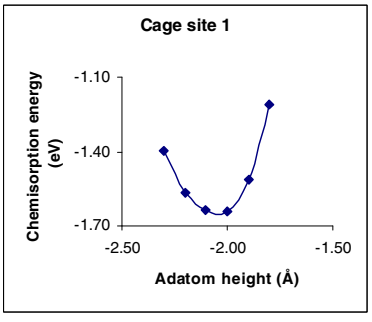

(j)

Figure 4.11 Chemisorption energy(eV) vs. adatom height(Å) for Cl adsorption on (4x2) surface in top2(a) top1(b) bridge 2(c) hollow 2(d) bridge 1(e) cave(f) hollow 1(g) trough(h) cage 2(i) and cage 1(j) sites

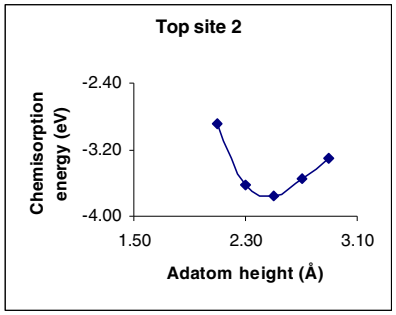

(a)

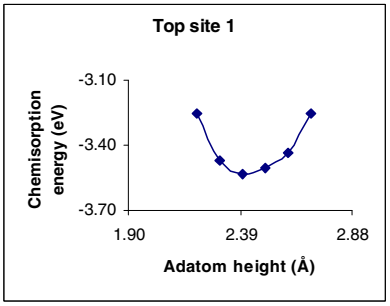

(b)

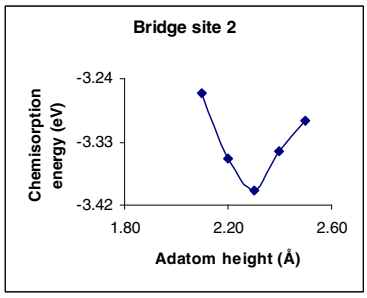

(c)

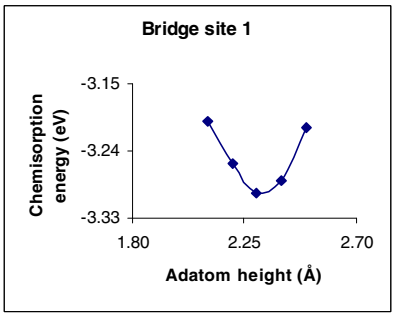

(d)

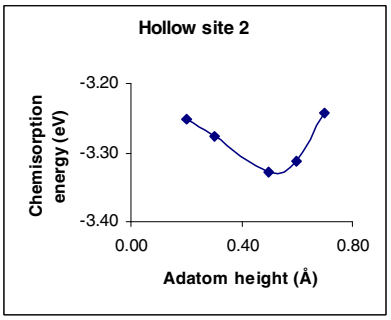

(e)

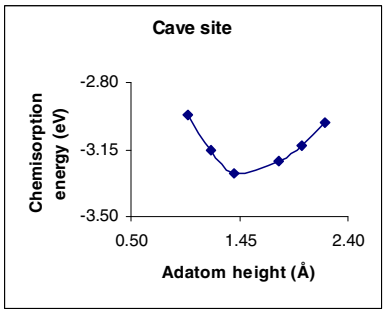

(f)

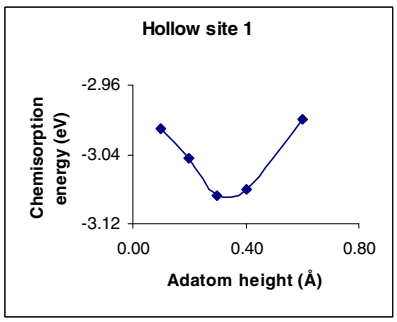

(g)

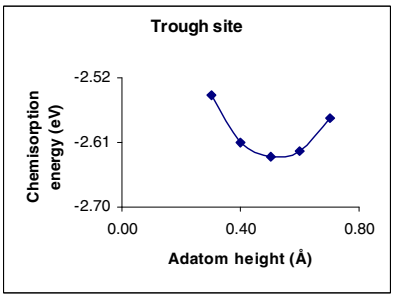

(h)

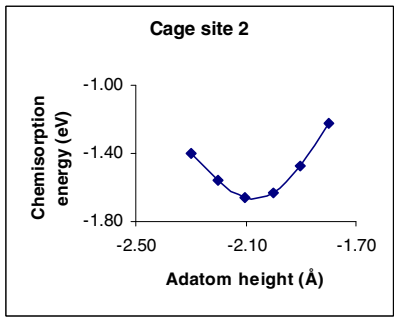

(i)

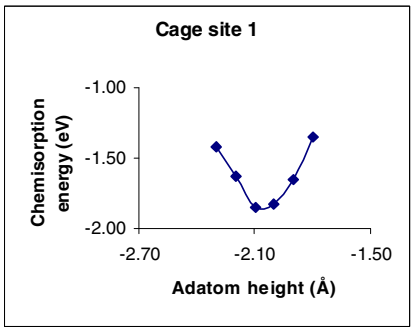

(j)

Figure 4.12 Chemisorption energy(eV) vs. adatom height(Å) for Cl adsorption on the InSb(100) c(8x2) surface in top 2(a) top 1(b) bridge 2(c) bridge 1(d) hollow 2(e) cave (f) hollow 1(g) trough (h) cage 2(i) and cage 1(j) sites

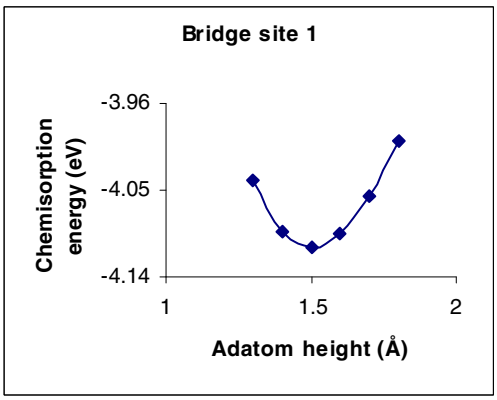

(a)

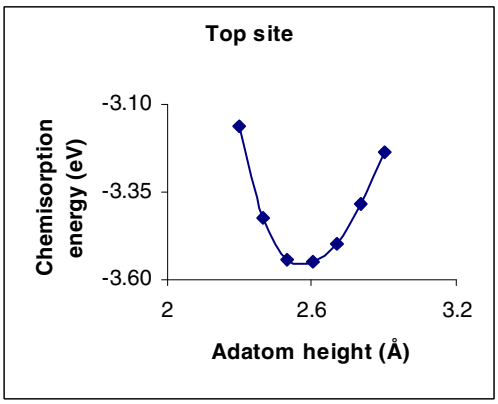

(b)

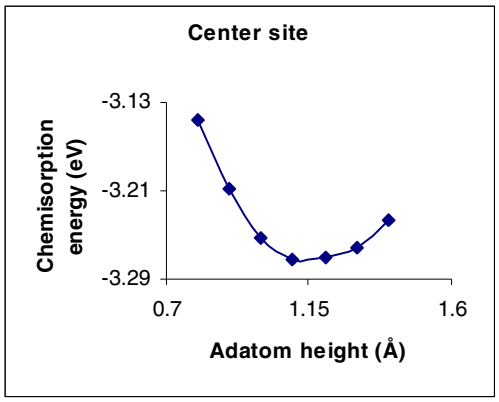

(c)

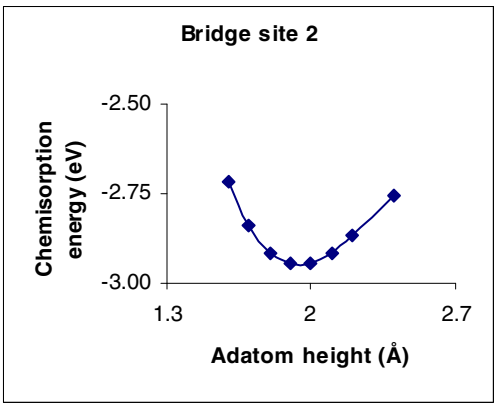

(d)

Figure 4.13 Chemisorption energy(eV) vs. adatom height(Å) for Br adsorption on the InSb(100) (1x1) surface in bridge 1(a) top(b) center(c) and bridge 2(d) sites

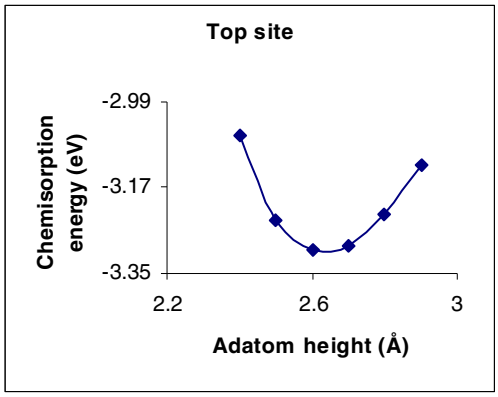

(a)

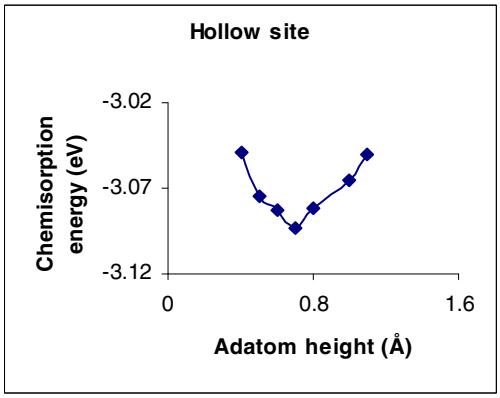

(b)

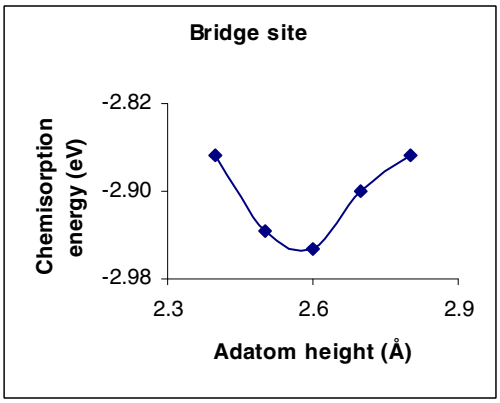

(c)

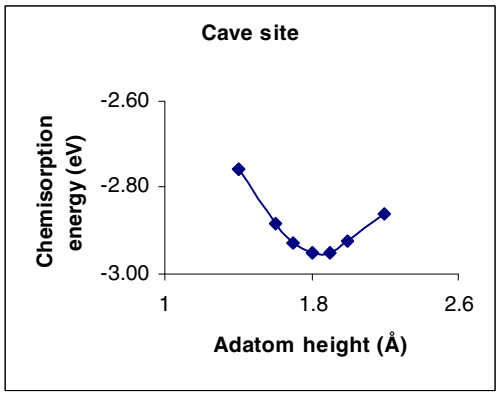

(d)

Figure 4.14 Chemisorption energy(eV) vs. adatom height(Å) for Br adsorption on the InSb(100) (2x1) surface in top(a) hollow(b) bridge(c) and cave(d) sites

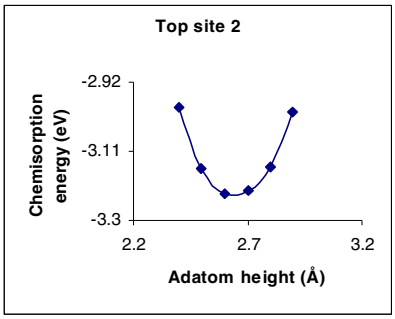

(a)

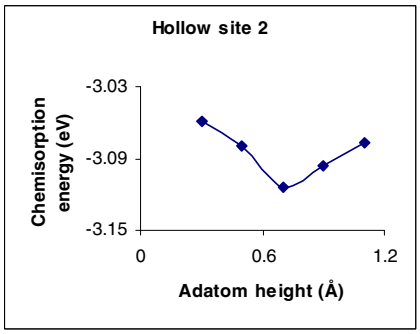

(b)

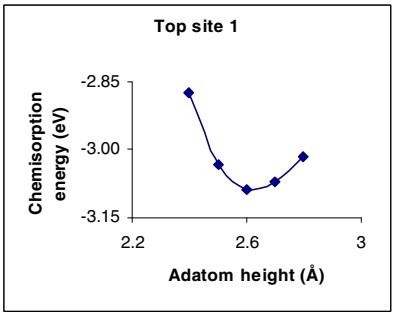

(c)

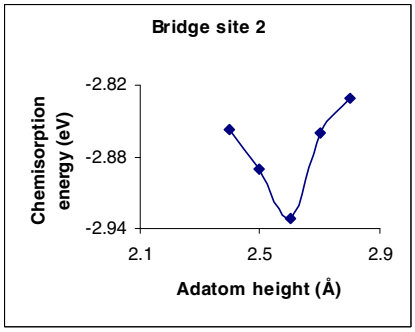

(d)

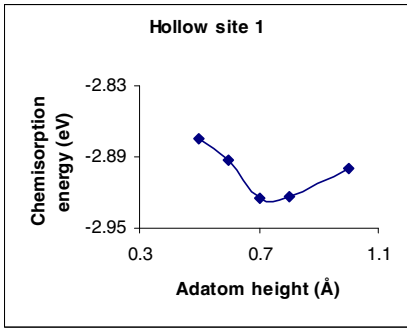

(e)

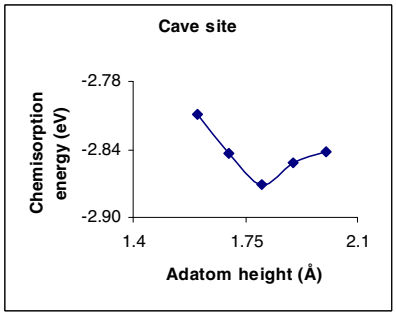

(f)

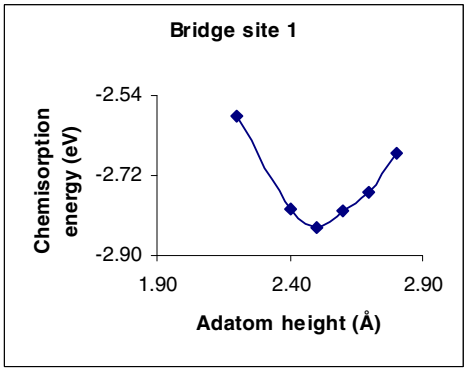

(g)

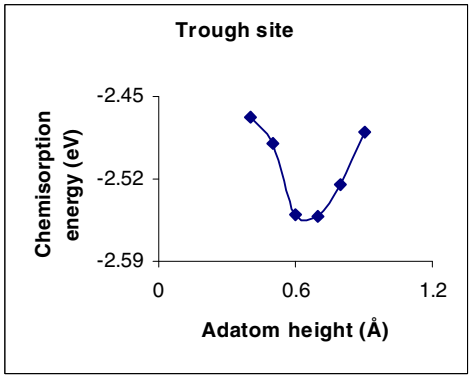

(h)

Figure 4.15 Chemisorption energy(eV) vs. adatom height(Å) for Br adsorption on the InSb(100) (4x2) surface in top 2(a) hollow 2(b) top 1(c) bridge 2(d) hollow 1(e) cave(f) bridge 1(g) and trough(h) sites

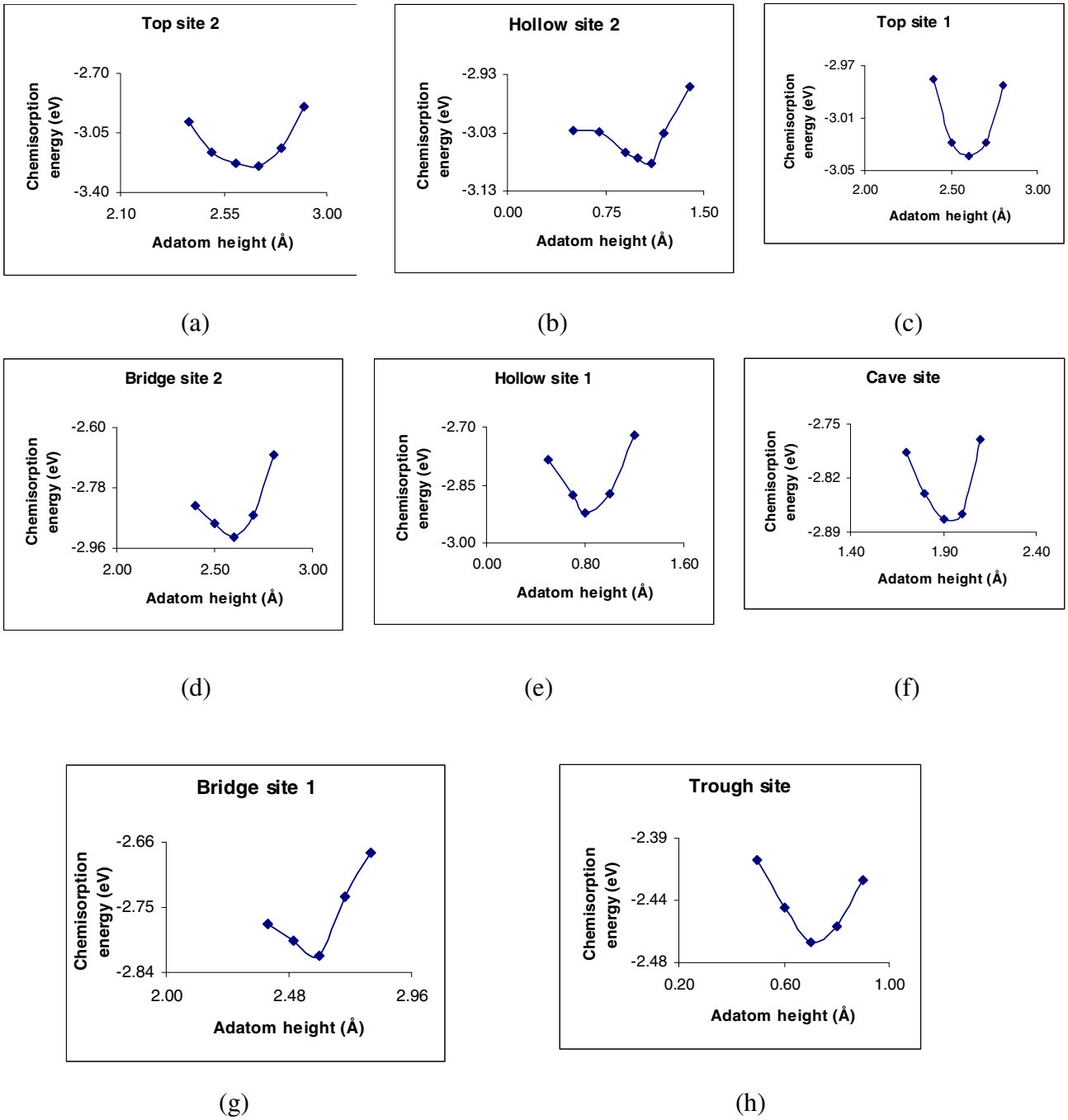

Figure 4.16 Chemisorption energy(eV) vs. adatom height(Å) for Br adsorption on the InSb(100) c(8x2) surface in top 2(a) hollow 2(b) top 1(c) bridge 2(d) hollow 1(e) cave(f) bridge 1(g) and trough(h) sites

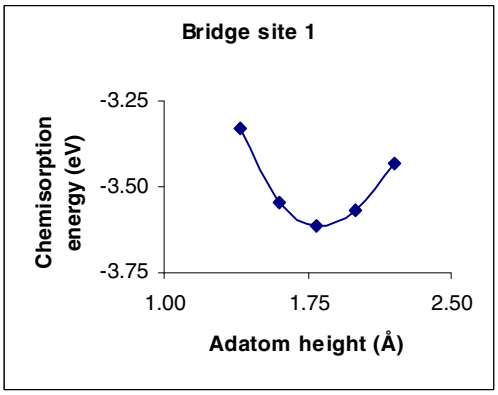

(a)

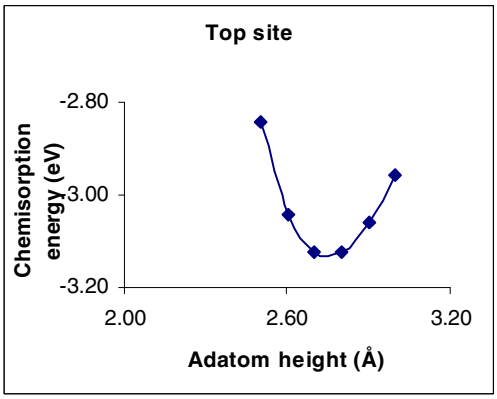

(b)

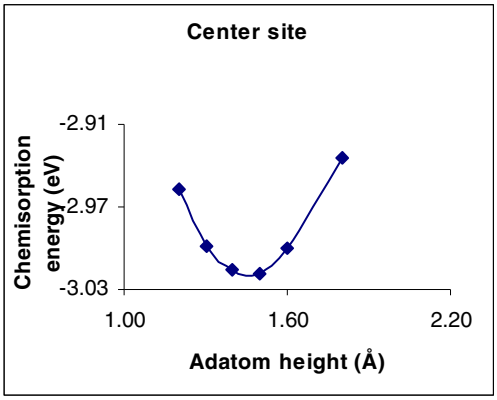

(c)

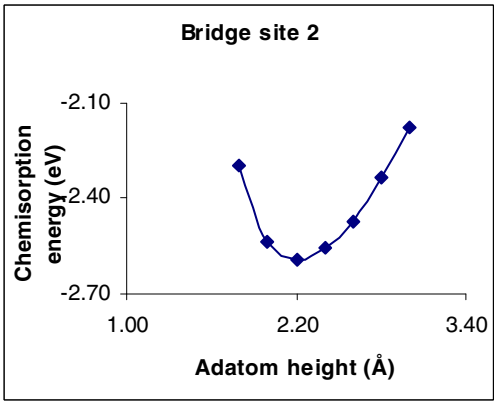

(d)

Figure 4.17 Chemisorption energy(eV) vs. adatom height(Å) for I adsorption on the InSb(100) (1x1) surface in bridge 1(a) top(b) center(c) and bridge 2(d) sites

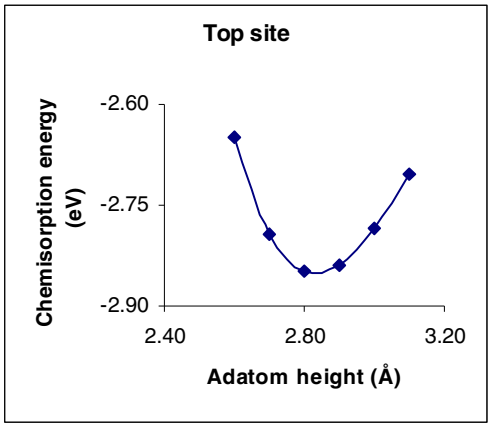

(a)

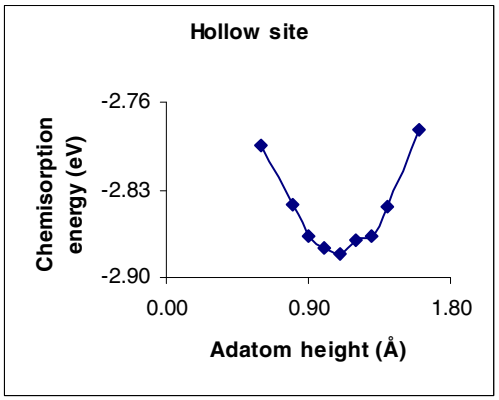

(b)

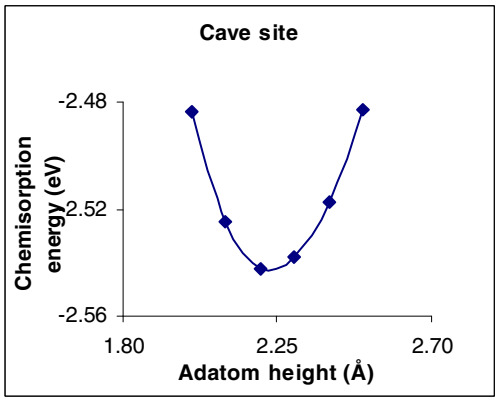

(c)

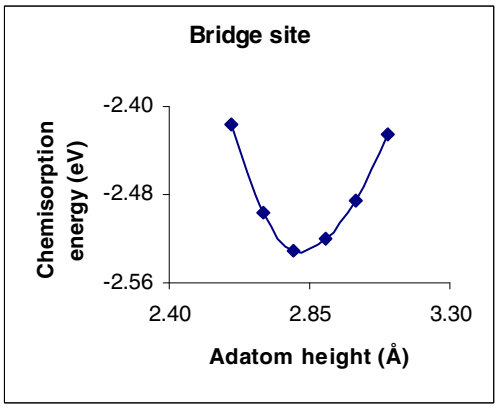

(d)

Figure 4.18 Chemisorption energy(eV) vs. adatom height(Å) for I adsorption on the InSb(100) (2x1) surface in top(a) hollow(b) cave(c) and bridge(d) sites

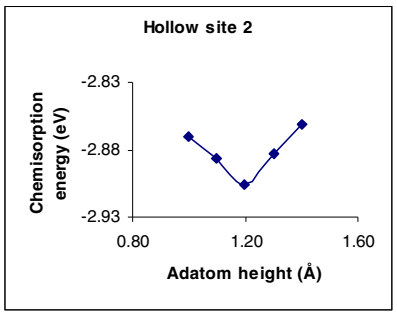

(a)

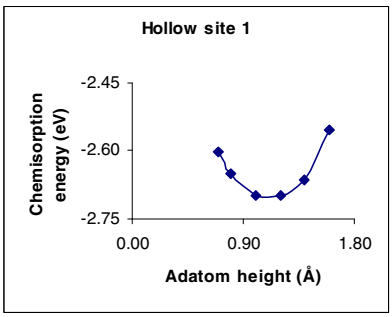

(b)

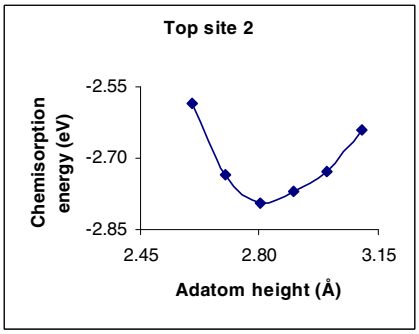

(c)

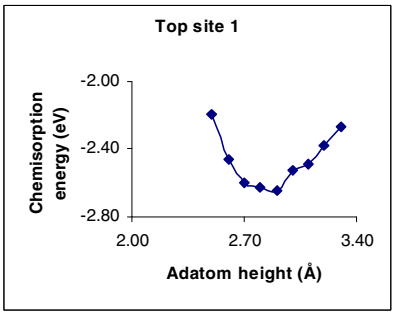

(d)

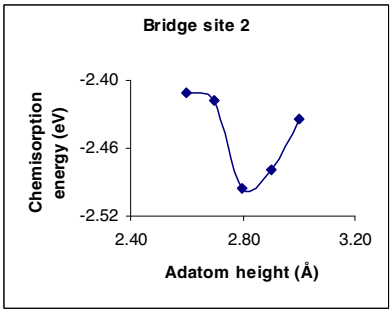

(e)

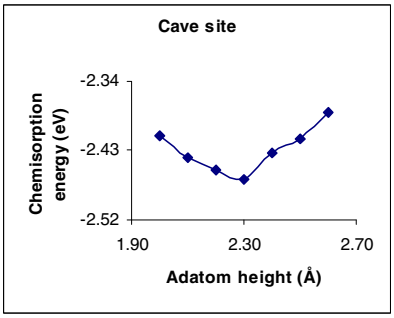

(f)

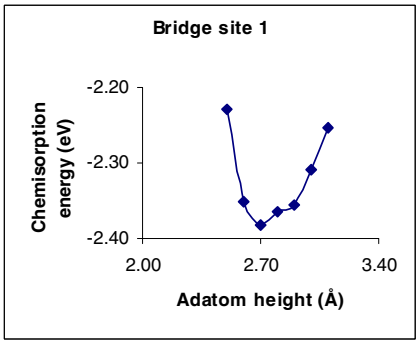

(g)

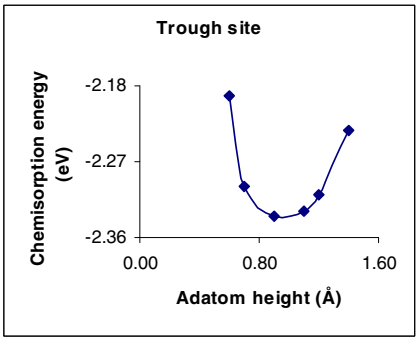

(h)

Figure 4.19 Chemisorption energy(eV) vs. adatom height(Å) for I adsorption on the InSb(100) (4x2) surface in hollow 2(a) hollow 1(b) top 2(c) top 1(d) bridge 2(e) cave(f) bridge 1(g) and trough(h) sites

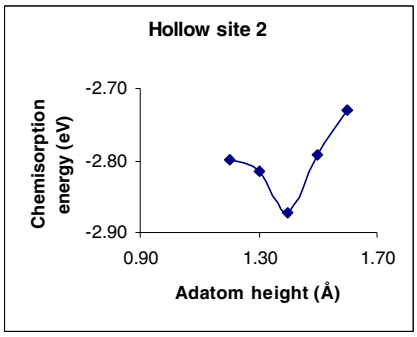

(a)

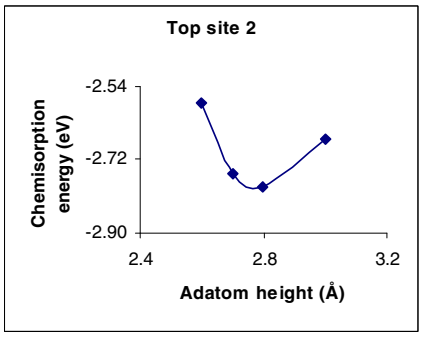

(b)

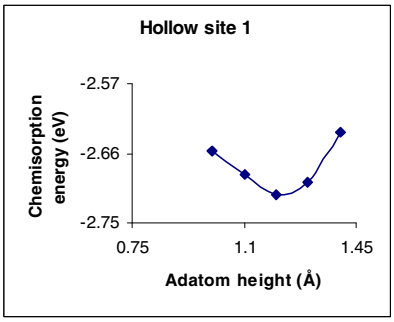

(c)

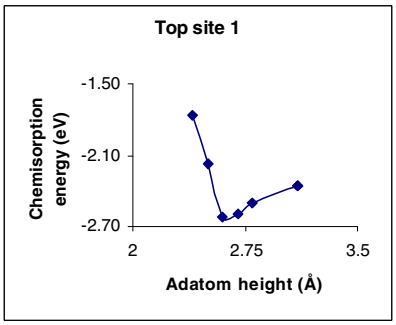

(d)

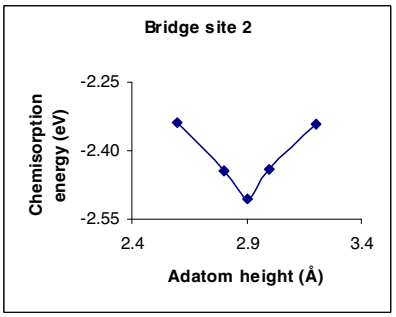

(e)

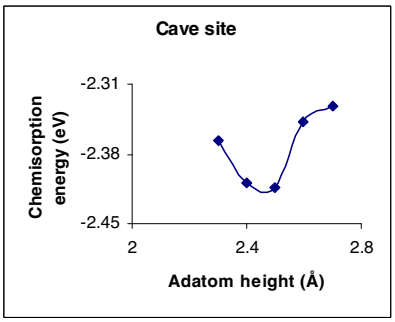

(f)

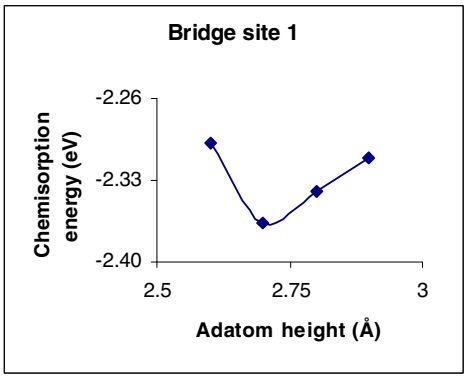

(g)

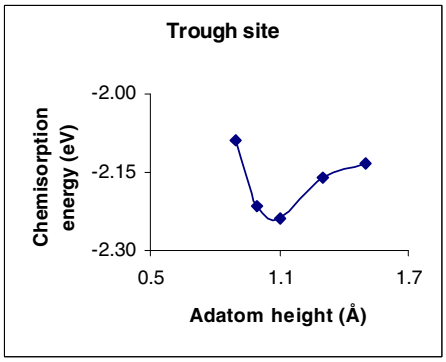

(h)

Figure 4.20 Chemisorption energy(eV) vs. adatom height(Å) for the I adsorption on the InSb(100) c(8x2) surface in hollow 2(a) hollow 1(b) top 2(c) top 1(d) bridge 2(e) cave(f) bridge 1(g) and trough(h) sites

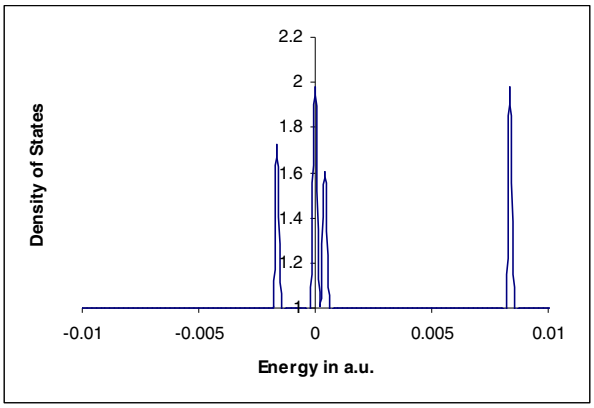

(a)

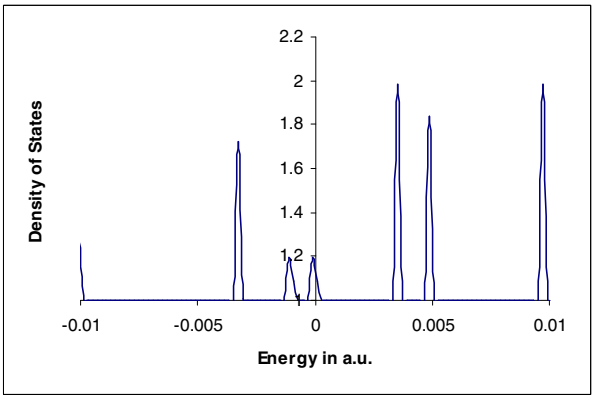

(b)

Figure 4.21 DOS Plot for (2x1) surface before(a) and after(b) lithium adsorption

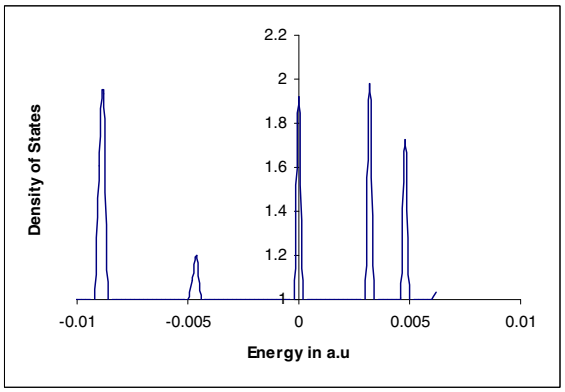

(a)

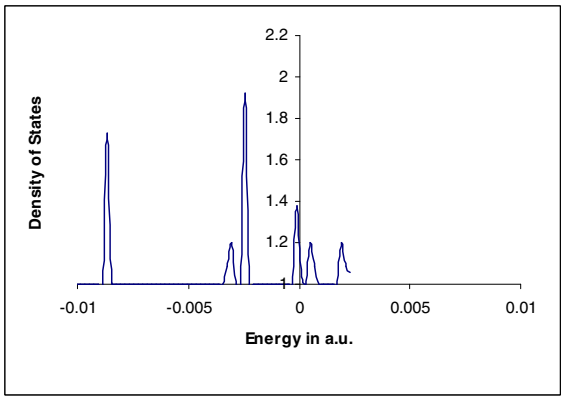

(b)

Figure 4.22 DOS plot for c(8x2) surface before(a) and after lithium adsorption(b)

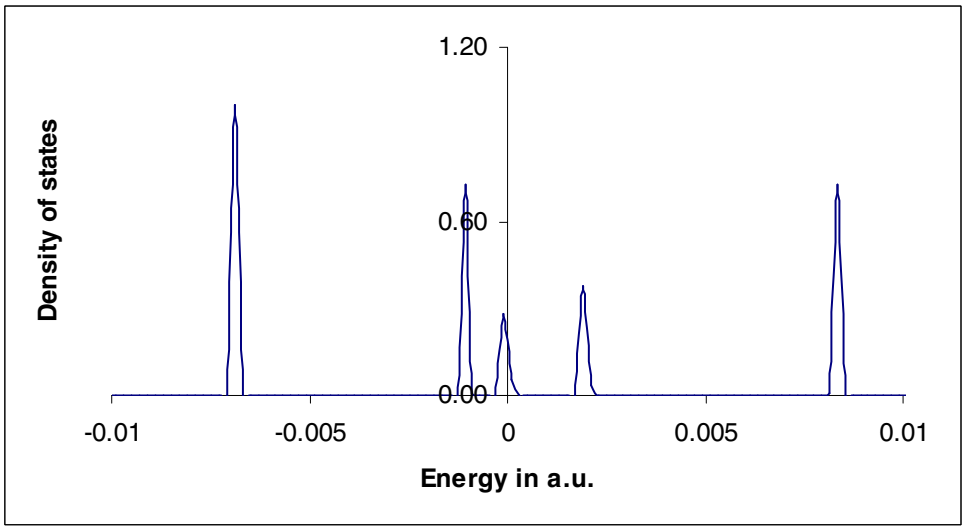

(a)

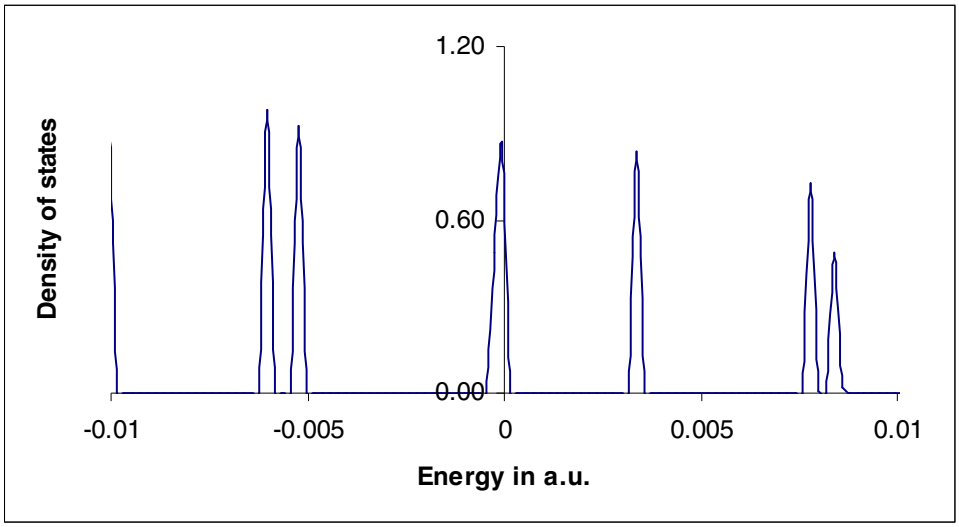

(b)

Figure 4.23 DOS plot for (1x1) surface before(a) and after(b) Cl adsorption

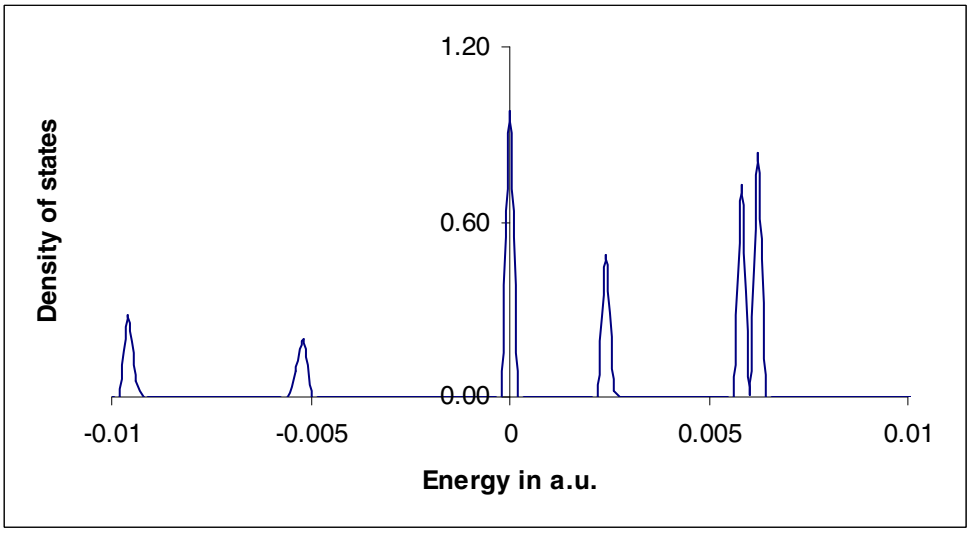

(a)

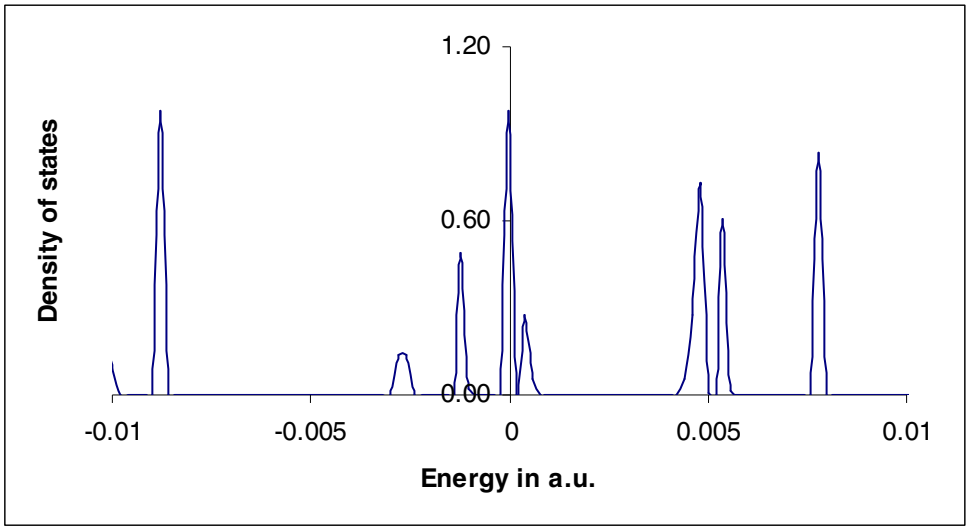

(b)

Figure 4.24 DOS plot for (4x2) surface before(a) and after(b)Cl adsorption

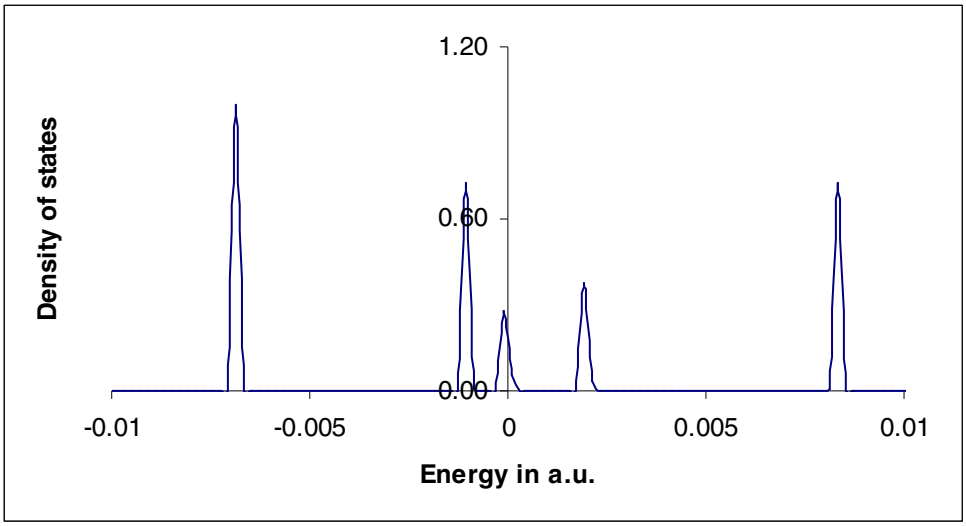

(a)

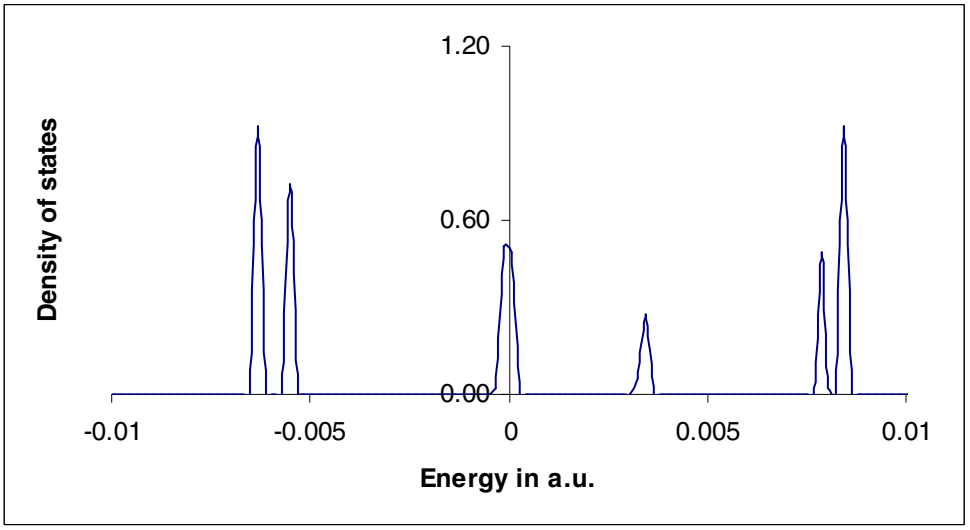

(b)

Figure 4.25 DOS plot for (1x1) surface before(a) and after(b) I adsorption

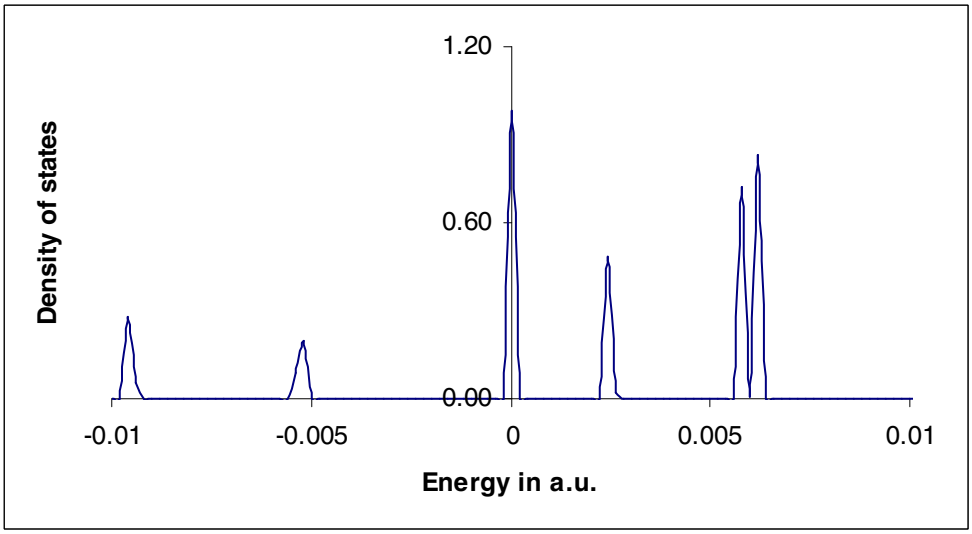

(a)

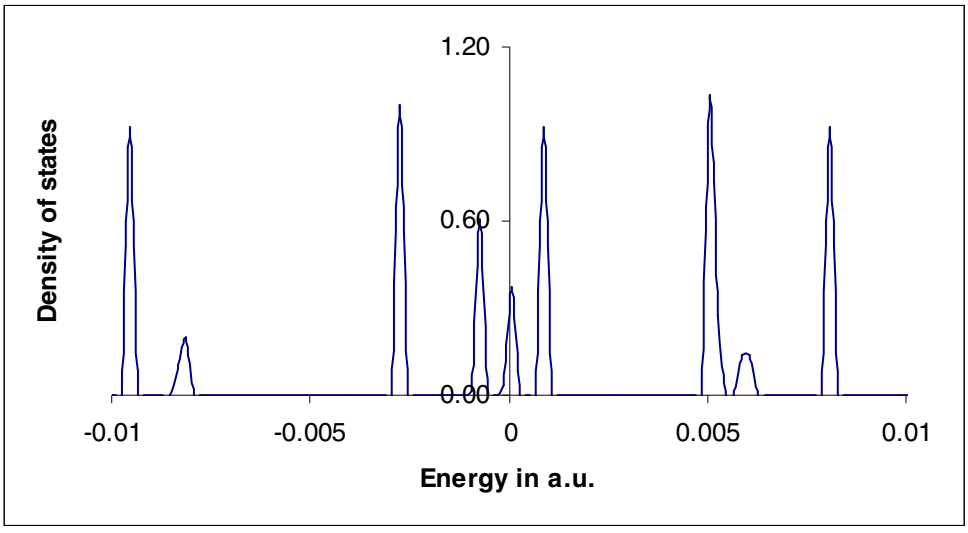

(b)

Figure 4.26 DOS plot for (4x2) surface before(a) and after(b) I adsorption

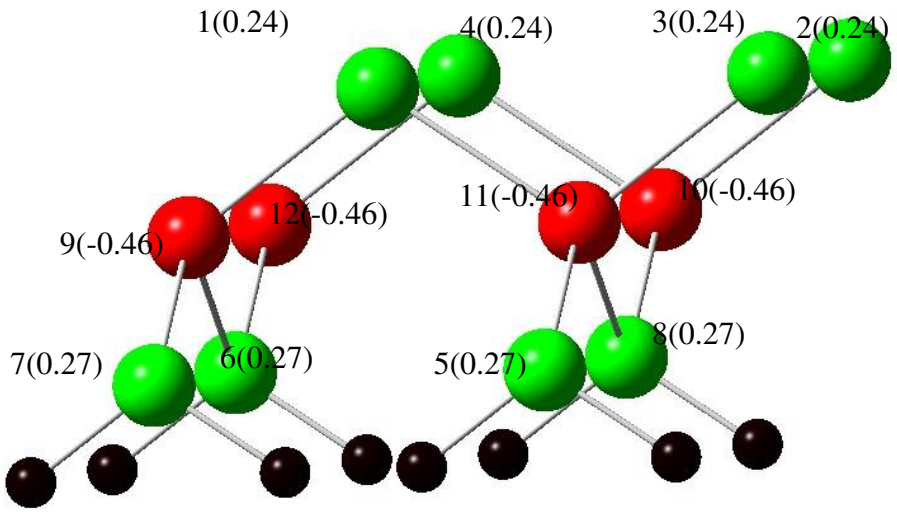

Figure 4.27 Atomic charge distribution of bare (1x1) surface

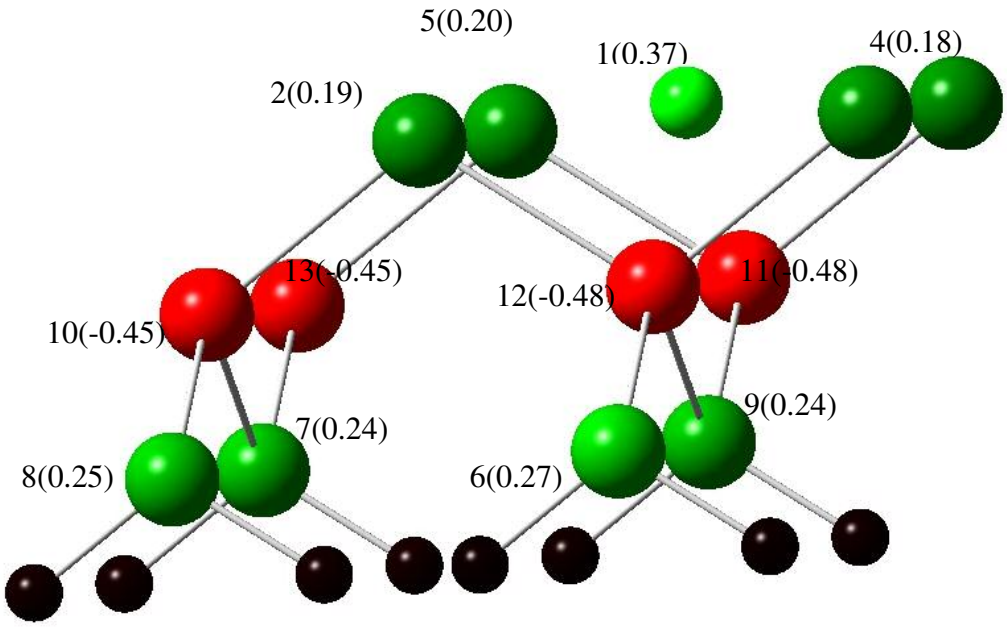

Figure 4.28 Atomic charge distribution of Li adsorbed (1x1) surface

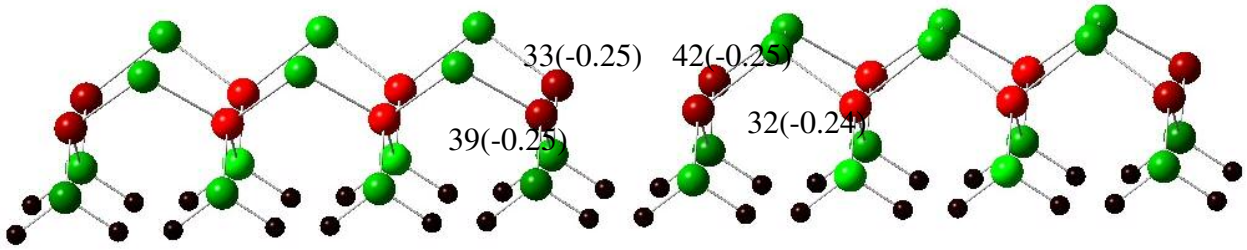

Figure 4.29 Atomic charge Distribution of bare c(8x2) surface

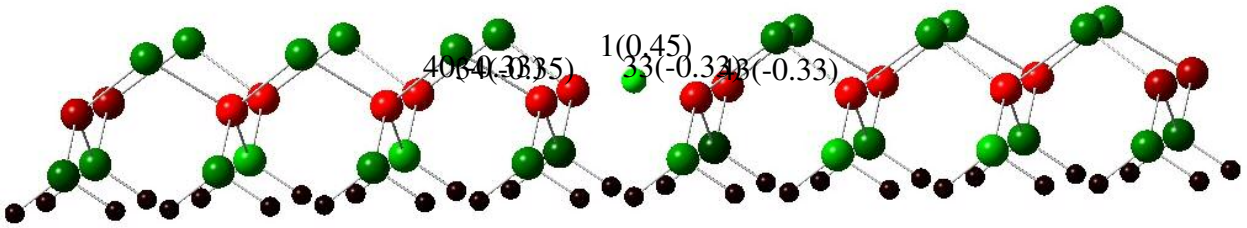

Figure 4.30 Atomic change Distribution of Li adsorbed c(8x2) surface

In all these atomic charge distribution figures, the bright red color represents the highest amount of charge gained by the particular atom and the bright green color represents the highest amount of charge gained by a particular atom.

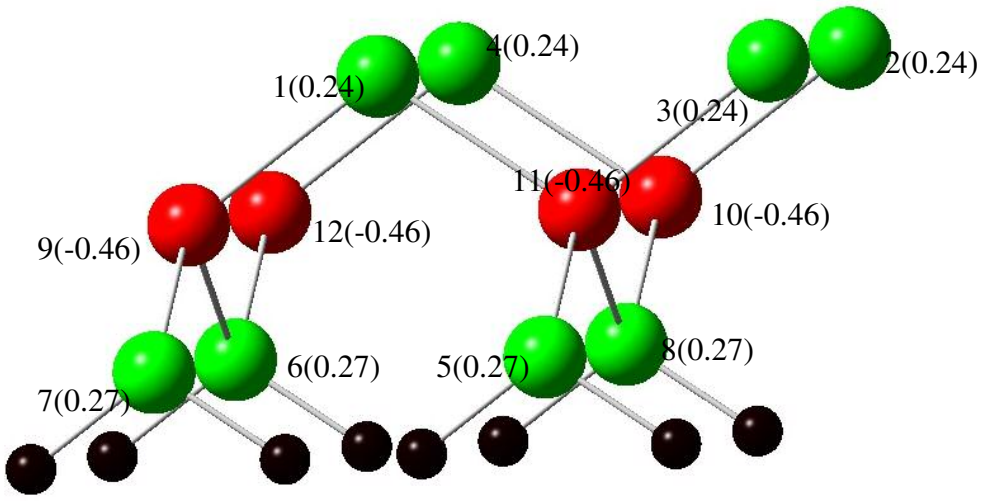

Figure 4.31 Atomic charge distribution of bare (1x1) surface

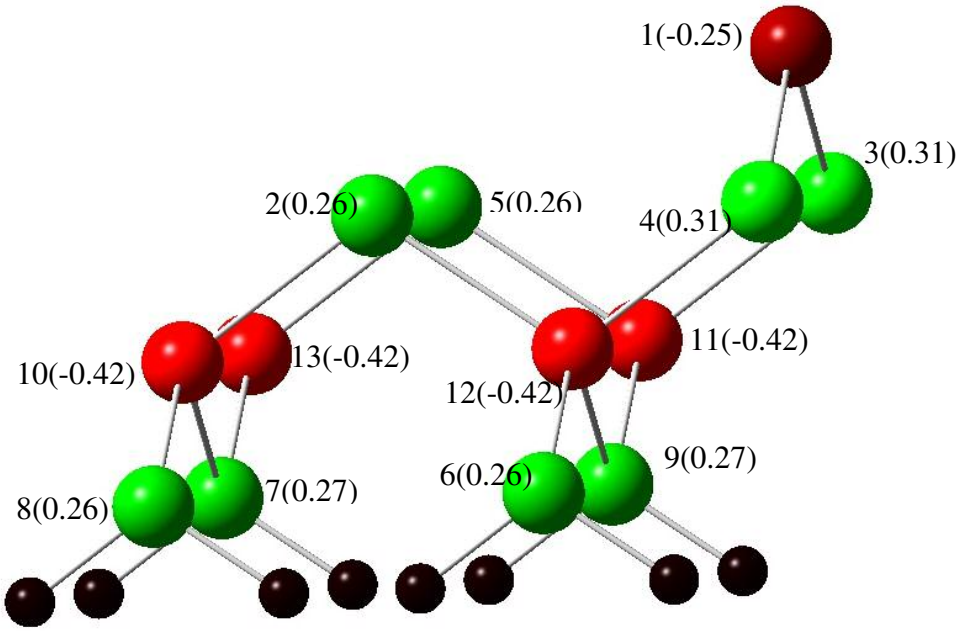

Figure 4.32 Atomic charge distribution of I adsorbed (1x1) surface

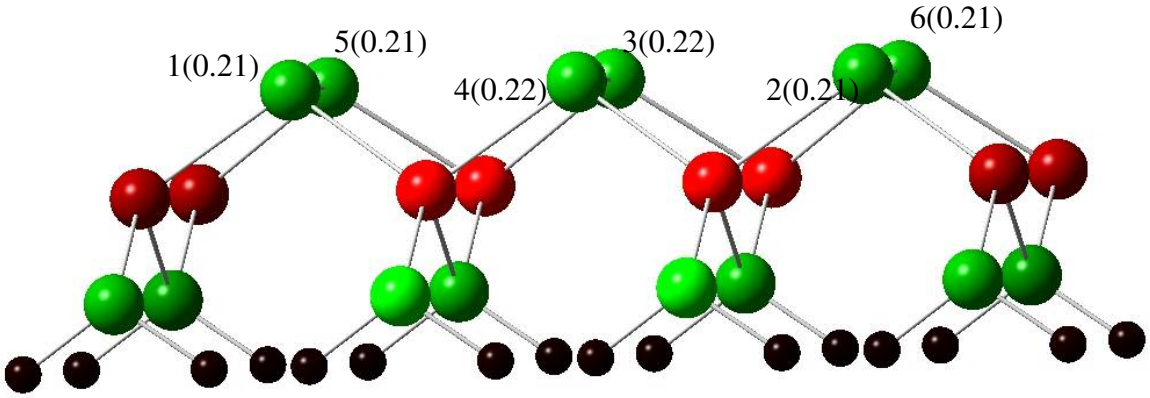

Figure 4.33 Atomic charge distribution of bare (4x2) surface

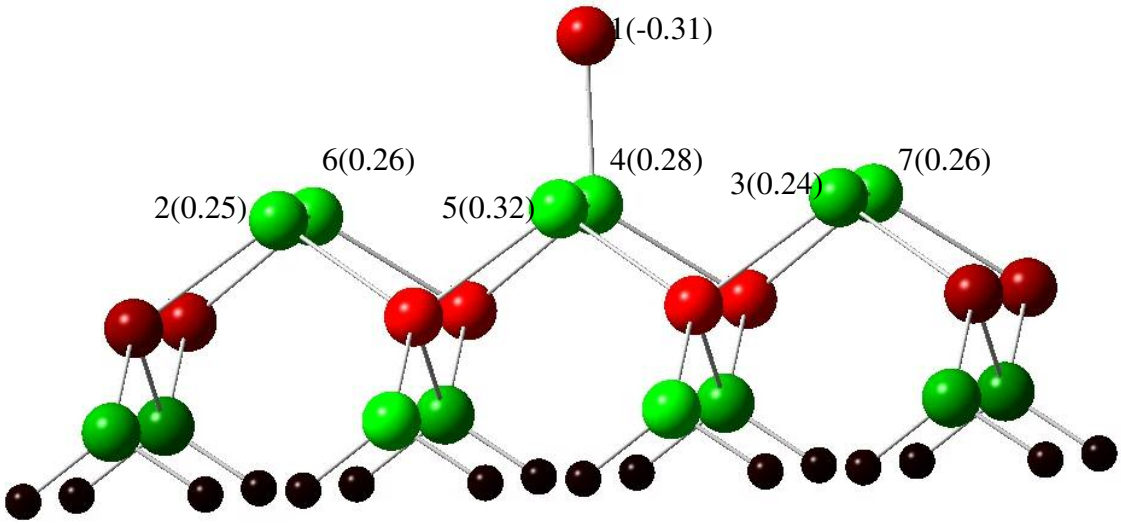

Figure 4.34 Atomic charge distribution of I adsorbed (4x2) surface

CHAPTER 5

MOLECULAR AND DISSOCIATIVE ADSORPTIONS OF I_2 ON InSb (4x2) SURFACE

5.1 Results and Discussions of Molecular Adsorption

Our atomic adsorption results of Li, Cl, Br and I on the (4x2) and c(8x2) unit cells were similar for the different comparable sites. Hence, the (4x2) surface of In-rich InSb(100) surface has been used to study the molecular halogen (I_2) reactions with the InSb(100) surface. In this molecular adsorption study, one I_2 molecule was chemisorbed on the unit cell of (4x2) surface in different symmetrical sites. For each of these positions, several approaches of chemisorptions were considered. They are i) I_2 molecular approaches vertically to the surface (vertical approach); ii) I_2 molecule approaching at an angle of 45˚ to the surface (angular approach); iii) I_2 molecule is parallel to the surface, but when the I_2 molecule comes parallel to the surface at Bridge site 1, Hollow site 1, Cave site and Top site 1, the atmosphere that this molecule sees is different due to the arrangement of the first layer of In atoms in the (4x2) surface; because of this it can approach in horizontal approach 1; and also in iv) horizontal approach 2; v) I_2 molecule parallel to the surface and have an angle of 45˚ with the x-axis. Hence considering the above described different approaches, it is obvious that for all of the horizontal approach positions, the iodine atoms of the I_2 molecule are at the same distance from the InSb surface, whereas for the vertical and angular approaches, one of the iodine atoms is closer to the surface than the other. For these I_2 adsorption calculations, one d function was added to the associated basis sets of

Hay-Wadt pseudopotentials of In, Sb and I for better performance during these molecular calculations. The chemisorption energies are calculated from the formula

$$E_c = E(In_{14}Sb_8H_{16}) + E(I_2) - E(In_{14}Sb_8H_{16}I_2)$$

Where $E(In_{14}Sb_8H_{16}I_2)$ is the total energy of the I_2 adsorbed (4x2) surface of InSb and $E(In_{14}Sb_8H_{16})$ is the total energy of the (4x2) surface and $E(I_2)$ is the total energy of the iodine dimer with the dimer bondlength of iodine fixed at the optimized value of 2.70 Angstroms. Hence during the molecular adsorption of I_2 on the (4x2) surface of InSb, the distance between the two iodine atoms is fixed at the optimized dimer bondlength found.

The sites considered for the I_2 molecular adsorption on the (4x2) surface in each of the five different approaches are described in the figures 5.1-5.5. These eight different symmetric sites are similar to the ones described for the atomic adsorption on the (4x2) surface as described in chapter 4. The results for the molecular adsorption of I_2 on the (4x2) surface for the vertical, angular, horizontal 1, horizontal 2 and horizontal 3 approaches are shown in the tables 5.1-5.5 respectively. The graphs concerning these molecular adsorptions are shown in the figures 5.11-5.15.

During the I_2 molecular adsorption in the vertical approach, bridge site 1 was found to be the most preferred site and trough site was found to be the least favored. In all the other approaches, such as, angular, horizontal 1 and horizontal 2, hollow site 2 was found to be the most preferred site. Also in horizontal approach 3, after cave site, hollow site 2 was found to be the most preferred site. During the angular approach, top site 1 was found to be the least favored site. On the other hand, in the horizontal approaches, bridge site 1 was found to be the least favored.

As compared to the atomic adsorption of I on the (4x2) surface discussed in chapter 4, where the adatom was found to lie 0.77 Å beneath the top layer of In atoms, during the molecular adsorption of I_2 in the trough site, it was found that the adatom was at 0.2 Å above the surface during vertical approach, 0.2 Å beneath the surface for the angular approach, 1.8 Å above the surface for horizontal approach 1 and 1.3 Å above the surface for the horizontal approach 3. This can be accounted for considering the size of the molecule and hence it stays above the surface.

Coming to the analysis of the atomic charge distributions, it was found that the charge distribution among the two atoms of the I_2 molecule was highly unsymmetrical, as seen from table 5.11, for the molecular adsorption in different sites during vertical approach. It was particularly noted that the Iodine atom that lies far away from the surface gains more charges as compared to the other Iodine atom that lies closer to the surface. A similar unsymmetrical charge distribution among the two iodine atoms was observed in case of molecular adsorption in all the sites for angular approach also, though the distribution was not as unsymmetrical as that of vertical approach. This is because of the fact that the second iodine atom is slightly more exposed to the surface in case of angular approach as compared to the vertical approach in all sites. The charge distribution between the two iodine atoms was found to be more symmetric in all sites during the molecular adsorption of I_2 in all the horizontal approaches as compared to the vertical approach or the angular approach. But, in the horizontal approaches, depending upon what site we are looking at, it was noted that the iodine atom that is closer to any of the atoms on the surface always gains slightly less charge than the other iodine atom that it is bonded to.

One other thing that was noted during the molecular adsorption study is that during the molecular adsorption of I_2 in any approach, it was found that the charges gained by the two

iodine atoms in the most favored site is always greater than that gained in the least favored site. This is seen from the mulliken charge distribution tables shown in tables 5.11-5.15.

The band gap of the (4x2) surface after I_2 adsorption in vertical approach was found to increase in the case of bridge sites 1 and 2 as well as in the hollow site 2. And in the case of bridge site 1, the increase was significantly high that the band gap of the system almost approached the value of bulk InSb. For the other sites, the band gap of the I_2 adsorbed system was found to be decrease with the cave site having the minimum decrease and trough site having the maximum decrease. In the case of I_2 adsorption in angular approach also, the band gap was found to increase for the bridge sites 1 and 2; whereas for the adsorption in case of other sites, the band gap was found to decrease where the decrease was found to be very less in case if adsorption in hollow site 2 and decrease being maximum in case of adsorption in the trough site. During the I_2 adsorption in all the horizontal approaches, the band gap was found to decrease for all the sites, with only the trough site as an exception. DOS plots are plotted for showing the increase in band gap for I_2 adsorption along the vertical approach in bridge site 1 of the (4x2) surface when compared to the bare (4x2) surface as shown in the figure 5.17 a and b.

5.2 Results and Discussions of Dissociative Adsorption

The dissociative adsorption calculations were performed for the most stable sites of the molecular adsorption performed in different approaches. Hence, a total of five different dissociative adsorptions were studied, one from each of the vertical, angular, horizontal 1, horizontal 2 and horizontal 3 approaches. By dissociative adsorption, we do not claim that the two iodine atoms of the I_2 molecular has totally dissociated. On the other hand, we only mean that we performed a total geometry optimization, that is, both the distance of the two iodine atoms from the surface (height from the surface) as well as the distance between the two iodine

atoms (the bondlength) are simultaneously optimized. During these dissociative adsorption studies, the chemisorption energies are calculated using the same formula 5.1, except for the fact that $E(I_2)$ is taken to be the total energy of the I_2 molecule at the corresponding bondlength at which the total energy $E(In_{14}Sb_8H_{16}I_{2)}$ is optimized.

The results of dissociative adsorption of I_2 are shown in tables 5.6-5.0 for different sites in different approaches. Also the optimized dimer bondlength as well as the height from the surface are shown in the figures 5.6-5.10 as compared to the corresponding initial geometry before dissociation. The dissociative adsorptions were performed for the I_2 adsorption in the bridge site 1 for vertical approach, hollow site 2 for angular approach and horizontal approach 1, hollow site 1 for horizontal approach 2 and cave site for horizontal approach 3 since these were the sites that were found to be the most stable ones during the molecular adsorptions in different approaches as seen from the tables 5.1-5.5.

It is seen from table 5.6 that after dissociative adsorption in vertical approach, the distance between the two iodine atoms is 3.10 Å as compared to 2.70 Å during the corresponding molecular adsorption. Also the adsorption energy was found to have increased from 1.3 eV to 2.1 eV during dissociative adsorption which tells us that a slight dissociation is still favored. But looking into the change in dimer bondlength, we note that the I_2 adsorption is not totally dissociative in vertical approach. It was also noted that the height of the molecule from the surface decreased from 2.8 Å in the case of molecular adsorption to 2.6 Å in the case of dissociative adsorption. The band gaps of the (4x2) surface after molecular and dissociative adsorptions of I_2 do not vary much.

In the case of dissociative adsorption of I_2 in the hollow site 2 in angular approach (table 5.7), it was found that the distance between the two iodine atoms was increased from 2.7 Å to 3.5

Å which is a slightly higher increase when compared to the dissociative adsorption in the case of vertical approach. Also a similar trend was found in the adsorption energies, that is the adsorption energy was found to have increased from 1.18 eV in the case of molecular adsorption to that of 2.96 eV in the case of dissociative adsorption of I_2 in the hollow site in angular approach. It was noted that there was a significant change in the height of the I_2 from the surface, from 0.7 Å in the case of molecular adsorption to that of 0.4 Å in the case of dissociative adsorption. Coming to the band gap analysis, it was found that the band gap decreased from 0.08 eV in the case of molecular adsorption to that of 0.03 eV in the case of dissociative adsorption.

In the dissociative adsorption study of I_2 in horizontal approach 1 (table 5.8), it is seen that the dimer bondlength of the I_2 molecular has significantly changed from 2.7 Å to that of 5.0 Å, going from molecular adsorption to that of dissociative adsorption. Here, we can claim that the I_2 molecule has completely dissociated. Also, it is seen that the adsorption energy during molecular adsorption is only 1.26 eV and in the case of dissociative adsorption, it was found to be 6.26 eV, which is almost five times more as compared to that of molecular adsorption. Hence it is concluded that dissociation is more favored in the case of horizontal approach 1. Another thing that was noted is that the final positions of the two iodine atoms after dissociative adsorption are the hollow sites as seen from the figure. During the atomic adsorption of I on the (4x2) surface, hollow site 2 was found to be the most favorable site and the corresponding adsorption energy was found to be 2.9 eV. And hence, from the adsorption energy (6.26 eV) of dissociative adsorption in the horizontal approach 1, it could be concluded that the dissociative adsorption is equivalent to the atomic adsorption of two iodine atoms in the hollow sites since the adsorption energy in this case is almost equivalent to twice the adsorption energy found in the case of atomic adsorption of I in the hollow site 2. It was found that the height of the two

iodine atoms from the surface decreased from 1.2 Å during molecular adsorption to 0.9 Å during dissociative adsorption of I_2. The band gaps were found to be 0.04 eV for both molecular and dissociative adsorptions.

In the dissociative adsorption study of I_2 in the horizontal approach 2 (table 5.9), it was found that the final geometry after optimization is exactly the same as that of the final geometry found for horizontal approach 1. The dimer bondlength was found to increase from 2.7 Å in the case of molecular adsorption to 4.9 Å in the case of dissociative adsorption and the corresponding adsorption energy after dissociative adsorption was found to be 6.25 eV. The explanation given for horizontal approach 1 holds good here also since the final geometry is the same as that. Again, the height of the iodine atoms from the InSb surface was found to decrease from 1.4 Å to 0.9 Å. The band gap was found to decrease from 0.09 eV to 0.03 eV.

In the dissociative adsorption study of I_2 in the horizontal approach 3 (table 5.10), it was found that the bondlength increased from 2.7 Å in the case of molecular adsorption to 4.2 Å in the case of dissociative adsorption. This is a considerable dissociation as compared to that of vertical and angular approaches, but still this is not a complete dissociation as in the cases of horizontal approaches 1 and 2. Also the adsorption energy was found to have increased from 1.17 eV in the case of molecular adsorption to that of 5.75 eV in the case of dissociative adsorption. The height of the iodine atoms from the surface was decreased from 2.7 Å in the case of molecular adsorption to that of 2.3 Å in the case of dissociative adsorption. Regarding band gaps, it was noted that the band gap decreased from 0.07 eV in the case of molecular adsorption to 0.02 eV in the case of dissociative adsorption.

The analysis of mulliken charge distribution, before and after dissociative adsorption of iodine atoms in different approaches was carried out and the comparable charge distributions are

as shown in the figures 5.21-5.25 and also the charges on each of the atoms are shown in tables 5.16-5.20 It is seen that after dissociative adsorption was performed in vertical approach, the iodine atoms gained more charges than the charges gained during molecular adsorption, though the difference in the charge gained when compared to the molecular adsorption is not very huge. But still, a similar trend of highly unsymmetrical charge distribution among the two iodine atoms is observed. It is seen from both the figures, that the iodine atom nearer to the In atom on the surface gains significantly less charges than the other iodine atom that is lying on the top, that is denoted by label 1.

In the case of dissociative adsorption in angular approach, it is seen that when compared to the corresponding molecular adsorption as shown in the figures, the charges gained by the two iodine atoms is more in the case of dissociative adsorption than that of molecular adsorption. Also, the charges gained after dissociative adsorption in the angular approach is significantly higher then that of the vertical approach , that is the difference in the gained charges before and after dissociative adsorption in the case of vertical approach is subtle when compared to that of angular approach. This is attributed to greater dissociation, in terms of adsorption energy and dimer bondlength, achieved in the case of angular approach. Also, it is seen that the unsymmetrical charge distribution before dissociative adsorption has slightly improved after dissociative adsorption. But still, here also it is seen that the iodine atom closer to one of the iodine atoms, that is the iodine atom labeled 1, gains significantly less charge when compared to the other iodine atom that is labeled 2 in the figure.

In the case of dissociative adsorption in horizontal approach 1, it is seen that there is a significant increase in the amount of charges gained after dissociation when compared to that of molecular adsorption. Again, this can be accounted for by considering the complete dissociation

of I_2 molecule occurred in this case of horizontal approach 1 where the bondlength as well as the adsorption energy has increased a lot when compared to that of molecular adsorption. A similar trend is noted in the case of horizontal approach 2 also, where the charge gained by the two iodine atoms is very high when compared to that before dissociative adsorption.

In the case of dissociative adsorption in horizontal approach 3, it was seen that the charges gained by the two iodine atoms is higher after dissociative adsorption as compared to that before dissociative adsorption. Also, it was noted that the charge distribution after dissociative adsorption has become more symmetrical when compared to the corresponding molecular adsorption.

Hence, overall, during the dissociative adsorption studies, it was noted that the height of the two iodine atoms from the surface decreased during the dissociative adsorption. The dissociative adsorption was always found to be more favored that that of molecular adsorption. It was found that the dissociation was minimal in the case of vertical approach, slightly higher in the case of angular approach which was still higher in the case of horizontal approach 3 and finally, the dissociation was found to be complete in the cases of horizontal approaches 1 and 2. It was also noted that more the dimer bondlength increases, going from vertical to angular to horizontal approach 3 to horizontal approaches 2 and 1, we find that the corresponding adsorption energy also increases consistently. Also it was seen that the values of adsorption energy in the case of molecular adsorption of I_2 in all sites in all approaches, range from 1.3 eV to 0.38 eV which is very less when compared to both dissociative as well as other atomic adsorption results of iodine atom. Hence it can be concluded that molecular adsorption of I_2 molecule is not favored when compared to the dissociative adsorption. This is in good agreement with the available experimental data which claims dissociative adsorption of I_2. Coming to the

analysis of HOMO-LUMO gaps, it was found that the band gaps do not vary after dissociative adsorption in the cases of vertical approach and horizontal approach 1, where as in the cases of dissociative adsorption in angular approach, horizontal approach 2 and 3, it was noted that the band gap after dissociative adsorption has decreased when compared to that of molecular adsorption. The iodine atoms gained more charges after dissociative adsorption compared to that of before dissociative adsorption in all the approaches.

Table 5.1 Summary of molecular adsorption of I_2 along vertical approach

Site	Height from the surface(Å)	Adsorption energy (eV)	Band gap (eV)	Δgap (eV)
Bridge 1	2.80	1.30	0.17	0.08
Bridge 2	2.60	1.26	0.12	0.03
Hollow 2	1.10	1.08	0.14	0.05
Hollow 1	1.40	0.99	0.07	-0.02
Top 2	2.90	0.97	0.03	-0.06
Cave	2.50	0.84	0.08	-0.01
Top 1	3.10	0.82	0.05	-0.04
Trough	0.20	0.80	0.03	-0.06

Table 5.2 Summary of molecular adsorption of I_2 along angular approach

Site	Height from the surface(Å)	Adsorption energy (eV)	Band gap (eV)	Δgap (eV)
Hollow 2	0.70	1.18	0.08	-0.01
Trough	-0.20	1.09	0.01	-0.08
Hollow 1	0.70	0.99	0.04	-0.05
Cave	2.30	0.98	0.07	-0.02
Bridge 2	2.80	0.87	0.14	0.05
Top 2	3.00	0.86	0.05	-0.04
Bridge 1	2.75	0.85	0.17	0.08
Top 1	2.90	0.71	0.04	-0.05

Table 5.3 Summary of molecular adsorption of I_2 along horizontal approach 1

Site	Height from the surface	Adsorption energy	Band gap	Δgap
Hollow 2	1.20	1.26	0.04	-0.05
Top 2	3.00	1.07	0.06	-0.03
Hollow 1	1.20	0.94	0.02	-0.07
Trough	1.80	0.81	0.15	0.06
Bridge 2	2.90	0.72	0.02	-0.07
Cave	3.20	0.65	0.04	-0.05
Top 1	3.00	0.59	0.05	-0.04
Bridge 1	3.40	0.38	0.05	-0.04

Table 5.4 Summary of molecular adsorption of I_2 along horizontal approach 2

Site	Height from the surface	Adsorption energy	Band gap	Δgap
Hollow 1	1.40	1.34	0.09	0.00
Top 1	3.00	1.06	0.08	-0.01
Cave	3.10	0.72	0.02	-0.07
Bridge 1	3.20	0.67	0.04	-0.05

Table 5.5 Summary of molecular adsorption of I_2 along horizontal approach 3

Site	Height from the surface(Å)	Adsorption energy (eV)	Band gap (eV)	Δgap (eV)
Cave	2.70	1.17	0.07	-0.02
Hollow 2	2.00	1.14	0.04	-0.05
Hollow 1	2.00	0.86	0.02	-0.07
Top 2	3.00	0.80	0.00	-0.09
Top 1	3.00	0.72	0.01	-0.08
Bridge 2	2.90	0.73	0.01	-0.08
Trough	1.30	0.52	0.11	0.02
Bridge 1	3.20	0.41	0.04	-0.05

Table 5.6 Results for molecular and dissociative adsorptions of I_2 in bridge site 1 along vertical approach

Type of adsorption	Height from the surface(Å)	Adsorption energy (eV)	Dimer bond length(Å)	Band gap (eV)
Molecular adsorption	2.8	1.3	2.70	0.17
Dissociative adsorption	2.6	2.1	3.10	0.18

Table 5.7 Results for molecular and dissociative adsorptions of I_2 in hollow site 2 along angular approach

Type of adsorption	Height from the surface(Å)	Adsorption energy (eV)	Dimer bond length(Å)	Band gap (eV)
Molecular adsorption	0.70	1.18	2.70	0.08
Dissociative adsorption	0.40	2.96	3.50	0.03

Table 5.8 Results for molecular and dissociative adsorptions of I_2 in hollow site 2 along horizontal approach 1

Type of adsorption	Height from the surface(Å)	Adsorption energy (eV)	Dimer bond length(Å)	Band gap (eV)
Molecular adsorption	1.20	1.26	2.70	0.04
Dissociative adsorption	0.90	6.26	5.00	0.04

Table 5.9 Results for molecular and dissociative adsorptions of I_2 in hollow site 1 along horizontal approach 2

Type of adsorption	Height from the surface(Å)	Adsorption energy (eV)	Dimer bond length(Å)	Band gap (eV)
Molecular adsorption	1.40	1.26	2.70	0.09
Dissociative adsorption	0.90	6.25	4.90	0.03

Table 5.10 Results for molecular and dissociative adsorptions of I_2 in cave site along horizontal approach 3

Type of adsorption	Height from the surface(Å)	Adsorption energy (eV)	Dimer bond length(Å)	Band gap (eV)
Molecular adsorption	2.70	1.17	2.70	0.07
Dissociative adsorption	2.30	5.75	4.20	0.02

Table 5.11 Charge distributions of (4x2) surface before and after molecular adsorption of I_2 along vertical approach

Layer	Label	Atom	(4x2) surface	Bridge 1	Bridge 2	Hollow 2	Hollow 1
Adatom	1	I	-	-0.23	-0.24	-0.19	-0.13
Adatom	2	I	-	-0.04	-0.02	-0.10	-0.05
1st	3	In	0.17	0.20	0.20	0.19	0.18
1st	4	In	0.17	0.27	0.20	0.20	0.24
1st	5	In	0.18	0.20	0.27	0.25	0.20
1st	6	In	0.18	0.20	0.27	0.25	0.20
1st	7	In	0.17	0.20	0.20	0.20	0.18
1st	8	In	0.17	0.27	0.21	0.20	0.24
2nd	9	Sb	-0.24	-0.22	-0.21	-0.22	-0.22
2nd	10	Sb	-0.27	-0.28	-0.27	-0.26	-0.27
2nd	11	Sb	-0.27	-0.27	-0.28	-0.27	-0.27
2nd	12	Sb	-0.22	-0.21	-0.21	-0.24	-0.22
2nd	13	Sb	-0.27	-0.27	-0.27	-0.27	-0.27
2nd	14	Sb	-0.22	-0.22	-0.26	-0.21	-0.22
2nd	15	Sb	-0.22	-0.22	-0.23	-0.24	-0.22
2nd	16	Sb	-0.27	-0.28	-0.27	-0.26	-0.27
3rd	17	In	0.13	0.14	0.13	0.14	0.14
3rd	18	In	0.15	0.14	0.15	0.15	0.15
3rd	19	In	0.11	0.11	0.12	0.12	0.11
3rd	20	In	0.18	0.16	0.17	0.16	0.16
3rd	21	In	0.11	0.12	0.11	0.12	0.12
3rd	22	In	0.13	0.13	0.13	0.14	0.13
3rd	23	In	0.17	0.17	0.17	0.17	0.17
3rd	24	In	0.16	0.13	0.15	0.15	0.13
4th	25	H	-0.02	-0.02	-0.02	-0.02	-0.02
4th	26	H	-0.02	-0.02	-0.02	-0.01	-0.02
4th	27	H	-0.01	-0.01	-0.01	-0.01	-0.01
4th	28	H	-0.01	-0.01	-0.01	-0.01	-0.01
4th	29	H	-0.01	-0.02	-0.01	-0.01	-0.01
4th	30	H	-0.01	-0.01	-0.02	-0.01	-0.01
4th	31	H	0.00	-0.01	-0.01	-0.01	-0.01
4th	32	H	-0.02	-0.01	-0.02	-0.01	-0.01
4th	33	H	-0.01	-0.01	-0.01	0.00	-0.01
4th	34	H	-0.01	-0.01	-0.02	-0.01	-0.01
4th	35	H	-0.01	-0.02	-0.01	-0.01	-0.01
4th	36	H	-0.01	-0.01	-0.02	-0.01	-0.01
4th	37	H	-0.01	-0.01	-0.01	-0.01	-0.01
4th	38	H	-0.01	-0.01	-0.01	0.00	-0.01
4th	39	H	-0.01	-0.02	-0.02	-0.02	-0.02
4th	40	H	-0.02	-0.02	-0.02	-0.01	-0.02

Table 5.11 - *Continued*

Layer	Atom label	Type of atom	(4x2) surface	Top 2	Cave	Top 1	Trough
Adatom	1	I	-	-0.20	-0.15	-0.19	-0.15
Adatom	2	I	-	-0.07	-0.08	-0.09	0.02
1st	3	In	0.17	0.22	0.19	0.20	0.20
1st	4	In	0.17	0.22	0.24	0.27	0.20
1st	5	In	0.18	0.26	0.24	0.23	0.18
1st	6	In	0.18	0.28	0.24	0.22	0.18
1st	7	In	0.17	0.23	0.19	0.20	0.20
1st	8	In	0.17	0.23	0.24	0.22	0.20
2nd	9	Sb	-0.24	-0.20	-0.21	-0.21	-0.22
2nd	10	Sb	-0.27	-0.28	-0.27	-0.28	-0.27
2nd	11	Sb	-0.27	-0.29	-0.28	-0.27	-0.27
2nd	12	Sb	-0.22	-0.27	-0.23	-0.22	-0.21
2nd	13	Sb	-0.27	-0.29	-0.28	-0.27	-0.27
2nd	14	Sb	-0.22	-0.24	-0.23	-0.21	-0.22
2nd	15	Sb	-0.22	-0.22	-0.24	-0.22	-0.22
2nd	16	Sb	-0.27	-0.29	-0.27	-0.28	-0.27
3rd	17	In	0.13	0.13	0.13	0.13	0.13
3rd	18	In	0.15	0.15	0.15	0.15	0.15
3rd	19	In	0.11	0.12	0.11	0.11	0.11
3rd	20	In	0.18	0.16	0.17	0.17	0.17
3rd	21	In	0.11	0.12	0.12	0.12	0.11
3rd	22	In	0.13	0.13	0.13	0.13	0.13
3rd	23	In	0.17	0.17	0.16	0.18	0.17
3rd	24	In	0.16	0.15	0.14	0.14	0.15
4th	25	H	-0.02	-0.01	-0.02	-0.01	-0.01
4th	26	H	-0.02	-0.02	-0.02	-0.02	-0.02
4th	27	H	-0.01	-0.01	-0.01	-0.01	-0.01
4th	28	H	-0.01	-0.01	-0.01	-0.01	-0.01
4th	29	H	-0.01	-0.01	-0.01	-0.02	-0.01
4th	30	H	-0.01	-0.01	-0.01	-0.02	-0.01
4th	31	H	0.00	-0.01	-0.01	-0.01	-0.01
4th	32	H	-0.02	-0.01	-0.01	-0.01	-0.01
4th	33	H	-0.01	0.00	-0.01	-0.01	-0.01
4th	34	H	-0.01	-0.01	-0.01	-0.01	-0.01
4th	35	H	-0.01	-0.01	-0.01	-0.01	-0.01
4th	36	H	-0.01	-0.01	-0.01	-0.01	-0.01
4th	37	H	-0.01	-0.01	-0.01	-0.01	-0.01
4th	38	H	-0.01	-0.01	-0.01	-0.01	-0.01
4th	39	H	-0.01	-0.02	-0.02	-0.02	-0.01
4th	40	H	-0.02	-0.02	-0.01	-0.02	-0.02

Table 5.12 Charge distributions of (4x2) surface before and after molecular adsorption of I_2 along angular approach

Layer	Atom label	Type of atom	(4x2) surface	Hollow 2	Trough	Hollow 1	Cave
Adatom	1	I	-	-0.09	0.00	-0.08	-0.10
Adatom	2	I	-	-0.17	-0.15	-0.13	-0.15
1st	3	In	0.17	0.19	0.22	0.19	0.19
1st	4	In	0.17	0.20	0.20	0.25	0.26
1st	5	In	0.18	0.26	0.17	0.20	0.23
1st	6	In	0.18	0.26	0.17	0.20	0.23
1st	7	In	0.17	0.19	0.23	0.19	0.19
1st	8	In	0.17	0.20	0.20	0.25	0.27
2nd	9	Sb	-0.24	-0.22	-0.24	-0.22	-0.24
2nd	10	Sb	-0.27	-0.26	-0.28	-0.30	-0.27
2nd	11	Sb	-0.27	-0.29	-0.27	-0.27	-0.27
2nd	12	Sb	-0.22	-0.23	-0.22	-0.18	-0.23
2nd	13	Sb	-0.27	-0.28	-0.28	-0.27	-0.28
2nd	14	Sb	-0.22	-0.24	-0.18	-0.23	-0.20
2nd	15	Sb	-0.22	-0.22	-0.23	-0.22	-0.24
2nd	16	Sb	-0.27	-0.26	-0.28	-0.29	-0.27
3rd	17	In	0.13	0.13	0.12	0.13	0.13
3rd	18	In	0.15	0.15	0.17	0.15	0.15
3rd	19	In	0.11	0.12	0.11	0.11	0.10
3rd	20	In	0.18	0.17	0.17	0.18	0.17
3rd	21	In	0.11	0.12	0.11	0.11	0.12
3rd	22	In	0.13	0.13	0.12	0.13	0.13
3rd	23	In	0.17	0.18	0.17	0.18	0.16
3rd	24	In	0.16	0.15	0.17	0.13	0.14
4th	25	H	-0.02	-0.02	-0.01	-0.01	-0.02
4th	26	H	-0.02	-0.02	-0.02	-0.02	-0.02
4th	27	H	-0.01	-0.01	-0.01	-0.01	-0.01
4th	28	H	-0.01	-0.01	-0.01	-0.01	-0.01
4th	29	H	-0.01	-0.01	-0.01	-0.01	-0.01
4th	30	H	-0.01	-0.01	-0.01	-0.02	-0.01
4th	31	H	0.00	0.00	-0.02	0.00	-0.01
4th	32	H	-0.02	-0.01	-0.01	-0.01	-0.02
4th	33	H	-0.01	0.00	-0.02	0.00	-0.01
4th	34	H	-0.01	-0.01	-0.01	-0.01	-0.01
4th	35	H	-0.01	-0.01	-0.01	-0.01	-0.01
4th	36	H	-0.01	-0.01	-0.01	-0.01	-0.01
4th	37	H	-0.01	-0.01	0.00	-0.01	-0.01
4th	38	H	-0.01	-0.01	-0.02	-0.01	-0.01
4th	39	H	-0.01	-0.02	-0.02	-0.02	-0.02
4th	40	H	-0.02	-0.02	-0.02	-0.02	-0.02

Table 5.12 - *Continued*

Layer	Label	Atom	(4x2) surface	Bridge 2	Top 2	Bridge 1	Top 1
Adatom	1	I	-	-0.06	-0.08	-0.03	-0.06
Adatom	2	I	-	-0.20	-0.19	-0.20	-0.16
1st	3	In	0.17	0.20	0.21	0.19	0.20
1st	4	In	0.17	0.21	0.22	0.26	0.24
1st	5	In	0.18	0.27	0.26	0.20	0.20
1st	6	In	0.18	0.27	0.25	0.20	0.19
1st	7	In	0.17	0.20	0.21	0.19	0.20
1st	8	In	0.17	0.21	0.22	0.26	0.25
2nd	9	Sb	-0.24	-0.22	-0.21	-0.24	-0.22
2nd	10	Sb	-0.27	-0.27	-0.28	-0.27	-0.29
2nd	11	Sb	-0.27	-0.27	-0.28	-0.27	-0.27
2nd	12	Sb	-0.22	-0.22	-0.23	-0.21	-0.17
2nd	13	Sb	-0.27	-0.27	-0.28	-0.28	-0.28
2nd	14	Sb	-0.22	-0.22	-0.23	-0.19	-0.22
2nd	15	Sb	-0.22	-0.23	-0.22	-0.21	-0.29
2nd	16	Sb	-0.27	-0.27	-0.27	-0.27	-0.26
3rd	17	In	0.13	0.13	0.13	0.12	0.13
3rd	18	In	0.15	0.15	0.15	0.15	0.15
3rd	19	In	0.11	0.11	0.12	0.10	0.11
3rd	20	In	0.18	0.17	0.17	0.17	0.17
3rd	21	In	0.11	0.11	0.12	0.11	0.12
3rd	22	In	0.13	0.12	0.13	0.12	0.13
3rd	23	In	0.17	0.17	0.17	0.18	0.18
3rd	24	In	0.16	0.15	0.15	0.14	0.13
4th	25	H	-0.02	-0.02	-0.02	-0.01	-0.01
4th	26	H	-0.02	-0.02	-0.02	-0.02	-0.01
4th	27	H	-0.01	-0.01	-0.01	-0.01	-0.01
4th	28	H	-0.01	-0.01	-0.01	-0.02	-0.01
4th	29	H	-0.01	-0.02	-0.01	-0.01	-0.02
4th	30	H	-0.01	-0.01	-0.01	-0.02	-0.02
4th	31	H	0.00	-0.01	-0.01	0.00	-0.01
4th	32	H	-0.02	-0.02	-0.01	-0.02	-0.01
4th	33	H	-0.01	-0.01	-0.01	-0.01	-0.01
4th	34	H	-0.01	-0.02	-0.01	-0.02	-0.01
4th	35	H	-0.01	-0.02	-0.01	-0.01	-0.01
4th	36	H	-0.01	-0.01	-0.01	-0.02	-0.01
4th	37	H	-0.01	-0.01	-0.01	-0.01	-0.01
4th	38	H	-0.01	-0.01	-0.01	-0.01	-0.01
4th	39	H	-0.01	-0.02	-0.02	-0.01	-0.02
4th	40	H	-0.02	-0.02	-0.02	-0.01	-0.01

Table 5.13 Charge distributions of (4x2) surface before and after molecular adsorption of I_2 along horizontal approach 1

Layer	Label	Atom	(4x2) surface	Hollow 2	Top 2	Hollow 1	Trough
Adatom	1	I	-	-0.17	-0.12	-0.09	-0.16
Adatom	2	I	-	-0.18	-0.17	-0.04	-0.02
1st	3	In	0.17	0.19	0.20	0.18	0.23
1st	4	In	0.17	0.21	0.23	0.25	0.18
1st	5	In	0.18	0.26	0.31	0.18	0.18
1st	6	In	0.18	0.26	0.24	0.19	0.18
1st	7	In	0.17	0.19	0.19	0.18	0.23
1st	8	In	0.17	0.20	0.22	0.24	0.18
2nd	9	Sb	-0.24	-0.21	-0.23	-0.24	-0.18
2nd	10	Sb	-0.27	-0.25	-0.28	-0.27	-0.26
2nd	11	Sb	-0.27	-0.26	-0.27	-0.27	-0.27
2nd	12	Sb	-0.22	-0.23	-0.23	-0.26	-0.22
2nd	13	Sb	-0.27	-0.26	-0.28	-0.27	-0.27
2nd	14	Sb	-0.22	-0.25	-0.23	-0.23	-0.22
2nd	15	Sb	-0.22	-0.19	-0.22	-0.15	-0.21
2nd	16	Sb	-0.27	-0.26	-0.25	-0.28	-0.26
3rd	17	In	0.13	0.14	0.13	0.13	0.13
3rd	18	In	0.15	0.15	0.15	0.15	0.15
3rd	19	In	0.11	0.11	0.11	0.12	0.11
3rd	20	In	0.18	0.15	0.17	0.18	0.17
3rd	21	In	0.11	0.12	0.12	0.11	0.11
3rd	22	In	0.13	0.14	0.12	0.13	0.13
3rd	23	In	0.17	0.18	0.17	0.18	0.16
3rd	24	In	0.16	0.14	0.13	0.12	0.15
4th	25	H	-0.02	-0.01	-0.02	-0.01	-0.02
4th	26	H	-0.02	-0.02	-0.01	-0.02	-0.02
4th	27	H	-0.01	-0.01	-0.01	-0.01	-0.01
4th	28	H	-0.01	-0.01	-0.01	-0.01	-0.01
4th	29	H	-0.01	-0.02	-0.02	-0.02	-0.02
4th	30	H	-0.01	-0.01	-0.02	-0.02	-0.02
4th	31	H	0.00	0.00	-0.01	0.00	-0.01
4th	32	H	-0.02	-0.01	-0.01	-0.02	-0.01
4th	33	H	-0.01	0.00	-0.01	-0.01	-0.01
4th	34	H	-0.01	-0.01	-0.01	-0.02	-0.01
4th	35	H	-0.01	-0.01	-0.01	-0.01	-0.02
4th	36	H	-0.01	-0.01	-0.01	-0.01	-0.01
4th	37	H	-0.01	-0.01	-0.01	-0.01	-0.01
4th	38	H	-0.01	-0.01	-0.01	-0.01	-0.01
4th	39	H	-0.01	-0.02	-0.02	-0.03	-0.02
4th	40	H	-0.02	-0.02	-0.01	-0.02	-0.01

Table 5.13 - *Continued*

Layer	Label	Atom	(4x2) surface	Bridge 2	Cave	Top 1	Bridge 1
Adatom	1	I		-0.16	-0.12	-0.10	-0.08
Adatom	2	I		-0.20	-0.08	-0.15	-0.07
1st	3	In	0.17	0.19	0.19	0.19	0.19
1st	4	In	0.17	0.23	0.26	0.23	0.23
1st	5	In	0.18	0.29	0.21	0.18	0.19
1st	6	In	0.18	0.29	0.21	0.19	0.19
1st	7	In	0.17	0.19	0.19	0.19	0.19
1st	8	In	0.17	0.23	0.26	0.29	0.23
2nd	9	Sb	-0.24	-0.20	-0.24	-0.21	-0.22
2nd	10	Sb	-0.27	-0.26	-0.27	-0.28	-0.27
2nd	11	Sb	-0.27	-0.27	-0.27	-0.27	-0.27
2nd	12	Sb	-0.22	-0.19	-0.23	-0.19	-0.21
2nd	13	Sb	-0.27	-0.27	-0.27	-0.27	-0.27
2nd	14	Sb	-0.22	-0.25	-0.23	-0.22	-0.22
2nd	15	Sb	-0.22	-0.23	-0.23	-0.22	-0.21
2nd	16	Sb	-0.27	-0.26	-0.27	-0.27	-0.27
3rd	17	In	0.13	0.12	0.13	0.13	0.13
3rd	18	In	0.15	0.15	0.15	0.15	0.15
3rd	19	In	0.11	0.11	0.11	0.11	0.11
3rd	20	In	0.18	0.17	0.17	0.17	0.17
3rd	21	In	0.11	0.12	0.12	0.11	0.12
3rd	22	In	0.13	0.12	0.12	0.13	0.12
3rd	23	In	0.17	0.17	0.17	0.18	0.17
3rd	24	In	0.16	0.14	0.14	0.14	0.14
4th	25	H	-0.02	-0.02	-0.02	-0.02	-0.02
4th	26	H	-0.02	-0.02	-0.01	-0.01	-0.02
4th	27	H	-0.01	-0.01	-0.01	-0.01	-0.01
4th	28	H	-0.01	-0.01	-0.01	-0.01	-0.01
4th	29	H	-0.01	-0.02	-0.02	-0.01	-0.01
4th	30	H	-0.01	-0.01	-0.02	-0.02	-0.02
4th	31	H	0.00	-0.01	-0.01	-0.01	-0.01
4th	32	H	-0.02	-0.01	-0.01	-0.01	-0.01
4th	33	H	-0.01	-0.01	-0.01	-0.01	-0.01
4th	34	H	-0.01	-0.01	-0.01	-0.01	-0.01
4th	35	H	-0.01	-0.01	-0.02	-0.01	-0.01
4th	36	H	-0.01	-0.02	-0.01	-0.01	-0.01
4th	37	H	-0.01	-0.01	-0.01	-0.01	-0.01
4th	38	H	-0.01	-0.01	-0.01	-0.01	-0.01
4th	39	H	-0.01	-0.02	-0.02	-0.02	-0.02
4th	40	H	-0.02	-0.02	-0.02	-0.02	-0.02

Table 5.14 Charge distributions of (4x2) surface before and after molecular adsorption of I_2 along horizontal approach 2

Layer	Label	Atom	(4x2) surface	Hollow 1	Cave	Top 1	Bridge 1
Adatom	1	I	-	-0.16	-0.09	-0.16	-0.15
Adatom	2	I	-	-0.13	-0.10	-0.10	-0.11
1st	3	In	0.17	0.19	0.20	0.19	0.19
1st	4	In	0.17	0.25	0.21	0.23	0.25
1st	5	In	0.18	0.20	0.27	0.21	0.22
1st	6	In	0.18	0.20	0.27	0.23	0.22
1st	7	In	0.17	0.19	0.20	0.19	0.19
1st	8	In	0.17	0.25	0.21	0.30	0.25
2nd	9	Sb	-0.24	-0.22	-0.23	-0.22	-0.22
2nd	10	Sb	-0.27	-0.25	-0.28	-0.30	-0.26
2nd	11	Sb	-0.27	-0.27	-0.27	-0.28	-0.28
2nd	12	Sb	-0.22	-0.21	-0.22	-0.21	-0.22
2nd	13	Sb	-0.27	-0.27	-0.27	-0.27	-0.28
2nd	14	Sb	-0.22	-0.22	-0.24	-0.22	-0.22
2nd	15	Sb	-0.22	-0.21	-0.23	-0.22	-0.22
2nd	16	Sb	-0.27	-0.25	-0.27	-0.25	-0.26
3rd	17	In	0.13	0.13	0.12	0.13	0.13
3rd	18	In	0.15	0.15	0.14	0.15	0.15
3rd	19	In	0.11	0.12	0.11	0.11	0.11
3rd	20	In	0.18	0.15	0.16	0.16	0.17
3rd	21	In	0.11	0.12	0.12	0.12	0.12
3rd	22	In	0.13	0.14	0.12	0.13	0.12
3rd	23	In	0.17	0.17	0.16	0.17	0.17
3rd	24	In	0.16	0.14	0.13	0.14	0.14
4th	25	H	-0.02	-0.01	-0.02	-0.02	-0.02
4th	26	H	-0.02	-0.01	-0.02	-0.02	-0.01
4th	27	H	-0.01	-0.01	-0.01	-0.01	-0.01
4th	28	H	-0.01	-0.01	-0.01	-0.01	-0.01
4th	29	H	-0.01	-0.02	-0.02	-0.02	-0.01
4th	30	H	-0.01	-0.01	-0.01	-0.02	-0.02
4th	31	H	0.00	0.00	-0.02	-0.01	-0.01
4th	32	H	-0.02	-0.01	0.00	0.00	-0.01
4th	33	H	-0.01	-0.01	-0.01	-0.01	-0.01
4th	34	H	-0.01	-0.01	-0.01	-0.02	-0.01
4th	35	H	-0.01	-0.01	-0.02	-0.01	-0.01
4th	36	H	-0.01	-0.01	-0.01	-0.01	-0.01
4th	37	H	-0.01	-0.01	-0.01	-0.01	-0.01
4th	38	H	-0.01	-0.01	-0.01	-0.01	-0.01
4th	39	H	-0.01	-0.03	-0.02	-0.02	-0.02
4th	40	H	-0.02	-0.02	-0.02	-0.02	-0.02

Table 5.15 Charge distributions of (4x2) surface before and after molecular adsorption of I_2 along horizontal approach 3

Layer	Label	Atom	(4x2) surface	Cave	Hollow 2	Hollow 1	Top 2
Adatom	1	I	-	-0.17	-0.18	-0.17	-0.12
Adatom	2	I	-	-0.08	-0.11	-0.07	-0.22
1st	3	In	0.17	0.19	0.20	0.18	0.19
1st	4	In	0.17	0.25	0.19	0.31	0.20
1st	5	In	0.18	0.25	0.21	0.20	0.32
1st	6	In	0.18	0.19	0.32	0.19	0.21
1st	7	In	0.17	0.19	0.20	0.19	0.19
1st	8	In	0.17	0.30	0.22	0.19	0.21
2nd	9	Sb	-0.24	-0.21	-0.21	-0.22	-0.23
2nd	10	Sb	-0.27	-0.28	-0.24	-0.26	-0.27
2nd	11	Sb	-0.27	-0.28	-0.26	-0.27	-0.27
2nd	12	Sb	-0.22	-0.23	-0.24	-0.20	-0.22
2nd	13	Sb	-0.27	-0.27	-0.25	-0.28	-0.28
2nd	14	Sb	-0.22	-0.26	-0.24	-0.23	-0.21
2nd	15	Sb	-0.22	-0.24	-0.24	-0.19	-0.21
2nd	16	Sb	-0.27	-0.27	-0.25	-0.26	-0.24
3rd	17	In	0.13	0.13	0.12	0.13	0.13
3rd	18	In	0.15	0.15	0.14	0.15	0.16
3rd	19	In	0.11	0.11	0.12	0.12	0.12
3rd	20	In	0.18	0.17	0.15	0.16	0.16
3rd	21	In	0.11	0.12	0.12	0.11	0.12
3rd	22	In	0.13	0.13	0.13	0.13	0.12
3rd	23	In	0.17	0.17	0.16	0.18	0.18
3rd	24	In	0.16	0.13	0.14	0.13	0.15
4th	25	H	-0.02	-0.02	-0.02	-0.01	-0.01
4th	26	H	-0.02	-0.01	-0.01	-0.01	-0.01
4th	27	H	-0.01	-0.01	-0.01	-0.01	-0.01
4th	28	H	-0.01	-0.01	-0.01	-0.01	-0.01
4th	29	H	-0.01	-0.01	-0.02	-0.02	-0.01
4th	30	H	-0.01	-0.02	-0.01	-0.01	-0.02
4th	31	H	0.00	-0.01	-0.01	-0.01	-0.01
4th	32	H	-0.02	-0.01	0.00	0.00	-0.01
4th	33	H	-0.01	-0.01	-0.01	0.00	0.00
4th	34	H	-0.01	-0.01	-0.02	-0.02	-0.01
4th	35	H	-0.01	-0.01	-0.01	-0.01	-0.01
4th	36	H	-0.01	-0.01	-0.01	-0.01	-0.01
4th	37	H	-0.01	-0.01	-0.02	-0.01	-0.01
4th	38	H	-0.01	-0.01	-0.01	-0.01	-0.01
4th	39	H	-0.01	-0.02	-0.02	-0.03	-0.02
4th	40	H	-0.02	-0.02	-0.01	-0.02	-0.02

Table 5.15 – *Continued*

Layer	Label	Atom	(4x2) surface	Bridge 2	Top 1	Trough	Bridge 1
Adatom	1	I	-	-0.14	-0.06	-0.18	-0.07
Adatom	2	I	-	-0.18	-0.13	0.00	-0.06
1st	3	In	0.17	0.20	0.19	0.20	0.19
1st	4	In	0.17	0.22	0.19	0.18	0.24
1st	5	In	0.18	0.34	0.19	0.18	0.20
1st	6	In	0.18	0.26	0.19	0.18	0.19
1st	7	In	0.17	0.20	0.19	0.21	0.19
1st	8	In	0.17	0.21	0.30	0.19	0.28
2nd	9	Sb	-0.24	-0.23	-0.20	-0.23	-0.24
2nd	10	Sb	-0.27	-0.27	-0.28	-0.27	-0.28
2nd	11	Sb	-0.27	-0.28	-0.27	-0.29	-0.27
2nd	12	Sb	-0.22	-0.23	-0.17	-0.21	-0.20
2nd	13	Sb	-0.27	-0.27	-0.27	-0.28	-0.28
2nd	14	Sb	-0.22	-0.22	-0.26	-0.11	-0.22
2nd	15	Sb	-0.22	-0.23	-0.23	-0.22	-0.23
2nd	16	Sb	-0.27	-0.26	-0.26	-0.26	-0.28
3rd	17	In	0.13	0.12	0.13	0.12	0.13
3rd	18	In	0.15	0.15	0.15	0.15	0.15
3rd	19	In	0.11	0.11	0.11	0.12	0.10
3rd	20	In	0.18	0.17	0.17	0.18	0.17
3rd	21	In	0.11	0.12	0.11	0.10	0.11
3rd	22	In	0.13	0.12	0.13	0.13	0.12
3rd	23	In	0.17	0.17	0.17	0.16	0.17
3rd	24	In	0.16	0.14	0.13	0.16	0.13
4th	25	H	-0.02	-0.02	-0.02	-0.01	-0.02
4th	26	H	-0.02	-0.02	-0.02	-0.02	-0.02
4th	27	H	-0.01	-0.01	-0.01	-0.02	-0.01
4th	28	H	-0.01	-0.01	-0.01	-0.02	-0.01
4th	29	H	-0.01	-0.02	-0.02	-0.01	-0.01
4th	30	H	-0.01	-0.02	-0.01	-0.01	-0.01
4th	31	H	0.00	-0.01	-0.01	0.00	-0.01
4th	32	H	-0.02	-0.01	-0.01	-0.01	-0.01
4th	33	H	-0.01	-0.01	-0.01	-0.01	-0.01
4th	34	H	-0.01	-0.01	-0.01	-0.01	-0.02
4th	35	H	-0.01	-0.01	-0.01	-0.02	-0.01
4th	36	H	-0.01	-0.01	-0.01	-0.02	-0.01
4th	37	H	-0.01	-0.01	-0.01	-0.01	-0.01
4th	38	H	-0.01	-0.01	-0.01	-0.01	-0.01
4th	39	H	-0.01	-0.02	-0.02	-0.02	-0.02
4th	40	H	-0.02	-0.02	-0.02	-0.02	-0.02

Table 5.16 Charge distributions of (4x2) surface before and after dissociative adsorption of I_2 along vertical approach

Layer	Atom label	Type of atom	Before dissociative adsorption	After dissociative adsorption
Adatom	1	I	-0.23	-0.31
Adatom	2	I	-0.04	-0.07
1st	3	In	0.20	0.20
1st	4	In	0.27	0.30
1st	5	In	0.20	0.23
1st	6	In	0.20	0.23
1st	7	In	0.20	0.20
1st	8	In	0.27	0.30
2nd	9	Sb	-0.22	-0.21
2nd	10	Sb	-0.28	-0.28
2nd	11	Sb	-0.27	-0.27
2nd	12	Sb	-0.21	-0.22
2nd	13	Sb	-0.27	-0.27
2nd	14	Sb	-0.22	-0.22
2nd	15	Sb	-0.22	-0.21
2nd	16	Sb	-0.28	-0.28
3rd	17	In	0.14	0.13
3rd	18	In	0.14	0.15
3rd	19	In	0.11	0.11
3rd	20	In	0.16	0.17
3rd	21	In	0.12	0.11
3rd	22	In	0.13	0.13
3rd	23	In	0.17	0.17
3rd	24	In	0.13	0.14
4th	25	H	-0.02	-0.01
4th	26	H	-0.02	-0.02
4th	27	H	-0.01	-0.01
4th	28	H	-0.01	-0.02
4th	29	H	-0.02	-0.01
4th	30	H	-0.01	-0.01
4th	31	H	-0.01	-0.01
4th	32	H	-0.01	-0.01
4th	33	H	-0.01	-0.01
4th	34	H	-0.01	-0.02
4th	35	H	-0.02	-0.01
4th	36	H	-0.01	-0.02
4th	37	H	-0.01	-0.01
4th	38	H	-0.01	-0.01
4th	39	H	-0.02	-0.01
4th	40	H	-0.02	-0.01

Table 5.17 Charge distributions of (4x2) surface before and after dissociative adsorption of I_2 along angular approach

Layer	Atom label	Type of atom	Before dissociative adsorption	After dissociative adsorption
Adatom	1	I	-0.09	-0.27
Adatom	2	I	-0.17	-0.40
1st	3	In	0.19	0.22
1st	4	In	0.20	0.25
1st	5	In	0.26	0.31
1st	6	In	0.26	0.31
1st	7	In	0.19	0.22
1st	8	In	0.20	0.25
2nd	9	Sb	-0.22	-0.21
2nd	10	Sb	-0.26	-0.23
2nd	11	Sb	-0.29	-0.26
2nd	12	Sb	-0.23	-0.21
2nd	13	Sb	-0.28	-0.26
2nd	14	Sb	-0.24	-0.22
2nd	15	Sb	-0.22	-0.21
2nd	16	Sb	-0.26	-0.24
3rd	17	In	0.13	0.15
3rd	18	In	0.15	0.15
3rd	19	In	0.12	0.12
3rd	20	In	0.17	0.15
3rd	21	In	0.12	0.12
3rd	22	In	0.13	0.14
3rd	23	In	0.18	0.16
3rd	24	In	0.15	0.14
4th	25	H	-0.02	-0.02
4th	26	H	-0.02	-0.02
4th	27	H	-0.01	-0.01
4th	28	H	-0.01	-0.01
4th	29	H	-0.01	-0.01
4th	30	H	-0.01	-0.01
4th	31	H	0.00	0.00
4th	32	H	-0.01	-0.01
4th	33	H	0.00	0.00
4th	34	H	-0.01	-0.01
4th	35	H	-0.01	-0.01
4th	36	H	-0.01	-0.01
4th	37	H	-0.01	-0.02
4th	38	H	-0.01	-0.01
4th	39	H	-0.02	-0.02
4th	40	H	-0.02	-0.02

Table 5.18 Charge distributions of (4x2) surface before and after dissociative adsorption of I_2 along horizontal approach 1

Layer	Atom label	Type of atom	Before dissociative adsorption	After dissociative adsorption
Adatom	1	I	-0.17	-0.39
Adatom	2	I	-0.18	-0.38
1st	3	In	0.19	0.22
1st	4	In	0.21	0.28
1st	5	In	0.26	0.28
1st	6	In	0.26	0.28
1st	7	In	0.19	0.21
1st	8	In	0.20	0.28
2nd	9	Sb	-0.21	-0.22
2nd	10	Sb	-0.25	-0.22
2nd	11	Sb	-0.26	-0.24
2nd	12	Sb	-0.23	-0.15
2nd	13	Sb	-0.26	-0.23
2nd	14	Sb	-0.25	-0.25
2nd	15	Sb	-0.19	-0.13
2nd	16	Sb	-0.26	-0.22
3rd	17	In	0.14	0.14
3rd	18	In	0.15	0.15
3rd	19	In	0.11	0.13
3rd	20	In	0.15	0.14
3rd	21	In	0.12	0.12
3rd	22	In	0.14	0.14
3rd	23	In	0.18	0.16
3rd	24	In	0.14	0.11
4th	25	H	-0.01	-0.01
4th	26	H	-0.02	-0.01
4th	27	H	-0.01	-0.01
4th	28	H	-0.01	-0.01
4th	29	H	-0.02	-0.02
4th	30	H	-0.01	-0.02
4th	31	H	0.00	0.00
4th	32	H	-0.01	-0.01
4th	33	H	0.00	0.00
4th	34	H	-0.01	-0.01
4th	35	H	-0.01	-0.01
4th	36	H	-0.01	-0.01
4th	37	H	-0.01	-0.02
4th	38	H	-0.01	-0.01
4th	39	H	-0.02	-0.03
4th	40	H	-0.02	-0.02

Table 5.19 Charge distributions of (4x2) surface before and after dissociative adsorption of I_2 along horizontal approach 2

Layer	Atom label	Type of atom	Before dissociative adsorption	After dissociative adsorption
Adatom	1	I	-0.16	-0.39
Adatom	2	I	-0.13	-0.39
1st	3	In	0.19	0.22
1st	4	In	0.25	0.27
1st	5	In	0.20	0.29
1st	6	In	0.20	0.28
1st	7	In	0.19	0.23
1st	8	In	0.25	0.28
2nd	9	Sb	-0.22	-0.25
2nd	10	Sb	-0.25	-0.21
2nd	11	Sb	-0.27	-0.24
2nd	12	Sb	-0.21	-0.12
2nd	13	Sb	-0.27	-0.25
2nd	14	Sb	-0.22	-0.19
2nd	15	Sb	-0.21	-0.21
2nd	16	Sb	-0.25	-0.21
3rd	17	In	0.13	0.14
3rd	18	In	0.15	0.14
3rd	19	In	0.12	0.14
3rd	20	In	0.15	0.14
3rd	21	In	0.12	0.12
3rd	22	In	0.14	0.15
3rd	23	In	0.17	0.16
3rd	24	In	0.14	0.11
4th	25	H	-0.01	-0.01
4th	26	H	-0.01	-0.01
4th	27	H	-0.01	-0.02
4th	28	H	-0.01	-0.01
4th	29	H	-0.02	-0.02
4th	30	H	-0.01	-0.01
4th	31	H	0.00	0.00
4th	32	H	-0.01	0.00
4th	33	H	-0.01	0.00
4th	34	H	-0.01	-0.01
4th	35	H	-0.01	-0.01
4th	36	H	-0.01	-0.01
4th	37	H	-0.01	-0.02
4th	38	H	-0.01	-0.01
4th	39	H	-0.03	-0.03
4th	40	H	-0.02	-0.01

Table 5.20 Charge distributions of (4x2) surface before and after dissociative adsorption of I_2 along horizontal approach 3

Layer	Atom label	Type of atom	Before dissociative adsorption	After dissociative adsorption
Adatom	1	I	-0.17	-0.36
Adatom	2	I	-0.08	-0.31
1st	3	In	0.19	0.20
1st	4	In	0.25	0.31
1st	5	In	0.25	0.30
1st	6	In	0.19	0.29
1st	7	In	0.19	0.21
1st	8	In	0.30	0.37
2nd	9	Sb	-0.21	-0.21
2nd	10	Sb	-0.28	-0.26
2nd	11	Sb	-0.28	-0.28
2nd	12	Sb	-0.23	-0.18
2nd	13	Sb	-0.27	-0.29
2nd	14	Sb	-0.26	-0.20
2nd	15	Sb	-0.24	-0.19
2nd	16	Sb	-0.27	-0.25
3rd	17	In	0.13	0.13
3rd	18	In	0.15	0.14
3rd	19	In	0.11	0.11
3rd	20	In	0.17	0.16
3rd	21	In	0.12	0.13
3rd	22	In	0.13	0.12
3rd	23	In	0.17	0.17
3rd	24	In	0.13	0.10
4th	25	H	-0.02	-0.02
4th	26	H	-0.01	0.00
4th	27	H	-0.01	-0.01
4th	28	H	-0.01	-0.01
4th	29	H	-0.01	-0.02
4th	30	H	-0.02	-0.02
4th	31	H	-0.01	-0.01
4th	32	H	-0.01	-0.01
4th	33	H	-0.01	-0.01
4th	34	H	-0.01	-0.01
4th	35	H	-0.01	-0.01
4th	36	H	-0.01	-0.01
4th	37	H	-0.01	-0.02
4th	38	H	-0.01	-0.02
4th	39	H	-0.02	-0.03
4th	40	H	-0.02	-0.01

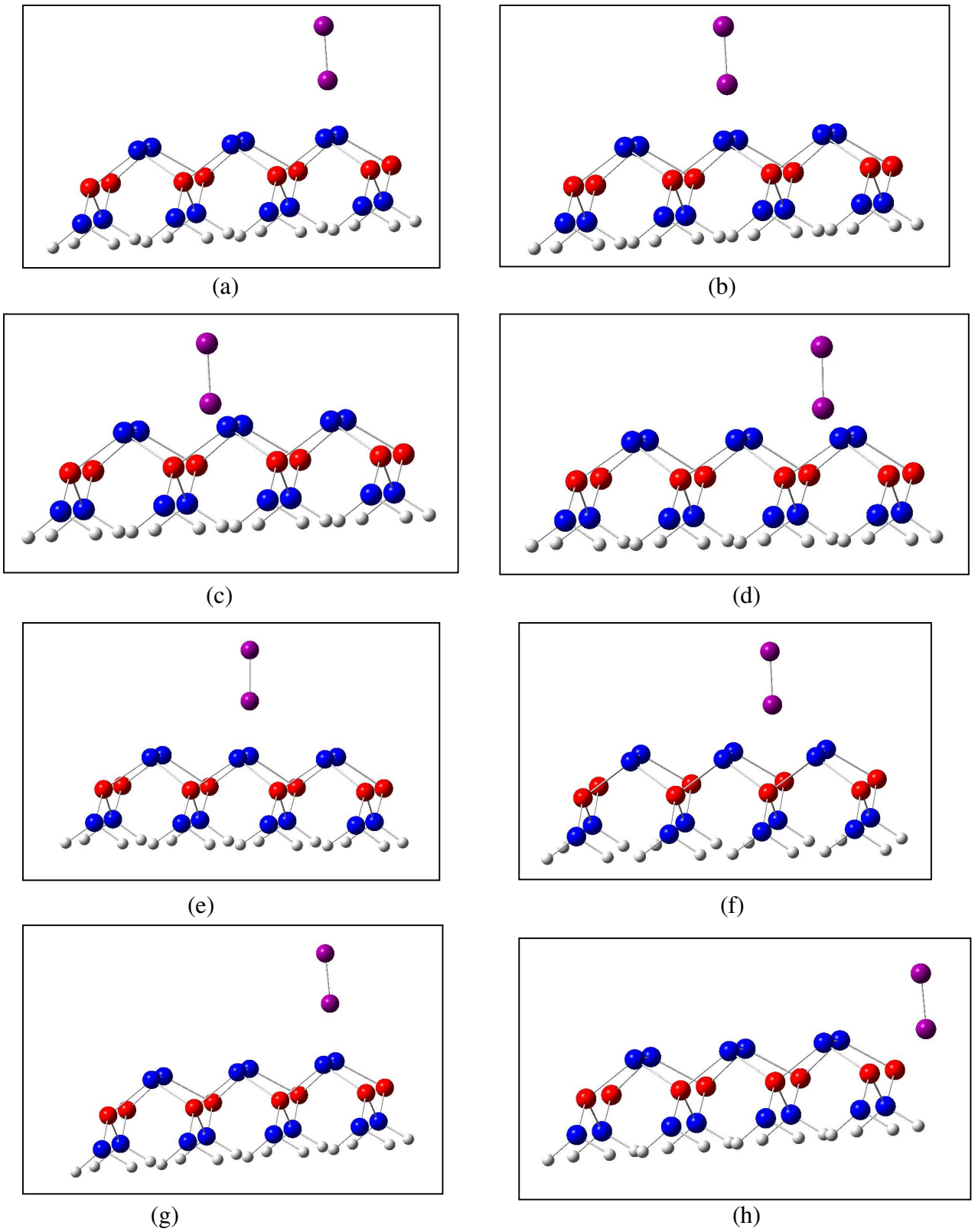

Figure 5.1 Molecular adsorption of I_2 on (4x2) surface along the vertical approach in bridge 1(a) bridge 2(b) hollow 2(c) hollow 1(d) top 2(e) cave(f) top 1(g) and trough(h) sites

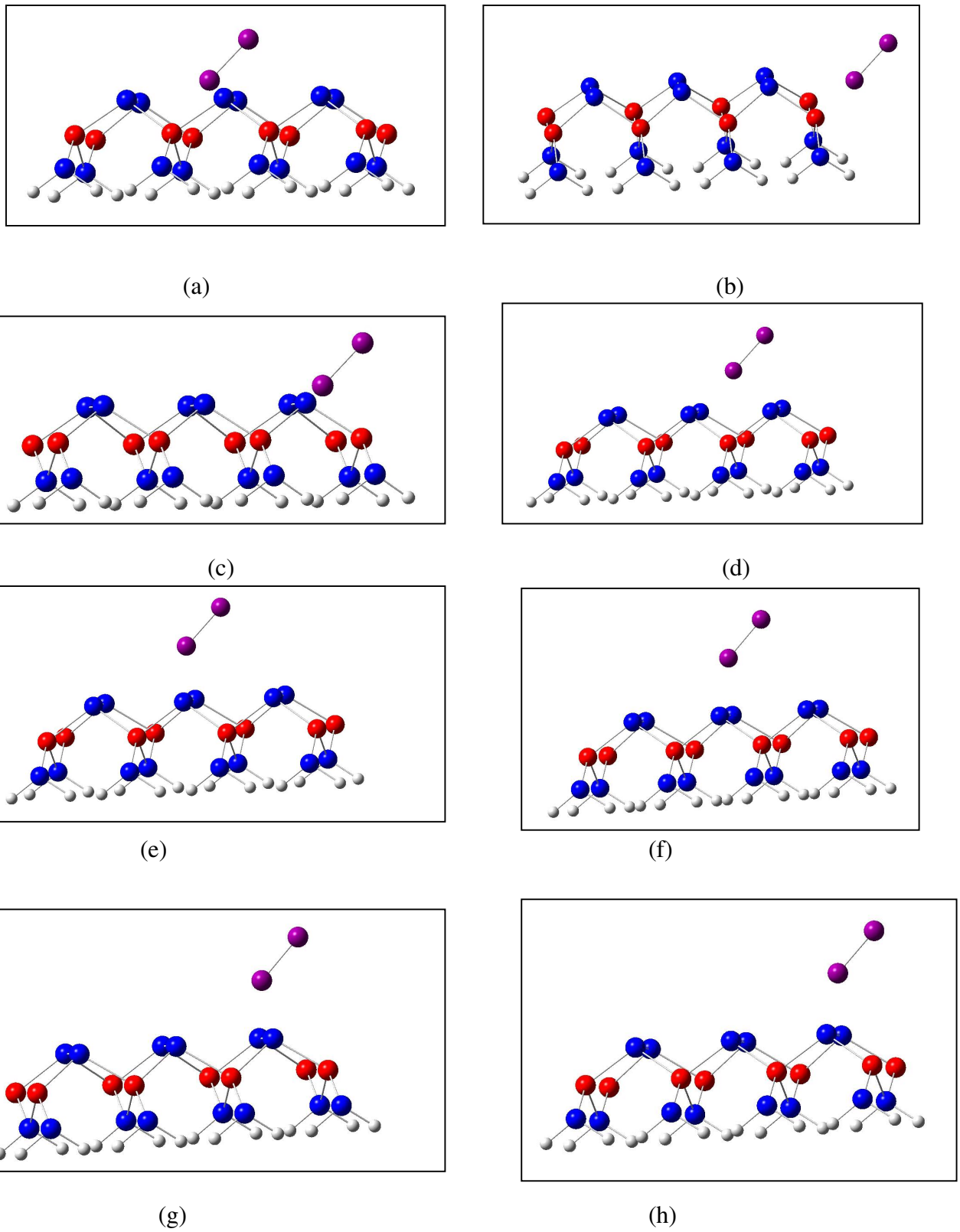

Figure 5.2 Molecular adsorption of I_2 on (4x2) surface along angular approach in hollow 2(a) trough(b) hollow 1(c) cave(d) bridge 2(e) top 2(f) bridge 1(g) and top 1(h) sites

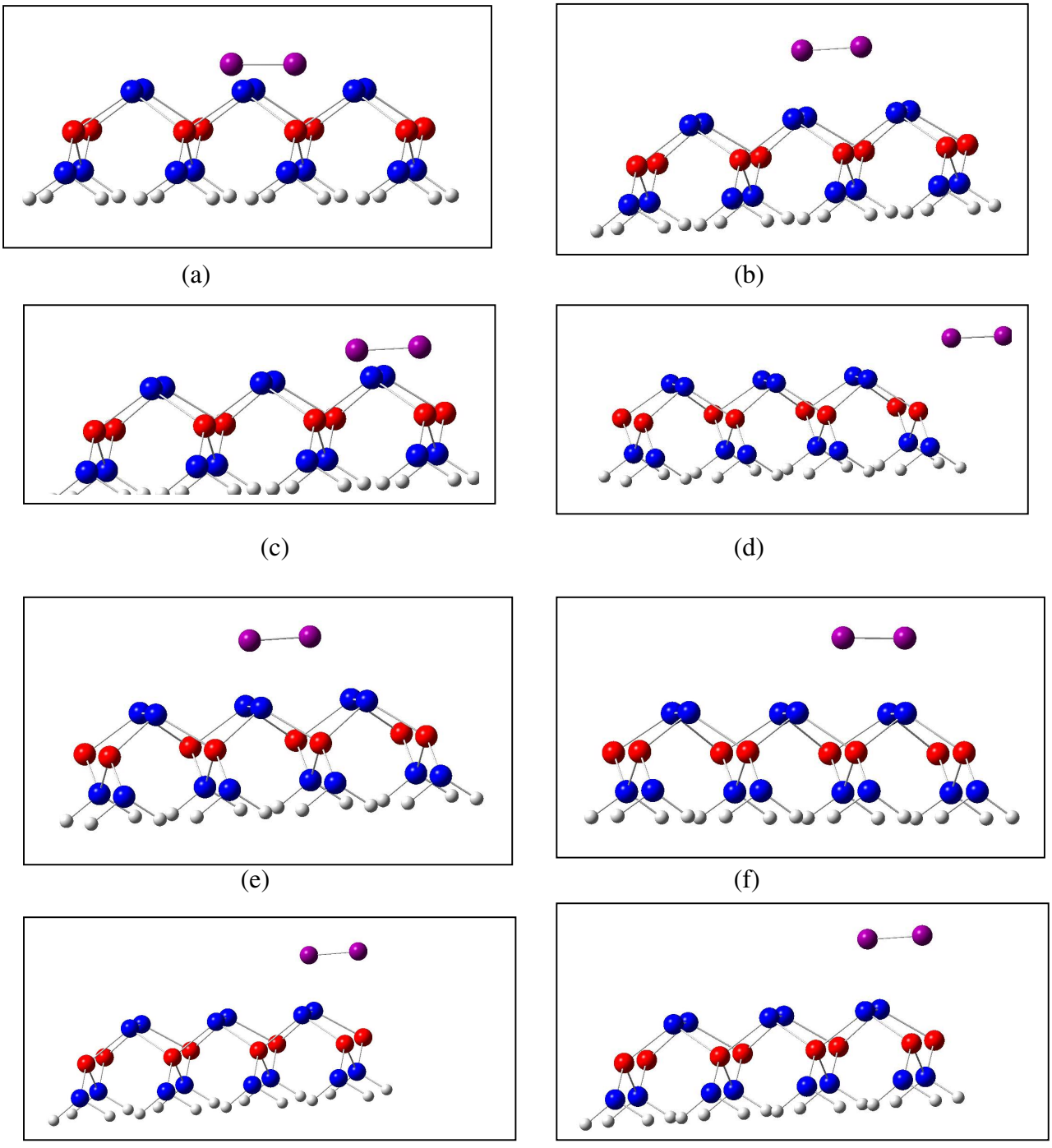

Figure 5.3 Molecular adsorption of I_2 on (4x2) surface along horizontal approach 1 in hollow 2(a) top 2(b) hollow 1(c) trough(d) bridge 2(e) cave(f) top 1(g) and bridge 1(h) sites

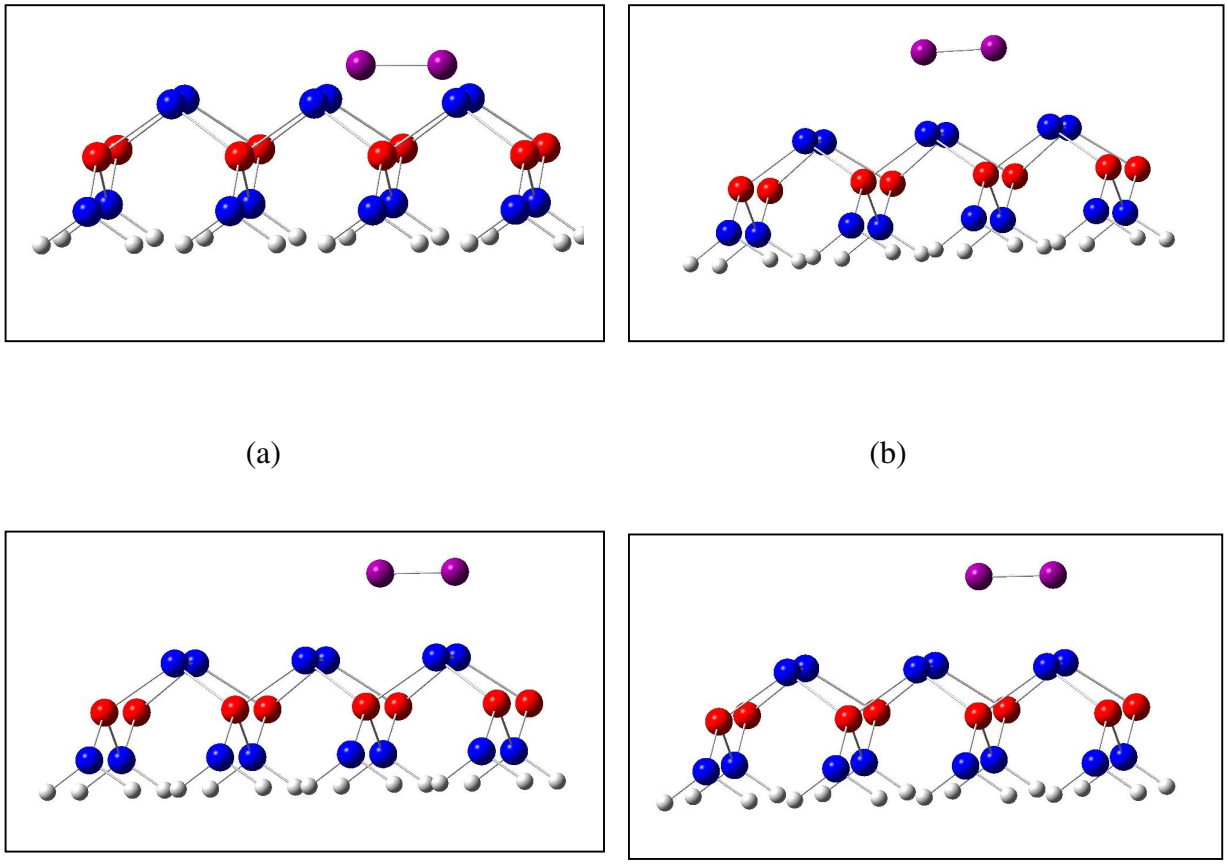

(a) (b)

(c) (d)

Figure 5.4 Molecular adsorption of I_2 on the (4x2) surface of In-rich InSb(100) surface in horizontal approach 2 on hollow 1(a) cave(b) top 1(c) and bridge 1(d) sites

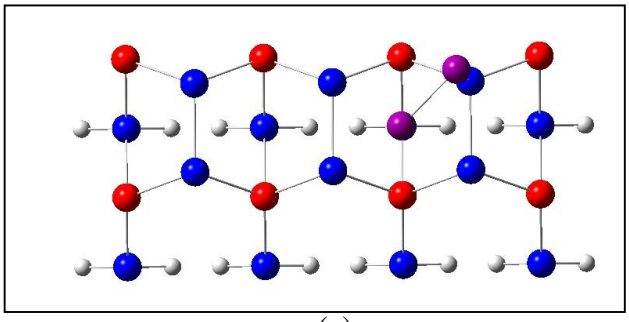

(a)

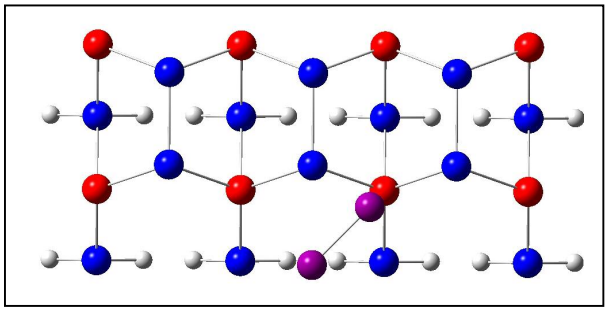

(b)

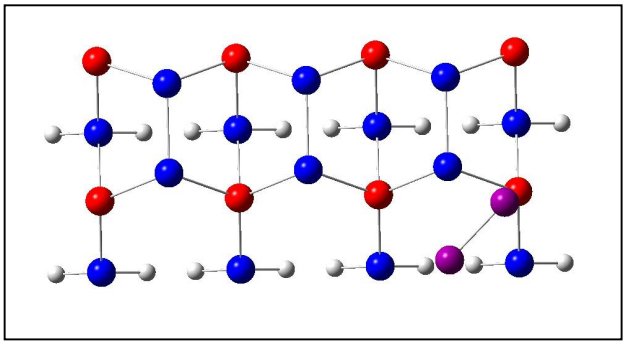

(c)

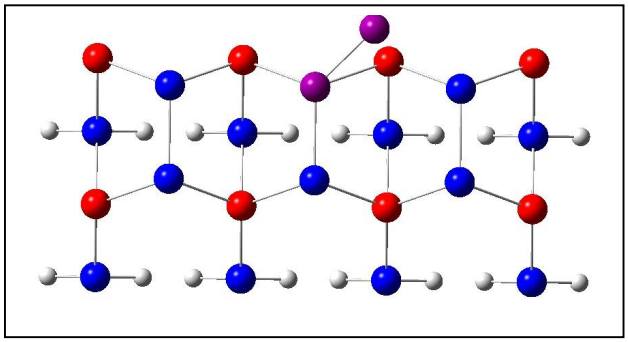

(d)

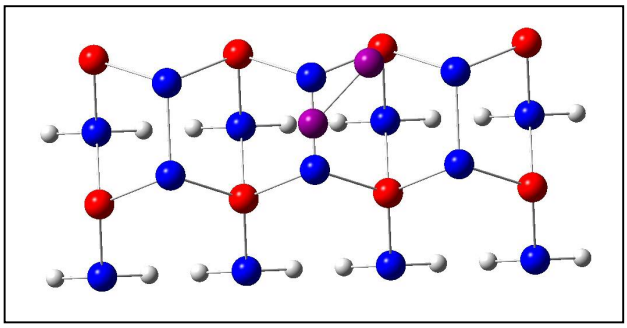

(e)

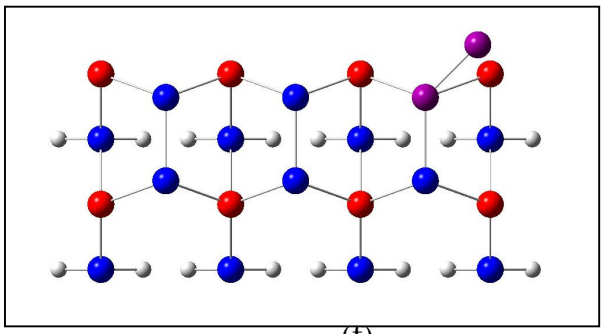

(f)

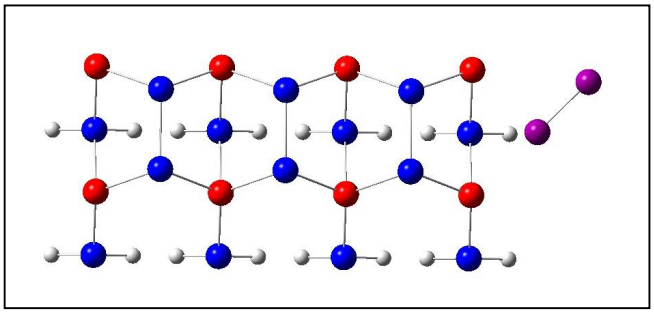

(g)

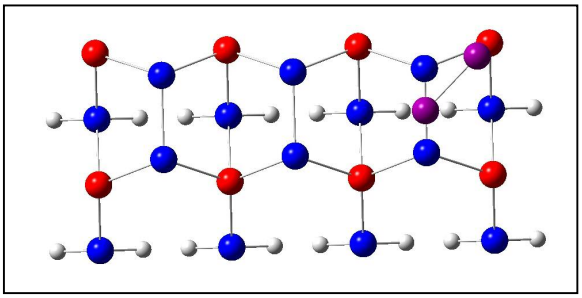

(h)

Figure 5.5 Molecular adsorption of I_2 on (4x2) surface along horizontal approach 3 in cave(a) hollow 2(b) hollow 1(c) top 2(d) bridge 2(e) top 1(f) trough(g) and bridge 1(h) sites

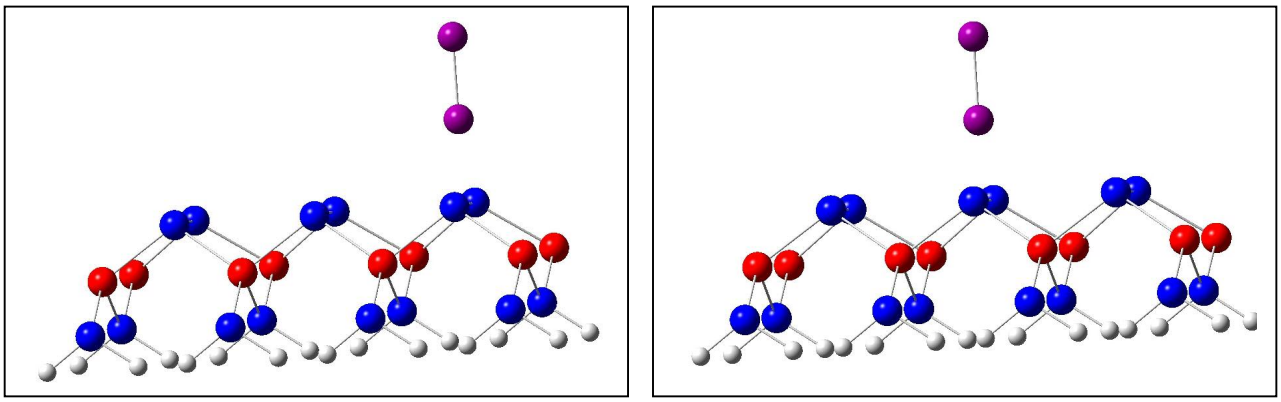

(a) (b)

Figure 5.6 I_2 adsorption on the (4x2) surface in bridge site 1 along vertical approach before (a) and after(b) dissociative adsorption

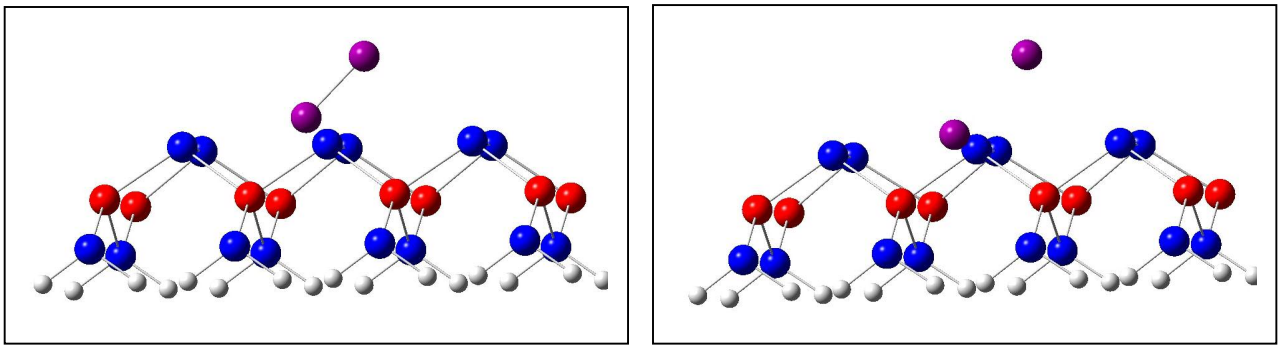

(a) (b)

Figure 5.7 I_2 adsorption on the (4x2) surface in hollow site 2 along angular approach before (a) and after(b) dissociative adsorption

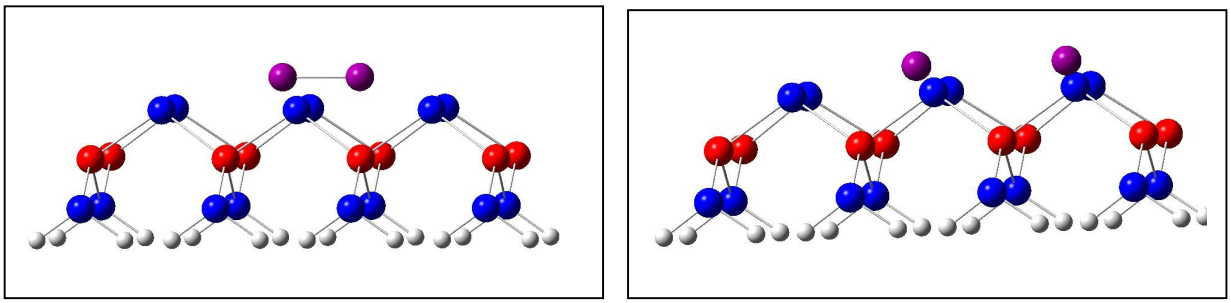

(a) (b)

Figure 5.8 I_2 adsorption on the (4x2) surface in hollow site 2 along horizontal approach 1 before (a) and after(b) dissociative adsorption

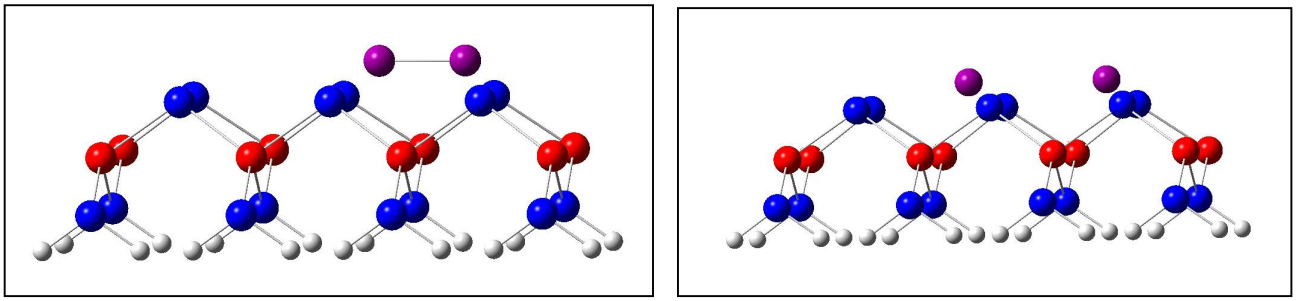

(b) (a)

Figure 5.9 I_2 adsorption on the (4x2) surface in hollow site 1 along horizontal approach 2 before(a) and after(b) dissociative adsorption

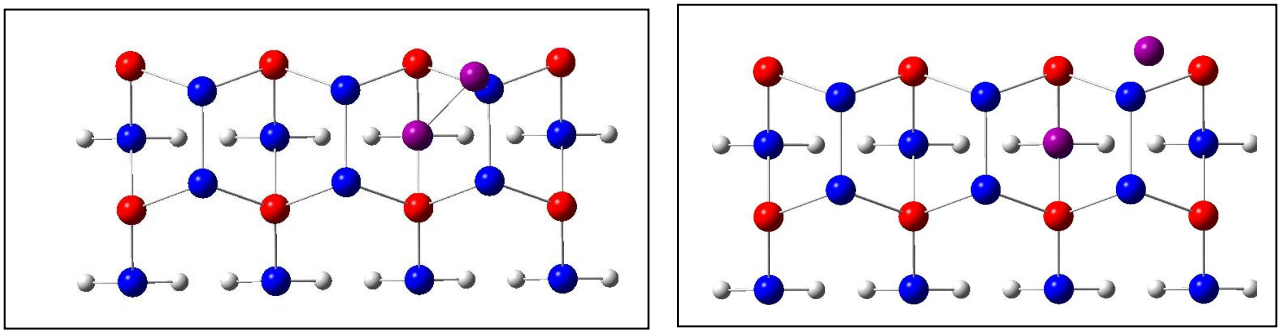

(a) (b)

Figure 5.10 I_2 adsorption on the (4x2) surface in cave site along horizontal approach 3 before(a) and after(b)dissociative adsorption

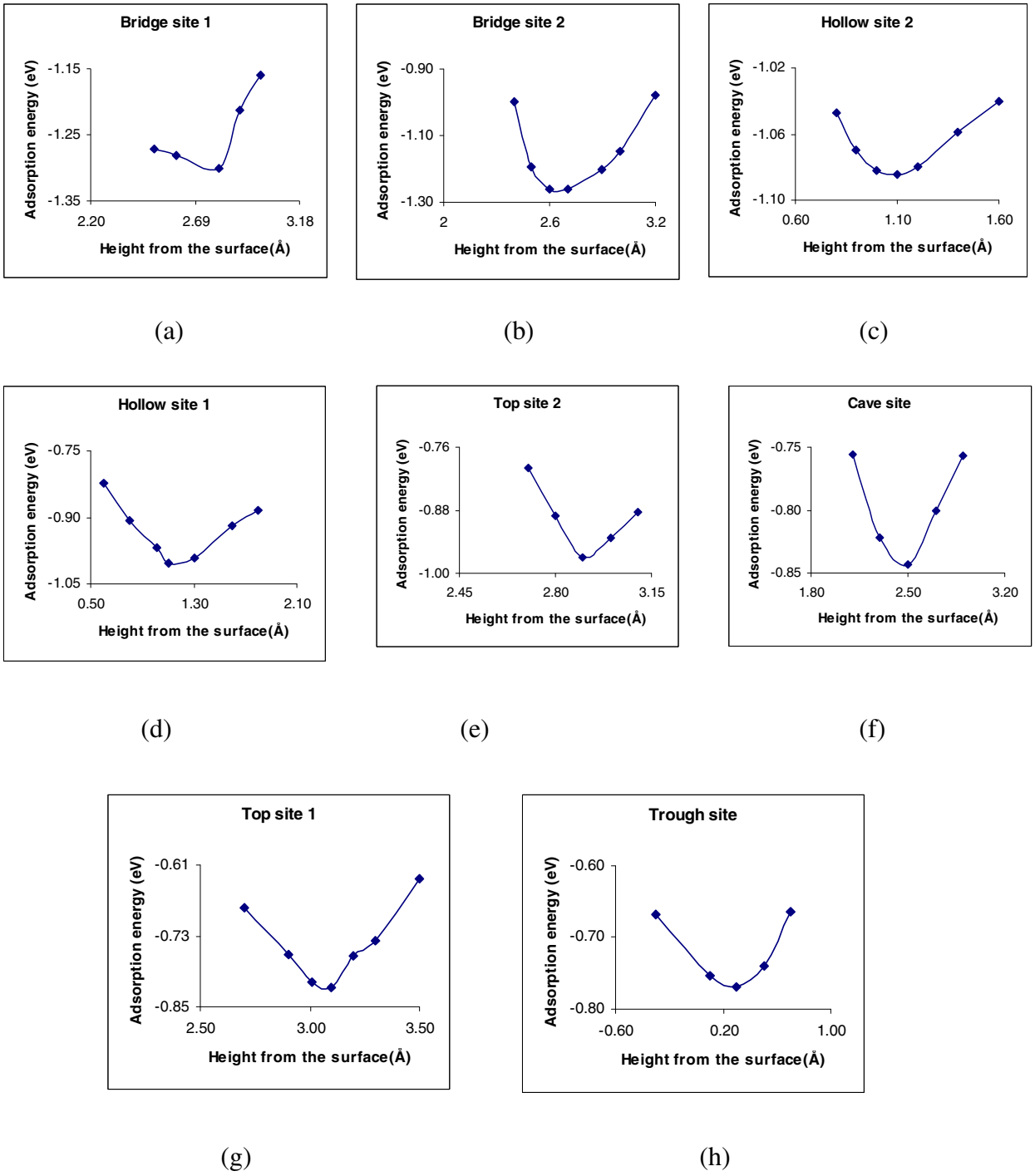

Figure 5.11 Adsorption energy (eV) vs. Height from the surface (Å) for the molecular adsorption of I_2 along vertical approach in bridge 1(a) bridge 2(b) hollow 2(c) hollow 1(d) top 2(e) cave(f) top 1(g) and trough(h) sites

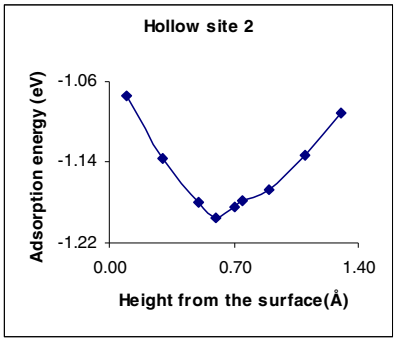

(a)

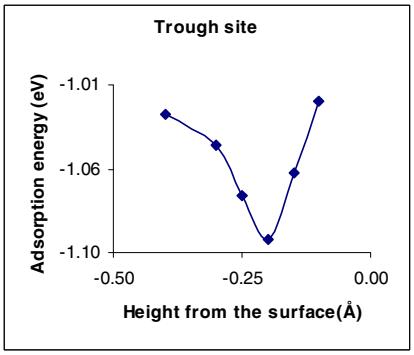

(b)

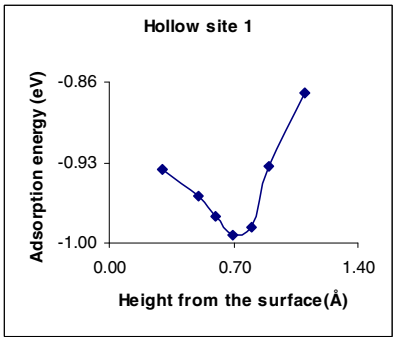

(c)

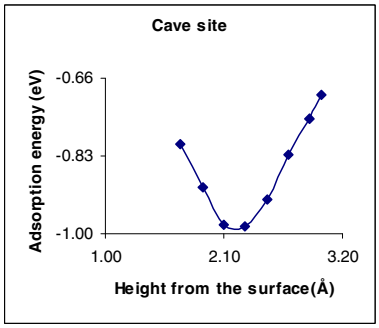

(d)

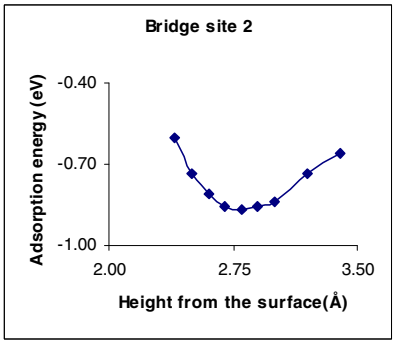

(e)

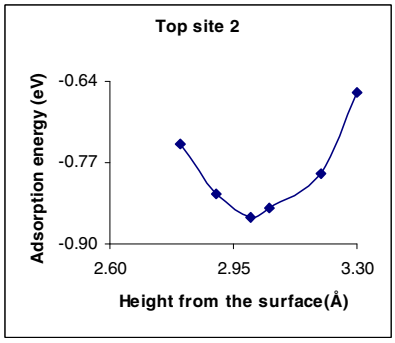

(f)

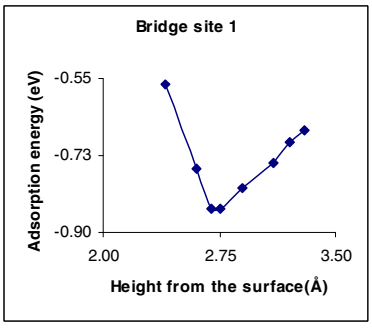

(g)

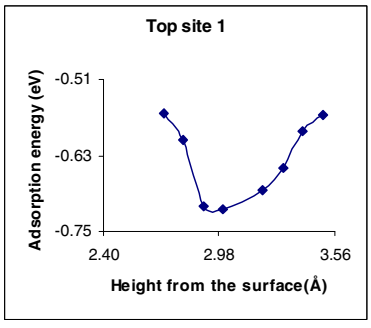

(h)

Figure 5.12 Adsorption energy (eV) vs. Height from the surface (Å) for the molecular adsorption of I_2 on (4x2) surface along angular approach in hollow 2(a) trough(b) hollow 1(c) cave(d) bridge 2(e) top 2(f) bridge 1(g) and top 1(h) sites

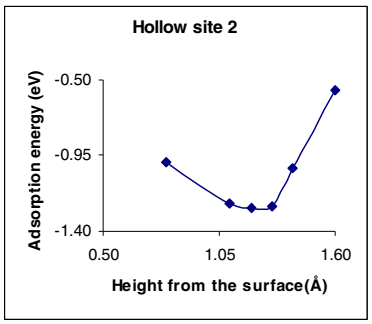

(a)

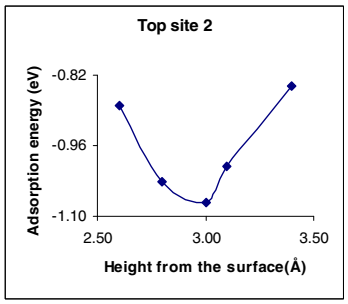

(b)

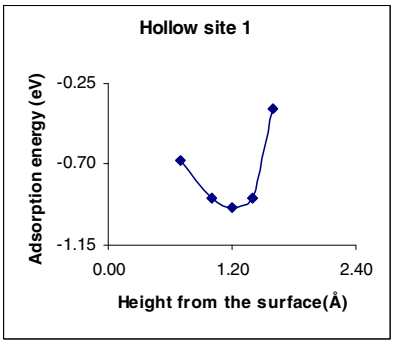

(c)

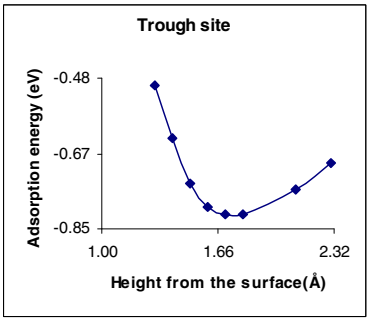

(d)

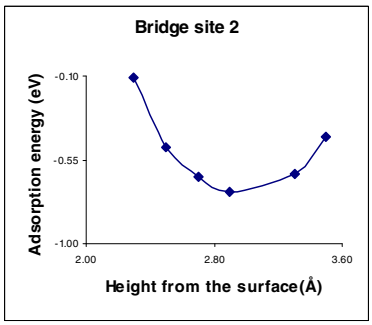

(e)

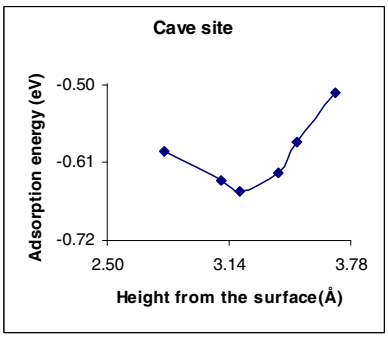

(f)

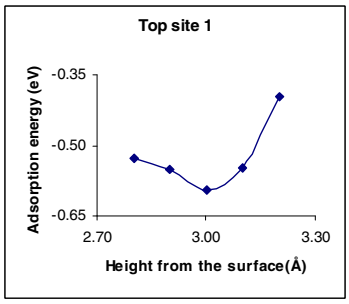

(g)

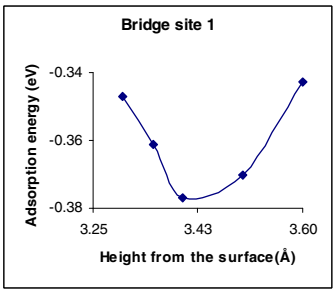

(h)

Figure 5.13 Adsorption energy (eV) vs. Height from the surface (Å) for the molecular adsorption of I_2 on (4x2) surface along the horizontal approach 1 in hollow 2(a) top 2(b) hollow 1(c) trough(d) bridge 2(e) cave(f) top 1(g) and bridge 1(h) sites

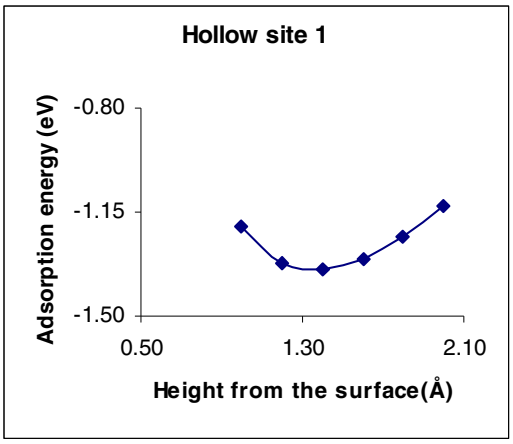

(a)

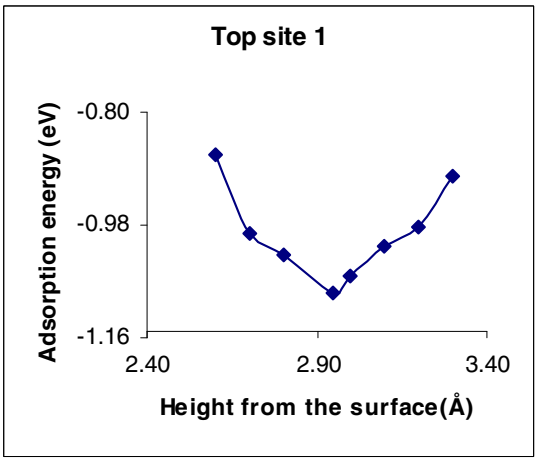

(b)

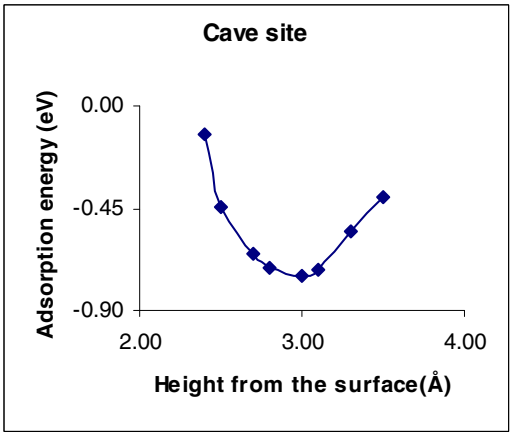

(c)

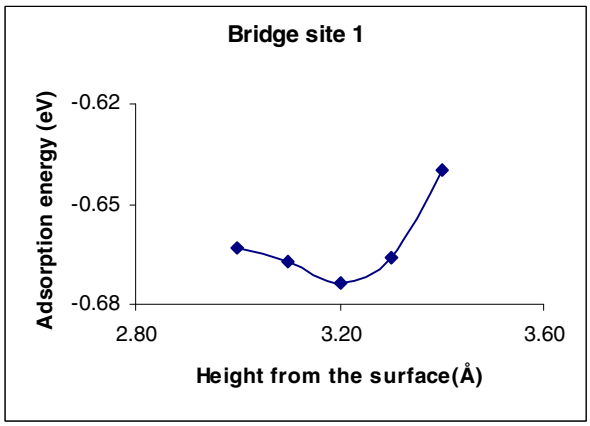

(d)

Figure 5.14 Adsorption energy (eV) vs. Height from the surface (Å) for the molecular adsorption of I_2 on the InSb(100) (4x2) surface along the horizontal approach 2 in hollow 1(a) top 1(b) cave(c) and bridge 1(d) sites

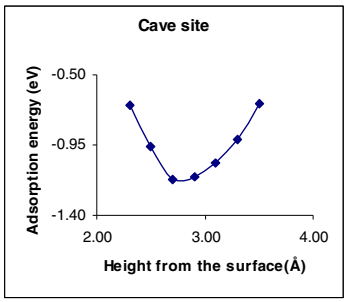

(a)

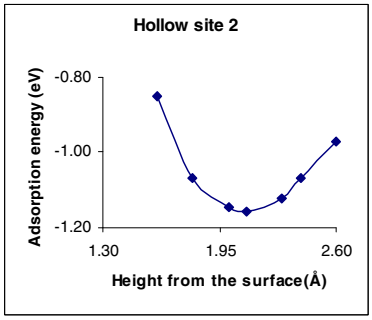

(b)

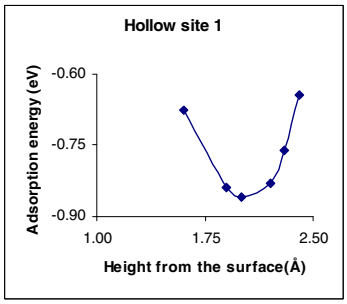

(c)

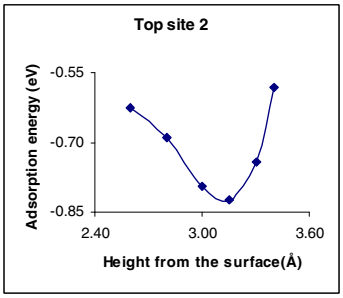

(d)

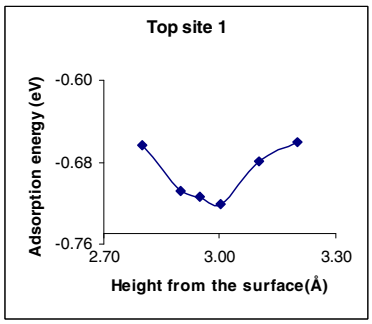

(e)

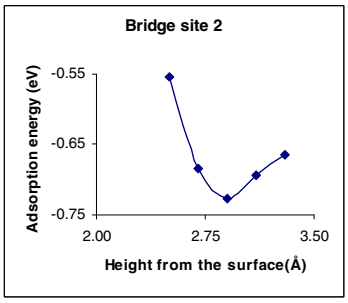

(f)

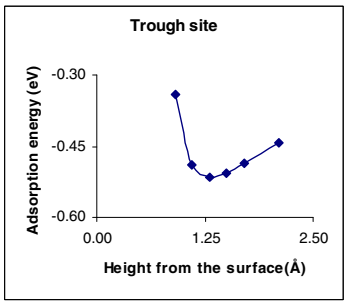

(g)

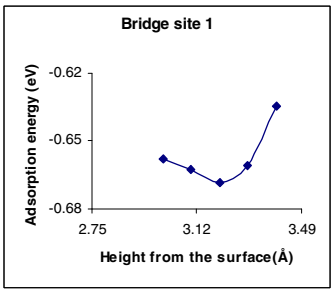

(h)

Figure 5.15 Adsorption energy (eV) vs. Height from the surface (Å) for the molecular adsorption of I_2 on (4x2) surface along horizontal approach 3 in cave(a) hollow 2(b) hollow 1(c) top 2(d) top 1(e) bridge 2(f) trough (g) and bridge 1(h) sites

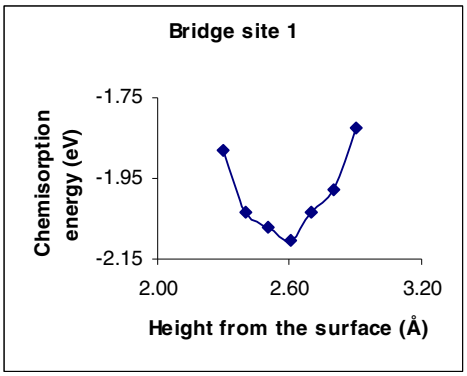

(a)

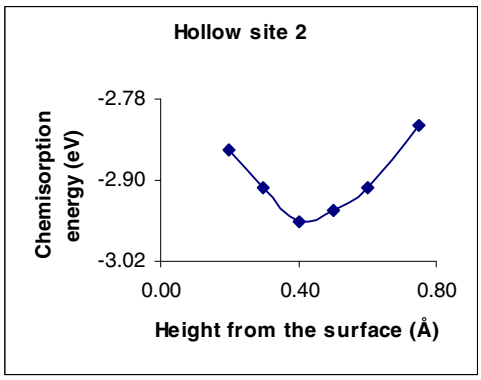

(b)

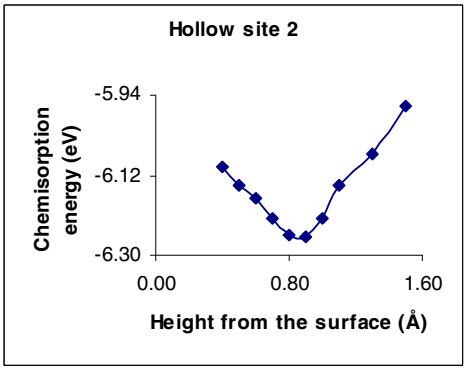

(c)

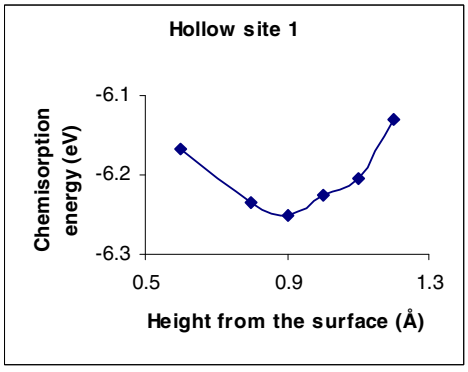

(d)

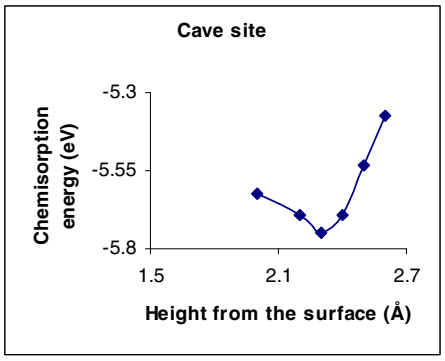

(e)

Figure 5.16 Chemisorption energy (eV) vs. Height from the surface (Å) for dissociative adsorption of I_2 along vertical(a) angular(b) horizontal 1(c) horizontal 2(d) and horizontal 3(e) approaches

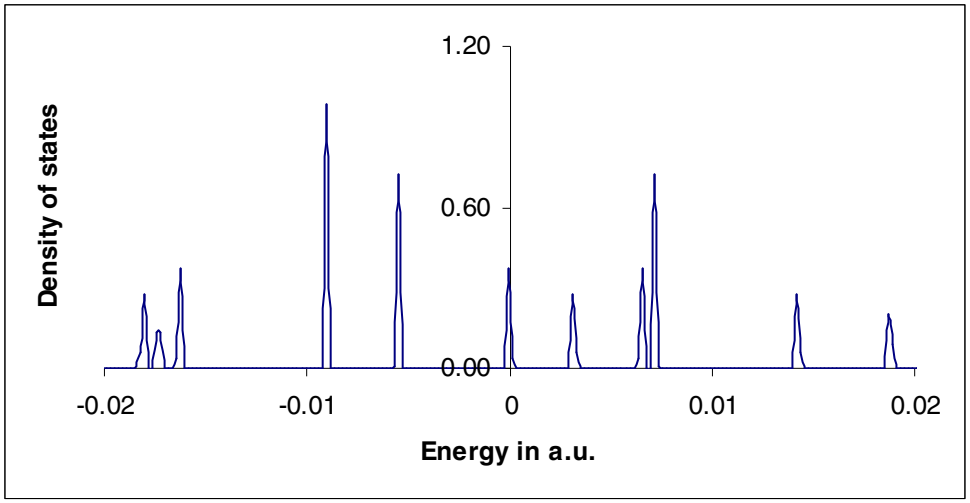

(a)

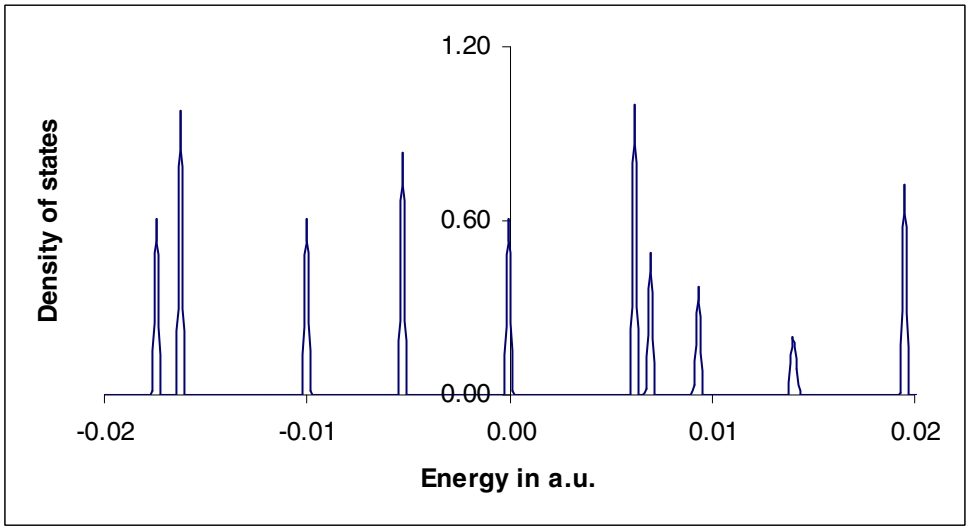

(b)

Figure 5.17 Density of states for (4x2) surface before(a) and after(b) molecular adsorption of I_2 along vertical approach

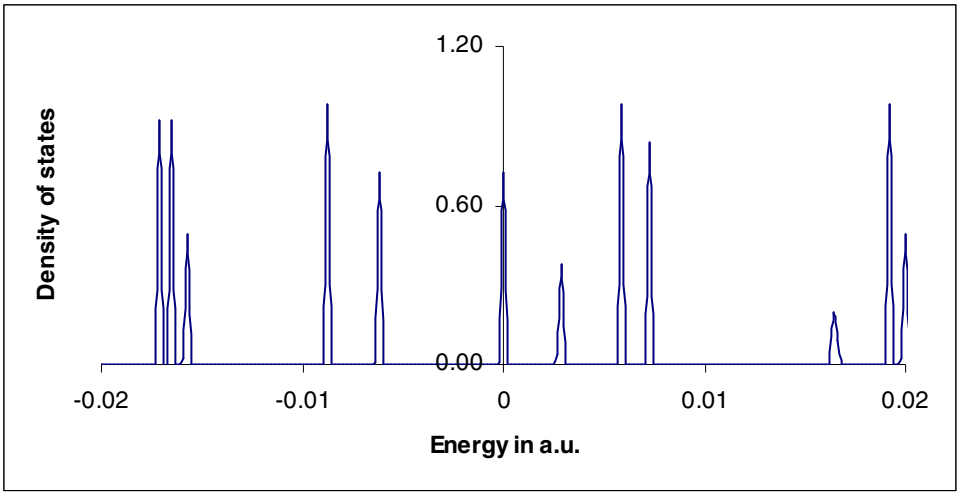

(a)

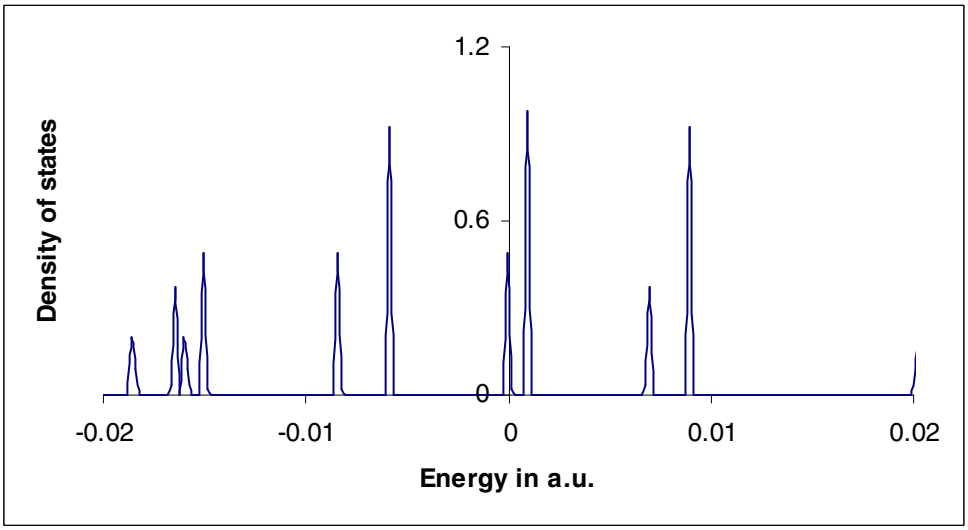

(b)

Figure 5.18 Density of states for (4x2) surface before(a) and after(b) dissociative adsorption of I_2 along angular approach

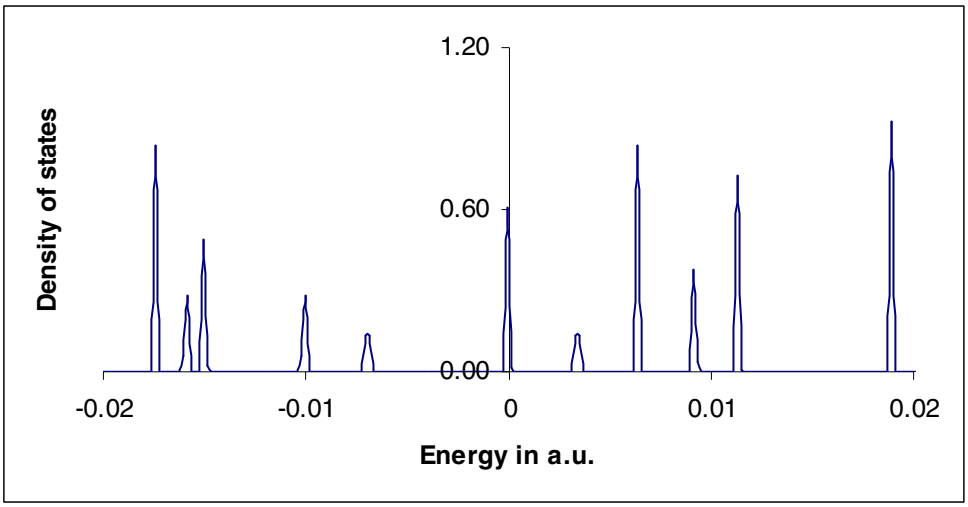

(a)

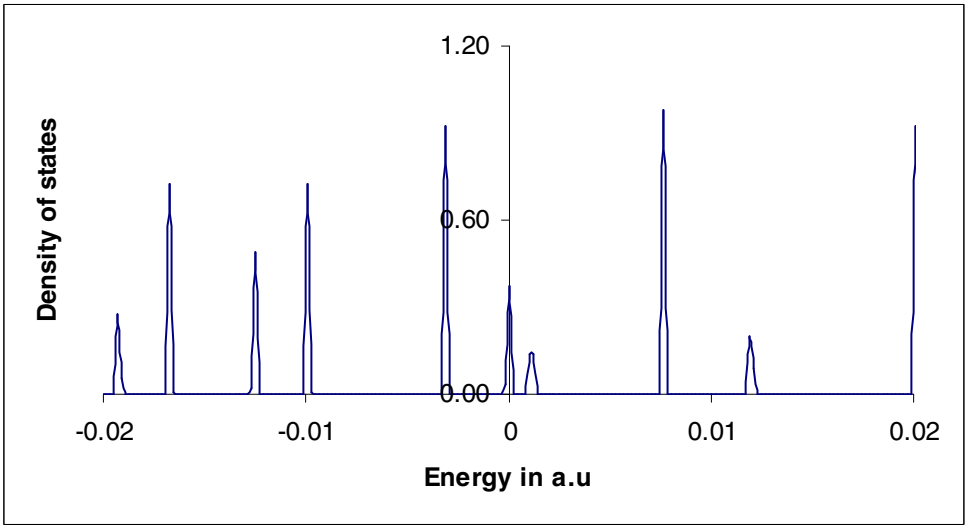

(b)

Figure 5.19 Density of states for (4x2) surface before(a) and after(b) dissociative adsorption of I_2 along horizontal approach 2

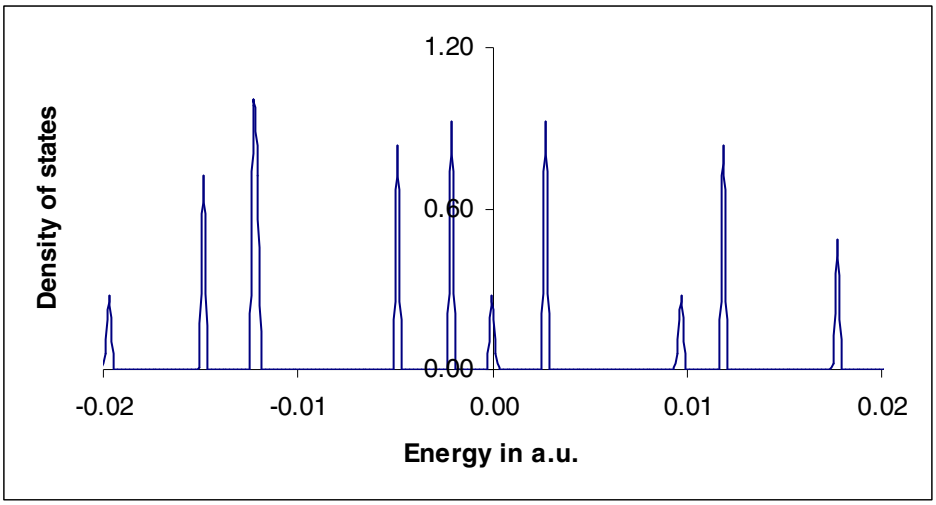

(a)

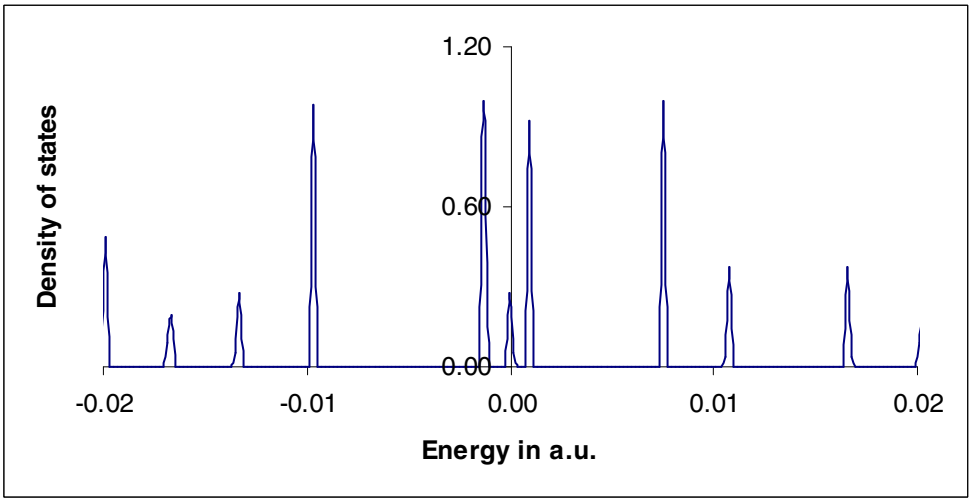

(b)

Figure 5.20 Density of states for (4x2) surface before (a) and after(b) dissociative adsorption of I_2 along horizontal approach 3

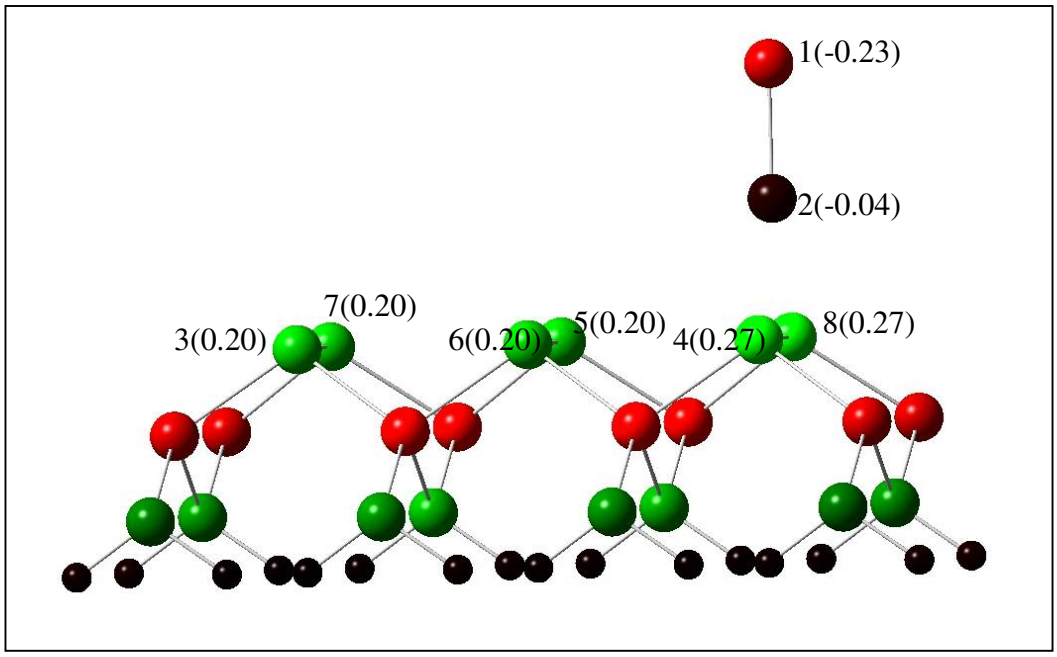

(a)

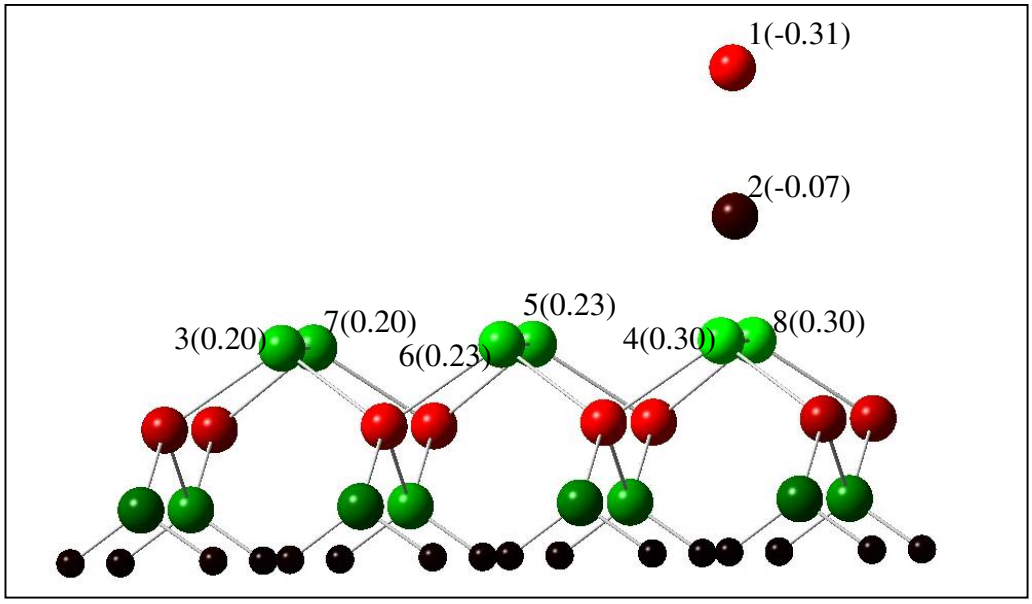

(b)

Figure 5.21 Atomic charge distribution of (4x2) surface before(a) and after(b) dissociative adsorption of I_2 along vertical approach

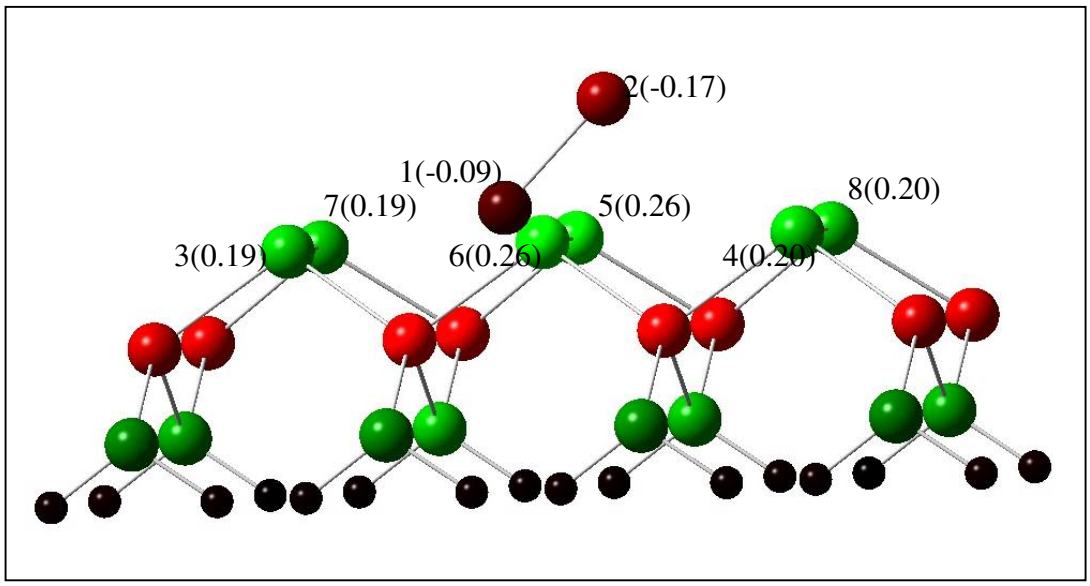

(a)

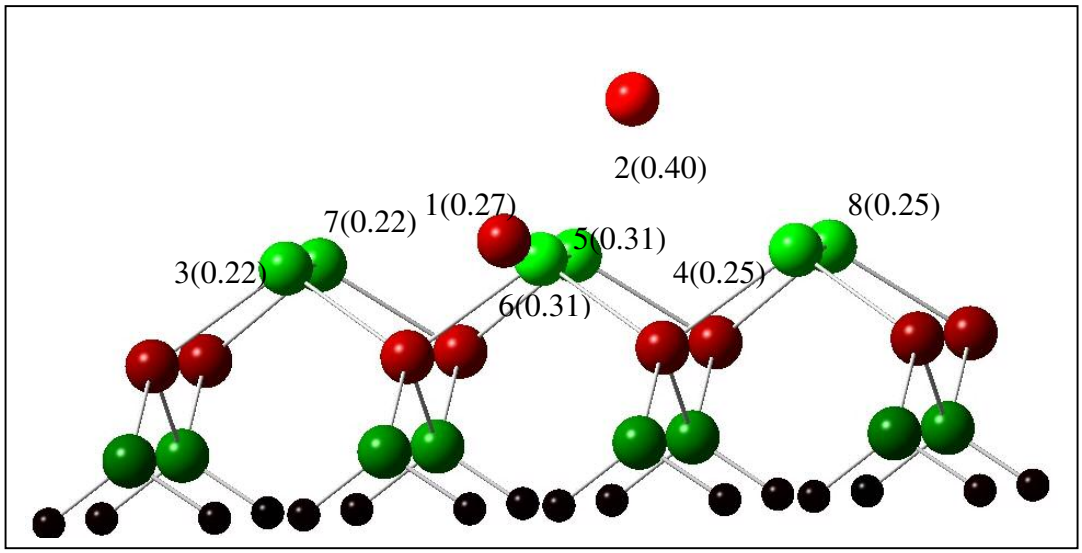

(b)

Figure 5.22 Atomic charge distribution of (4x2) surface before(a) and after(b) dissociative adsorption of I_2 in the hollow site 2 angular approach

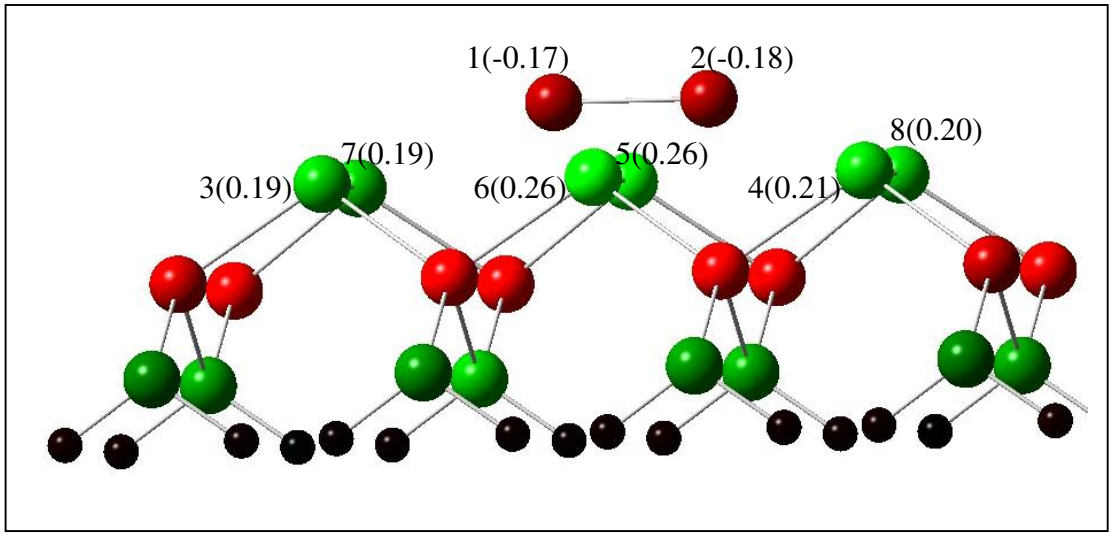

(a)

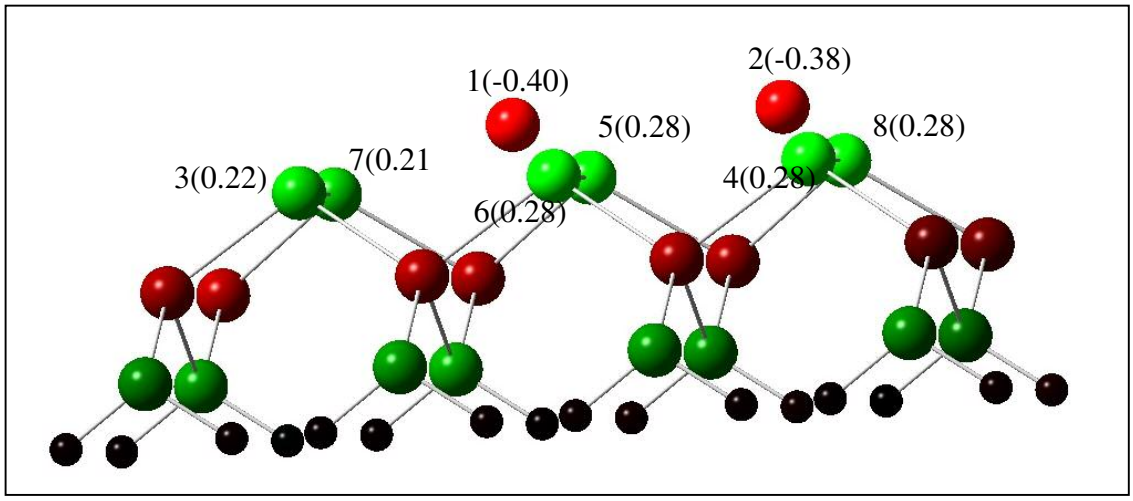

(b)

Figure 5.23 Atomic charge distribution of (4x2) surface before(a) and after(b) dissociative adsorption of I_2 along horizontal approach 1

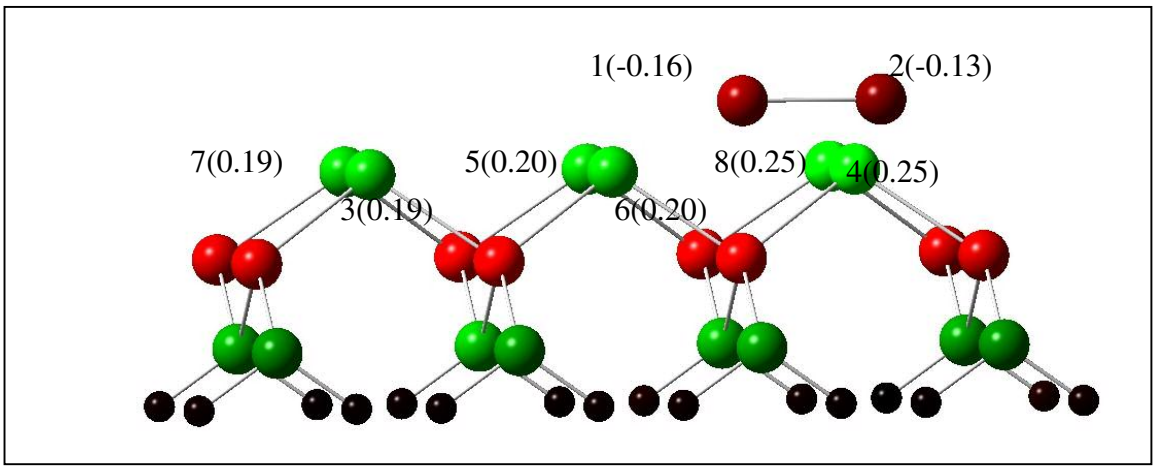

(a)

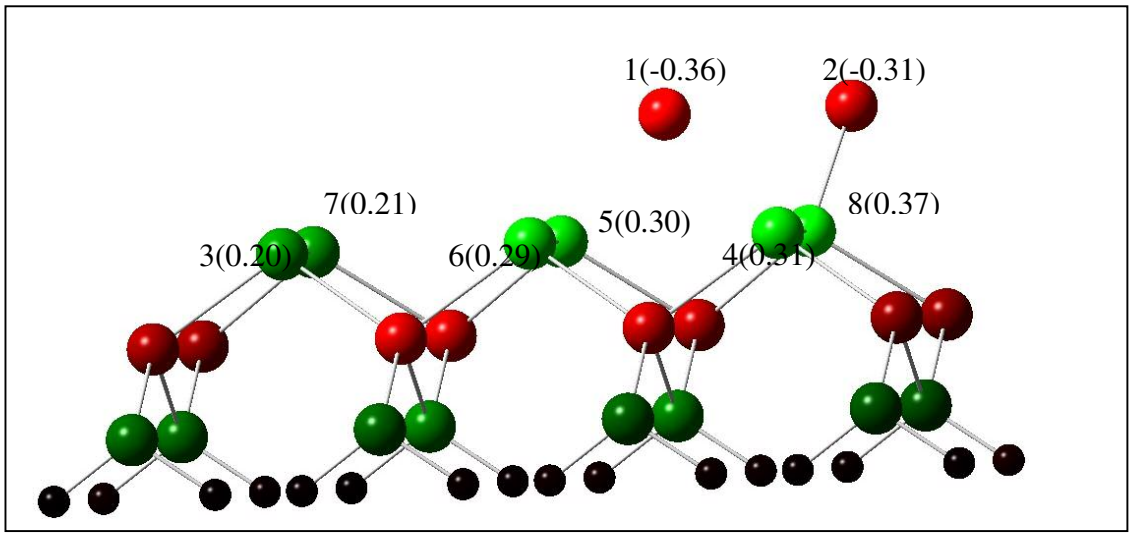

(b)

Figure 5.24 Atomic charge distribution of the (4x2) surface before(a) and after(b) dissociative adsorption of I_2 along horizontal approach 3

CHAPTER 6

CONCLUSIONS AND DIRECTIONS FOR FUTURE WORK

6.1 Relaxations and Reconstructions of In-rich InSb Surfaces.

During the study of relaxations and reconstructions of InSb(100) surfaces, the (2x1) surface was found to have comparatively higher binding energy compared to the (1x1), (4x2) and c(8x2) surfaces of InSb(100), though there were no experimental data reported about the existence of this surface. This surface was found to be more metallic when compared to the other (1x1), (4x2) and c(8x2) surfaces. This is in good agreement with the other available data found in the literature [74] concerning the (2x1) surface of the Ga-rich GaAs (100) surface. Also, both (4x2) surface and c(8x2) surfaces yielded similar binding energy per atom, dimer bondlengths and band gaps.

6.2 Atomic Adsorptions on InSb Surfaces

6.2.1 Li adsorption

During the adsorption studies of Li, the center site was found to be the most preferred site on (1x1) surface, hollow site for (2x1) surface and trough site for (4x2) and c(8x2) surfaces. In particular, the order of preferred sites for adsorption of Li on (1x1) surface is Center>Bridge>Top. For (2x1) surface, this ordering was Hollow>Cage>Cave>Bridge>Top. For both (4x2) and c(8x2) surfaces, this was found to be Trough>Hollow>Cage>Cave>Bridge>Top. The justification for this kind of preference lies in the fact that the coordination of the adatom with the neighboring

atoms decreases in the same order as listed above for each of the surfaces. For example, in the case of (1x1) surface, the center site was found to be the most coordinated site, followed by the bridge sites and then the top site. As discussed above, adsorption of Li on both (4x2) and c(8x2) surfaces yielded exactly very similar chemisorption energies for the different corresponding sites showing the equivalence of these two surfaces. From DOS plots as well as ΔGaps, it was clear that the adsorption of Li on the (1x1), (4x2) and c(8x2) surfaces reduced the band gaps of these surfaces. Similarly, the adsorption of Li on the (2x1) surface seems to increase the band gap of this surface. From the Mulliken Population Analysis, it was observed that Li atom loses charges and the In or Sb atoms, whichever lie closer to the adatom depending upon the site in which the adsorption is done gain the maximum amount of charges. It was noted that the Li atom loses maximum charges in the case of most preferred site during adsorption on each of the surfaces; for example 0.37 e during adsorption in the center site of (1x1) surface; 0.30 e for adsorption in hollow site of (2x1) surface; 0.47 e in trough site of (4x2) surface; and again 0.45 e in the trough site of c(8x2) surface.

6.2.2 Halogen(Cl, Br and I) Adsorption

During the adsorption of Cl, Br and I on the (1x1) surface, the order of preferred sites was found to be Bridge 1>Top>Center>Bridge 2. It was found that top site is the most preferred site for the adsorption of Cl, Br and I on the InSb(100) (2x1), (4x2) and c(8x2) surfaces where halogens can form strong, and directional bond. Also, it was found that the cage site was the least favored site during Cl adsorption, however, this site was not bound for Br and I. During the adsorptions of Br and I on (4x2) and c(8x2)

surfaces, trough site was found to be the least preferred site. It was noted that in the sites that were found to be least preferred, the adatom was found to have more coordination with the nearest neighbors. Overall, it was observed that chemisorption of Cl, Br and I on the (1x1) surface was more favorable than that of (2x1), (4x2) and c(8x2) surfaces. This is in good agreement with the available experimental data where it was found that after I_2 adsorption, the c(8x2) reconstruction was removed and a (1x1) LEED pattern was observed.

The order of the preferential sites is exactly the same for the cases of halogen adsorption on the (4x2) and c(8x2) surfaces and the adsorption energies are also very close in both these cases. The same trend was observed during the Lithium adsorption on the (4x2) and c(8x2) surfaces which allows us to conclude that the (4x2) and c(8x2) surfaces are equivalent [17].

The chemisorption energies for Cl adsorption on the InSb surfaces are found to be much than that of Br and the chemisorption energies for I was found to be the least for the comparable sites of different surfaces. Hence, the order of reactivity of halogens on InSb surfaces is Cl>Br>I which is expected because their electronegativities. This shows the possibility of Iodine being used as “gentler” etchant in semiconductor device processing where minimal amount of etchant-induced disorder is desired.

Several other trends were also obvious during this chemisorption studies. It was noted that the distance of the adatom from the surfaces decreases in the order of Top>Bridge>Cave>Hollow>Trough sites in the cases of adsorption on the (2x1), (4x2) and c(8x2) surfaces; for (1x1) surface, this ordering was found to be Top>Bridge

2>Bridge 1>Center site. The halogen-In dimer bondlengths were found to increase in the order of Cl<Br<I. This could be justified by considering the fact that the sizes of the different adatoms increase in the same order.

In general, the halogen adsorption on the (1x1), (4x2) and c(8x2) surfaces was found to lower the band gaps of these surfaces. In the case of (2x1) surface, the halogen adsorbed InSb(100) surface tends to have higher band gaps compared to that of the corresponding bare (2x1) surfaces.

From the Mulliken Population Analysis, it was observed that the halogens always gained charges and the In or Sb atoms whichever lie closer to the adatom was found to lose more charges; these charges were distributed as per the electronegativities of the different atoms involved. However, the highest charge gain was found to occur in the case of center site in (1x1) surface; in the hollow site for the cases of (2x1), (4x2) and c(8x2) surfaces during the adsorptions of Cl, Br and I. It was also found that in general, the charges gained by halogens follow the pattern Cl>Br>I. This is expected due to the fact the electronegativities of Cl>Br>I.

6.3 Molecular and Dissociative Adsorptions of I_2 on InSb (4x2) Surface

One important conclusion from the study of the different InSb surfaces and the atomic adsorptions of Li and halogen (Cl, Br and I) atoms on these surfaces is that the (4x2) and c(8x2) surfaces are equivalent. Similar values for dimer bondlengths, binding energy per atom and band gaps of these two surfaces and the one to one correspondence in the order of preferred sites during the atomic adsorptions of Li, Cl, Br and I on these (4x2) and c(8x2) surfaces allow us to conclude that these two surfaces are equivalent

Hence during our adsorption studies of I_2, (4x2) surface was used to study the reaction of I_2 on the InSb surface since this is a subunit of c(8x2) surface.

Overall, the adsorption energies of the molecular adsorption of I_2 was found to be very low ranging from 1.3 eV to 0.38 eV , from highest to lowest among all the approaches of the I_2 molecule. This, compared to the higher chemisorption energies found during the dissociative adsorptions, 6.26 eV to 2.36 eV, from highest to lowest in all the approaches of I_2 during dissociative adsorption. It was also observed that the dimer bondlengths of the I_2 molecule was found to increase, going from vertical to angular to horizontal approaches during dissociative adsorption. Both these tremendous increase in chemisorption energies and also in the dimer bondlengths during dissociative adsorptions tell us that the iodine molecule prefers dissociative adsorption when compared to molecular adsorption. This is in good agreement with the experimental studies as discussed in the introduction. Also, it was noted that going from vertical approach to angular to horizontal approaches, there is a consistent increase in the chemisorption energies during dissociative adsorption studies. The heights of the two iodine atoms were found to have decreased after dissociative chemisorptions when compared to their molecular counterparts.

During the dissociative adsorption of I_2 along horizontal approach 1, the iodine atoms were found to occupy the hollow sites, each iodine atom occupying separate hollow sites and the chemisorption energy for this geometry was found to be 6.26 eV. This chemisorption energy is almost equivalent to that of twice the chemisorption energy of 2.89 eV found during the atomic adsorption of Iodine in the hollow site.

Hence this particular dissociative chemisorption of I_2 along horizontal approach 1 could to though of as being equivalent to adsorption of two different iodine atoms in the hollow sites.

From the Mulliken Population Analysis, it was found that the electronic charges gained by both the iodine atoms in the case of dissociative adsorption were considerably high compared to their molecular counterparts. This is speculated to be the reason for the preference of dissociative adsorption. The charge distribution among the iodine atoms was found to become more symmetric, moving from the I_2 adsorption along vertical approach to angular approach to horizontal approaches. Also, the DOS plots show the reduction in band gaps for the (4x2) surface during dissociative adsorption in the angular approach, horizontal approach 2 and horizontal approach 3.

6.4 Directions for Future Work

In future, it would be interesting to study the reactions of oxygen and hydrogen atoms on the InSb surfaces as we know the abundance of these elements in the atmosphere and also hydrogen, due to its small size have more chances of interacting with these semiconductors during the storing process in any industry.

Also, there is a plenty of room for further research in the area of molecular adsorptions of halogens on the semiconductor surfaces. The coverage of the I_2 molecule on the surfaces could be increased and the changes in the geometric and electronic structure properties could be studied as a function of coverage of I_2

APPENDIX A

COORDINATES FOR InSb SURFACES AND CHEMISORPTIONS

Table A.1 Coordinates for (1x1) surface

Atom	X(Å)	Y(Å)	Z(Å)
In1	4.248135	4.248135	4.423193
In2	8.968285	8.968285	4.423193
In3	8.968285	4.248135	4.423193
In4	4.248135	8.968285	4.423193
In5	6.608210	1.888060	1.085543
In6	1.888060	6.608210	1.085543
In7	1.888060	1.888060	1.085543
In8	6.608210	6.608210	1.085543
Sb1	1.888060	4.248135	2.754368
Sb2	6.608210	8.968285	2.754368
Sb3	6.608210	4.248135	2.754368
Sb4	1.888060	8.968285	2.754368
H1	0.353046	6.608210	0.000125
H2	0.353046	1.888060	0.000125
H3	5.073284	6.607945	0.000000
H4	5.073196	1.888060	0.000125
H5	3.423074	6.608210	0.000125
H6	3.423074	1.888060	0.000125
H7	8.143223	6.608210	0.000125
H8	8.143223	1.888060	0.000125
TV	9.4403	0.0	0.0
TV	0.0	9.4403	0.0

Table A.2 Coordinates for (2x1) surface

Atom	X(Å)	Y(Å)	Z(Å)
In1	4.247944	5.097960	4.422919
In2	8.967882	8.117866	4.422919
In3	8.967882	5.097960	4.422919
In4	4.247944	8.117866	4.422919
In5	6.607913	1.887975	1.085419
In6	1.887975	6.607913	1.085419
In7	1.887975	1.887975	1.085419
In8	6.607913	6.607913	1.085419
Sb1	1.887975	4.247944	2.754169
Sb2	6.607913	8.967882	2.754169
Sb3	6.607913	4.247944	2.754169
Sb4	1.887975	8.967882	2.754169
H1	0.352962	6.607913	0.000000
H2	0.352962	1.887975	0.000000
H3	5.072899	6.607913	0.000000
H4	5.072899	1.887975	0.000000
H5	3.422989	6.607913	0.000000
H6	3.422989	1.887975	0.000000
H7	8.142926	6.607913	0.000000
H8	8.142926	1.887975	0.000000
TV	9.4399	0.0	0.0
TV	0.0	9.4399	0.0

Table A.3 Coordinates for (4x2) surface

Atom	X(Å)	Y(Å)	Z(Å)
In1	4.247944	5.072959	4.423135
In2	13.687820	5.072959	4.423135
In3	8.967882	8.142866	4.423135
In4	8.967882	5.072959	4.423135
In5	4.247944	8.142866	4.423135
In6	13.687820	8.142866	4.423135
In7	6.607913	1.887975	1.085635
In8	1.887975	6.607913	1.085635
In9	16.047788	1.887975	1.085635
In10	11.327851	6.607913	1.085635
In11	1.887975	1.887975	1.085635
In12	11.327851	1.887975	1.085635
In13	6.607913	6.607913	1.085635
In14	16.047788	6.607913	1.085635
Sb1	1.887975	4.247944	2.754385
Sb2	11.327851	4.247944	2.754385
Sb3	6.607913	8.967882	2.754385
Sb4	16.047788	8.967882	2.754385
Sb5	6.607913	4.247944	2.754385
Sb6	1.887975	8.967882	2.754385
Sb7	16.047788	4.247944	2.754385
Sb8	11.327851	8.967882	2.754385
H1	0.352962	6.607913	0.000217
H2	0.352962	1.887975	0.000217
H3	5.072899	6.607913	0.000217
H4	5.072899	1.887975	0.000217
H5	9.792837	6.607913	0.000217
H6	9.792837	1.887975	0.000217
H7	14.512928	6.608373	0.000217
H8	14.512775	1.887975	0.000217
H9	3.422989	6.607913	0.000217
H10	3.422989	1.887975	0.000217
H11	8.142926	6.607913	0.000217
H12	8.142926	1.887975	0.000217
H13	12.862864	6.607913	0.000217
H14	12.862864	1.887975	0.000217
H15	17.582802	6.607913	0.000217
H16	17.582802	1.887975	0.000217
TV	18.8798	0.0	0.0
TV	0.0	9.4399	0.0

Table A.4 Coordinates for c(8x2) surface

Atom	X(Å)	Y(Å)	Z(Å)
In1	4.247944	3.422929	4.423135
In2	13.687820	3.422929	4.423135
In3	8.967882	9.792897	4.423135
In4	23.127695	5.072959	4.423135
In5	32.567571	5.072959	4.423135
In6	27.847633	8.142866	4.423135
In7	8.967882	3.422929	4.423135
In8	4.247944	9.792897	4.423135
In9	13.687820	9.792897	4.423135
In10	27.847633	5.072959	4.423135
In11	23.127695	8.142866	4.423135
In12	32.567571	8.142866	4.423135
In13	6.607913	1.887975	1.085635
In14	1.887975	6.607913	1.085635
In15	16.047788	1.887975	1.085635
In16	11.327851	6.607913	1.085635
In17	25.487664	1.887975	1.085635
In18	20.767726	6.607913	1.085635
In19	34.927539	1.887975	1.085635
In20	30.207602	6.607913	1.085635
In21	1.887975	1.887975	1.085635
In22	11.327851	1.887975	1.085635
In23	6.607913	6.607913	1.085635
In24	20.767726	1.887975	1.085635
In25	16.047788	6.607913	1.085635
In26	30.207602	1.887975	1.085635
In27	25.487664	6.607913	1.085635
In28	34.927539	6.607913	1.085635
Sb1	1.887975	4.247944	2.754385
Sb2	11.327851	4.247944	2.754385
Sb3	6.607913	8.967882	2.754385
Sb4	20.767726	4.247944	2.754385
Sb5	16.047788	8.967882	2.754385
Sb6	30.207602	4.247944	2.754385
Sb7	25.487664	8 .967882	2.754385
Sb8	34.927539	8.967882	2.754385
Sb9	6.607913	4.247944	2.754385
Sb10	1.887975	8.967882	2.754385
Sb11	16.047788	4.247944	2.754385
Sb12	11.327851	8.967882	2.754385
Sb13	25.487664	4.247944	2.754385

Table A.4 - *Continued*

Sb14	20.767726	8.967882	2.754385
Sb15	34.927539	4.247944	2.754385
Sb16	30.207602	8.967882	2.754385
H1	0.352962	6.607913	0.000217
H2	0.352962	1.887975	0.000217
H3	5.072899	6.607913	0.000217
H4	5.072899	1.887975	0.000217
H5	9.792837	6.607913	0.000217
H6	9.792837	1.887975	0.000217
H7	14.512775	6.607913	0.000217
H8	14.512775	1.887975	0.000217
H9	19.232713	6.607913	0.000217
H10	19.232713	1.887975	0.000217
H11	23.952650	6.607913	0.000217
H12	23.952650	1.887975	0.000217
H13	28.672588	6.607913	0.000217
H14	28.672588	1.887975	0.000217
H15	33.392679	6.608373	0.000000
H16	33.392526	1.887975	0.000217
H17	3.422989	6.607913	0.000217
H18	3.422989	1.887975	0.000217
H19	8.142926	6.607913	0.000217
H20	8.142926	1.887975	0.000217
H21	12.862864	6.607913	0.000217
H22	12.862864	1.887975	0.000217
H23	17.582802	6.607913	0.000217
H24	17.582802	1.887975	0.000217
H25	22.302740	6.607913	0.000217
H26	22.302740	1.887975	0.000217
H27	27.022677	6.607913	0.000217
H28	27.022677	1.887975	0.000217
H29	31.742615	6.607913	0.000217
H30	31.742615	1.887975	0.000217
H31	36.462553	6.607913	0.000217
H32	36.462553	1.887975	0.000217
TV	37.7595	0.0	0.0
TV	0.0	9.4399	0.0

Table A.5 Coordinates for Li adsorption in the hollow site of (2x1) surface

Atom	X(Å)	Y(Å)	Z(Å)
Li	8.967882	1.887963	2.322919
In1	4.247944	5.097960	4.422919
In2	8.967882	8.117866	4.422919
In3	8.967882	5.097960	4.422919
In4	4.247944	8.117866	4.422919
In5	6.607913	1.887975	1.085419
In6	1.887975	6.607913	1.085419
In7	1.887975	1.887975	1.085419
In8	6.607913	6.607913	1.085419
Sb1	1.887975	4.247944	2.754169
Sb2	6.607913	8.967882	2.754169
Sb3	6.607913	4.247944	2.754169
Sb4	1.887975	8.967882	2.754169
H1	0.352962	6.607913	0.000000
H2	0.352962	1.887975	0.000000
H3	5.072899	6.607913	0.000000
H4	5.072899	1.887975	0.000000
H5	3.422989	6.607913	0.000000
H6	3.422989	1.887975	0.000000
H7	8.142926	6.607913	0.000000
H8	8.142926	1.887975	0.000000
TV	9.4399	0.0	0.0
TV	0.0	9.4399	0.0

Table A.6 Coordinates for Li adsorption in the cage site of (2x1) surface

Atom	X(Å)	Y(Å)	Z(Å)
Li	8.967882	6.607913	1.622919
In1	4.247944	5.097960	4.422919
In2	8.967882	8.117866	4.422919
In3	8.967882	5.097960	4.422919
In4	4.247944	8.117866	4.422919
In5	6.607913	1.887975	1.085419
In6	1.887975	6.607913	1.085419
In7	1.887975	1.887975	1.085419
In8	6.607913	6.607913	1.085419
Sb1	1.887975	4.247944	2.754169
Sb2	6.607913	8.967882	2.754169
Sb3	6.607913	4.247944	2.754169
Sb4	1.887975	8.967882	2.754169
H1	0.352962	6.607913	0.000000
H2	0.352962	1.887975	0.000000
H3	5.072899	6.607913	0.000000
H4	5.072899	1.887975	0.000000
H5	3.422989	6.607913	0.000000
H6	3.422989	1.887975	0.000000
H7	8.142926	6.607913	0.000000
H8	8.142926	1.887975	0.000000
TV	9.4399	0.0	0.0
TV	0.0	9.4399	0.0

Table A.7 Coordinates for Li adsorption in the cave site of (2x1) surface

Atom	X(Å)	Y(Å)	Z(Å)
Li	6.607913	6.607913	4.222919
In1	4.247944	5.097960	4.422919
In2	8.967882	8.117866	4.422919
In3	8.967882	5.097960	4.422919
In4	4.247944	8.117866	4.422919
In5	6.607913	1.887975	1.085419
In6	1.887975	6.607913	1.085419
In7	1.887975	1.887975	1.085419
In8	6.607913	6.607913	1.085419
Sb1	1.887975	4.247944	2.754169
Sb2	6.607913	8.967882	2.754169
Sb3	6.607913	4.247944	2.754169
Sb4	1.887975	8.967882	2.754169
H1	0.352962	6.607913	0.000000
H2	0.352962	1.887975	0.000000
H3	5.072899	6.607913	0.000000
H4	5.072899	1.887975	0.000000
H5	3.422989	6.607913	0.000000
H6	3.422989	1.887975	0.000000
H7	8.142926	6.607913	0.000000
H8	8.142926	1.887975	0.000000
TV	9.4399	0.0	0.0
TV	0.0	9.4399	0.0

Table A.8. Coordinates for Li adsorption in the bridge site of (2x1) surface

Atom	X(Å)	Y(Å)	Z(Å)
Li	8.967882	6.607913	6.722919
In1	4.247944	5.097960	4.422919
In2	8.967882	8.117866	4.422919
In3	8.967882	5.097960	4.422919
In4	4.247944	8.117866	4.422919
In5	6.607913	1.887975	1.085419
In6	1.887975	6.607913	1.085419
In7	1.887975	1.887975	1.085419
In8	6.607913	6.607913	1.085419
Sb1	1.887975	4.247944	2.754169
Sb2	6.607913	8.967882	2.754169
Sb3	6.607913	4.247944	2.754169
Sb4	1.887975	8.967882	2.754169
H1	0.352962	6.607913	0.000000
H2	0.352962	1.887975	0.000000
H3	5.072899	6.607913	0.000000
H4	5.072899	1.887975	0.000000
H5	3.422989	6.607913	0.000000
H6	3.422989	1.887975	0.000000
H7	8.142926	6.607913	0.000000
H8	8.142926	1.887975	0.000000
TV	9.4399	0.0	0.0
TV	0.0	9.4399	0.0

Table A.9 Coordinates for Li adsorption in the top site of (2x1) surface

Atom	X(Å)	Y(Å)	Z(Å)
Li	8.967882	8.117866	7.122919
In1	4.247944	5.097960	4.422919
In2	8.967882	8.117866	4.422919
In3	8.967882	5.097960	4.422919
In4	4.247944	8.117866	4.422919
In5	6.607913	1.887975	1.085419
In6	1.887975	6.607913	1.085419
In7	1.887975	1.887975	1.085419
In8	6.607913	6.607913	1.085419
Sb1	1.887975	4.247944	2.754169
Sb2	6.607913	8.967882	2.754169
Sb3	6.607913	4.247944	2.754169
Sb4	1.887975	8.967882	2.754169
H1	0.352962	6.607913	0.000000
H2	0.352962	1.887975	0.000000
H3	5.072899	6.607913	0.000000
H4	5.072899	1.887975	0.000000
H5	3.422989	6.607913	0.000000
H6	3.422989	1.887975	0.000000
H7	8.142926	6.607913	0.000000
H8	8.142926	1.887975	0.000000
TV	9.4399	0.0	0.0
TV	0.0	9.4399	0.0

REFERENCES

[1] http://www.reed-electronics.com/electronicnews/article/CA149786.html

[2] http://www.onr.navy.mil/sci_tech/information/312_electronics/ncsr/glossary.asp

[3] http://www.intel.com/pressroom/archive/releases/20050208corp.htm

[4] I. Kanno, F. Yoshihara, R. Nouchi, Osamu Sugiura, Y. Murase, T. Nakamura and M. Katagiri, Rev. Sci. Instr. **74**, 3968 (2003).

[5] T. Nakamura, M. Katagiri, Y. Aratone, I. Kanno, S. Hishiki, O. Sugiura and Y. Murase, Nucl. Instr. Mthds. Phys. Res. A **520**, 76 (2004).

[6] C. Kumpf, D. Smilgies, E. Landemark, M. Nielson, R. Feidenhans'1, O. Bunk, J. H. Zeysing, Y. Su, R. L. Johnson, L. Cao, J. Zegenhagen, B. O. Fimland, L. D. Marks, and D. Ellis, Phys. Rev. B **64**, 075307 (2001).

[7] See, for example: *The Technology and Physics of Molecular Beam Epitaxy*, Ed. E. N. C. Parker (Plenum, New York, 1985).

[8] M. O. Schweitzer, F. M. Leibsle, T. S. Jones, C. F. McConville and N. V. Richardson, Surf. Sci. **280**, 63 (1993).

[9] W. Mo¨ nch, *Semiconductor Surfaces and Interfaces*, (Plenum, New York, 1992).

[10] K. Oe, S. Ando and K. Sugiyama, Jap. J. Appl. Phys. **19**, L417 (1980).

[11] A. J. Noreika, M. H. Francombe and C. E. C. Wood, J. Appl. Phys. **52,** 7416 (1981).

[12] P. John, T. Miller and T. C. Chiang, Phys. Rev B **39**, 1730 (1989).

[13] R. G. Jones, N. K. Singh, C. F. McConville, Surf. Sci. **208**, L34 (1989).

[14] D. P. Woodruff and K. Horn, Vac. **33**, 633 (1983).

[15] M. O. Schweitzer, F. M. Leibsle, T. S. Jones, C. F. McConville and N. V. Richardson, J. Vac. Sci. Tech. A **11,** 981 (1993).

[16] C. F. McConville, T. S. Jones, F. M. Leibsle, S. M. Driver, T. C. Q. Noakes, M. O. Schweitzer and N. V. Richardson, Phys. Rev. B **50**, 14965 (1994).

[17] W. K. Liu and M. B. Santos, Surf. Sci. **319**, 172 (1994).

[18] N. Jones, C. Norris, C. L. Nicklin, P. Steadman, S. H. baker, A.D. Johnson and S. L. Bennett, Surf. Sci. **409**, 17 (1998).

[19] C. Kumpf, L.D. Marks, D. Smilgies, E. Landemark, M. Nielsen, R. Feidenhans'1, J. Zegenhagen, O. Bunk, J. H. Zeysing, Y. Su, and R. L. Johnson, Phys. Rev. Lett. **86**, 3586 (2001).

[20] I. P. Batra, Prog. Surf. Sci. **25**, 175 (1987)

[21] E. H. Rhoderick and R. H. Williams, *Metal-Semiconductor Contacts* (Clarendon, Oxford, 1988).

[22] W. Monch, in *Proc. Metallization and Metal-Semiconductor Interfaces*, edited by I. P. Batra (Plenum, New York, 1989)

[23] W. C. Simpson and J. A. Yarmoff, Ann. Rev. Phys. Chem. **47**, 527 (1996).

[24] G. Margaritondo, J. E. Rowe, C. M. Bertoni, C. Calandra, F. Manghi, Phys. Rev. B. **23**, 509 (1981).

[25] R. D. Schnell, D. Rieger, A. Bogen, K. Wandelt, W. Steinmann, Sol. St. Comm. **53**, 205 (1985).

[26] D. J. D. Sullivan, H. C. Flaum, A. C. Kummel, J. Chem. Phys. **101**, 1582 (1994).

[27] A. J. Murrell, R. J. Price, R. B. Jackman, J. S. Foord, Surf. Sci. **227**, 197 (1990).

[28] D. K. Shuh, C. W. Lo, J. A. Yarmoff, A. Santoni, L. J. Terminello, F. R. McFeely, Surf. Sci. **303**, 89 (1990).

[29] V. Montgomery, R. H. Williams, R.R. Varma, J. Phys. C **11**, 1989 (1978).

[30] A. Mowbray, R. G. Jones, C. F. McConville, J. Chem. Soc. Faraday Trans. **87**, 3259 (1991).

[31] A. Mowbray, R. G. Jones, Vacuum **41**, 672 (1990)

[32] A. Mowbray, R. G. Jones, Appl. Surf. Sci. **48-49**, 27 (1991)

[33] P. R. Varekemp, M. C. Håkonsson, J. Kanski, B. J. Kowalski, L. Ö, Olsson, L. Ilver, Z. Q. He, J. A. Yarmoff and U. O. Karlsson, Surf. Sci. **352**, 387 (1996).

[34] P. R. Varekemp, M. C. Håkonsson, J. Kanski, D. K. Shuh, M. Björkqvist and M. Gothelid, W. C. Simpson, U. O. Karlsson, J. A. Yarmoff, Phys. Rev. B **54,** 2101 (1996).

[35] P. R. Varekemp, M. C. Håkonsson, J. Kanski, Björkqvist and M. Gothelid, B. J. Kowalski, Z.Q. He, D. K. Shuh and J. A. Yarmoff and U. O.Karlsson, Phys. Rev. B **54**, 2114 (1996).

[36] R. G. Parr and W. Yang, *Density Functional Theory of Atoms and Molecules* (Oxford University Press, Oxford, 1989).

[37] K. Capelle, *A Bird's-Eye View of Density Functional Theory,* www.arxiv:cond-mat/0211443 (2004).

[38] Á. Nagy, Phys. Rep. **298**, 1 (1998).

[39] P. Hohenberg and W. Kohn, Phys. Rev. **136,** B864 (1964).

[40] T. Kato, Commun. Pure Appl. Math. **10**, 151 (1957).

[41] M. Levy, Proc. Natl. Academy Sci. USA, **76**, 6002 (1972).

[42] M. Levy, Phys. Rev. A **26**, 1200 (1982).

[43] M. Leib, Int. J. Quant. Chem. **24**, 243 (1982).

[44] W. Kohn and L. J. Sham, Phys. Rev. **140**, A1133 (1965).

[45] E. R. Davidson and D. Feller, Chem. Rev. **86,** 681 (1986).

[46] J. C. Slater, *Quantum Theory of Molecules and Solids*, *Vol. 4: The Self-Consistent-Field for Molecules and Solids* (McGraw-Hill, New York, 1974).

[47] S. H. Vosko, L. Wilk, and M. Nusair, Can. J. Phys. **58**, 1200 (1980).

[48] S. B. Trickey (Ed.), *Density Functional Theory for Many Fermion Systems* (Academic, San Diego, 1990.

[49] R. M. Dreialer and E. K. U. Gross, *Density Functional Theory: An Approach to Quantum Many Body Problem* (Springer, Berlin, 1990).

[50] J. F. Dobson, G. Vignale, and M. P. Das (Eds.), *Electronic Density Functional Theory – Recent Progress and New Directions* (Plenum, New York, 1998).

[51] P. J. Hay and W. R. Wadt, J. Chem. Phys. **82,** 270 (1985).

[52] P. J. Hay and W. R. Wadt, J. Chem. Phys. **8**2, 284 (1985).

[53] D. R. Lide, *Handbook of Chemistry and Physics, 76th edition* (1995-1996).

[54] A. Brunot, M. Cottin, M. H. Donnart, and J. C. Muller, Int. J. Mass Spec. Ion Phys. **33**, 417 (1980).

[55] W. W. Williams, D. L. Carpenter, A. M. Covington, and J. S. Thompson, T. J. Kvale, and D. G. Seely, Phys. Rev. A. **58**, 3582 (1998).

[56] B. M. Smirnov, and A. S. Yatsenko, Physics – Uspekhi **39**, 211 (1996).

[57] B. Paulus and P. Flude, Phys. Rev. B. **54,** 2556 (1996).

[58] C. Kittel, *Introduction to Solid State Physics*, 6th Ed., (New York: John Wiley, 1986), p. 185.

[59] K. N. Kudin and G. E. Scuseria, Chem. Phys. Lett. **289**, 611 (1998).

[60] K. N. Kudin and G. E. Scuseria, Chem. Phys. Lett. **283**, 61 (1998).

[61] K. N. Kudin and G. E. Scuseria, Phys. Rev. B **61**, 16440 (2000).

[62] O. V. Yazyev, K. N. Kudin, and G. E. Scuseria, Phys. Rev. B **65**, 205117 (2002).

[63] R. Schailey: "*An Ab Initio Cluster Study of Chemisorption of Atomic Cesium and Hydrogen on Reconstructed Surfaces of Gallium Rich Gallium Arsenide (100) Surface*", Ph. D. Dissertation, The University of Texas at Arlington (1999).

[64] R. Schailey and A. K. Ray, J. Chem. Phys. **111,** 8628 (1999).

[65] R. Schailey and A. K. Ray Comp. Mat. Sci. **22**, 169 (2001).

[66] K. M. Song, "*An Ab Initio Study of Alkali Metal Adsorption on Gallium Arsenide (110) Surface,"* (Ph. D. Dissertation, The University of Texas at Arlington, 1994).

[67] K. M. Song, D. C. Khan, and A. K. Ray, Phys. Rev. B **49**, 1818 (1994).

[68] K. M. Song and A. K. Ray, Phys. Rev. B **50**, 14255 (1994).

[69] K. M. Song and A. K. Ray, J. Phys: Cond. Matt. **6**, 9571 (1994).

[70] K. M. Song and A. K. Ray, J. Phys: Cond. Matt. **8**, 6617 (1996).

[71] M. L. Mayo, "*A Many Body Perturbation Theoretic study of Atomic Oxygen and Aluminum Chemisorption on GaAs (100) (2x1) and β (4x2) Surfaces*", M. S. Thesis, the University of Texas at Arlington (2003).

[72] M. L. Mayo and A. K. Ray, Eur. Phys. J. D **33**, 413 (2005).

[73] Gaussian '03 (Revision A.1), M. J. Frisch *et al* Gaussian Inc., Pittsburgh. PA, 2003.

[74] G. - X. Qian, R. M. Martin, and D. J. Chadi, Phys. Rev. B. **38**, 7649 (1988).

[75] G. Pacchioni and P. S. Bagus, Phys. Rev. B 36, 2813 (1987)

[76] R. S. Mulliken, J. Chem. Phys. **23**, 1833 (1955).

[77] R. S. Mulliken, J. Chem. Phys. **23**, 1841 (1955).

[78] R. S. Mulliken, J. Chem. Phys. **23**, 234 (1955).

[79] *GaussView3.0* User's Reference, 2003, Gaussian, Inc, Pittsburgh, PA.

[80] T. H. Dunning Jr. and P. J. Hay, in *Modern Theoretical Chemistry*, Ed. H. F. Schaefer III, Vol. 3(Plenum, New York, 1976) pp. 1-28.

[81] S. Kunsági-Máte, C. Schür, T. Marek, and H. P. Strunk, Phys. Rev. B **69**, 193301 (2004).

[82] M. Panda, "*Interactions of Alkali Atom with the GaAs (110) Surface: A Density Functional Approach*," M. S. Thesis, The University of Texas at Arlington (1997).

[83] M. Panda and A. K. Ray, J. Vac. Sci. Tech. A **17**, 2647 (1999).

BIOGRAPHICAL INFORMATION

The author completed her undergraduate degree in electrical engineering in the University of Madras, Chennai, India. Her undergraduate project was in the design of three-axis robot endowed with artificial intelligence that has capability of lifting and transferring loads upto 2 kg., sensing fire and high temperature. She stood first in her undergraduate in a class of 70 students and also received the best student award and the best project award. After completion of her undergraduate, she worked in an electronics company where she was involved in the design and development of automation products, such as, window annunciators used in the fault detection systems. She also inspected the quality of the products and programmed 8081,8086 microprocessors. In the course of her masters', she was involved in the simulations of reconstructions and relaxations of ABCS (antimony-based compound semiconductor) surfaces and in the analysis of interactions of Li and halogen atoms with these surfaces which are of great industrial importance. She has authored and co-authored quite a few papers in scientific journals and has also presented papers at international conferences. She has held John D. McNutt Scholarship for the year 2004-2005. Also, in the field of electrical engineering, she was involved in projects utilizing PSPICE to determine the resistance characteristics of a diode and wrote several research papers in the area of advanced electronics. In future, she seeks an opportunity to work in the research labs in the field

of semiconductors, especially in the areas of IC fabrication where she can utilize her knowledge in theoretical simulations.